**The Dissertation Committee for David Hamilton Van Wagener Certifies that this is the approved version of the following dissertation:**

# Stripper Modeling for $CO_2$ Removal Using Monoethanolamine and Piperazine Solvents

**Committee:**

Gary T. Rochelle, Supervisor

A. Frank Seibert

Thomas F. Edgar

Thomas M. Truskett

Craig N. Schubert

# Stripper Modeling for $CO_2$ Removal Using Monoethanolamine and Piperazine Solvents

**by**

**David Hamilton Van Wagener, B.S.**

**Dissertation**

Presented to the Faculty of the Graduate School of

The University of Texas at Austin

in Partial Fulfillment

of the Requirements

for the Degree of

**Doctor of Philosophy**

**The University of Texas at Austin**

**August 2011**

# Dedication

To my family

# Acknowledgements

First and foremost, I would like to thank my research advisor, Dr. Gary Rochelle. He has provided immense support throughout this work with his guidance, encouragement, and enthusiasm. He has incredible passion and dedication to the field of carbon capture, and working with him on this topic has been a privilege. He was always ready to discuss the problem at hand, whether it would take 2 minutes or 2 hours. His love and knack for chemical engineering was always apparent when he would quickly resolve a quandary by pulling an equation, seemingly out of nowhere, to explain the phenomenon in question. I will carry the influence of Dr. Rochelle as I continue my career in the field of chemical engineering research.

I would also like to thank the funding sources for this project. The Luminant Carbon Management Program and the Industrial Associates Program for $CO_2$ capture directly supplied funding support for this project. Specifically, I really appreciate the support of Aspentech and Chau-Chyun Chen to resolve the occasional software glitch. Additionally, the $CO_2$ Capture Pilot Plant Project (C2P3) supported the pilot plant campaigns that were analyzed in this project.

I also gratefully acknowledge the help that I received from the entire chemical engineering support staff. Maeve Cooney has been immensely helpful and accommodating. Maeve is always willing to lend a hand whether the task is large or small. T Stockman also deserves my gratitude for helping sort through the "graduate student rules" when the handbooks were not so easy to comprehend. Jim Smitherman, Butch Cunningham, and Kevin Haynes also served vital roles for me. The doors, furniture, and stairwell were not always designed with handicap accessibility in mind, but

you went out of your way to make sure that I was comfortable and could get my work done. I have also had the pleasure of working occasionally with Randy Rife and Patrick Danielewski to resolve hardware and Aspen issues.

The support and camaraderie of the other students in the Rochelle Group was invaluable to my successes: Babatunde Oyenekan, Marcus Hilliard, Eric Chen, Jason Davis, Andrew Sexton, Ross Dugas, Bob Tsai, Stephanie Freeman, Xi Chen, Jorge Plaza, Sepideh Ziaii, Qing Xu, Fred Closmann, Stephanie Freeman, Thu Nguyen, Stuart Cohen, Peter Frailie, Alex Voice, Chao Wang, Lynn Li, Mandana Ashouri, Steven Fulk, Humera Rafique, and Omkar Namjoshi. Sharing an office with Jorge, Peter, and Bob was a great experience, and they were always helpful for the instances where a quick group discussion avoided hours of searching for the solution alone. Also, having now gone through the experience of writing a dissertation and preparing for the defense, I appreciate every minute that was spared by previous group members when they were on the verge of defending. I learned the basics of stripper modeling from Babatunde Oyenekan as he was just finishing his writing; it certainly was not the most stress-free moment in time for him, and I appreciate the valuable lessons! Working in the Rochelle group was a great experience.

I have met a number of great people that I had shared my time with while studying in Austin. In addition to other members of the group like Jorge, Peter, Bob, Stephanie, Alex, Ross, and Andrew, I've enjoyed unwinding from the stresses of grad school with other good friends. I still have memories of working on the homework for first-year classes alongside Dan Miller, Adam Stephens, Grant Offord, Scott Owens, Sara Jones, and David Trombly. The hours spent in the graduate lounge went by much quicker with your company.. I also appreciate the friends and support that has come from my roommates over the last 5 years: Dan Miller, Matt Panthani, Tarik Khan, Yevgeniy

Reznik, Thomas Nguyen, and Thomas Lewis. There is not enough space for everyone here, but thank you to all of my Austin friends!

Above all, I would like to thank my family. You have always been my greatest supporter. You are continually the source of my drive to succeed! To my parents, thank you for all the encouragement to find what makes me happy while giving a helpful nudge when needed. You have raised us to value family, even after venturing out on our own. To my brother and sister, you are great siblings and the best friends I could ask for. Whether sharing new music, offering advice, or exploring the world together, I always value having you in my life.

# Stripper Modeling for $CO_2$ Removal by Monoethanolamine and Piperazine Solvents

Publication No._____

David Hamilton Van Wagener, Ph.D.

The University of Texas at Austin, 2011

Supervisor: Gary T. Rochelle

This dissertation seeks to reduce the energy consumption of steam stripping to regenerate aqueous amine used for $CO_2$ capture from coal-fired power plants. Rigorous rate-based models in Aspen Plus® were developed, and rate-based simulations were used for packed vapor/liquid separation units. Five main configurations with varying levels of complexity were evaluated with the two solvents. 8 m piperazine (PZ) always performed better than 9 m monoethanolamine (MEA). More complex flowsheets stripped $CO_2$ with higher efficiency due to the more reversible separation. Multi-stage flash configurations were competitive at their optimal lean loadings, but they had poor efficiency at low lean loading. The most efficient configuration was an interheated column, with more effective and distributed heat exchange. It had a secondary benefit of a cooler overhead temperature, so less water vapor exited with the $CO_2$. Using a rich loading of 0.40 mol $CO_2$/mol alkalinity in 8 m PZ, the optimal lean loading was 0.28 and the energy requirement was 30.9 kJ/mol $CO_2$.

Case studies were also performed on cold rich bypass and the use of geothermal heat. When cold rich bypass is used with the 2-stage flash and 8 m PZ, it reduces equivalent work by 11% to 30.7 kJ/mol $CO_2$. PZ benefited the most from cold rich bypass because it had a higher water concentration in the overhead vapor than with MEA. In an advanced 2-stage flash with 8 m PZ, geothermal heat available from 150 down to 100 °C requires 35.5 kJ work/mol $CO_2$. The heat duty and equivalent work was higher than other optimized configurations, but it would be a valid option if separating the heat source from the steam cycle of a coal-fired power plant was highly valued.

Pilot plant campaigns were simulated with the available thermodynamic models. Two campaigns with 8 m PZ were simulated within small deviation from the measured values. The average absolute errors in these campaigns were 2.5 and 2.7%. A campaign with 9 m MEA in a simple stripper demonstrated that the MEA model did not predict the solvent properties well enough to appropriately represent the pilot plant operation.

# Table of Contents

# List of Tables

# List of Figures

# Chapter 1: Introduction

This chapter introduces the need for stripper modeling in the context of carbon dioxide ($CO_2$) capture from coal-fired power plants. Coal combustion for power production is a significant point source of $CO_2$. Post-combustion capture by absorption/stripping with alkanolamines is the state-of-the-art technology which has prior applications in the field of acid gas treating. Modeling of the stripper component is essential to help evaluate and optimize the process operation to reduce the overall cost. The penalty of using a standard technology absorption/stripping process for $CO_2$ removal from coal-fired power plants has been estimated to be approximately 30% of the total electricity produced, and the majority of the energy is used in the stripper and $CO_2$ compression. The expected benefits of stripper modeling are discussed in this chapter. The research objectives are defined, and the scope of this work is described.

## 1.1. $CO_2$ Capture from Coal-Fired Power Plants

A study of atmospheric carbon dioxide concentrations at Mauna Loa, Hawaii was initiated in 1960, and it determined that $CO_2$ levels have risen by about 17% in 41 years (Keeling et al., 2004). Additionally, Antarctic ice cores show that trends over geologic scales of the average Earth surface temperature and the atmospheric $CO_2$ concentration nearly track each other. This observation suggests a direct correlation of atmospheric $CO_2$ concentration with global surface temperatures (Petit et al., 1999). The annual worldwide carbon emissions continue to rise each year, which have increased the

atmospheric $CO_2$ concentration to 390 ppm from preindustrial levels of 300 ppm (Bates et al., 2008; Tans, 2010). In order to attempt to mitigate global climate change by reducing greenhouse gases in the atmosphere, the release of carbon dioxide should be addressed. While the $CO_2$ emission rate of each individual coal-fired power plant is highly dependent on plant technology and type of coal, an emission rate of approximately 10,000 ton/day is typical for a 500 $MW_e$ plant (Fisher et al., 2005). Moreover, coal is the largest electricity producer in the United States, accounting for nearly 50% of the total production (EIA, 2006). For this reason, coal-fired power plants have been recognized as the most important target for reducing point source emissions of $CO_2$.

## 1.2. ABSORPTION/STRIPPING WITH AMINE SOLVENTS

Absorption/stripping using alkanolamine solvents is the state-of-the-art technology for removing $CO_2$ from the flue gas of coal-fired power plants. It is a post-combustion technology, and a flowsheet describing its expected integration with a power plant is shown in Figure 1-1. It is a tail-end process which could be installed with new plants, but it could also be retrofitted to current plants with few changes to the existing power plant. Most coal-fired power plants already use an electrostatic precipitator (ESP) to remove fly ash and a flue gas desulfurization unit (FGD) to remove SOx. The absorption/stripping unit would treat the flue gas after exiting the FGD. After $CO_2$ removal, the cleaned flue gas travels to the stack, and the removed $CO_2$ is compressed for sequestration. To heat the reboiler, the absorption/stripping unit uses low-pressure steam taken between the IP and LP steam turbines in the coal plant. Electricity is used to run the $CO_2$ compressor and solvent circulation pumps.

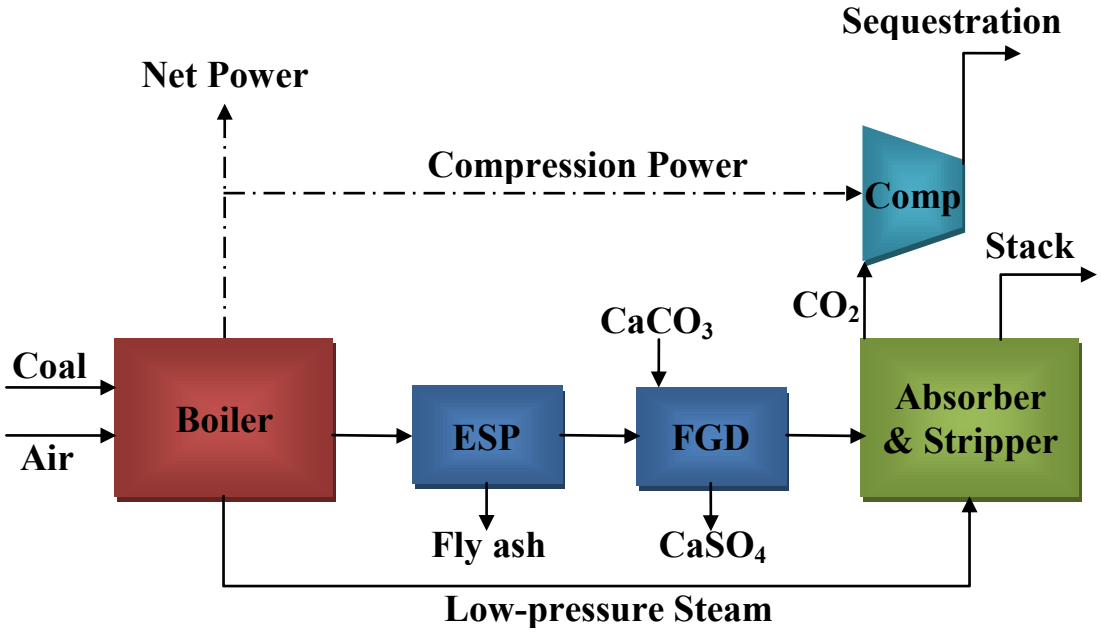


Figure 1-1: Absorption/Stripping As a Post-Combustion Process for $CO_2$ Capture from Coal-Fired Power Plants

A generic flowsheet of the absorption process is shown in Figure 1-2. Flue gas enters the absorber with approximately 12 mol% $CO_2$ and is counter-currently contacted by the amine solvent, which absorbs 90% of the $CO_2$ by a reversible chemical reaction. The treated gas is then sent to the stack. The rich solvent exits the bottom of the absorber and is heated by hot lean solvent in a cross heat exchanger, then enters the top of the stripper. Steam supplied to the reboiler of the stripper generates steam, which countercurrently contact the amine solution. The steam strips $CO_2$ from the solvent as it travels up the column. The lean solvent exits from the reboiler and is recycled to the top of the absorber after being cooled by the cross exchanger and an additional trim cooler.

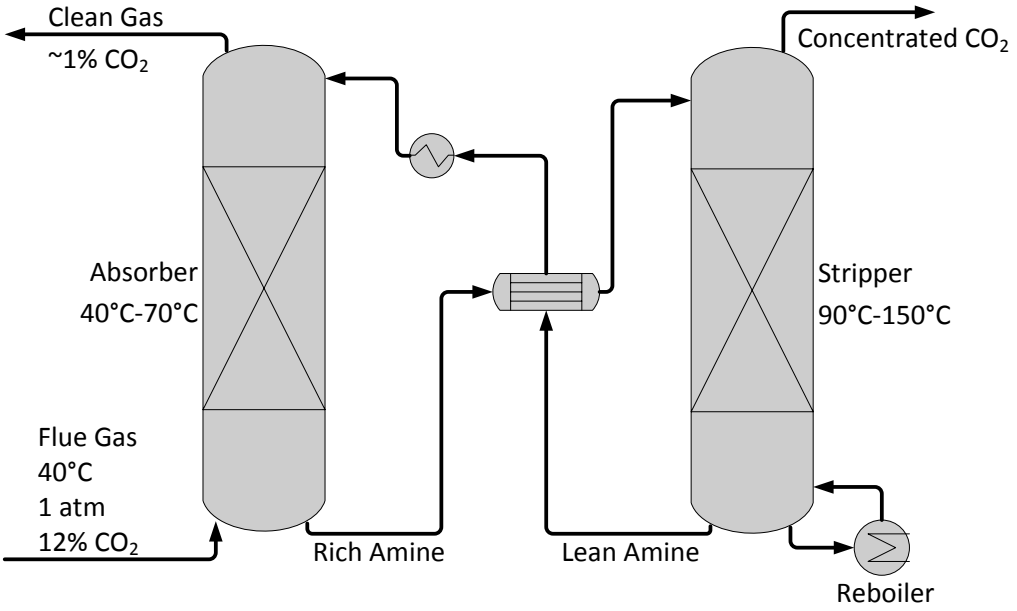


Figure 1-2: Absorption/Stripping with Alkanolamine Solutions

Aqueous monoethanolamine (MEA) is the current standard solvent in a concentration of 7 m (30 wt%); it has the most substantial research base. It has also been used in the past for similar applications like $H_2S$ removal from natural gas. Removing 90% of $CO_2$ using MEA is possible with this technology, but the capital cost and energy requirement of current systems are currently prohibitive (Rochelle, 2007). The steam and electricity used for operating the pumps, compressors, and stripper reboiler typically accounts for 20-30% of the total power plant output. In order to be a practical solution for industrial $CO_2$ producers, the total energy penalty must be reduced.

## 1.3. STRIPPER MODELING

Although the energy consumption of a base case stripper with 7 m MEA is high, computer modeling of these process units can improve the understanding of the underlying mechanisms and help locate areas where work is lost. This knowledge can

aid in the implementation of advanced technologies to reduce the overall energy usage. An accurate model is an important tool for the design and optimization of a full-scale process.

There are two important considerations in the development of a stripper with high efficiency. As with any chemical process, configurations with more complex heat and material recycles improve the overall reversibility by reducing driving forces (Leites et al., 2003). Any realistic process has innate inefficiencies due to the driving forces required to minimize overall capital costs, but the efficiency of a simple stripper case can be drastically improved by introducing some complexity to the flowsheet. The second important consideration is solvent choice. Certain properties of the amine solvent can significantly affect the performance; these properties include $CO_2$-carrying capacity, heat of absorption, heat capacity, and thermal degradation rate. Reaction rate with $CO_2$ at low temperature affects the performance of the absorber, which has a secondhand effect on the stripper operation.

Although developing a process with a reduced energy requirement is the desired output of stripper modeling, another important aspect of developing a good model is ensuring accurate representation of the solvent and process. Truthful representation of the solvent properties is accomplished by utilizing equilibrium and rate-based models to describe the behavior. After selecting and cultivating the model of choice, additional checks of the model predictions are required. Stripper models and pilot plant campaigns assist each other in being successful. The model helps guide decisions of run conditions for pilot plant campaigns, and measurements from completed campaigns are used in the stripper model to verify accurate portrayal of the process. A model verified with pilot scale data is a powerful tool to reliably suggest configurations and conditions for a full-scale process.

## 1.4. PRIOR WORK

Table 1-1 briefly summarizes previous simulation work in the area of absorption/stripping. The contributions are categorized into system models (combined absorber and stripper modeling), absorber models, and stripper models. Nearly all authors included an analysis of rate-based calculations, but kinetically controlled reactions were not usually considered.

The majority of previous work in modeling of $CO_2$ capture with aqueous amines focused on improving capture in the absorber; fewer papers have been published that emphasize the importance of optimizing the stripper performance. Previous efforts in stripper modeling by other authors have implemented a variety of types of solvent models. The models ranged in complexity; the simplest consisted of sets of equation-based correlations to predict a minimum number of properties, and the most complicated utilized full thermodynamic models (like the e-NRTL model) to be internally consistent. Each model developed for an individual solvent system required a substantial amount of data to properly regress relevant model parameters, and was typically approached as an individual task separate from process modeling. Several papers addressed the concept of chemical absorption and desorption with chemical reaction (Weiland et al., 1982; Bosch et al., 1990). Some work progressed further to investigate theory of mass transfer and kinetic modeling (Astarita et al., 1980a; Astarita et al., 1980b; Escobillana et al., 1991; Cadours et al., 1997).

Pilot plant results have been replicated by capture process simulations represented by equilibrium and rate-based models. This type of work had two objectives: validating the stripper simulation and verifying the accuracy of pilot plant measurements. There

was varying success in the ability to match pilot plant data. Oyenekan constructed equilibrium and rate-based stripper models, but representing pilot plant data proved to be difficult (Oyenekan, 2007). Conversely, Tobiesen constructed a stripper simulation whose sole purpose was to accurately represent pilot plant data. The conditions in the column were successfully predicted with low deviation, but the model was not further implemented to develop or optimize stripper configurations (Tobiesen et al., 2008). In addition to pilot plant reconciliation, stripper models have been used to evaluate the extent to which new configurations or solvents reduce the energy requirement in the stripper (Jassim et al., 2006). Previous configurations of interest have included multi-pressure columns and double matrix configurations. Of all the prior work, some simulations were done in Aspen Plus®, but many were executed with in-house codes programmed in FORTRAN or other languages.

**Table 1-1. Simulations of $CO_2$ Capture with Amines**

| Author | Year | Tool | Simulation Method | Solvent | Focus of work | Accomplishments/conclusions |
|---|---|---|---|---|---|---|
| **System Models** | | | | | | |
| Desideri | 1999 | Aspen Plus RadFrac | Equilibrium Reactions | MEA | System modeling for MEA in Aspen Plus | Full system model and cost analysis. Electricity price doubles with $CO_2$ capture |
| Freguia | 2002 | Aspen Plus RateFrac | Kinetics/ Equilibrium Reactions | MEA | Development of rigorous system model using $K^+$/PZ | An optimum lean loading exists which minimizes the stripper energy requirement. |
| Alie | 2005 | Aspen Plus RateFrac | Equilibrium Reactions | MEA | Model $CO_2$ capture using decomposition method | Energy cost is more important than capital costs, so reducing reboiler duty is key. |
| Jassim | 2006 | Aspen Plus RateFrac | Kinetics/ Equilibrium Reactions | MEA | Analysis of advanced stripper configurations for reducing work | Multi-level stripping can be beneficial because energy used by work is more efficient than heating. |
| Oexmann | 2008 | Aspen Plus RadFrac | Equilibrium Stages | $K^+$/PZ | K+/ PZ system modeling (2.5/2.5) | An optimal solvent blend is a complex. Factors = energy use, amine cost, and degradation rates. |
| Zheng | 2009 | In-House Code | Equilibrium stages | MEA, DMAP | Verification with pilot plant, new amine evaluation | 8wt% MEA, 22wt% DMAP reduced heat requirement by 20% over 30wt% MEA base case. |
| Kvamsdal | 2011 | CO2SIM | Equilibrium Stages | AMP, PZ | Verification with pilot plant, evaluation of new features | Intercooling in the absorber and vapor recompression in the stripper reduced heat by 19%. |

| Author | Year | Tool | Simulation Method | Solvent | Focus of work | Accomplishments/conclusions |
|---|---|---|---|---|---|---|
| **Absorber Models** | | | | | | |
| Al-Baghli | 2001 | In-House Code | Kinetics | MEA, DEA | Rate-based absorption of $CO_2$ using MEA and DEA | Boundary layer rigorously calculated, important for absorber with multiple controlling rates. |
| Chen | 2007 | Aspen Plus RateSep | Kinetics | $K^+$/PZ | Pilot plant modification, kinetic absorber model reconciliation | F1Y packing in absorber showed good results in model with 80% of air-water measured value. |
| **Stripper Models** | | | | | | |
| Oyenekan | 2007 | Aspen Custom Modeler | All model types | Various | Advanced stripper configuration development and analysis | High P and T stripping is not kinetically controlled. High $\Delta H_{abs}$ decreases overall energy use. Complexity improves efficiency. |
| Tobiesen | 2008 | In-House Code | Kinetics/ Equilibrium Reactions | MEA | Validation of rigorous stripper model with pilot plant | Equilibrium and rate-based reactions give similar predictions in the stripper. $k_g$ is more important in stripper than in absorber. |
| van Nierop | 2011 | MATLAB | Equilibrium Stages | MEA | Effect of $\Delta H_{abs}$ on overall performance | Increased $\Delta H_{abs}$ can decrease stripper temperature, but increases solvent rate and cooling load. |
| This Work | 2011 | Aspen Plus RateSep | Equilibrium Reactions | MEA, PZ | Analyze performance of advanced configurations using MEA and PZ solvents | Quantify benefit of stripping with concentrated PZ. Determine relationship between complexity and efficiency. Develop new configurations. |

## 1.5. RESEARCH OBJECTIVES

This work addresses the following objectives:

1. Compare the energy performance of configurations with varying levels of complexity and determine the most efficient alterations.
2. Evaluate the energy benefit of using concentrated PZ over MEA in the stripper.
3. Quantify and qualify the difference in performance enhancement between MEA and PZ when using configurations with varying levels of complexity.
4. Propose and evaluate the performance of innovative stripper configurations.
5. Evaluate pilot plant campaigns with MEA and PZ to validate the thermodynamic models.

The goal of this project is to use the results of a rigorous stripper model to make conclusions regarding improving the overall efficiency of the stripper. Prior thermodynamic models for MEA and PZ are used to calculate the performance of each solvent. In-depth analysis of each simulation of a configuration/solvent combination provides insight regarding the location of inefficiency within the process. Additionally, the use of Aspen Plus provides the opportunity to simulate many new innovative stripper configurations. Lastly, validation of the thermodynamic solvent models with pilot plant data provides the verification that laboratory scale measurements can be scaled to a full-size process with an adequate modeling tool.

This work improves upon prior efforts by using a rate-based stripper model in Aspen Plus® to investigate the combined effects of the stripper configuration and solvent choice. The solvent models used in this work use the e-NRTL framework to predict all

relevant properties in the simulation while maintaining thermodynamic consistency. In addition to comprehensive solvent models and simulation methods, the flowsheets proposed in this work are more practical than previous proposals, while effectively increasing stripper complexity and improving efficiency. For example, multi-stage flash configurations are evaluated that increase the flowsheet complexity but would most likely decrease capital investment. This work takes a strategic approach to analyzing the improvement in stripper performance with an increase in configuration complexity with both MEA and PZ.

# Chapter 2: Stripper Modeling in Aspen Plus®

This project focused on comparing the performance of different solvents and configurations. In order to make conclusions on the potential improvement by using a novel solvent and/or configuration, a reliable stripper simulation method was established. Aspen Plus® v7.1 was used with thermodynamic models for monoethanolamine and piperazine to represent the behavior of the solvents in a $CO_2$ capture process. The solvent models were developed by other authors. This chapter introduces the chemistry of $CO_2$ absorption and stripping with aqueous amines solvents. The models that represent monoethanolamine and piperazine in this work are also described.

An understanding of the individual contributions to the overall energy requirement enabled an adequate analysis of stripper simulations. Energy was required for pumping the solvent, heating the solvent to regenerate the lean solvent and produce $CO_2$, and compressing the $CO_2$ to pipeline specifications for transport and sequestration. The basis of these contributions is also introduced.

## 2.1. AMINE CHEMISTRY

In the absorber amines react with $CO_2$ from the flue gas to chemically bind the compound to the solvent. The reaction is reversible and requires heat in the stripper to release the $CO_2$. Several reactions can occur with any given solvent, but every reaction follows the same arrangement:

$$A + CO_2 + B \rightarrow ACOO^- + BH^+ \qquad \text{2-1}$$

"A" represents an amine/acid molecule, and "B" represents a molecule acting as a base. With the exception of amines that cannot form a carbamate, the $CO_2$ replaces a $H^+$ ion on the nitrogen of the amine, and the base picks up the $H^+$. The base can be another amine molecule or a water molecule. $CO_2$ absorbed into solution is no longer in its original molecular state, but its apparent concentration in a loaded solution is described by the $CO_2$ loading. The loading value expresses the moles of $CO_2$ absorbed per mole of alkalinity of the solvent, effectively accounting for the number of reactive nitrogen sites on each amine molecule.

Monoethanolamine (MEA), the industry-standard solvent, is a primary amine and forms a single carbamate. It has a moderate balance between the $CO_2$ reaction rate, capacity, heat of absorption, and thermal/oxidative degradation rates. The structure of MEA and ionic species are shown in Figure 2-1.

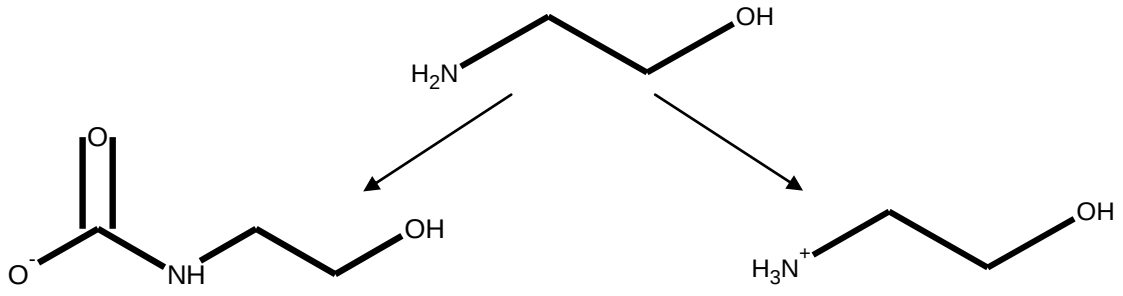


Figure 2-1: Monoethanolamine (MEA), carbamate (bottom left), and protonated (bottom right) species in a $CO_2$ loaded solution.

Piperazine (PZ) is a cyclic molecule with two amine groups on each molecule. It has gained recent interest as a potential solvent for $CO_2$ capture because it has greater $CO_2$ capacity and lower degradation rates compared to MEA (Freeman et al., 2010). Since each molecule has two amine groups, the number of possible reactions and the

number of ion types in a loaded solution are greater than in an MEA solution. Piperazine had previously only been studied as a solvent promoter, increasing the reaction rate of a slow solvent that otherwise had good properties. Some examples of amines that have been studied with PZ promotion are potassium (Cullinane, 2005), diethylethanolamine (DEEA) (Vaida et al., 2009), methyldiethanolamine (MDEA) (Closmann et al., 2009), and MEA (Nainar et al., 2009). The main reason that piperazine had not been considered for a solvent on its own was its poor solubility in water; at ambient temperature (20 °C) a solution higher than 2 m PZ precipitates solids. However, a solution in the $CO_2$ loading range of 0.3-0.4, which is expected in the absorption/stripping process, has been found to be soluble down to 0 °C, and the wider, more conservative loading range of 0.2-0.4 is soluble down to at least 30 °C (Freeman et al., 2010). A maximum concentration of 8 m PZ is being considered due to prohibitively high viscosity at higher concentration. The structure of PZ and its ionic species are shown in Figure 2-2.

Amine solvents absorb $CO_2$ by chemisorption, as opposed to physical solvents that use physisorption. Physical solvents dissolve the $CO_2$ and hold it in solution by weak van der Waals forces. The heat of absorption is generally very low, but a high driving force for dissolution is required in the absorber. Chemical absorption attains a faster reaction rate with $CO_2$ with a small driving force. Chemisorption is preferred for carbon capture from industrial sources like coal-fired power plants because the $CO_2$ partial pressure of the flue gas is relatively low. A partial pressure of approximately 12 kPa can be expected in the flue gas of coal-fired power plants, and the $CO_2$ content in natural gas applications is even smaller (Fisher et al., 2005).

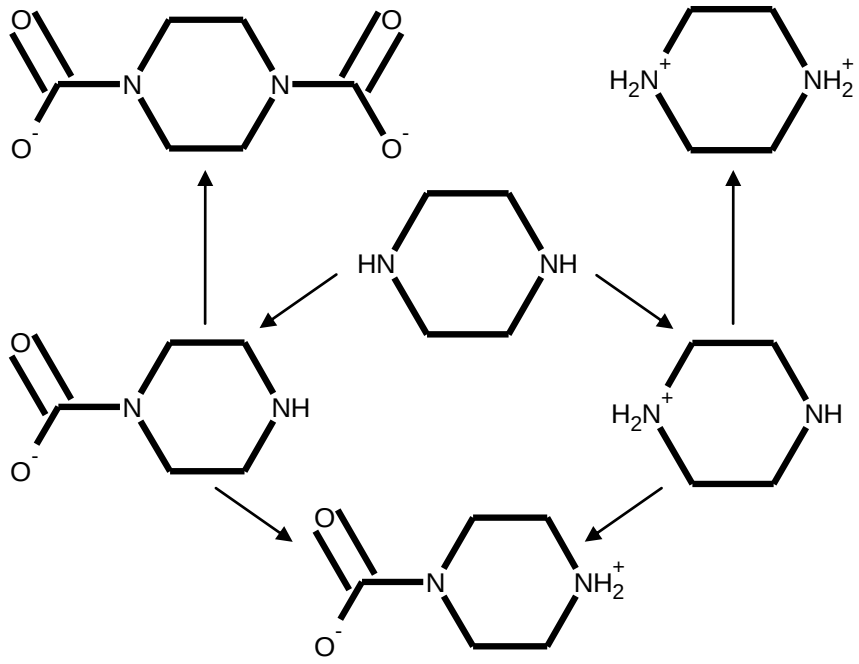


Figure 2-2: Piperazine (PZ) in center and species in a $CO_2$ loaded solution (clockwise from top left): dicarbamate, diprotonated, protonated, protonated carbamate (zwitterion), carbamate.

## 2.2. SOLVENT THERMODYNAMIC MODEL FRAMEWORK

There is a significant history of solvent models, especially for 30 wt% (7 m) MEA. The foundation of a correct simulation of the stripper is an accurate solvent model, a product of reliable data. Various authors have contributed data on VLE and mass transfer characteristics of solvents other than MEA, including MEA/PZ, $K^+$/PZ, and even potential new solvents like 2-amino-2-hydroxymethyl-1,3-propanediol (AHPD), an amine, promoted with carbonic anhydrase to increase its reaction rate with $CO_2$ (Aroonwilas et al., 1997; Dang, 2001; Cullinane, 2002; Le Tourneux et al., 2008). A significant contribution to solvent data was made by Hilliard (2008), who measured VLE, heat capacity, heat of absorption, and speciation for MEA, PZ, $K^+$/PZ, and MEA/PZ.

The type of thermodynamic model used for simulations typically depended on the modeling tool available to a specific author. FORTRAN was often utilized to implement either equilibrium or rate-based models. The level of model complexity was a choice of the modeler, and it can predict solvent properties using either individual correlations for each property or a full solvent model (i.e. e-NRTL) to predict everything. For example, a model developed by Tobiesen used Fortran to define a rate-based simulation that accounted for heat and mass transfer in the liquid and vapor films (2008). A number of models have been developed in Aspen Plus® to represent alkanolamine solutions for use in $CO_2$ capture. The thermodynamic framework most suited for modeling the solutions is the electrolyte Nonrandom Two-Liquid (e-NRTL) model. This model uses interaction parameters between molecules and electrolytes to calculate activity coefficients for all components in solution. An early solvent model was developed by Austgen (1991) which broadly predicted VLE for $CO_2$ and $H_2S$ in MEA, MDEA, MDEA/MEA, and MDEA/DEA solutions. This MEA model was updated by Freguia (2003) to include VLE data collected by Jou (1995). In his work Freguia also developed a full process model for the absorber and stripper, incorporating reaction rates in the absorber by utilizing experimental kinetic data at absorber conditions. Cullinane produced a standalone FORTRAN model for PZ promoted potassium. PZ was used as an additive to the potassium solvent to increase the reaction rate with $CO_2$ (Cullinane et al., 2004). A broad thermodynamic model for MEA was recently developed by Hilliard (2008) which included data sets for MEA from 3.5 to 11 m and temperatures from 40 to 120 °C. In addition to the MEA model, further solvent models were developed for PZ, $K^+$, and selected blends, including a global $K^+$/MEA/PZ representation. His work found that attempting to represent a broad range of solvents and conditions sacrificed accuracy of predictions.

### 2.2.1. Electrolyte-NRTL model

The Electrolyte Non-Nonrandom Two Liquid (e-NRTL) model is an extension of the NRTL model, and it calculates activity coefficients and Gibbs free energy for the liquid phase (Chen et al., 1982). The molar Gibbs free energy is calculated as a contribution of individual chemical potential terms, but an excess Gibbs free energy, $G^{ex}$, is also calculated to account for non-ideality. The excess Gibbs free energy has three components: the Pitzer-Debye-Hückel contribution from long range ion-ion interactions, the Born correction for the change in mixed solvent reference state, and the local contribution for short range ion-ion interactions (Chen et al., 2004). The calculation method for the local contribution in the e-NRTL is as follows:

$$\frac{\boldsymbol{G_m^{*ex,lc}}}{\boldsymbol{RT}} = \sum_{\boldsymbol{m}} \boldsymbol{X_m} \frac{\sum_{\boldsymbol{m}} \boldsymbol{X_j G_{jm} \tau_{jm}}}{\sum_{\boldsymbol{k}} \boldsymbol{X_k G_{km}}} + \sum_{\boldsymbol{c}} \boldsymbol{X_c} \sum_{\boldsymbol{a'}} \left( \frac{\boldsymbol{X_{a'}}}{\sum_{\boldsymbol{a''}} \boldsymbol{X_{a''}}} \right) \frac{\sum_{\boldsymbol{j}} \boldsymbol{G_{jc,a'c} \tau_{jc,a'c}}}{\sum_{\boldsymbol{k}} \boldsymbol{X_k G_{kc,a'c}}} + \sum_{\boldsymbol{a}} \boldsymbol{X_a} \sum_{\boldsymbol{c'}} \left( \frac{\boldsymbol{X_{c'}}}{\sum_{\boldsymbol{c''}} \boldsymbol{X_{c''}}} \right) \frac{\sum_{\boldsymbol{j}} \boldsymbol{G_{ja,a'c} \tau_{ja,a'c}}}{\sum_{\boldsymbol{k}} \boldsymbol{X_k G_{ka,a'c}}} \quad \textbf{2-2}$$

where

$$\boldsymbol{G_{cm}} = \frac{\sum_{\boldsymbol{a}} \boldsymbol{X_a G_{ca,m}}}{\sum_{\boldsymbol{a'}} \boldsymbol{X_{a'}}}, \qquad \boldsymbol{G_{am}} = \frac{\sum_{\boldsymbol{c}} \boldsymbol{X_c G_{ac,m}}}{\sum_{\boldsymbol{c'}} \boldsymbol{X_{c'}}}$$

$$\boldsymbol{\alpha_{cm}} = \frac{\sum_{\boldsymbol{a}} \boldsymbol{X_a \alpha_{ca,m}}}{\sum_{\boldsymbol{a'}} \boldsymbol{X_{a'}}}, \qquad \boldsymbol{\alpha_{am}} = \frac{\sum_{\boldsymbol{c}} \boldsymbol{X_c \alpha_{ac,m}}}{\sum_{\boldsymbol{c'}} \boldsymbol{X_{c'}}}$$

$$\boldsymbol{G_{jc,a'c}} = \boldsymbol{exp}\left(-\boldsymbol{\alpha_{jc,a'c} \tau_{jc,a'c}}\right), \quad \boldsymbol{G_{jc,c'a}} = \boldsymbol{exp}\left(-\boldsymbol{\alpha_{ja,c'a} \tau_{ja,c'a}}\right)$$

$$G_{im} = exp(-\alpha_{im}\tau_{im}), \qquad G_{ca,m} = exp\left(-\alpha_{ca,m}\tau_{ca,m}\right)$$

Subscripts and indices of $\boldsymbol{m}$, $\boldsymbol{c}$, and $\boldsymbol{a}$ refer to molecules, cations, and anions, respectively. The binary interaction parameters, τ, are defined within the e-NRTL model as a function of temperature:

$$\boldsymbol{\tau_{x,y}} = \boldsymbol{A_{x,y}} + \frac{\boldsymbol{B_{x,y}}}{\boldsymbol{T}} \quad \textbf{2-3}$$

$$\boldsymbol{\tau_{x,y}} = \boldsymbol{\tau_{m,m}}, \quad \boldsymbol{\tau_{ca,m}}, \quad \boldsymbol{\tau_{m,ca}}, \quad \boldsymbol{\tau_{c'a,c'b}}, \quad \boldsymbol{\tau_{ca',ca''}}$$

Equation 2-3 also has higher order parameters that can be regressed, but they are typically excluded to promote model stability. Aspen Plus® has non-temperature dependent default binary interaction parameters for the e-NRTL model. The default values are given below in Table 2-1.

**Table 2-1: Default Binary Interaction Parameters for the E-NRTL Model in Aspen Plus®**

| Pair type | Default Value |
|---|---|
| **Molecule-Electrolyte** | 10 |
| **Electrolyte-Molecule** | -2 |
| **Water-Electrolyte** | 8 |
| **Electrolyte-Water** | -4 |

Appropriate interaction parameters, Gibbs free energy of formation, enthalpy of formation, and component heat capacities can be individually regressed to ensure that a solvent model accurately represents its physical system. A rigorous methodology for this regression can be found in the dissertation by Hilliard (2008). The simulations in this work all used the ELECNRTL property method in Aspen Plus®. This method used the e-NRTL model for liquid phase calculations and the Redlich-Kwong equation of state for vapor phase calculations.

### 2.2.2. Solvent Representation in Aspen Plus®

Each model to be used in this work had been regressed by other authors in Aspen Plus® to fit laboratory data of an individual solvent. A sequential regression method was used; this approach determined the values of parameters which affected only pure

component properties, and then values of parameters for binary mixtures were regressed, and so forth. This method typically resulted in more stable regressions since fewer parameters were being regressed at once. Models have been developed for use in Aspen Plus® for both MEA (Hilliard, 2008) and PZ (Rochelle et al., 2010).

#### *2.2.2.1 Monoethanolamine*

The model used for MEA was developed by Hilliard as part of doctoral work. In the regression first step, three MEA heat of vaporization parameters were regressed to match heat of vaporization and heat capacity data for pure MEA. In the next step, binary interaction parameters for $H_2O$-MEA were regressed to predict total vapor pressure, vapor-liquid equilibrium, heat capacity, and freezing point depression. Finally, the ternary system $H_2O$-MEA-$CO_2$ was regressed. $CO_2$ solubility, MEA vapor pressure, heat capacity, heat of absorption, and speciation data were used to regress values of $AG_{aq,fm}$, $AH_{aq,fm}$, $C_p$ temperature dependent parameters A and B for the calculation of $\tau$ (Equation 2-3). The number of regressed parameters was reduced as much as possible while maintaining appropriate representation of the system. Solvent models were also developed for solutions with more complex combinations including $K^+$ and PZ, but they suffered a drop in accuracy as a wider range of conditions was represented. The input file for the $H_2O$-MEA-$CO_2$ model can be found in Appendix A.

The solvent of interest in this work is 9 m MEA, but the model was designed to represent 3.5-11 m MEA. The data used to generate the model included concentrations of 3.5 m, 5 m, 7 m, and 11 m MEA. Data for 9 m MEA has never been collected. Property data and model predictions for 7 m MEA can be found in the dissertation by Hilliard (Hilliard, 2008). Figures 2-3 to 2-8 compare model predictions 9 m MEA to

available experimental data. The VLE data for solutions of varying amine concentration collapsed on each other when plotted versus loading, so the predictions for 9 m MEA are compared to the data for 3.5 m-11 m MEA. The best fit of $CO_2$ solubility data was with 7 m MEA. Experimental data demonstrates the VLE of solutions of different amine concentration should fall in line with each other. However, the values of $P^*_{CO2}$ increased with increasing amine concentration in Aspen Plus® model for MEA. This effect is demonstrated in Figure 2-4 for a sample temperature of 60 °C.

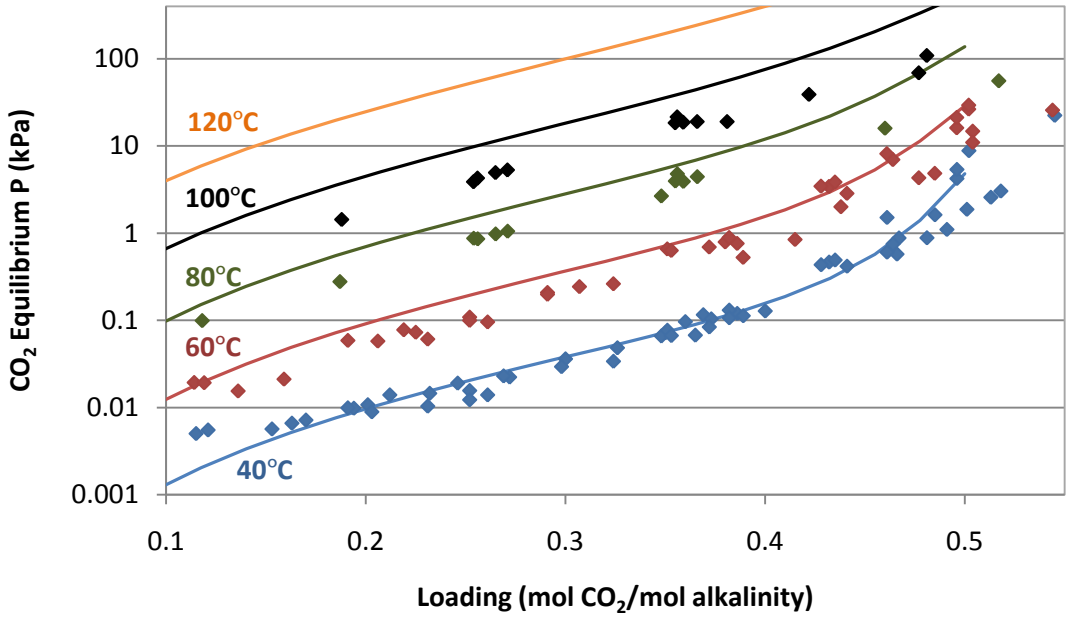


Figure 2-3. Equilibrium $CO_2$ partial pressure of MEA. Points = MEA solubility data for 3.5-13 m by Hilliard, Dugas, and Jou, Curves = Hilliard model predictions for 9 m MEA. Blue = 40 °C, Red = 60 °C, Green = 80 °C, Black = 100 °C, Orange = 120 °C.

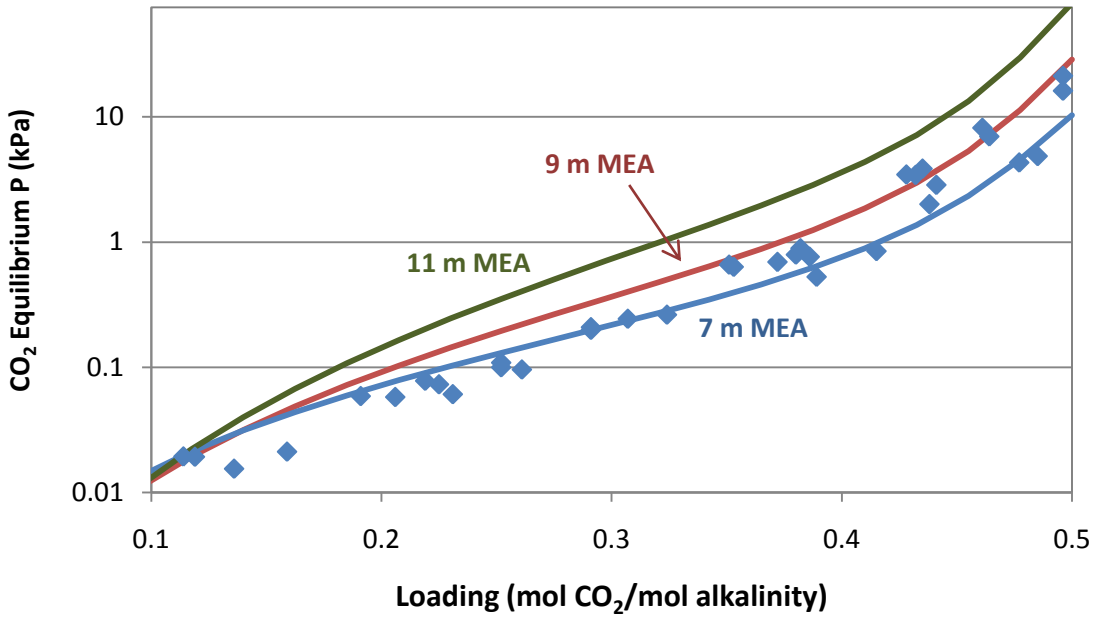


Figure 2-4. Increasing $CO_2$ partial pressure predictions of MEA model with increasing amine concentration. Points = MEA solubility data at 60 °C in 3.5-13 m by Hilliard, Dugas, and Jou. Curves = Hilliard model: blue = 7 m MEA, Red = 9 m MEA, Green = 11 m MEA.

Heat capacity, heat of absorption, speciation, and the amine volatility demonstrate some change with amine concentration. Model predictions for heat capacity for 9 m MEA is displayed in Figure 2-5. Model predictions for heat of absorption for 9 m MEA is displayed in Figure 2-6. Predicted speciation behavior of 9 m MEA at 40 °C and 60 °C is shown in Figure 2-7. Amine volatility is not generally a heavy concern in stripper modeling, but a model with accurate volatility predictions generally has better amine activity coefficient specifications. Figure 2-8 shows that the amine volatility does not increase dramatically with amine concentration, and the predictions for 9 m MEA are accurate within a small margin of error.

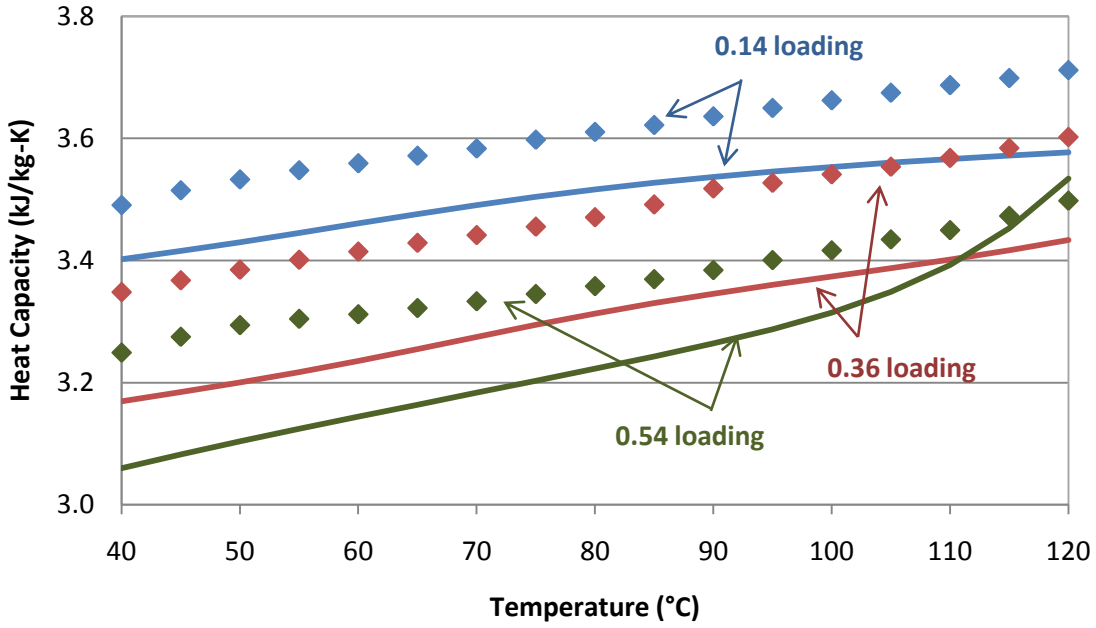


Figure 2-5. Heat capacity for 9 m MEA. Curves = Hilliard model predictions, Points = Hilliard experimental data for 7 m MEA.

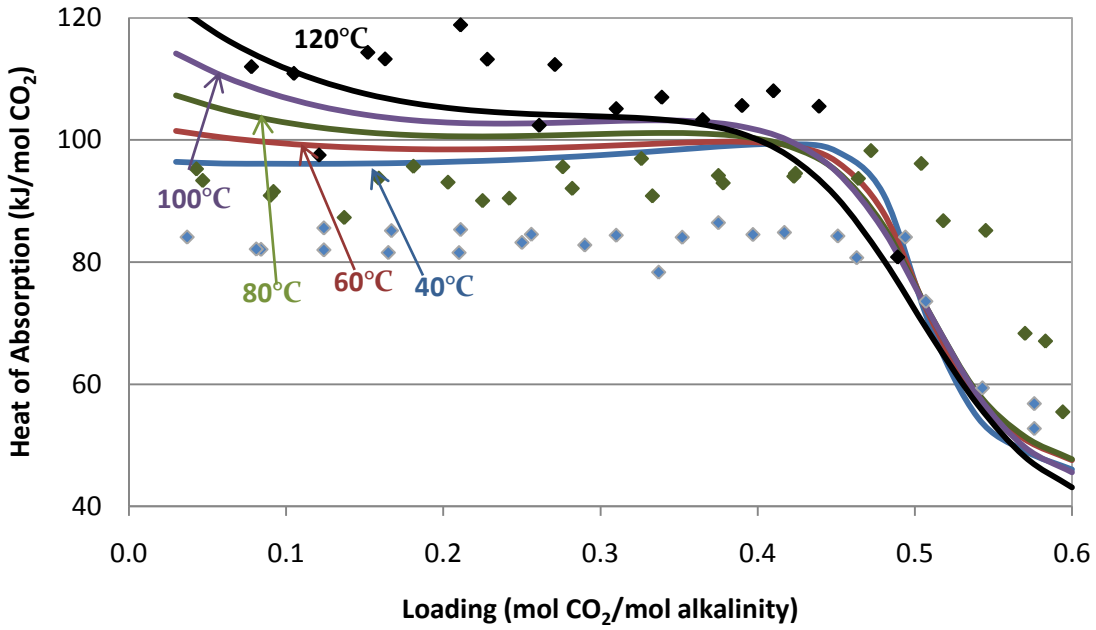


Figure 2-6. Heat of absorption for 9 m MEA. Curves = Hilliard model predictions by Gibbs-Helmholtz method, Points = Kim (Kim et al., 2007) experimental data for 7 m MEA.

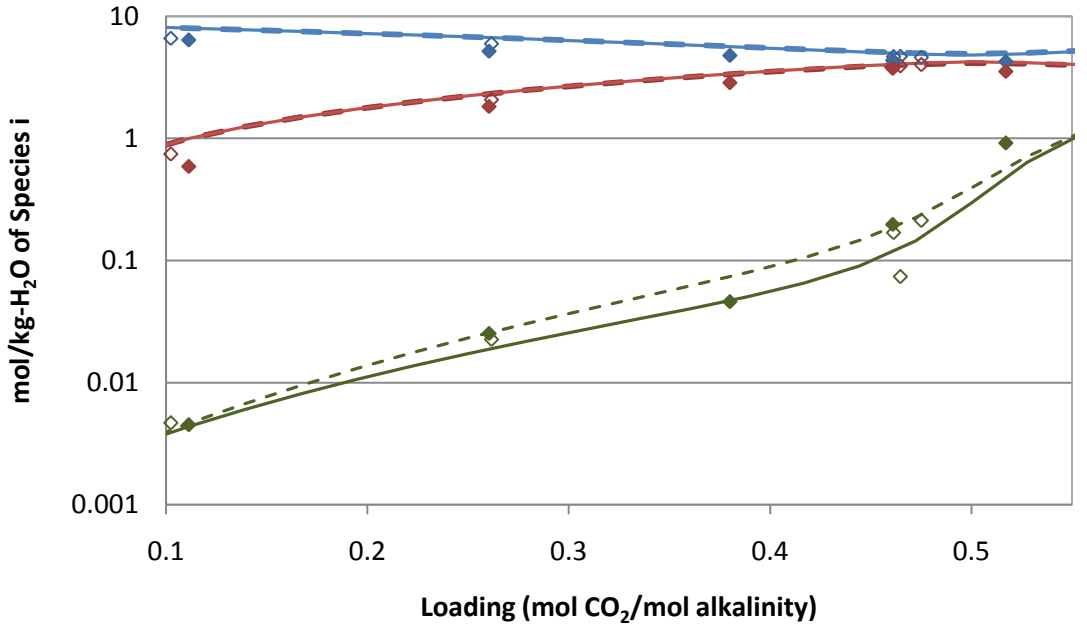


Figure 2-7. Speciation of 9 m MEA. Curves = Hilliard model predictions, Points = Hilliard experimental data for 7 m MEA. Blue = MEA, Red = $MEACOO^-$, Green = $HCO_3^-$. Solid/Filled = 40 °C, Dashed/Hollow = 60 °C.

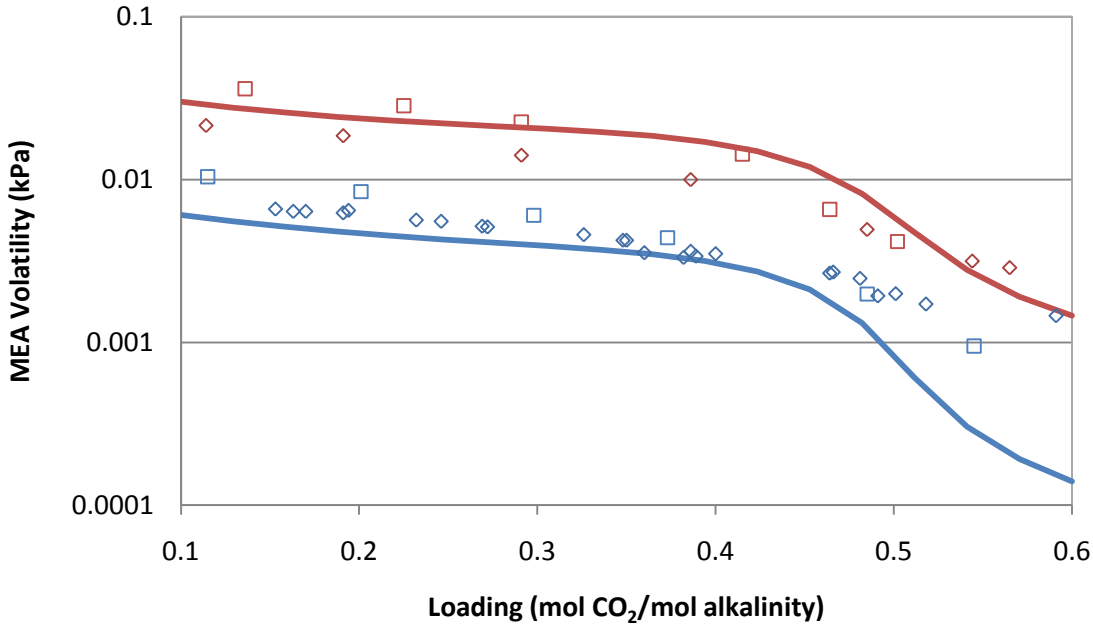


Figure 2-8. Amine volatility of loaded 9 m MEA . Curves = Hilliard model predictions. Diamonds = Hilliard experimental data for 7 m MEA, Squares = Hilliard experimental data for 11 m MEA. Blue = 40 °C, Red = 60 °C.

The thermodynamic model for MEA regressed by Hilliard was an adequate model to simulate 9 m MEA, but it had its downfalls. As shown in Figure 2-2, the model overestimated $CO_2$ partial pressure as amine concentration increased. This effect was exaggerated at high temperature since the model was regressed mainly with data at 40 °C and 60 °C. In a simulation, this error would result in a larger $CO_2$ partial pressure in the stripper. The effect of this larger pressure would reduce the stripping steam requirement of the heat duty (see section 2.3), reducing the overall energy requirement. The accuracy of the heat capacity predictions cannot be appropriately assessed since there is no data for 9 m MEA, but the predictions for 7 m MEA were generally accurate within 1.5%. Similarly, experimental data was not available for heat of absorption of $CO_2$ in 9 m MEA, but the fit for 7 m MEA was within the scatter of the data. The speciation in Figure 2-5 predictions fit the expected trends. Lastly, MEA volatility was predicted reasonably well at 40 °C and 60 °C.

#### *2.2.2.2 Piperazine*

A solvent model used for PZ initially was developed by Hilliard as part of doctoral work, but the model was only designed for low concentrations (2-3.6 m PZ) and low temperature (40-60 °C). Based on recent experiments (Freeman et al., 2010), 8 m PZ was the concentration of interest for this work. Additionally, the ceiling temperature for PZ in the stripper is 150 °C, so accurate representation to this high temperature was needed. The model was updated by Frailie and Plaza to accurately represent the desired concentration, 8 m PZ. The sequential regression method was also used for developing this model. The updating by Frailie and Plaza, culminating in the 5deMayo (Cinco de Mayo) model, repeated the third step of the regression, which only regressed parameters

applicable to the ternary system. The new regression focused on available data for concentrated PZ. The number of regressed parameters was also reduced.

Figures 2-9 through 2-13 compare model predictions to experimental data for 8 m PZ. Experimental data was available for VLE, heat capacity, heat of absorption, and amine volatility. The heat of absorption data was collected by Freeman (2010), and its accuracy was debated due to the exceptionally high values and scatter in the data. Speciation data was not available, but predictions by the Aspen Plus® model are included in Figure 2-12.

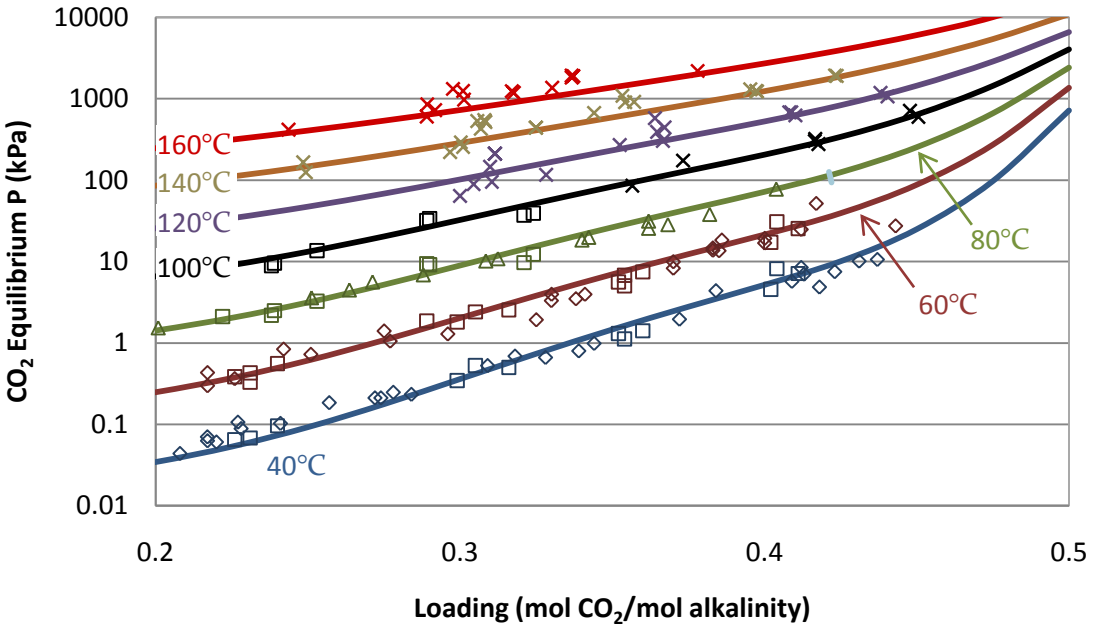


Figure 2-9. Equilibrium $CO_2$ partial pressure for 8 m PZ. Curves = 5deMayo model predictions, Points = experimental data: Diamonds = Hilliard, Squares = Dugas, Triangles = Ermatchkov, Crosses = Xu (Ermatchkov et al., 2006; Hilliard, 2008; Dugas, 2009; Xu et al., 2011).

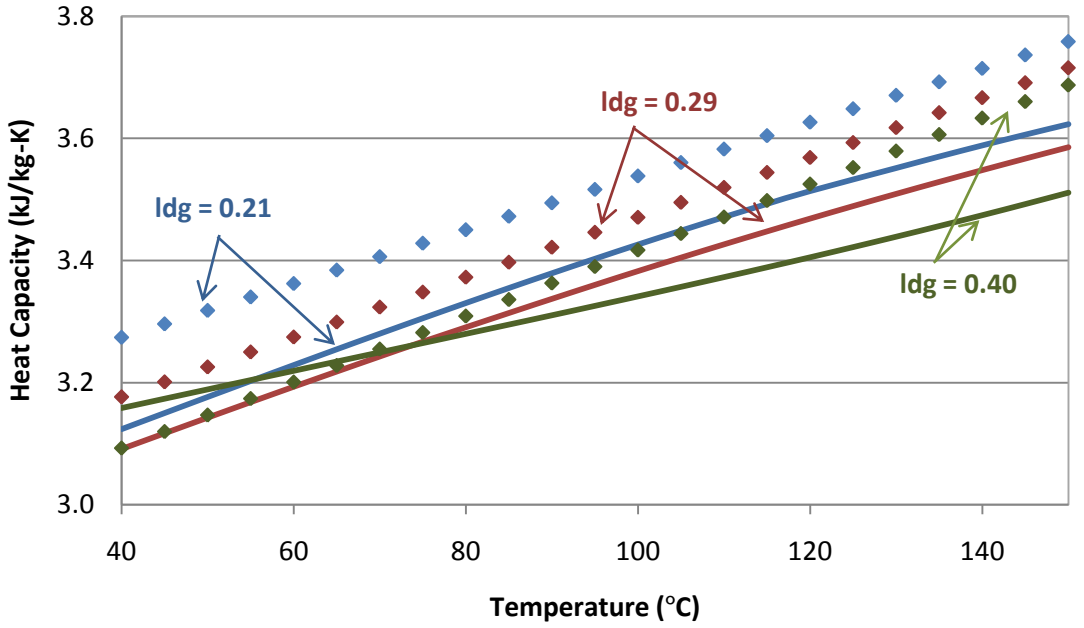


Figure 2-10. Heat capacity for 8 m PZ. Curves = 5deMayo model predictions, Points = experimental data (Rochelle et al., 2009).

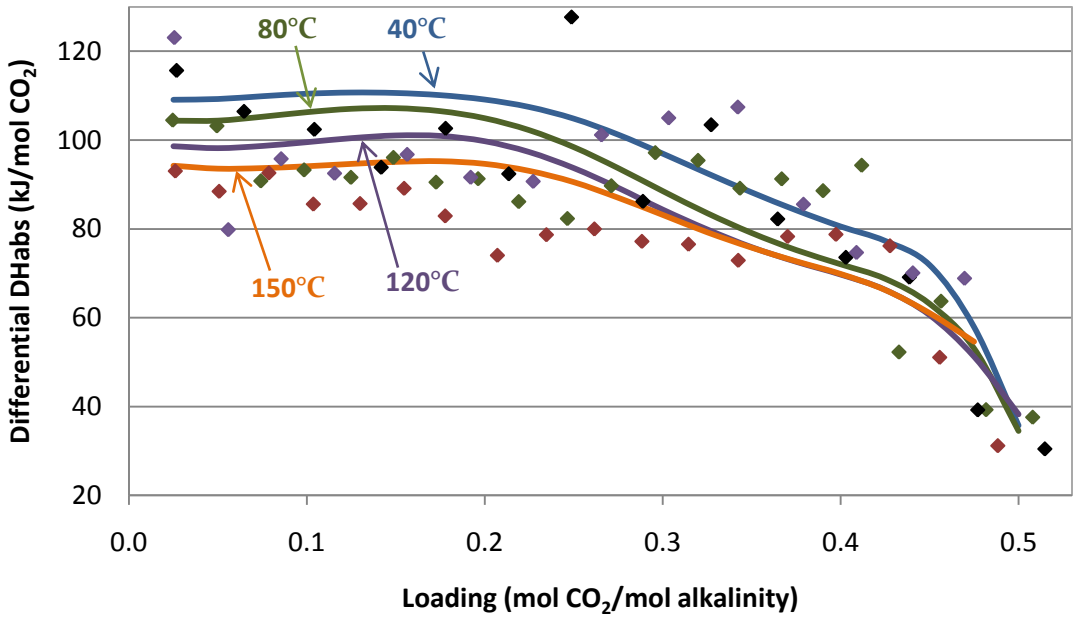


Figure 2-11. Heat of absorption for 8 m PZ . Curves = 5deMayo model predictions by Gibbs-Helmholtz method, Points = experimental data (Freeman, 2011).

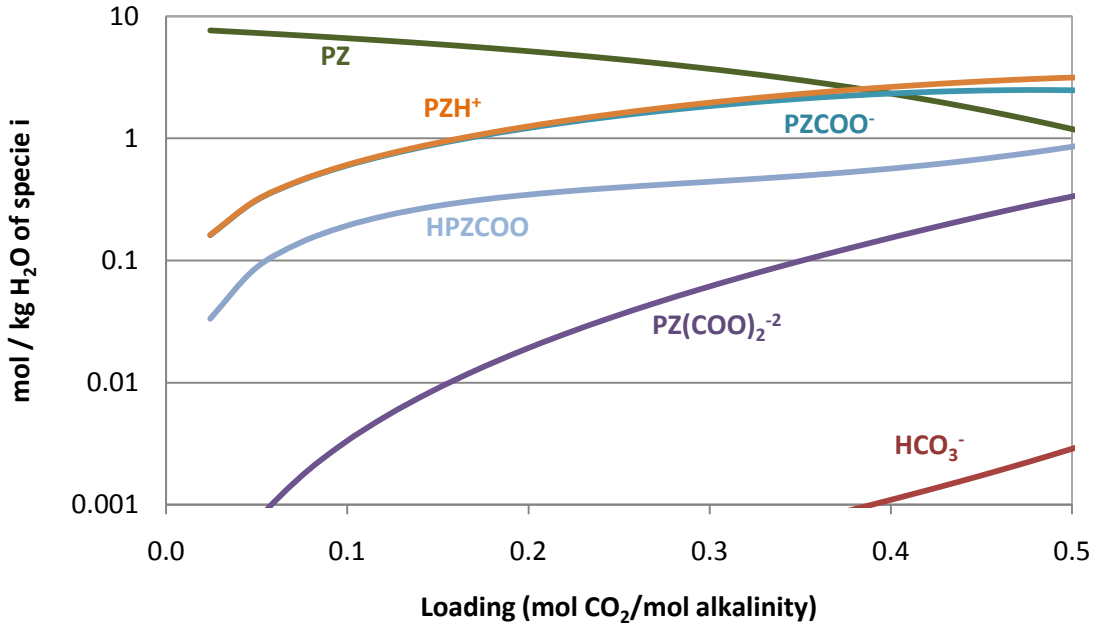


Figure 2-12. Prediction of speciation at 40 °C for 8 m PZ by 5deMayo model.

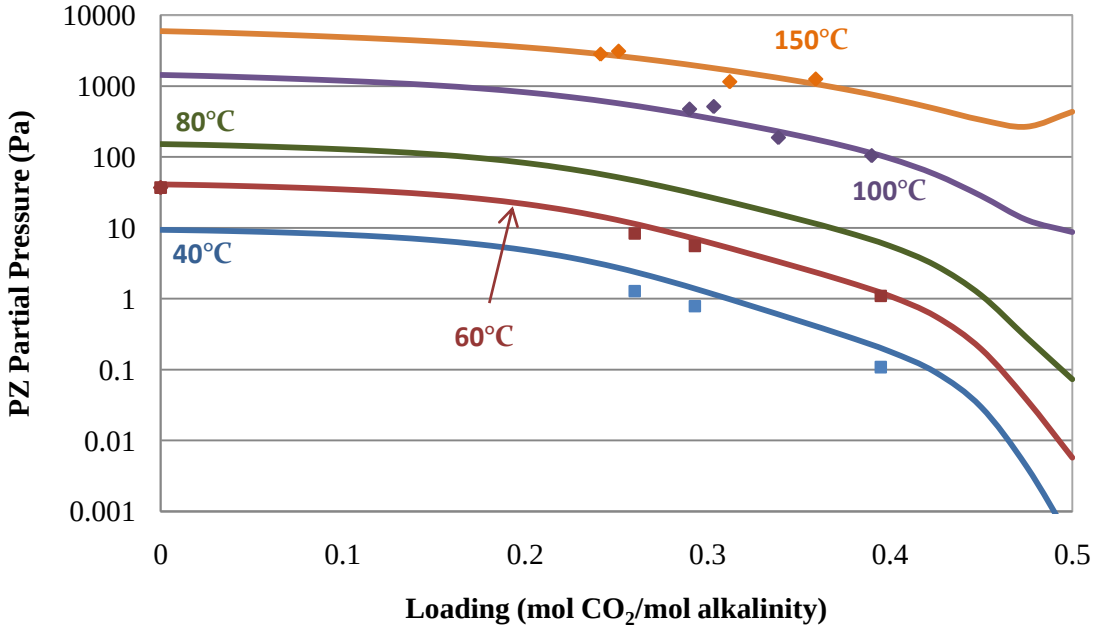


Figure 2-13. Amine volatility for 8 m PZ. Curves = 5deMayo model predictions, Points = experimental data: Squares = Xu, Diamonds = Nguyen (Nguyen et al., 2011; Xu, 2011 (expected)).

Comparing to the available thermodynamic data for 8 m PZ, the 5deMayo model represents the solvent well. The most significant offset from experimental data was in the heat capacity. The 5deMayo model underpredicted heat capacity consistently by about 0.2 kJ/kg-K, or about 6%. This error would surface in a lower sensible heat calculation by the model. Additionally, the 5deMayo model predicts a heat capacity at a loading of 0.40 that crossed over the heat capacity at a loading of 0.29. This error would result in slightly inaccurate heat exchanger calculations. The rich solvent with a high loading would have a smaller temperature change in the main cross exchanger due to its higher heat capacity, so the rich inlet temperature to the stripper would be underestimated.

Near the conclusion of this project, additional work by Frailie produced the Guy Fawkes model for concentrated PZ (Frailie et al., 2011). This model addressed the inaccurate calculation of equilibrium constants, which was unknowingly offset in 5deMayo by changing activity coefficients. The new Fawkes model required fewer parameters to be regressed. Additionally, the Fawkes model has the capability to predict the behavior of MDEA and the MDEA/PZ blend, though these solvents were not in the scope of this work. This model aimed to predict more accurate activity coefficients and heat capacities. The predictions of the Fawkes model are shown in Figures 2-14 through 2-18. This model will be licensed, so its input file is not included in this work.

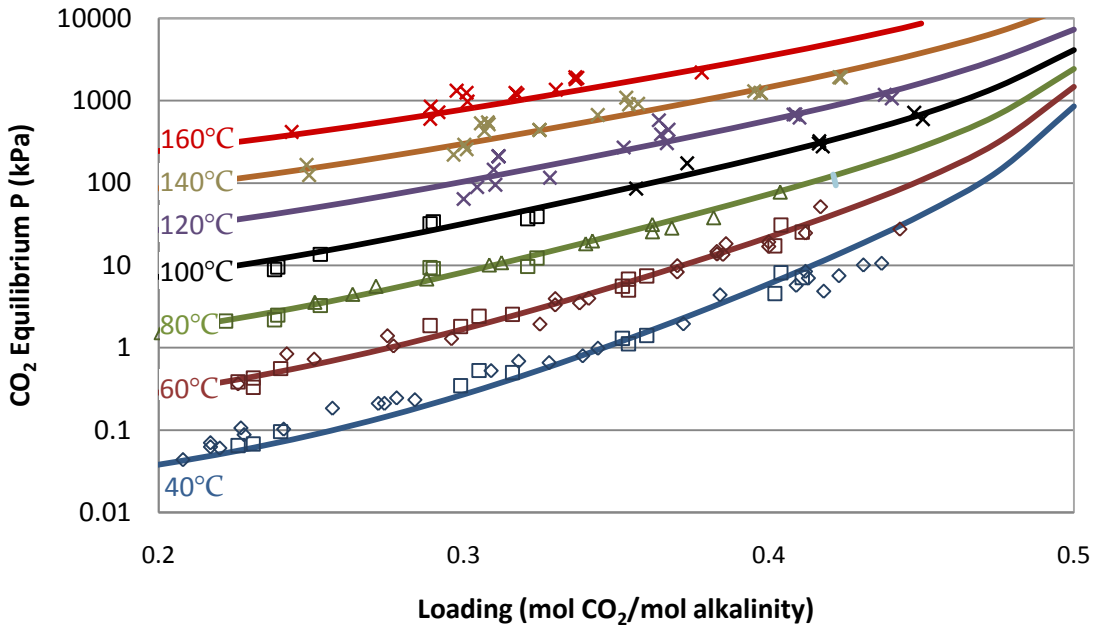


Figure 2-14. Equilibrium $CO_2$ partial pressure for 8 m PZ. Curves = Fawkes model prediction, Points = experimental data: Diamonds = Hilliard, Squares = Dugas, Triangles = Ermatchkov, Crosses = Xu (Ermatchkov et al., 2006; Hilliard, 2008; Dugas, 2009; Xu et al., 2011).

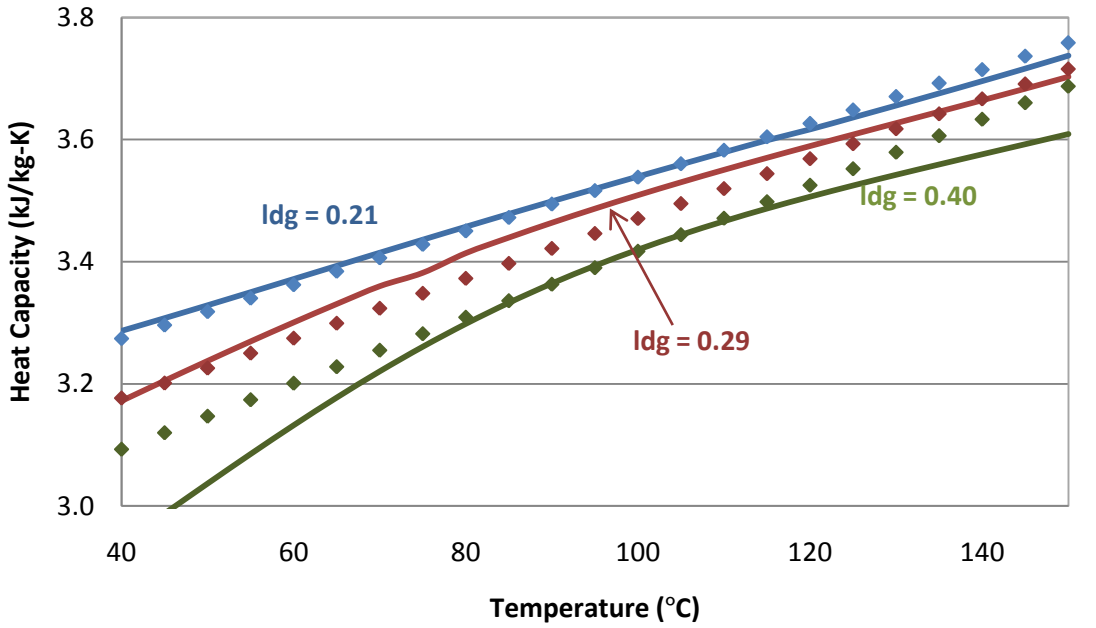


Figure 2-15. Heat capacity for 8 m PZ. Curves = Fawkes model prediction, Points = experimental data (Rochelle et al., 2009).

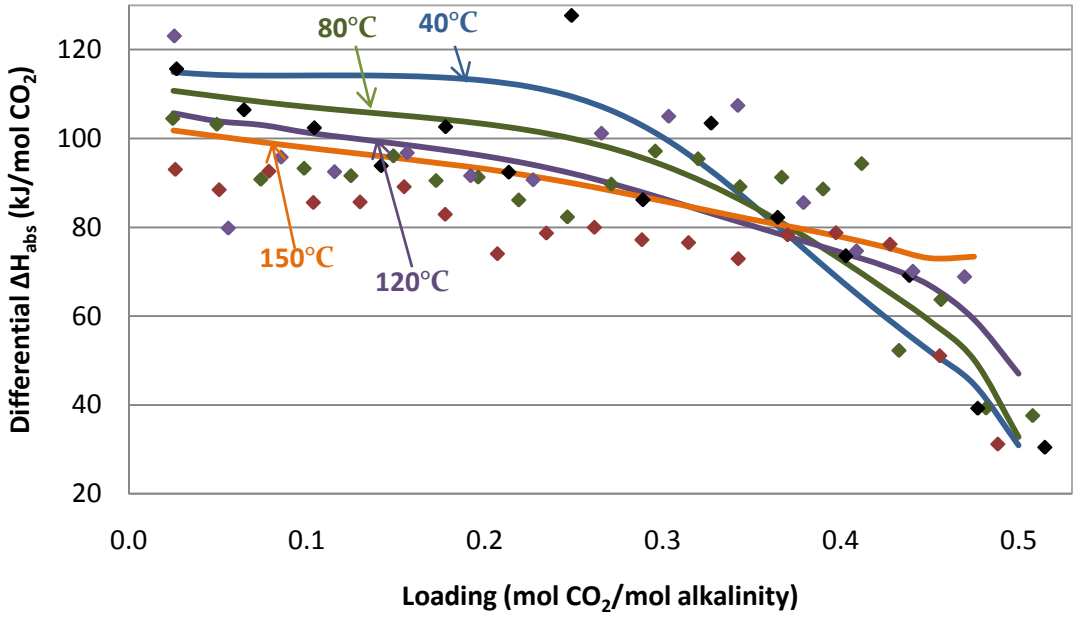


Figure 2-16. Heat of absorption for 8 m PZ. Curves = Fawkes model prediction by Gibbs-Helmholtz method, Points = experimental data (Freeman, 2011).

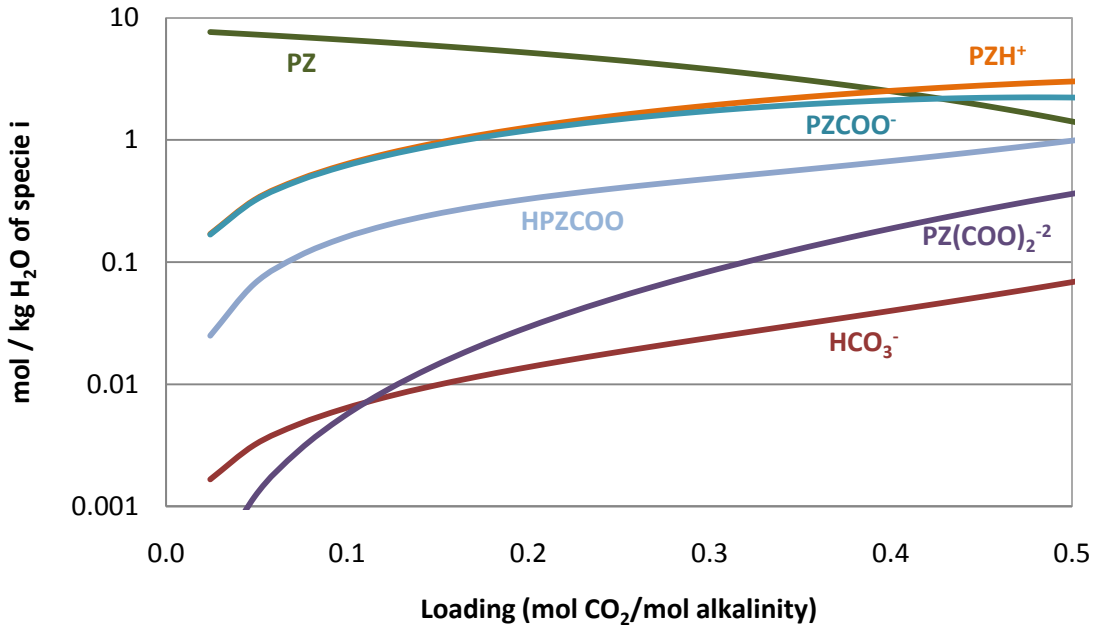


Figure 2-17. Prediction of speciation at 40 °C for 8 m PZ by Fawkes model.

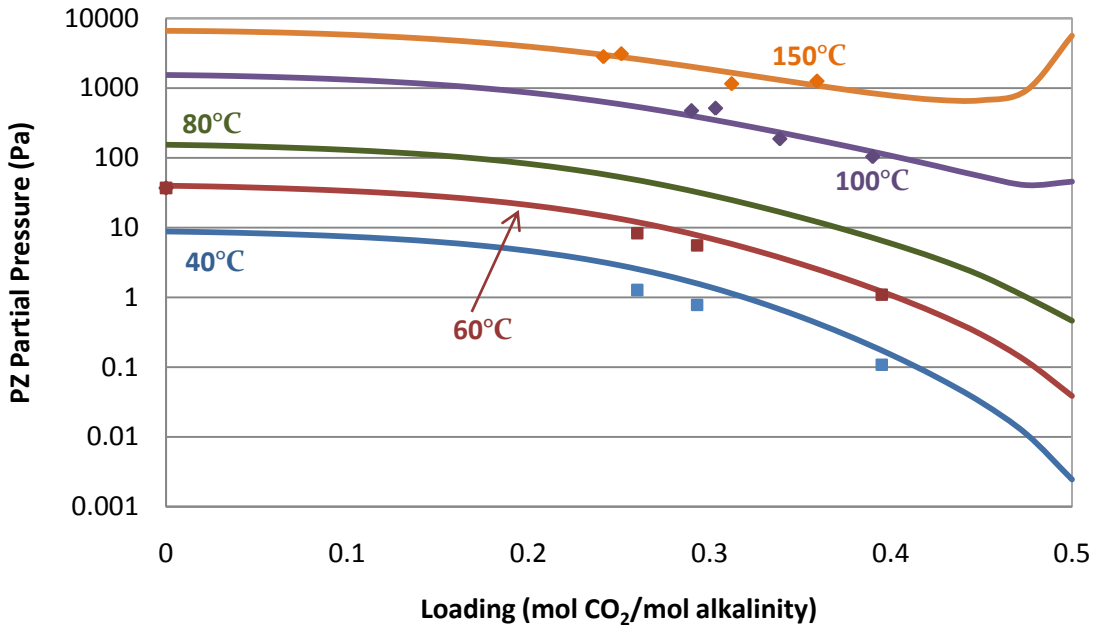


Figure 2-18. Amine volatility for 8 m PZ. Curves = Fawkes model predictions, Points = experimental data: Squares = Xu, Diamonds = Nguyen (Nguyen et al., 2011; Xu, 2011 (expected)).

The thermodynamic property predictions for 8 m PZ were very accurate with both 5deMayo and Fawkes. The most noticeable differences in the properties shown in this report were in the heat capacity and speciation. The most significant improvement with the newer Fawkes model was in the activity coefficients. The $CO_2$ activity in the liquid phase is small due to its low concentration, but accurately representing this activity is essential to describing the kinetic rate of reactions involving $CO_2$. Therefore, any modeling which utilized reaction kinetics would benefit from the Fawkes model, but 5deMayo was sufficient if equilibrium reactions could be assumed.

## 2.3 CONTRIBUTIONS TO ENERGY REQUIREMENT

In the scope considered in this work, there were three main contributions to the overall energy requirement: heating in the reboiler, pump work, and compression work.

The pump and compression work would be taken as electricity directly from the turbine generators on the power plant site. Typically steam was used for the heat source in the reboiler. Earlier work suggested the use of an equivalent work term to evaluate the heat duty on the same basis as the pump and compression work (Oyenekan, 2007). The total equivalent work was calculated as the sum of the three individual contributions, shown in Equation 2-4.

$$W_{eq} = W_{heat} + W_{pump} + W_{comp} \quad \textbf{2-4}$$

The heating work, $W_{heat}$, is the amount of electricity that could be extracted from the steam used in the reboiler. Without modeling the complex steam cycle of the power plant, the heating work was be approximated by Equation 2-5 below. The equation assumed a Carnot efficiency based on the heating temperature and a heat sink at 40 °C. An additional 75% turbine efficiency was also included. This method of evaluation also assumed that the steam was taken between the IP and LP turbines at the exact pressure required to heat the stripper. Any superheating of the steam was neglected. This calculation easily allowed for comparison of stripper configurations operating at different temperatures and variable proportions of steam and electricity usage.

$$W_{heat} = 0.75\, Q_{reb} \left(\frac{T_{heat} - T_{sink}}{T_{sink}}\right) \quad \textbf{2-5}$$

$T_{heat}$ was the temperature of the heat source, which was the temperature of the reboiler plus an expected approach temperature. $T_{sink}$ was the assumed heat sink temperature.

The heat duty can be further broken down into three components: sensible heat requirement, latent heat requirement, and stripping steam requirement. The sensible heat goes into heating the solvent over the temperature difference of the rich to lean solutions. Typically the rich solvent is pressurized through the heat exchanger to overcome the head

of the column, so the rich temperature is the temperature of the solvent once it flashes to the pressure of the column. The solvent heats up as it travels down the column until it exits at the reboiler. As the solvent travels down the column and $CO_2$ is stripped out, both the mass flow rate, $\dot{m}$, and the heat capacity, $C_p$, change. The magnitude of the sensible heat can be calculated as an integral:.

$$Q_{sens} = \int_{T_{rich}}^{T_{lean}} \dot{m}\, C_p\, T\ dT \qquad \textbf{2-6}$$

The latent heat requirement is the amount of energy that goes into moving the $CO_2$ from the liquid to vapor phase. The latent heat has three components: the heat of reaction, heat of non-ideal mixing, and heat of vaporization. Reaction heat is necessary to $CO_2$ from the amine molecule within the liquid phase. Next, as with any non-ideal process, heat is associated with mixing components. The heat of vaporization transitions $CO_2$ from the liquid to vapor phase. The three heats are measured together experimentally as the opposite of the heat of absorption, $-AH_{abs}$ (Kim et al., 2009). The magnitude of the latent heat is simply calculated as the product of the heat of absorption and $CO_2$ removal rate.

$$Q_{latent} = -A\, H_{abs}\, n_{CO_2} \qquad \textbf{2-7}$$

The stripping steam requirement is the amount of energy that goes into vaporizing steam that exits in the overhead with $CO_2$. In the generic stripper flowsheet, this energy is wasted because the stripped steam is condensed either in the cooler preceding the multistage compressor or and an intercooler between compression stages. This wasted energy can be minimized by using a solvent or configuration which reduces the ratio of water to $CO_2$ exiting in the overhead. The magnitude of the stripping steam requirement is normalized for the $CO_2$ removal rate by calculating the product of the $H_2O/CO_2$ ratio and heat of vaporization of water, $AH_{vap,H_2O}$.

$$Q_{steam} = \frac{n_{H_2O}}{n_{CO_2}} A H_{vap,H_2O} \quad \text{2-5}$$

The wasted heat in stripped steam cannot be eliminated completely by solvent choice alone. At an elevated stripper temperature, water always has a substantial vapor pressure and, therefore, constitutes a significant portion of the exiting vapor.

The search for new solvents often focuses on reducing the energy of regeneration in the stripper. This search is often misguided, emphasizing the benefit of solvents with a low heat of absorption. Considering only Equation 2-5, the heat of regeneration is directly correlated with the heat of absorption. However, the three contributions to the heat duty are not independent of each other. A simple approximation can demonstrate this concept, though a more rigorous analysis has been performed by another author (Oexmann et al., 2009). The Gibbs-Helmholtz relation can be modified to represent $CO_2$ in the reactive amine solvent, and it clearly demonstrates that an increase in the heat of absorption of a solvent also increases the equilibrium partial pressure of $CO_2$ in the stripper for a given temperature swing between the absorber and stripper.

$$\frac{d\left(ln\ p^*_{CO_2}\right)}{d\left(1/T\right)} = -\frac{\Delta H_{abs}}{R} \quad \text{2-6}$$

The equilibrium partial pressure of water is roughly constant with varying heat of absorption, though slight variations may occur with a difference of the interaction of water with the amine or $CO_2$. Nonetheless, due to the increase in $P^*_{CO_2}$, an increase in the heat of absorption of a solvent leads to an improvement in the selectivity for $CO_2$ over water at the top of the column. Moreover, the increase in column pressure reduced electricity demand of the process because a portion of the mechanical compression in the multistage compressor is replaced by compression in the rich pump. Achieving higher pressure by pumping is much more efficient because the volumetric flow rate of the liquid is far smaller than the vapor in the first stages of the compressor. The benefits of

using a solvent with a high heat of absorption to reduce stripping steam generation and achieve higher column pressure outweigh the penalty of supplying more heat for $CO_2$ desorption.

## 2.4 SIMULATION METHODS

Aspen Plus® 7.1 was used for this work due to its ability to model a wide range of rate-based systems. The software used a sequential modeling method to converge stripper flowsheets. Numerous convergence methods were available to close recycle loops and design-specification loops; generally recycle loops used the Wegstein method, and design-specifications used for simpler Secant method. The simulations used thermodynamic models in the e-NRTL framework, as described in section 2.2.1. Similar to most simulation software used for modeling $CO_2$ capture with aqueous amines, the performance of the basic process units were calculated with equilibrium assumptions. These process units included heat exchangers, pumps, compressors, splitters/mixers, and flash/separation vessels.

### 2.4.1. Vapor/Liquid Separation Modeling

The stripping columns were represented using RadFrac blocks, which modeled the direct, counter-current contact of liquid and vapor. These vapor/liquid separation columns had the option of running with equilibrium or rate-based assumptions for heat transfer, mass transfer, and reaction kinetics.

The separation column was broken up into individual stages where a total amount of heat and mass transfer between phases was calculated. The standard RadFrac block assumed equilibrium between the liquid and vapor phases in each stage. Additionally,

chemical equilibrium was assumed within the liquid and vapor phases of each stage. Stage efficiencies, like a Murphree efficiency, can assist in translating equilibrium stages to a total packed height.

Shortly before the start of this work, Aspentech released a feature called RateSep™, a new function within their RadFrac block. The RateSep™ function provided the ability to perform rigorous rate-based calculations in gas/liquid separations. Several standard correlations were built in for heat transfer, mass transfer, column hydraulics, and interfacial area, but user-defined subroutines for each could be substituted. This capability permitted modeling the gas/liquid separation with a higher level of complexity: equilibrium reactions. In the equilibrium reactions method, the interfacial area, heat transfer rates, mass transfer rates, and hydraulics in each stage were calculated. Chemical equilibrium was still assumed at each discretized point within the liquid and vapor films of each stage. As a final layer of complexity, kinetic reactions could be specified within the liquid and vapor phases. This simulation method can be called kinetic reactions. All of the rate-based calculations from the equilibrium reactions method were also performed in the kinetic reactions method, and kinetic limited reaction rates were added to the set of equations to solve. The kinetic reactions method was the most rigorous calculation approach in Aspen Plus®.

The increase in complexity from equilibrium stages, to equilibrium reactions, to kinetic reactions each increased the simulation time and convergence issues for a stripper flowsheet. The simplest method should be used to achieve results of a desired accuracy. For example, a simple separation with two components would be a good candidate for the equilibrium stages calculation method if its performance in a separation column would be expected to follow the predictions of the McCabe-Thiele method. In contrast, a complex

separation with many components with slow heat and mass transfer in reaction rates would benefit from the kinetic reactions method.

### 2.4.2. Simulation Specifications

This report over a range of process configurations and solvents required a specific set of process specifications to allow for an adequate comparison between cases. If certain specifications were not held constant across cases, the effect on one or more work contributions would not be accounted for and would be mistakenly attributed to the change in configuration or solvent. The following process conditions were held constant unless otherwise specified:

- Constant rich loading: this work follows with the decomposition method (Alie et al., 2005), and the stripper was run and optimized independently of the absorber.
- 5 °C cold side approach on main cross exchanger.
- 5 °C approach on steam heated reboilers.
- Equal moles of vapor produced in each pressure stage: this specification yields the highest efficiency from a reversibility standpoint.
- Constant reboiler temperature (variable stripping pressure).
- 50 kPa of pressure drop over cross exchanger.
- 150 kPa of liquid head for packed absorber height.
- 150 kPa of liquid head for packed stripper height.
- 5 m stripper packed height.
- 150 bar compressed $CO_2$ pressure: typical pipeline specification for sequestration.

Stripper columns were modeled using the equilibrium reactions method. The equilibrium stages method was too simple of a model because the Murphree efficiency of each individual stage could be an unpredictable function of temperature, $CO_2$ loading, liquid and/or gas rate, etc. Conversely, the kinetic reactions method was an overly complex method since the desorption reaction can be expected to be nearly instantaneous at elevated temperature in the stripper. Mass transfer of the components would be the rate limiting contribution, so the equilibrium stages method was the best modeling option.

# Chapter 3: Stripper Complexity

The majority of the energy requirement for an absorption/stripping system stems from regenerating the solvent in the stripper. The base case stripper technology is a simple stripper. Various inefficiencies arise in this process due to its simplistic nature and lack of advanced heat recovery. This chapter introduces several advanced configurations that improve the reversibility in the stripper, which consequently improve the efficiency. These configurations were evaluated for the base case solvent of 9 m MEA. The effect of switching to 8 m PZ was also investigated.

## 3.1. ADVANCED CONFIGURATIONS

Fundamental work showed the benefit of reducing driving forces for generic chemical processes. Driving forces surface in several forms: temperature driving forces, mass transfer driving forces, and chemical reaction driving forces. Typical strippers for this application have very large driving forces in several locations. Stripping columns with optimized conditions have large driving forces in the reboiler and bottom sections of packing and pinches at the top (Oyenekan, 2007). Introducing more complexity to the flowsheet by means of splits, recycles, and multiple pressure stages can reduce the existing driving forces to cut down on total exergy loss (Leites et al., 1993; Leites et al., 2003). Complex flowsheets had previously been proposed that introduced many types of complexity simultaneously to improve the energy efficiency of the stripper. These

process flow diagrams are shown in Figures 3-1 and 3-2. Figure 3-1 shows an example of a process that incorporates interheating with two separate lean streams, and the incorporation of a semi-lean that is fed to the absorber at an optimized location.

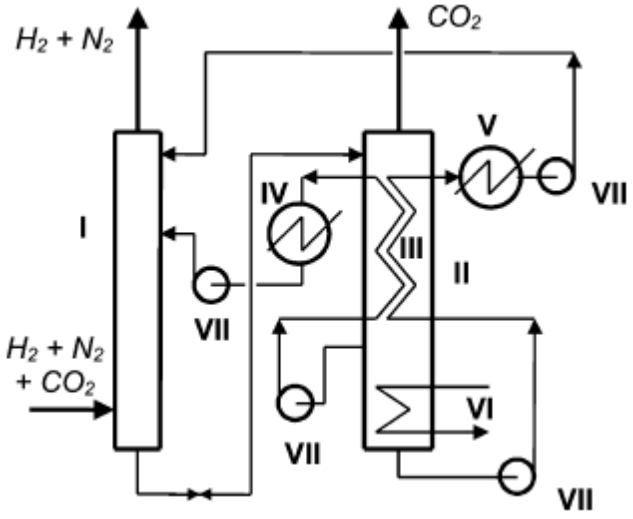


Figure 3-1. Process flow diagram for purification of gas from $CO_2$ with MEA solution with integration of solution regeneration and heat recycling. *I*—absorber, *II*—regenerator, *III*—heat exchanger, *IV*—cooler of solution, *V*—cooler (condenser) for steam-gas mixture, *VI*—reboiler, *VII*—pumps (Leites et al., 1993).

Figure 3-2 shows a complex example of incorporating splits of the rich stream into the stripper. This flowsheet has three feeds to the stripper at varying temperatures. Like the previous example, a semi-lean stream is drawn from the stripper and fed to an optimized location in the absorber. A complex network of heat exchangers was used to not only recover heat from the hot lean solvent, but also from the flue gas feed and treated gas product.

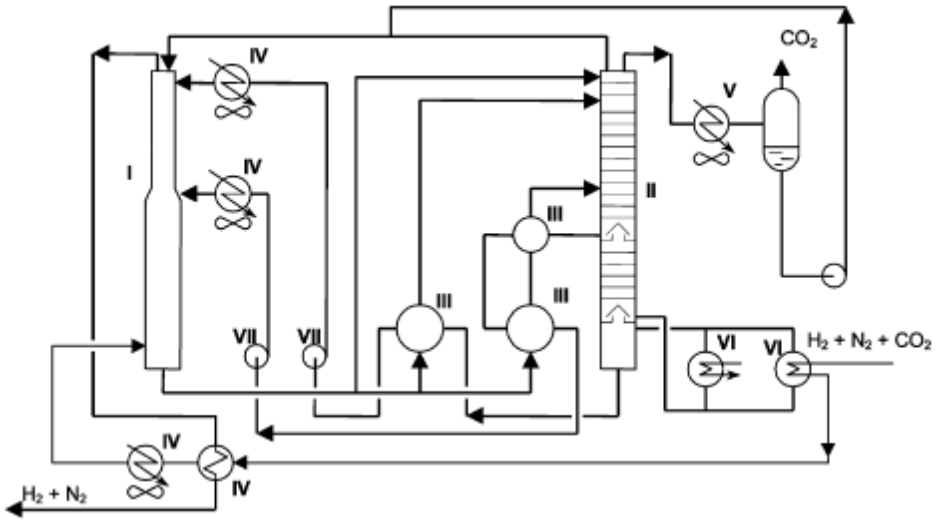


Figure 3-2. Process flow diagram for purification of gas from CO2 with MEA solution with three flows of rich solution and two flows of lean solutions. I —absorber, II—regenerator, III—heat exchanger, IV—cooler, V—cooler (condenser) for steam-gas mixture, VI—reboiler, VII—pumps (Leites et al., 1993).

Stripping in multiple pressure stages is another increase in complexity that improves reversibility by separating $CO_2$ in multiple steps instead of all at once. Additionally, stripping with multiple pressure stages provides the opportunity to collect a portion of the $CO_2$ at high pressure and reduce the compressor workload. Essentially, stripping at multiple pressures yields the benefit of both high pressure and low pressure stripping. High pressure stripping is beneficial to improve the selectivity of $CO_2$ while collecting at high pressure. Ambient pressure stripping is helpful to achieve a desired lean loading at lower temperature, which can avoid excessive thermal degradation of the solvent. Several authors investigated the benefit of running selected complex configurations (Jassim et al., 2006; Oyenekan et al., 2007).

Recent work in industry has also shown interest in the development of more complex configurations with higher efficiency. MHI has been focused on more efficient heat recovery for the stripper and investigated an interheated column (Yagi et al., 2004). This configuration attempted to be a more reversible process by recycling a portion of the

heat contained in the lean solvent directly into the column. Fluor also acquired a number of patents on the implementation of advanced configurations, including a lean flash configuration which is further described in section 3.1.3 (Benson et al., 1979; Reddy et al., 2004; Reddy et al., 2007).

For this study, the complexity was represented as the total number of major pieces of equipment, excluding typical pumping and compression equipment. The pumps and multistage compressor were excluded because they were a constant across all configurations. As an example, a single stage heated flash had a complexity value of 2 (a heater and separation vessel), and a simple stripper had a value of 3 (a heater, vessel, and packing). The complexity value of a configuration was decreased if an intercooler was eliminated by integrating a compression stage into the flowsheet. This was the case in the 2-stage multi-pressure configuration. It was expected that more complex configurations would improve performance but exhibit a diminishing return at higher complexity. It was also expected that different configurations with similar complexity values might have different performance according to how efficiently the process units were arranged.

Building upon prior conclusions (Oyenekan, 2007), this work continued the investigation of complexity by including new variations of advanced configurations. The configurations can be separated into three subcategories: multi-stage flash, double matrix, and columns. The analysis began with the most simple separation method, a 1-stage flash, and built upward systematically in complexity and total number of pressure stages. Each stage had a number of options: flash vs. packing, heated vs. adiabatic, and recompression of the vapor to the prior stage. Even though these flowsheets aimed to investigate the effect of complexity on stripper performance, they are simpler and more practical than those presented by Oyenekan. In this work, the multi-pressure had two

pressure stages instead of three, the double matrix had heated flashes in the place of packed, heated vessels, and the interheated column was heated in one location instead of using continuous countercurrent heat exchange.

### 3.1.1. Multi-Stage Flash

The multi-stage flash configurations included a specified number of equilibrium flashes arranged in series. The 1- and 2-stage flash flowsheets are shown in Figures 3-3 and 3-4. In these configurations each equilibrium stage was heated to maintain isothermal operation. Mainly $CO_2$ and water flashed off in each stage, and the equilibrium pressure decreased as the $CO_2$ loading decreased. In the configurations with more than one stage (like the 2-stage flash), the low pressure vapor stream was condensed at 40 °C, compressed, and combined with the vapor from the stage before it. The final combined vapor stream was sent to the multi-stage compressor train. 3- and 4-stage flash configurations are not shown, but they were also simulated and follow the same progression.

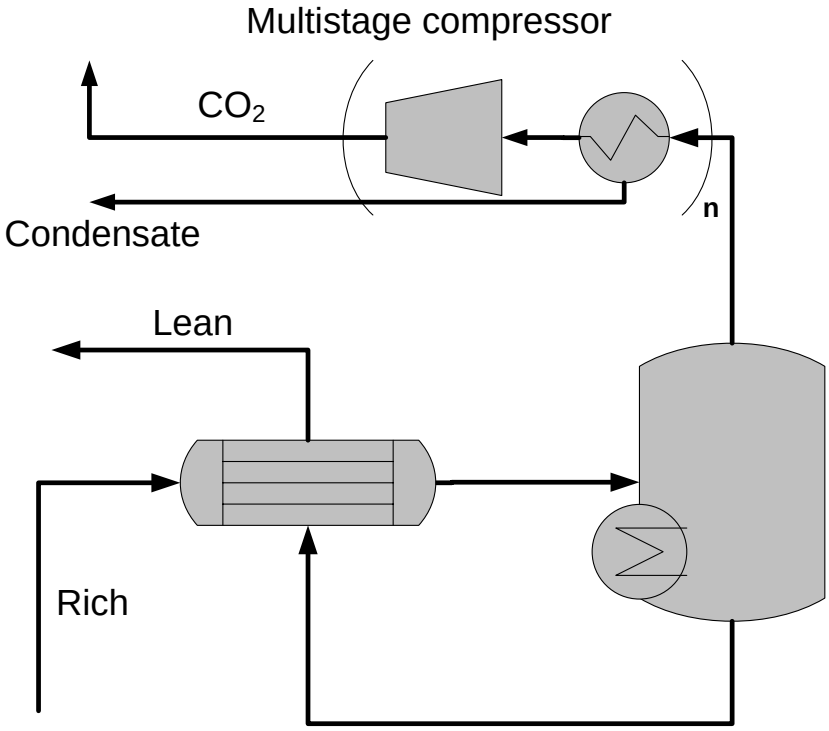


Figure 3-3. 1-Stage Flash with intercooled multi-stage compressor.

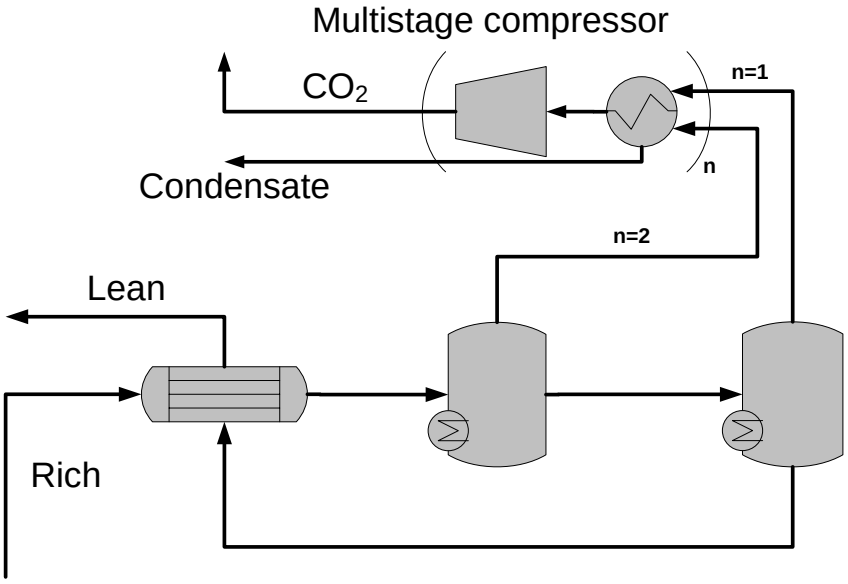


Figure 3-4. 2-Stage Flash with intercooled multi-stage compressor.

### 3.1.2. Double Matrix

The double matrix was derived from the 2-stage flash. Like the 2-stage flash, rich solvent was heated by the lean solvent in the main cross exchanger, and $CO_2$ was stripped in two heated equilibrium flashes in series. The double matrix added complexity by splitting a portion of the cold rich stream and contacting it in a flash with the vapor exiting the low-pressure second flash. The double matrix was designed to achieve better efficiency than the 2-stage flash by using the water-rich low-pressure vapor as a heat source to condense steam and strip additional $CO_2$ from the split solvent stream. Once treated, the split solvent stream exited the vessel as a semi-lean stream, was cross exchanged with the corresponding split rich stream, and was returned to the absorber. The semi-lean would ideally be fed to the absorber at an optimized midpoint location. Each of the three flashes could also be packed columns, so three variations of the double matrix were simulated:

1. Three equilibrium flashes, 20% solvent split to LP section
2. Three equilibrium flashes, optimized solvent split for all lean loadings
3. Two equilibrium flashes for heat stages, packed vessel for top of LP, optimized solvent split

The two heated flashes provided enough driving force that very little packing would be needed before a mass-transfer pinch appeared, so the option of a packed column in the place of either heated flash was not explored. An example flowsheet of variation 3 is shown in Figure 3-5.

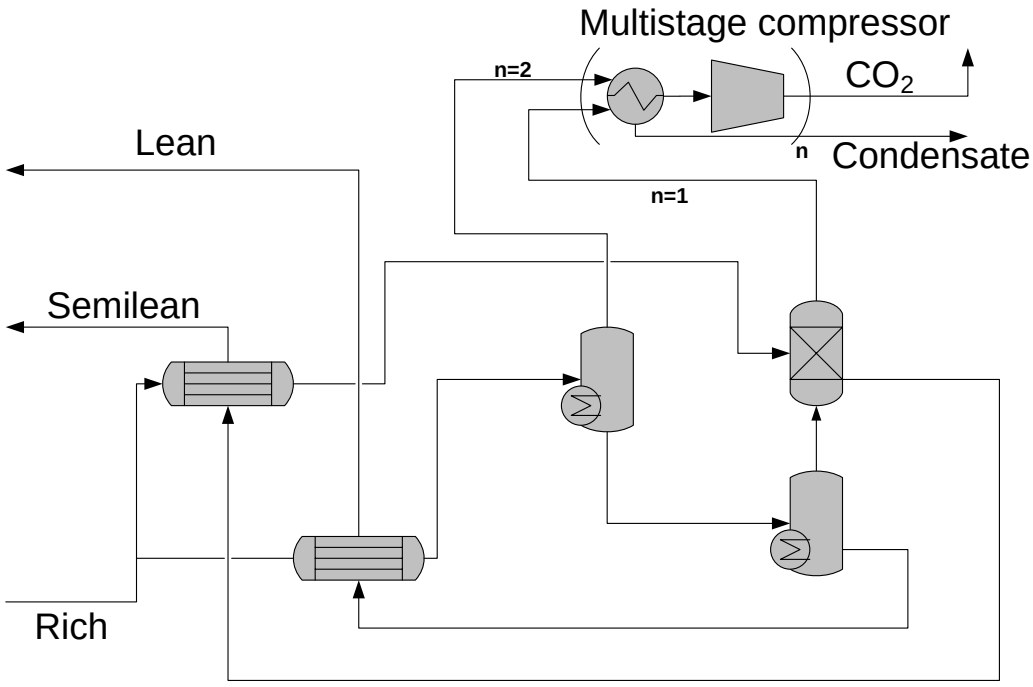


Figure 3-5. Double matrix with two heated equilibrium flashes, packed top low-pressure section, and multi-stage compressor.

### 3.1.3. Columns

This category contains process configurations which were stacked vertically, resembling columns. This included modifications of the simple stripper as well as configurations with vapor recompression. One design included in this section was the 2-stage multi-pressure. This flowsheet stripped $CO_2$ at two pressure levels, recompressed the low pressure vapor, and fed the vapor to the higher pressure stage. Like the multi-stage flash and double matrix, both stages were heated to the same temperature. The pressure in each vessel was dictated by the temperature and solvent composition. The vapor production in each stage was specified to be equal, so fixing the pressures was not possible. Three variations of the multi-pressure were simulated. First, the flowsheet was

run using equilibrium flashes for both stages. Next, the flowsheet was altered by replacing the flash in the top, high-pressure stage with a section of packing, depicted in Figure 3-6. Finally, this second flowsheet with packing in the high-pressure stage was altered by applying heat only to the top stage, and the bottom stage was specified to be an adiabatic flash. This third flowsheet resembled a simple stripper with an adiabatic flash. The separate adiabatic lean flash flowsheet (Fluor configuration) is shown in Figure 3-7.

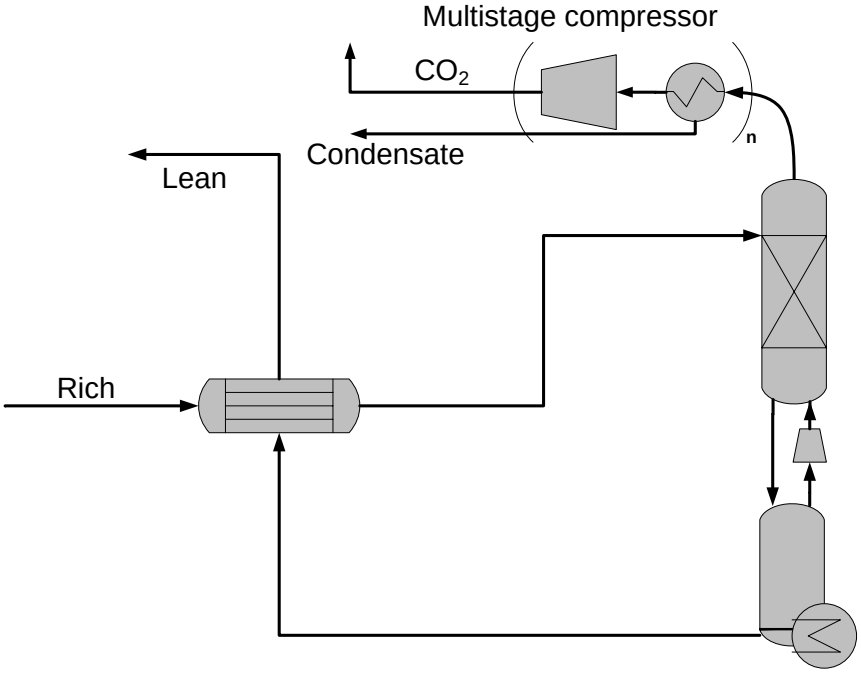


Figure 3-6. Multi-pressure column with isothermal sections and intercooled multi-stage compressor.

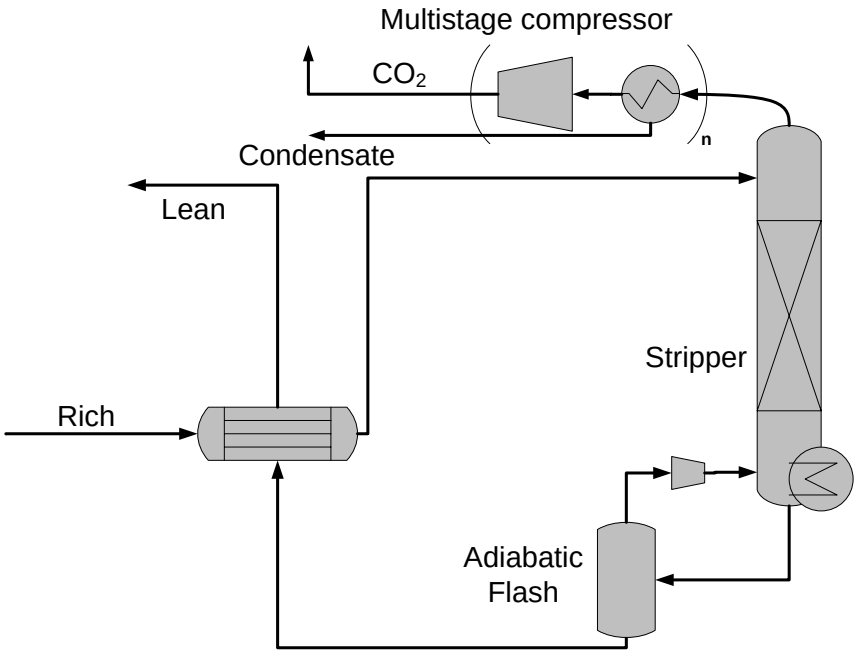


Figure 3-7. Fluor configuration with simple stripper, adiabatic lean flash, and intercooled multi-stage compressor.

In addition to the three multi-pressure configurations, an interheated configuration was simulated. This arrangement split the simple stripper column into two sections and used an additional heat exchanger to recycle some of the heat in the lean solvent back to the column to more efficiently strip out $CO_2$. A previous author predicted that this type of configuration should be beneficial (Leites et al., 2003). In a simple stripper, exchanging all of the heat with the rich feed in a single cross exchanger inevitably resulted in substantial flashing at the top of the column. Interheating reduced the amount of heat exchanged to the rich stream in the main exchanger, so the degree of flashing would be reduced. Additionally, the entering rich solvent would be cooler, so more stripping steam in the vapor would be condensed and the $CO_2$ selectivity would be enhanced. This interheated configuration was simulated in two forms. In the first configuration, the solvent exiting the bottom of a packed column was exchanged with the hot lean stream, and then it was fed to an equilibrium flash which functioned as the

reboiler. In the other variation, the liquid was drawn from the middle of the packed column and exchanged with the hot lean solvent, and then it was returned to the column in the stage below the drawoff. To improve convergence and reduce the risk of a dry stage, only 80% of the liquid was drawn off in the simulation. A 5 °C LMTD was specified on the exchanger for this arrangement. Since a log mean approach was specified, the cold side approach was less than 5 °C. This mid-column interheating flowsheet is shown in Figure 3-8.

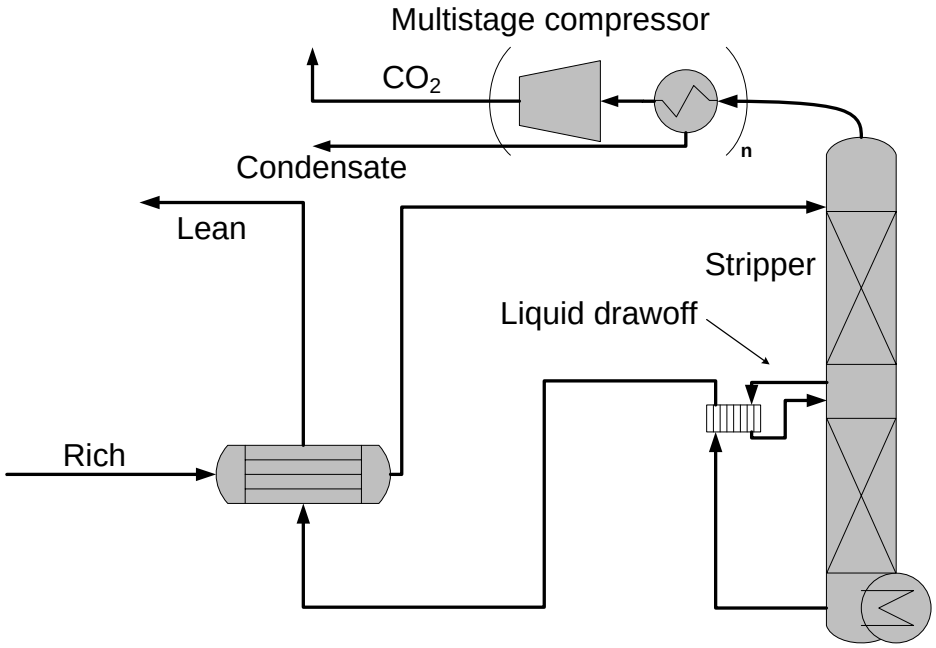


Figure 3-8. Interheated column with interheated position in middle of the column, intercooled multi-stage compressor. 80% liquid drawoff.

### 3.1.4. Compression Work Calculation

The compression section was specified identically for all configurations. For flowsheets with product vapor exiting at multiple pressures, the low pressure vapor streams were cooled to 40 °C with knockout and removal of condensed water,

compressed to the pressure in the stage above, and combined with the vapor from the stage above. The final mixed product vapor was also cooled to 40 °C with water knockout, and then it was fed to a multi-stage compressor train, which intercooled to 40 °C, knocked out water between stages, and pressurized the $CO_2$ to a final pressure of 150 bar. The Aspen Plus® multi-stage compressor block, Mcomp, was temperamental, even when using the property method of SRK, which was more stable than e-NRTL for high pressure $CO_2$-$H_2O$ systems. Additionally, it was desired to use a minimum number of total compression stages while maintaining a compression ratio of no greater than 2. Manually manipulating the compression stages would slow down the total simulation time.

A workaround for both of these problems was to develop a correlation for compressing a $CO_2$ stream saturated with water to 150 bar. The correlation used data collected from a separate Aspen Plus® flowsheet. Compression work was calculated for trains with inlet pressures ranging from 0.8 atm to 20 atm. In the isolated simulation, the convergence of the compressor block was less of an issue, and work values were calculated for the range of inlet pressures with 3–8 compression stages. The number of compression stages was minimized while maintaining a compression ratio of 2 or lower. There was no pressure drop in the intercoolers. The Aspen Plus® simulation assumed a compressor polytropic efficiency of 72%. The correlation demonstrated a near linear fit the compression work versus $\ln(P_{final}/P_{initial})$ since this term is found in the expression for calculating compression work of an ideal gas. A 2-piece function provided a better fit than a single linear regression, so the final form of the correlation was piecewise and is shown in Equation 3-1. This correlation is a continuous function at the transition point, though its first derivative is discontinuous. However, if the compressor was simulated and its work was calculated within each simulation, discontinuities would exist when the

number of compression stages changed to meet the desired specifications, so the discontinuous first derivative of the correlation was not an issue.

$$W_{comp}\left(\frac{\mathbf{kJ}}{\mathbf{mol\ CO_2}}\right) = \begin{cases} \mathbf{4.572}\ ln\left(\mathbf{150}/P_{in}\right) - \mathbf{4.096}, & P_{in} \leq \mathbf{4.56\ bar} \\ \mathbf{4.023}\ ln\left(\mathbf{150}/P_{in}\right) - \mathbf{2.181}, & P_{in} > \mathbf{4.56\ bar} \end{cases} \quad \mathbf{3\text{-}1}$$

Equation 3-1 was used for all of the compressor work calculations in this work. The sensitivity of the compressor work calculation was evaluated for variable polytropic efficiency and intercooler pressure drop. The polytropic efficiency of 72% that was used in the generation of Equation 3-1 was possibly lower than what would be observed in a real compressor; 80% efficiency could be possible. Additionally, a real process would most likely experience pressure drop in the intercoolers. The magnitude of the pressure drop in each intercooler would be proportional to the pressure of the gas fed to the cooler. The pressure drop for the intercooler of stage $n$ could be calculated using Equation 3-2, using an individual pressure drop factor, $\varepsilon$, for the multi-stage compressor train.

$$\Delta P_n = \varepsilon \cdot P_{inlet,n} \quad \mathbf{3\text{-}2}$$

The total work of the multi-stage compressor was calculated at 80% polytropic efficiency with pressure drop factors of 0, 0.1, and 0.2. These calculations were compared against the original calculations with 72% efficiency and no pressure drop. This comparison is shown in Figure 3-9.

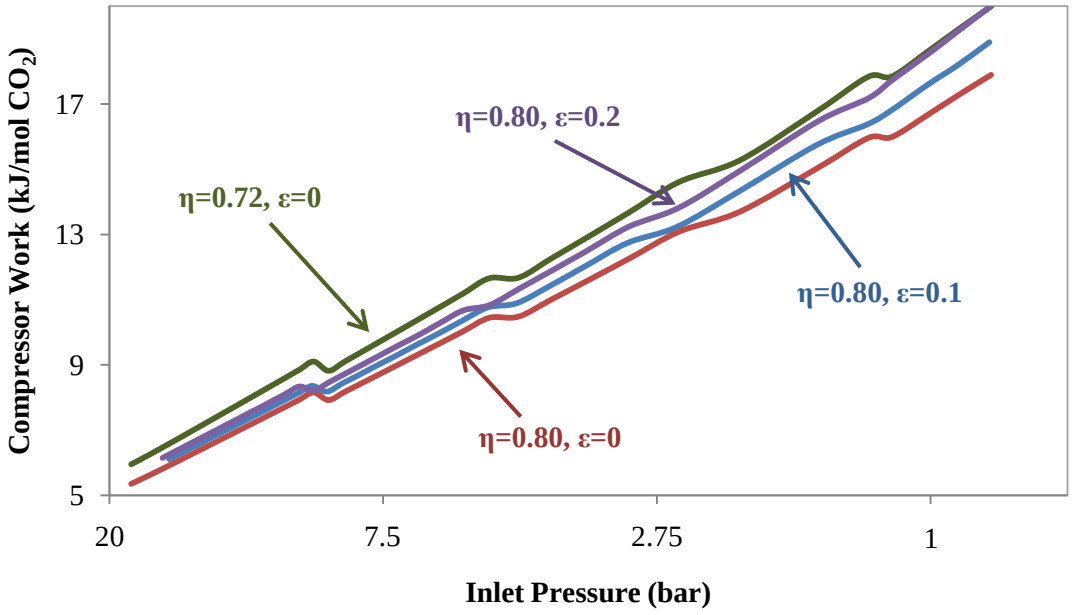


Figure 3-9. Sensitivity of $CO_2$ compression work to compression efficiency and intercooler pressure drop.

The compressor work was plotted as a function of the natural log of the inlet pressure to show the approximate linear trend as it was regressed in Equation 3-1. The actual inlet pressures are displayed in the figure.

A compressor efficiency of 80% and pressure drop factor of 0.2 may be a realistic set of parameters to expect in a real multi-stage compressor. The estimation with 72% efficiency and no pressure drop was close to the calculations with the more realistic parameters (Figure 3-9). Therefore, it was concluded that Equation 3-1 was a reasonable tool to predict the relative magnitude of the compressor work in relation to the heating work and pump work for the stripper.

These calculations of compressor work were also compared against the theoretical minimum for isothermal compression at 40 °C. The minimum work was equal to the change in process-initiating work, or the change in the Gibbs free energy. Using data

from NIST (NIST, 2011), the minimum work for $CO_2$ compression to 150 bar was calculated for varying inlet pressures using Equation 3-3.

$$\Delta G = \Delta H - T\Delta S \qquad \textbf{3-3}$$

Figure 3-10 ratioed the calculated compressor work of Equation 3-1 to the minimum work calculated by Equation 3-3. The overall thermodynamic efficiency was mostly constant, but it varied slightly with inlet pressure. The discontinuities in the ratio are associated with the introduction of additional compressor stages. The efficiency was 56 to 59%. As a comparison, the ratios of raw Aspen Plus® predictions of two scenarios to the minimum work are also shown. Again, the scenario with 80% efficiency and 20% pressure drop per intercooler had a slightly lower compressor work then the scenario with 72% efficiency and no pressure drop, but the predictions were roughly equivalent.

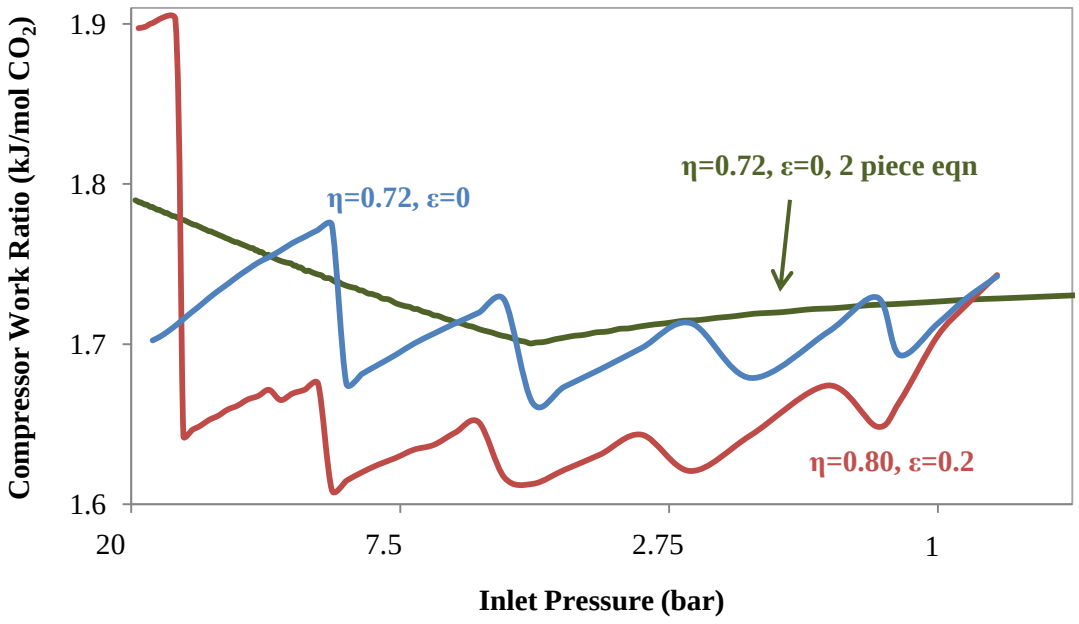


Figure 3-10. Ratio of compressor work predictions to minimum work calculations. Blue and red lines = ratio of Aspen Plus® calculations to thermodynamic minimum. Green line = Equation 3-1, 72% efficiency, no intercooler pressure drop, 2 piece correlation.

## 3.2. PERFORMANCE WITH MEA

The widest range of configurations was evaluated with MEA. The amine concentration was held constant at 9 m (35 wt%), and the rich loading was assumed constant at 0.5, which corresponded to a $CO_2$ partial pressure of 5 kPa at 40 °C. Since performance generally improves at higher stripper temperature with a greater temperature swing between the absorber and stripper, the maximum allowable temperature of 120 °C was the main case of interest. The results are graphically presented for 120 °C reboilers, grouped into the four categories: multi-stage flash (Figure 3-11), double matrix (Figure 3-12), columns (Figure 3-13), and interheated columns (Figure 3-14). Each figure shows the optimization of lean loading to minimize total equivalent work. The performance of a simple stripper is shown in each figure as a baseline comparison.

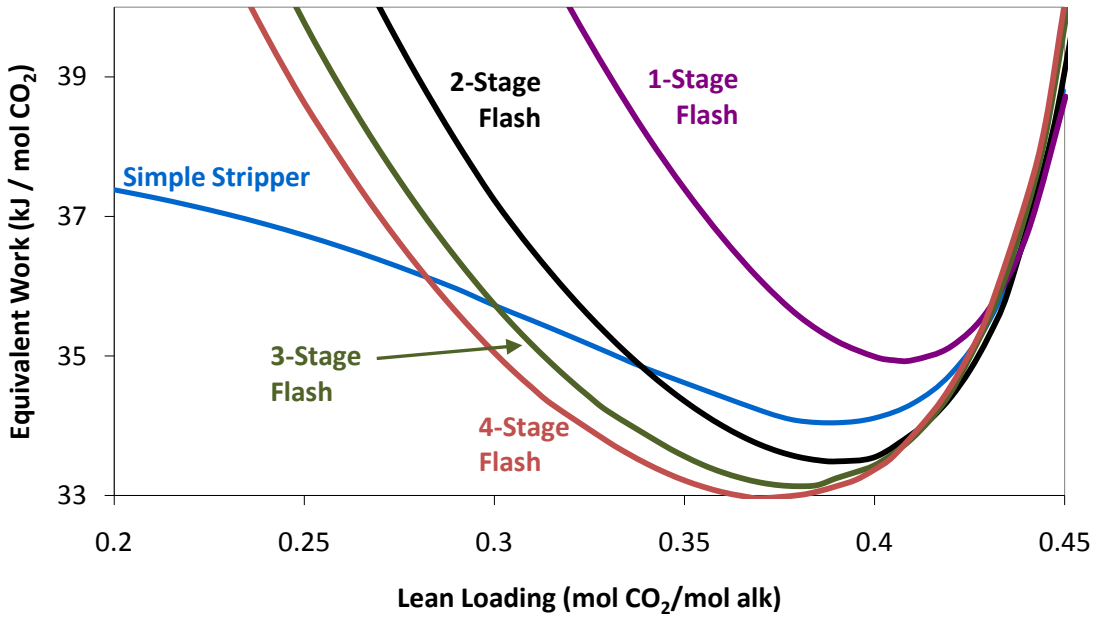


Figure 3-11. Performance of multi-stage flash configurations with 9 m MEA. 0.5 rich loading, 120 °C reboilers, 5 °C cold side approach on main heat exchanger, $CO_2$ compression to 150 bar, equal molar vapor production per pressure stage.

Increasing complexity with the multi-stage flash configurations demonstrated the improvement when the reversibility of the process was enhanced by adding pressure stages. Compared to the simple stripper base case with an optimum performance of 34.0 kJ/mol $CO_2$, the 1-stage flash configuration had a substantially higher optimum equivalent work of 34.9 kJ/mol $CO_2$. Additionally, the optimal lean loading of the 1-stage flash was 0.41 compared to 0.39 with the simple stripper. The equivalent work and optimal lean loading both decreased as the number of flash stages increased. At the higher number of pressure stages, however, each additional pressure stage yielded a diminishing amount of improvement. Increasing the number of pressure stages from 1 to 2 decreased the minimum equivalent work requirement from 34.9 to 33.5 kJ/mol $CO_2$, respectively, an improvement of 4.2%. Increasing the number of pressure stages from 3 to 4 decreased the minimum equivalent work requirement from 33.1 to 33.0 kJ/mol $CO_2$, respectively, an improvement of 0.5%.

Figure 3-12 shows the performance results of double matrix configurations. This figure makes several important conclusions. First, the best double matrix configuration decreased the total equivalent work from the simple stripper by 1.6 kJ/mol $CO_2$, or 4.8 %. Next, the benefit of optimizing a split ratio in these complex flowsheets was apparent.

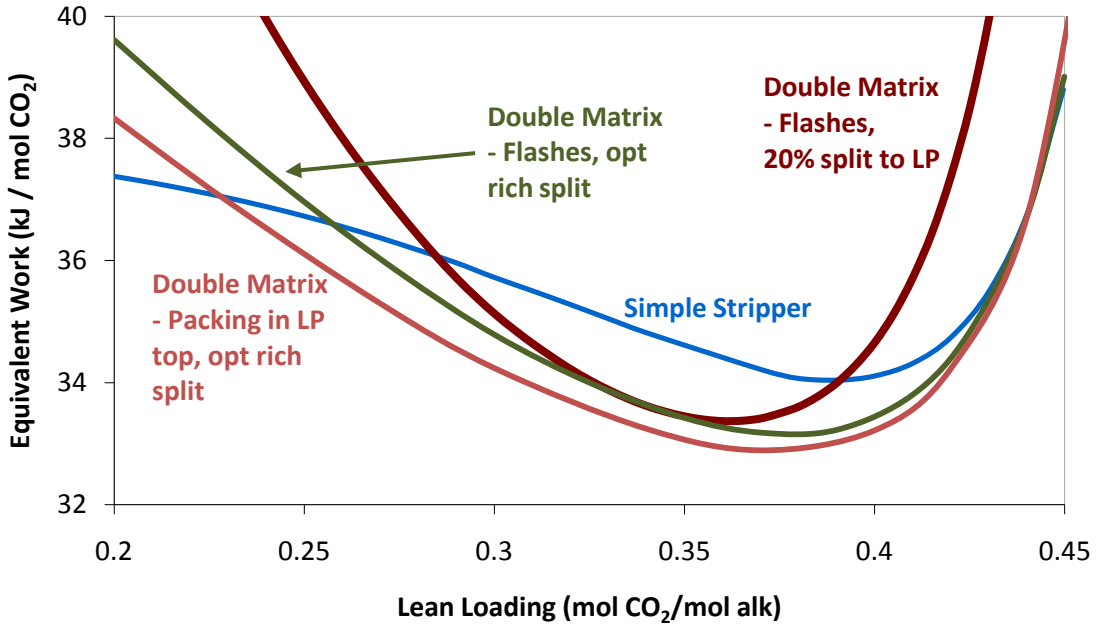


Figure 3-12. Performance of double matrix configurations with 9 m MEA. 0.5 rich loading, 120 °C reboilers, 5 °C cold side approach on main heat exchanger, $CO_2$ compression to 150 bar, equal molar vapor production per pressure stage.

In the two cases where all vessels were flashes, the constant 20% split to the low pressure vessel only coincided with one point on the optimized split curve, where the optimal split was 20%. At very low lean loading, the split optimized to high flow toward the low pressure vessel, but between lean loading values of 0.30 and 0.40, the split toward the low pressure vessel was between 7% and 37%. The split when running at the optimal lean loading of 0.37 was 13%. Adding packing to the top vessel decreased the required split, with optimal values of 5 to 27% between lean loading 0.30 and 0.40. With packing in the top low-pressure vessel, the split when running at the optimal lean loading of 0.36 was 11%. In addition to reducing the minimum equivalent work and split ratio, adding packing to the top section improved the performance at low lean loading. The effect was minimal in this configuration, and there was a more noticeable benefit in the next subset of configurations, columns, in Figure 3-13.

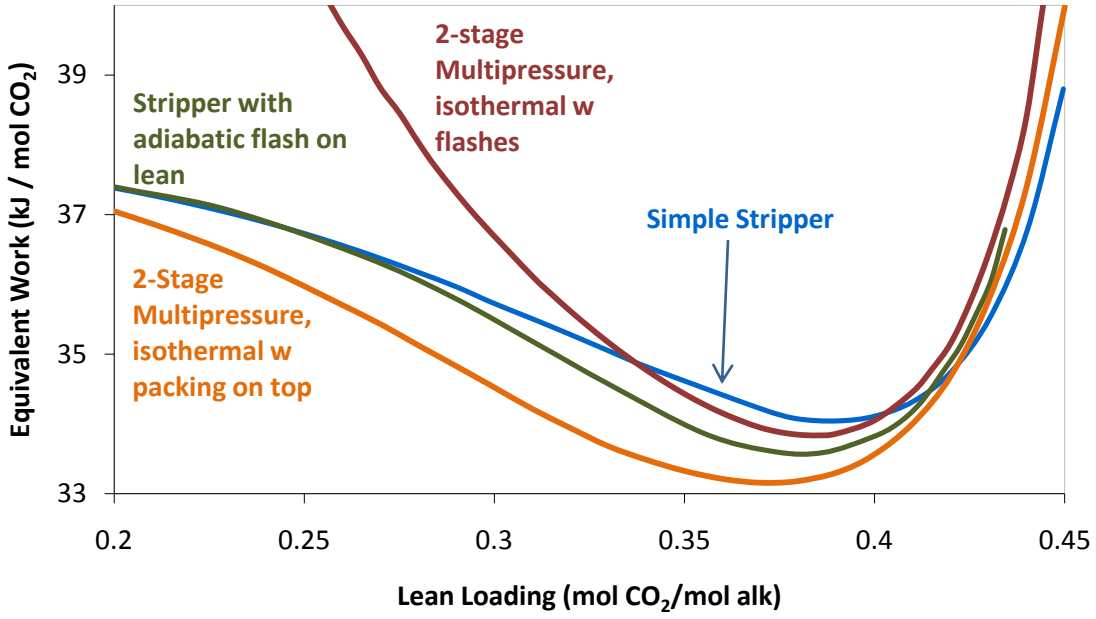


Figure 3-13. Performance of column configurations with 9 m MEA. 0.5 rich loading, 120 °C reboilers, 5 °C cold side approach on main heat exchanger, $CO_2$ compression to 150 bar, equal molar vapor production per pressure stage.

The stripper with an adiabatic lean flash (Fluor configuration) and the 2-stage multi-pressure configurations both improved performance over the simple stripper. The multi-pressure column greatly benefited from packing in the top section, especially at low loading. The Fluor configuration improved performance over the simple stripper by 0.4 kJ/mol $CO_2$, or 1.3%. The multi-pressure column with a packed top section improved performance over the simple stripper by 0.8 kJ/mole $CO_2$, or 2.6%. The benefit of packing was greater for the multi-pressure column than for the double matrix configuration because all of the liquid and vapor received this benefit, unlike in the case of the double matrix where only the split liquid and half of the vapor passed through the packing.

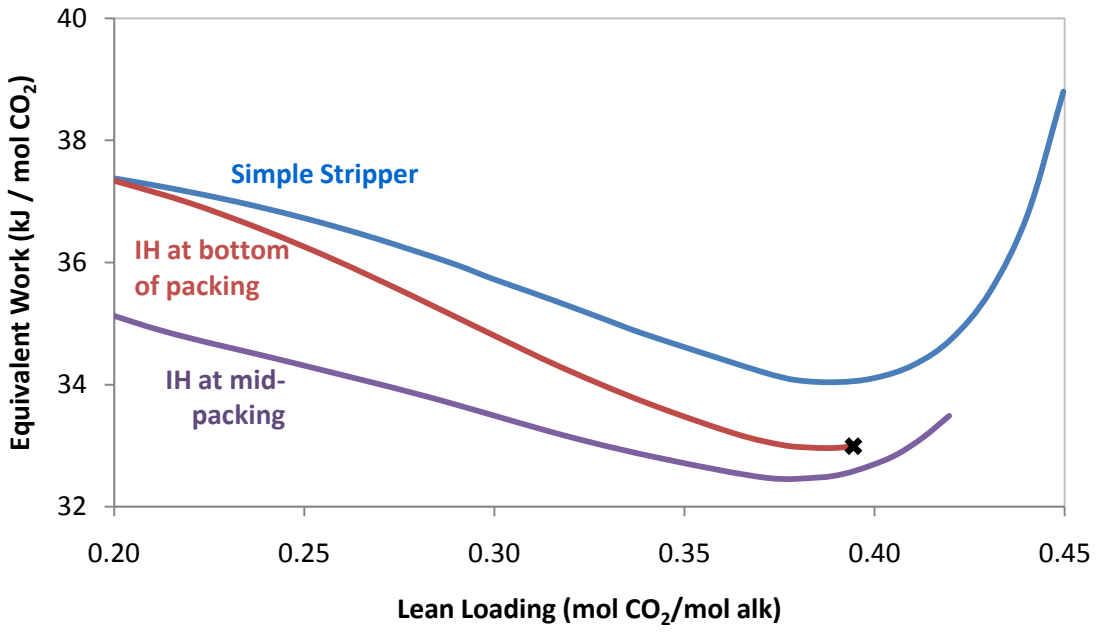


Figure 3-14. Performance of interheated columns with 9 m MEA. 0.5 rich loading, 120 °C reboilers, 5 °C cold side approach on main heat exchanger, $CO_2$ compression to 150 bar, equal molar vapor production per pressure stage, 80% extracted solvent.

The black "x" in Figure 3-14 represents a maximum lean loading where the stripper model would converge. The interheated column had the best performance of all of the configurations. Additionally, the interheating had the greatest effect when placed at the midpoint of the stripper column. When the interheating exchanger was placed at the bottom of the column, directly above reboiler, the extracted liquid was much hotter than at the middle of the column, so less heat could be exchanged. Moreover, the passing liquid and vapor streams were further from equilibrium at the bottom of the column. By performing the interheating at the middle the column where the vapor and liquid were close to a mass transfer pinch, the interheating step was more separate from the heating in the reboiler. Therefore, the mid-point interheated was more efficient. Interheating improved the performance in several ways. The optimal lean loading decreased from the simple stripper value, so the pump work and sensible heat requirements also decreased.

Next, the temperature at the top of the column was cooler than when running similar conditions for a simple stripper. The cooler temperature reduced the stripping steam requirement. Lastly, the rich solvent entering the column was cooler than with the simple stripper, so it did not flash upon entering the stripper. By using this configuration, the total equivalent work was reduced from the simple stripper by 1.5 kJ/mol $CO_2$, or 4.6%, at a lean loading of 0.37.

### 3.2.1. Performance Effect with Temperature

Performance generally improved with increasing reboiler temperature. The partial pressure of $CO_2$ rises faster than the partial pressure of water with increasing temperature, so a higher temperature always results in better $CO_2$ selectivity and less energy required for stripping steam. As a simple example, Figure 3-15 shows the effect of temperature between 100 °C and 130 °C in the 1-stage flash. The minimum equivalent work and optimal lean loading both decreased as temperature increased. The improvement was not consistent with each equal temperature step. The heating and compression work requirements consistently increased and decreased, respectively, but the pumping energy requirement increased exponentially with temperature since it was related to the pressure of the vessel. The downside to higher stripper temperature and exponentially increasing vessel pressure was the increasing pump work requirement with respect to the compression work benefit. Since it was assumed that extra pressurization of the lean solvent could not be recovered through a liquid expander, high stripper temperature with overpressurization resulted in lost work from a flash valve that would be implemented.

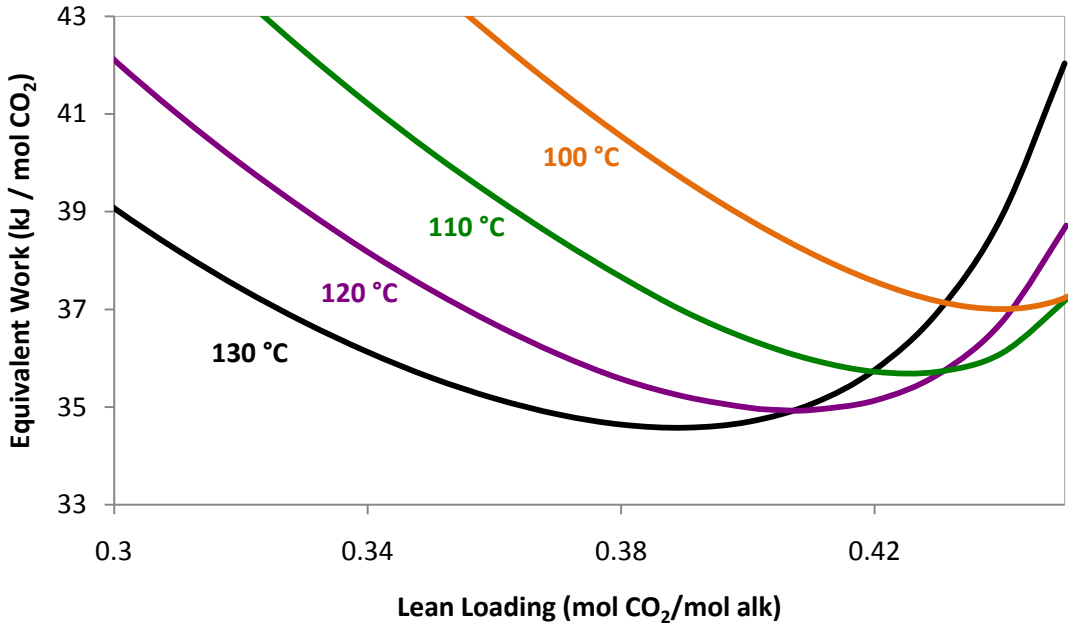


Figure 3-15. 1-stage flash performance with varying reboiler temperature using 9 m MEA. 0.5 rich loading, 5 °C cold side approach on main heat exchanger, $CO_2$ compression to 150 bar.

Figure 3-16 shows the trends in the heating work, compression work, and pump work for a 1-stage flash at optimal lean loadings for reboiler temperatures between 100 and 130 °C. Since the maximum operation temperature of MEA would be 120 °C, the increasing pump work requirement at high temperature was not significant enough to start increasing the total equivalent work.

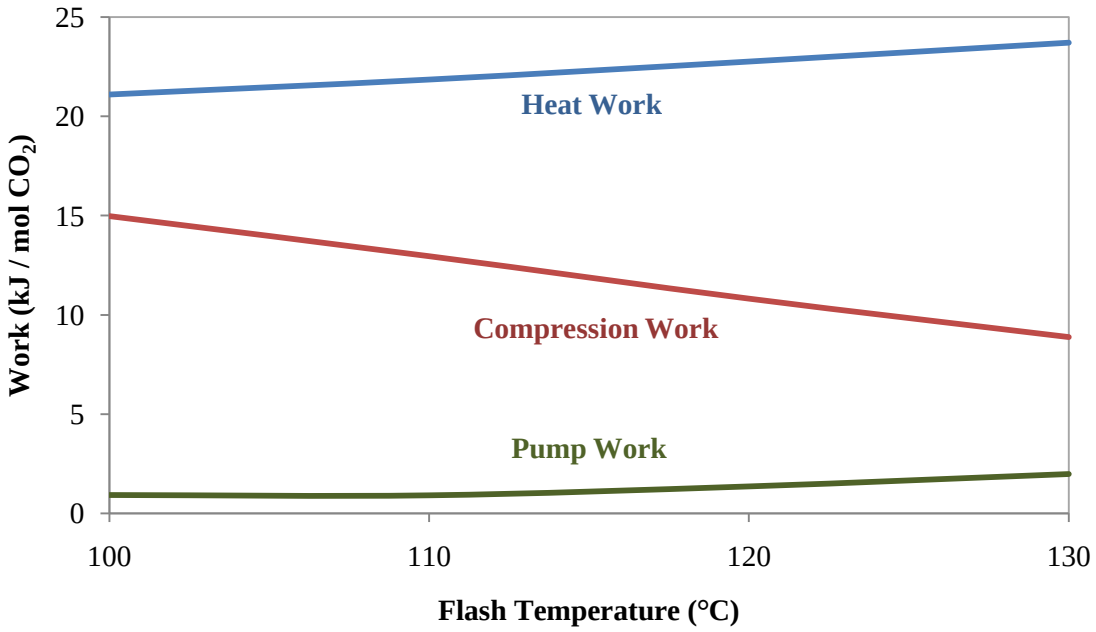


Figure 3-16. Equivalent work contributions for 1-stage flash. 9 m MEA, optimal lean loadings, 5 °C cold side approach on main heat exchanger, $CO_2$ compression to 150 bar.

Tables 3-1 to 3-3 display the equivalent work values for reboiler temperatures of 100 °C and 110 °C in addition to the 120 °C cases. The number of process units, equivalent work, lean loading, and vessel pressure(s) are listed for each configuration. The number of process units included vessels and heaters within the stripper section, but it excluded the main heat exchanger, pumps, and compressors because these process units were constant across all configurations. The stripper with an adiabatic lean flash received a credit in the number of process units because the first compression stage between the flash and stripper column would not require the typical pre-cooler and condenser. The total number of process units would roughly be related to configuration complexity since more process units would require a higher capital investment.

**Table 3-1. Results summary for all configurations at 100 °C. 9 m MEA, 0.5 rich loading, 5 °C main cross exchanger cold side temperature approach, $CO_2$ compression to 150 bar.**

| Configuration | Process units | Equivalent Work (kJ/mol $CO_2$) | | | Opt. ldg | P at opt. |
|---|---|---|---|---|---|---|
| | | *0.3 ldg* | *0.37 ldg* | *Opt. ldg* | *mol/mol* | *bar* |
| 1-stage flash | 2 | 50.1 | 41.5 | 37.0 | 0.44 | 2.3 |
| Simple stripper | 3 | 39.0 | 37.5 | 36.9 | 0.41 | 1.8 |
| Stripper with adiabatic lean flash | 3 | 37.9 | 36.9 | 36.0 | 0.42 | 2.3 / 1.3 |
| 2-stage flash | 4 | 44.5 | 37.9 | 35.1 | 0.43 | 3.1 / 2.1 |
| 2-stage multi-pressure, packed top | 4 | - | 36.5 | 35.2 | 0.41 | 2.3 / 1.7 |
| Interheated column | 5 | 35.6 | 34.7 | 34.5 | 0.41 | 1.7 |
| 3-stage flash | 6 | 42.5 | 36.6 | 34.5 | 0.43 | 3.7 / 2.5/ 2.0 |
| Double matrix, packed LP top | 6 | 38.2 | 36.0 | 35.0 | 0.42 | 2.9 / 1.9 |
| 4-stage flash | 8 | 41.4 | 35.9 | 34.2 | 0.42 | 4.0 / 2.8 / 2.2 / 1.8 |

**Table 3-2. Results summary for all configurations at 110 °C. 9 m MEA, 0.5 rich loading, 5 °C main cross exchanger cold side temperature approach, $CO_2$ compression to 150 bar.**

| Configuration | Process units | Equivalent Work (kJ/mol $CO_2$) | | | Opt. lldg | P at opt. |
|---|---|---|---|---|---|---|
| | | *0.3 ldg* | *0.37 ldg* | *Opt. ldg* | *mol/mol* | *bar* |
| 1-stage flash | 2 | 45.9 | 38.4 | 35.7 | 0.42 | 3.6 |
| Simple stripper | 3 | 36.9 | 35.6 | 35.1 | 0.40 | 2.9 |
| Stripper with adiabatic lean flash | 3 | 37.0 | 35.1 | 34.5 | 0.41 | 4.0 / 2.3 |
| 2-stage flash | 4 | 40.6 | 35.2 | 33.9 | 0.41 | 5.2 / 3.2 |
| 2-stage multi-pressure, packed top | 4 | 36.1 | 34.3 | 33.8 | 0.40 | 4.4 / 2.9 |
| Interheated column | 5 | 34.5 | 33.6 | 33.3 | 0.39 | 2.8 |
| 3-stage flash | 6 | 38.7 | 34.2 | 33.4 | 0.41 | 6.4 / 4.1/ 3.1 |
| Double matrix, packed LP top | 6 | 36.3 | 33.9 | 33.4 | 0.39 | 4.7 / 2.7 |
| 4-stage flash | 8 | 37.7 | 33.8 | 33.3 | 0.40 | 7.1 / 4.8 / 3.6 / 2.9 |

**Table 3-3. Results summary for all configurations at 120 °C. 9 m MEA, 0.5 rich loading, 5 °C main cross exchanger cold side temperature approach, $CO_2$ compression to 150 bar.**

| Configuration | Process units | Equivalent Work (kJ/mol $CO_2$) | | | Opt. lldg | P at opt. |
|---|---|---|---|---|---|---|
| | | *0.3 ldg* | *0.37 ldg* | *Opt. ldg* | *mol/mol* | *bar* |
| 1-stage flash | 2 | 42.1 | 36.1 | 34.9 | 0.41 | 6.3 |
| Simple stripper | 3 | 35.7 | 34.2 | 34.0 | 0.39 | 5.1 |
| Stripper with adiabatic lean flash | 3 | 35.5 | 33.6 | 33.6 | 0.39 | 6.6 / 3.7 |
| 2-stage flash | 4 | 37.3 | 33.7 | 33.5 | 0.39 | 8.9 / 5.1 |
| 2-stage multi-pressure, packed top | 4 | 34.5 | 33.2 | 33.2 | 0.37 | 6.7 / 4.2 |
| Interheated column | 5 | 33.5 | 32.5 | 32.5 | 0.37 | 4.2 |
| 3-stage flash | 6 | 35.8 | 33.2 | 33.1 | 0.38 | 10.9 / 6.6 / 4.6 |
| Double matrix, packed LP top | 6 | 34.1 | 32.4 | 32.9 | 0.37 | 8.0 / 4.3 |
| 4-stage flash | 8 | 35.0 | 33.0 | 33.0 | 0.37 | 12.1 / 7.7 /5.4 / 4.2 |

Plaza et al. (2010) showed that 90% $CO_2$ removal could be achieved at a lean loading of 0.41 and rich loading a 0.495 with 15 meters of packing and intercooling at the absorber midpoint to 40 °C. If a shorter absorber were used, a lower lean loading could be desired to still achieve 90% removal. Many of the optimal lean loadings were 0.41 or below, but the tables also document stripper performance of each configuration for lean loadings of 0.3 and 0.37 in addition to the optimal lean loading in case a lower lean loading would be necessary to achieve adequate absorber performance. These equivalent work values at lower lean loading reiterated the concept that packed columns operate more efficiently under conditions with high solvent capacity.

### 3.2.2. Complexity effect with 9 m MEA

Increasing complexity clearly demonstrated an improvement in stripper performance. Improved stripper performance was characterized by a reduced optimum equivalent work. A lower optimal lean loading also indirectly demonstrated better configurations because the absorber could run with less packing or higher purity with a lower lean loading. The reduction in optimum equivalent work and lean loading was especially apparent in Figure 3-11, showing the difference between the various multi-stage flash configurations. Not only did the energy requirement decrease with more flash stages, but the optimal lean loading also decreased. This figure also demonstrated a diminishing return effect; the improvement from the 1-stage flash to 2-stage flash was much more substantial than the improvement from the 3-stage flash to 4-stage flash. If higher levels of multi-stage flash configurations were simulated, the realized improvement would be even less significant as the configurations approached a completely reversible process for flashing $CO_2$ and water.

Vapor recompression was used in the Fluor configuration (adiabatic lean flash). Recompression improved performance by condensing some of the stripping steam contained in the low-pressure vapor, vaporizing $CO_2$ in the high-pressure vessel. However, the trend of its benefit was unexpected. Since the flash took a downward step in pressure, it would be expected that this lean flash configuration would be most beneficial at high reboiler temperature, where the stripper pressure was high and extra pressurization in the lean solvent was lost. However, since this configuration was non-isothermal, the high-pressure stripper column ran at a higher pressure than for the simple stripper. At high reboiler temperature, this stripper pressure elevation effect was magnified. Therefore, although the lean flash attempted to more reversibly bring the lean solvent from stripper pressure to absorber pressure, increasing pump work lessened the benefit of the adiabatic lean flash at high reboiler temperature.

Unlike vapor recompression, inserting packing sections in place of equilibrium flashes did not improve performance at optimal lean loading as much as expected. The effect of this addition was seen directly in the double matrix and 2-stage multi-pressure configurations. In the case of the double matrix, the baseline configuration with three equilibrium flashes was altered by replacing the top flash of the low-pressure section with a packed column. Adding packing in this location was expected to have the greatest effect on performance because a large amount of stripping steam was produced in the bottom flash of the low-pressure section, and the stripping steam required an adequate number of transfer units to fully condense and vaporize $CO_2$ from the split rich stream. The other flashes included reboilers which mostly eliminated the need for transfer units. Similarly, in the 2-stage multi-pressure configuration, packing was inserted in the high-pressure stage to better reach equilibrium with the inlet rich solvent to reduce the amount of stripping steam exiting in the vapor before it was cooled and compressed. As seen in

Figures 3-12 and 3-13, including packing in these two configurations had only a minor effect at high lean loading where the $CO_2$ capacity was low. However, packing substantially improved performance in both configurations at low lean loadings when an increased number of transfer units was beneficial to achieve the increased amount of $CO_2$ liberation per unit solvent.

The interheated column at 120 °C showed very promising results. The configuration with interheating at the bottom of the packing had a minimum equivalent work of 33.0 kJ/mol $CO_2$ at an optimal lean loading of 0.37. However, the configuration with interheating in the middle of the packing performed even better with a minimum equivalent work of 32.5 kJ/mol $CO_2$ at an optimal lean loading of 0.37. This alternative placement of the interheating was believed to be beneficial because the vapor rising from the reboiler was allowed to approach equilibrium with the falling solvent before the extra heat was applied in the interheater. This arrangement made the individual step changes smaller, therefore making it more reversible and more efficient. At 120 °C, the interheated column had comparable performance to the double matrix, but the interheated column was only slightly more complex than a simple stripper.

In Tables 3-1 to 3-3 the general trend of decreasing equivalent work with increasing complexity is displayed, though the trend did not fit a direct correlation with the number of process units. Figure 3-17 shows the relationship between complexity and performance, quantified by the minimum total equivalent work. This figure shows the decreasing trend in the equivalent work with increasing temperature for all configurations. The points seemed to suggest a minimum at a complexity level of 5, but the minimum was an illusion of "scatter" that was inherent in each complexity level. The configuration with a complexity of 5 was the interheated column, the most efficient of all of the flowsheets that were evaluated. The interheated column does not represent an

actual minimum with respect to complexity since the equivalent work should approach an asymptote at infinite complexity. Instead, this suggests that interheating was the most beneficial single flowsheet improvement, and it could be coupled with other improvements like vapor recompression or more pressure stages.

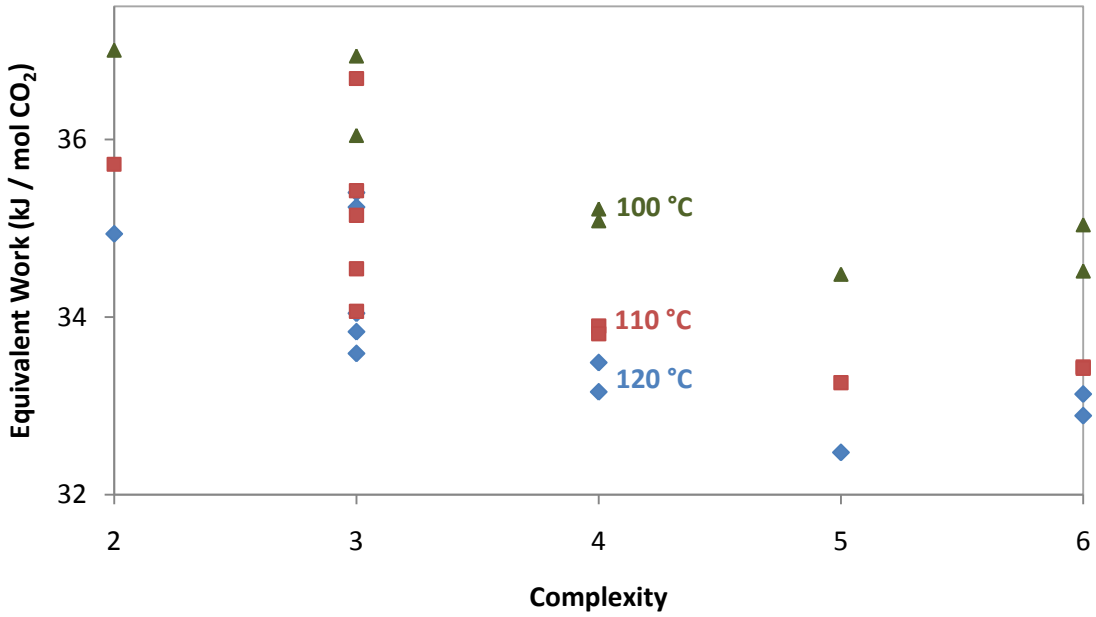


Figure 3-17. Decreasing trend of equivalent work with increasing complexity for 100 °C, 110 °C, and 120 °C reboiler temperatures. 5 °C cold side approach on main heat exchanger, $CO_2$ compression to 150 bar, equal molar vapor production per pressure stage.

### 3.2.3. Reboiler temperature effect with 9 m MEA

The difference in performance at varying reboiler temperatures demonstrated the importance of using packing at high temperature. The multi-stage flash configurations demonstrated a reduced benefit from increasing the reboiler temperature from 100 °C to 120 °C compared to the other configurations that used packing. Table 3-4 demonstrates this conclusion more clearly by forming two configuration categories of multi-stage flash and packed configurations. All configurations showed a relatively similar drop in the

equivalent work when increasing the reboiler temperature from 100 °C to 110 °C, but there was very little additional benefit for the multi-stage flash configurations by increasing the temperature to 120 °C.

**Table 3-4. Higher benefit of increasing reboiler temperature with packed configurations. Difference in minimum equivalent work values for each configuration.**

| Configuration | Process units | Benefit of increasing T by 10 °C to: | |
|---|---|---|---|
| | | *110 °C* | *120 °C* |
| 1-stage flash | 2 | 1.3 | 0.8 |
| 2-stage flash | 4 | 1.2 | 0.4 |
| 3-stage flash | 6 | 1.1 | 0.3 |
| 4-stage flash | 8 | 0.9 | 0.3 |
| Simple stripper | 3 | 1.8 | 1.1 |
| Stripper with adiabatic lean flash | 3 | 1.5 | 1.0 |
| 2-stage multipressure, packed top | 4 | 1.4 | 0.7 |
| Interheated column | 5 | 1.2 | 0.8 |
| Double matrix, packed LP top | 6 | 1.6 | 0.5 |

As the reboiler temperature increased, the vapor pressure of water increased exponentially. Similarly, the benefit from countercurrent cooling with rich solvent in a packed column had an exponentially increasing benefit. Therefore, the improvement for packed configurations at the high temperature of 120 °C was better than the improvement for multi-stage flash configurations. Moreover, the improvement at 120 °C was greater for fully packed configurations (simple stripper) compared to those that had exiting vapor that was not countercurrently contacted by rich solvent (double matrix, packed LP top).

The 1-stage flash experienced the greatest benefit by increasing its temperature from 110 °C to 120 °C because all of the $CO_2$ was stripped at the low, lean pressure where the stripping steam contribution was highest. The configurations with more pressure stages did not realize as high of an improvement due to a relatively lower average improvement in $CO_2$ selectivity.

### 3.2.4. Significance of Equivalent Work Evaluation

This analysis also demonstrated the significance of evaluating performance by equivalent work as opposed to heat duty. An analysis using heat duty would neglect the effect of temperature on the value of steam. A heat duty analysis would also overlook the pumping and compression contributions to overall energy requirement. An example of this difference can be seen in the comparison of the 2-stage flash with the simple stripper in Figure 3-18.

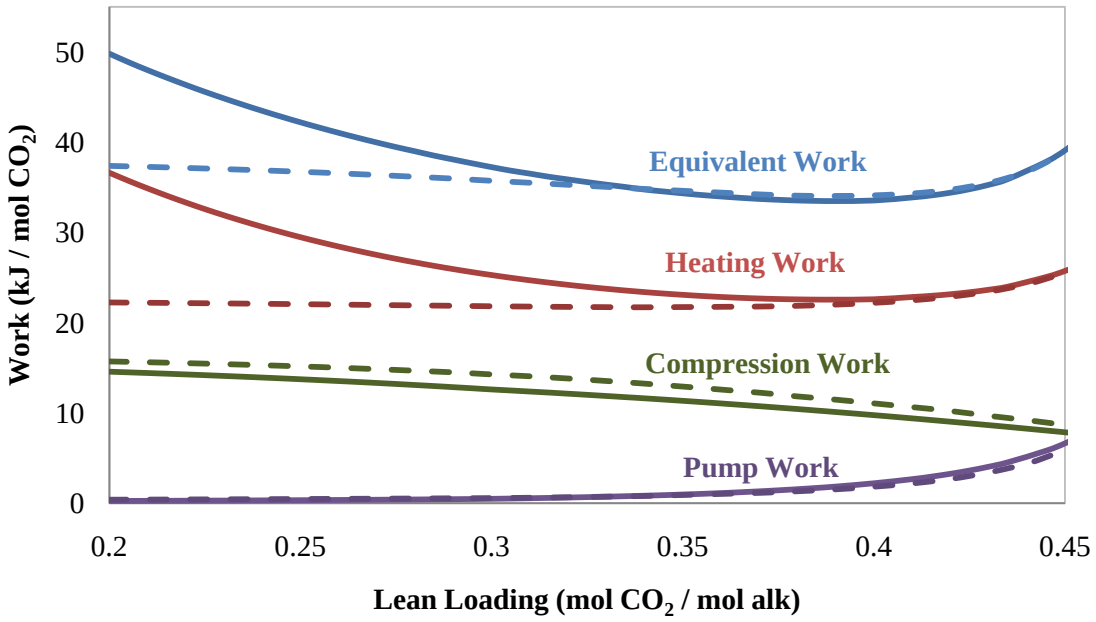


Figure 3-18. Total equivalent work and individual contributions for simple stripper and 2-stage flash at 120 °C. Dashed = simple stripper, Solid = 2-stage flash. 9 m MEA, 0.5 rich loading, 5 °C cold side approach on main heat exchanger, $CO_2$ compression to 150 bar.

The 2-stage flash had a lower minimum equivalent work but higher heat duty than the simple stripper. The pump work requirements of the two configurations were fairly equivalent, except at very high lean loading when the 2-stage flash had a higher requirement. The increase in pump work of the 2-stage flash at high loading was due to the growing pressure in the first stage, which directly impacted the work for the rich

solvent pump. The improvement of the 2-stage flash over the simple stripper stemmed from reduction in compression work due to collection of $CO_2$ at high pressure in the first flash, so the heat duty analysis did not recognize this benefit.

The importance of equivalent work analysis with regards to varying reboiler temperature is demonstrated in Figure 3-19. The total equivalent work, individual contributions, and total heat duty for a 2-stage flash with reboiler temperatures of 100 °C and 120 °C are compared. The minimum total heat duties were 153 and 135 kJ/mol $CO_2$ for 100 °C and 120 °C, respectively, a 12% decrease. However, converting these heat duties to heat works demonstrated a reduced benefit with values of 23.4 and 22.6 kJ/mol $CO_2$, respectively, a 3% benefit. The total work analysis also showed a 29% decrease in compression work and 50% increase in pump work by stripping at the higher temperature (Table 3-5). Therefore, the equivalent work analysis provided a more accurate description of the source of improvement by stripping at higher temperature: when increasing the stripper temperature, the pump work increased, but the decreases in heat and compression work offset the pump work increase to result in a lower total equivalent work.

In general, the trends for change in each individual work contribution were characterized. Since this work was isothermal at desired reboiler temperatures, the stripper pressure was variable as the lean loading was optimized. As lean loading increased, two effects occurred. First, since the rich loading was constant, the $CO_2$ carrying capacity decreased with increasing lean loading since the $\Delta_{loading}$ was nearing zero. Next, the stripper vessel pressure increased with increasing lean loading as dictated by VLE curves for $CO_2$, water, and, to a lesser extent, amine. Pump work was a direct function of solvent capacity and stripper pressure, so it increased with lean loading and reboiler temperature. Compression work decreased with increasing stripper pressure, so

the work for compression decreased with increasing lean loading and stripper temperature. Heat duty in heating work did not have monotonic trends with lean loading like pump and compression work. Normalized heat duty always reached a minimum at a lean loading where the sensible and stripping steam heat requirements were balanced (as in Figure 3-19). Additionally, heat duty always decreased with increasing reboiler temperature. It reached a minimum that balanced the sensible heat and stripping steam heat inputs. The trend of change in heating work with reboiler temperature was complicated. Heating work confounded the trend with lean loading and reboiler temperature since it accounted for the higher value of high temperature steam. Nonetheless, the minimum heating work was found to decrease with increasing temperature when stripping to the optimal lean loading.

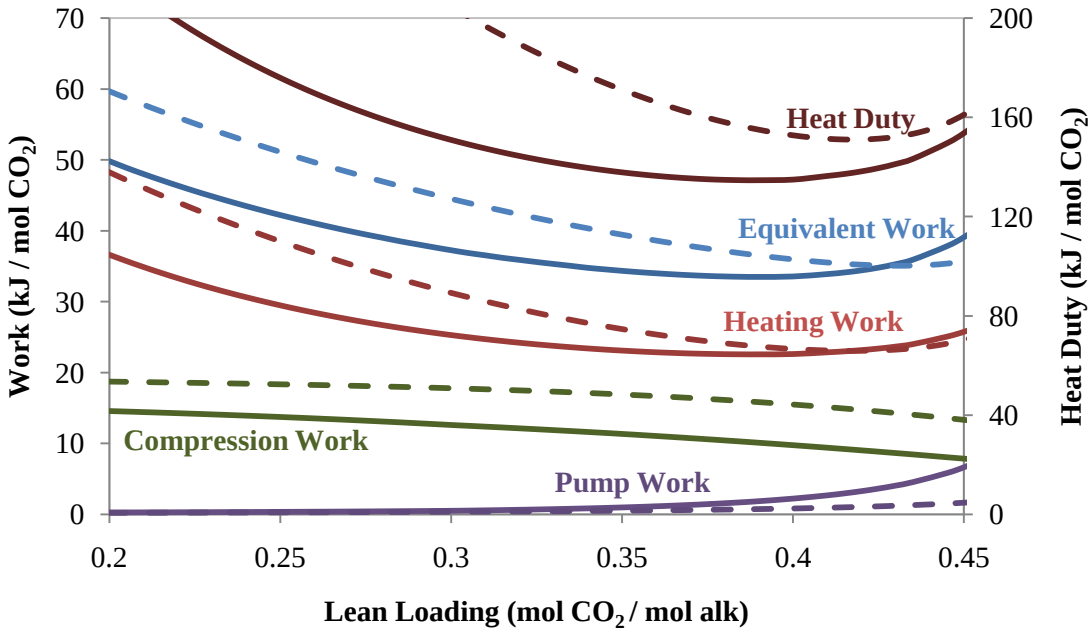


Figure 3-19. Total equivalent work and individual contributions for 2-stage flash. Dashed = 100 °C, Solid = 120 °C. 9 m MEA, 0.5 rich loading, 5 °C cold side approach on main heat exchanger, $CO_2$ compression to 150 bar.

**Table 3-5. Total heat duty and work contributions from 2-stage flash at 100 °C and 120 °C and optimal lean loadings for 9 m MEA.**

| | Total Q | $W_{heat}$ | $W_{comp}$ | $W_{pump}$ |
|---|---|---|---|---|
| | *kJ/mol $CO_2$* | | | |
| 100 °C | 152 | 23.2 | 14.3 | 1.2 |
| 120 °C | 135 | 22.6 | 10.1 | 1.8 |

Evaluating by equivalent work instead of heat duty can demonstrate significantly different optimal lean loadings. This effect is shown in Figure 3-20. The response of equivalent work and heat duty with varying lean loading are shown for 9 m MEA with reboiler temperature of 120 °C. Heat duty had a flat optimum, but the minimum heat duty occurred at a lean loading of 0.34. In contrast, the equivalent work minimum occurred at a lean loading of 0.39.

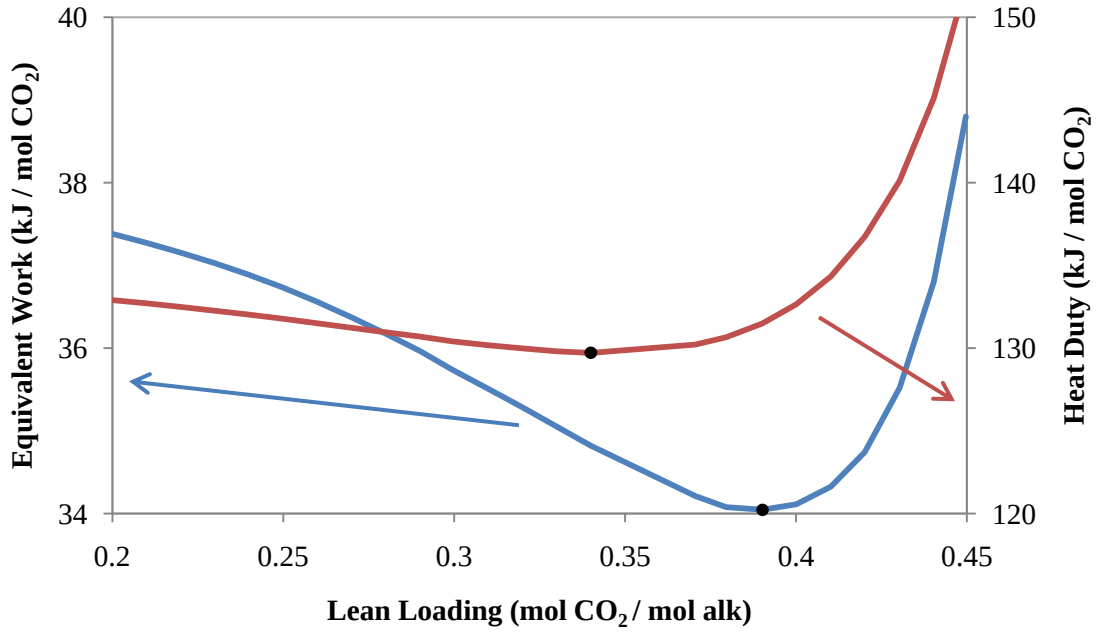


Figure 3-20. Optimization of heat duty (red) and equivalent work (blue) for 9 m MEA. 0.5 rich loading, 120 °C reboiler, 5 °C cold side approach, $CO_2$ compression to 150 bar.

## 3.3. PERFORMANCE WITH PZ

The typical concentrated PZ solvent concentration of 8 m was evaluated. The rich loading was assumed to be constant at 0.4, which corresponded to 5 kPa at 40 °C. The preferred stripping temperature was chosen to be the ceiling temperature of the solvent, which is generally considered to be 150 °C due to elevated thermal degradation rates above that temperature (Freeman, 2011). The performance was also evaluated at 120 °C to investigate whether PZ could be an adequate replacement solvent for MEA in a plant whose reboiler temperatures were already designed to be 120 °C. The number of configurations that were simulated with concentrated PZ was reduced from the work with MEA. The most relevant configurations were simulated to determine the specific benefit of complexity with this solvent. Concentrated PZ has twice the capacity of 7 m MEA, but its heat of absorption is lower; therefore, the magnitude of its benefit was uncertain. This solvent was evaluated with 1- and 2-stage flash (Figures 3-3 and 3-4), simple stripper (Figure 1-2), adiabatic lean flash (Figure 3-7), interheated column (Figure 3-8), and double matrix configurations (Figure 3-5).

The lean loading was optimized for each configuration. However, the optimal lean loading demonstrated understripping in many cases. A saturated optimized lean loading represented a case where the optimal lean loading had a $P^*_{CO2}$ at 40 °C equal to 10% of the rich solvent $P^*_{CO2}$ at 40 °C. The saturated lean loading for 8 m PZ with a rich loading of 0.40 was 0.31. An overstripped lean loading had a $P^*_{CO2}$ at 40 °C less than saturation, and an understripped lean loading had a $P^*_{CO2}$ at 40 °C greater than saturation. Figure 3-21 shows the lean loading optimization for all 6 configurations running with a reboiler temperature of 150 °C.

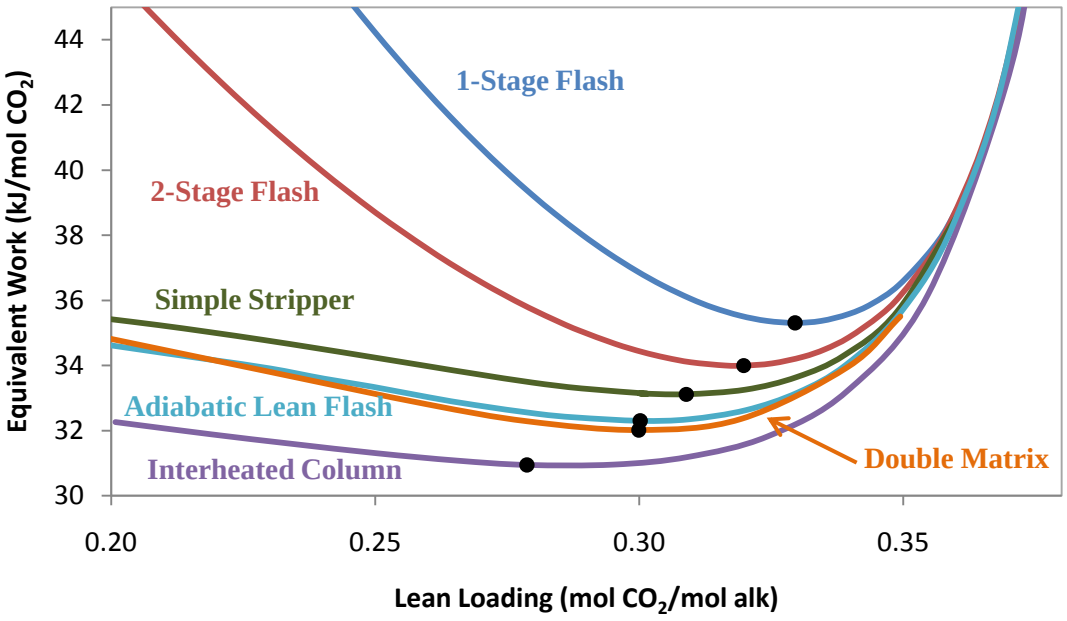


Figure 3-21. Performance of various stripper configurations with 8 m PZ at 150 °C. 0.4 rich loading, 5 °C cold side approach, $CO_2$ compression to 150 bar.

Some cases, particularly those with high complexity and/or high operating temperature, yielded a saturated optimal lean loading which was equal to the 90% removal spec. The only case which had an optimal lean loading that was overstripped was the interheated column. The equivalent work values are reported for each configuration at both 120 °C and 150 °C in Tables 3-6 and 3-7, respectively.

**Table 3-6. Minimum equivalent work for various configurations at 120 °C and using 8 m PZ.**

| Configuration | Opt. Lean Loading | Pressure | $W_{eq}$ | Heat Duty | Pump Work | $W_{eq}$ @ $P^*_{CO2}$<= 0.5 kPa |
|---|---|---|---|---|---|---|
| | *mol $CO_2$/mol alk* | *bar* | *kJ/mol $CO_2$* | | | *kJ/mol $CO_2$* |
| 1SF | 0.35 | 3.9 | 35.6 | 138.9 | 0.8 | 39.2 |
| SS | 0.33 | 3.3 | 33.5 | 120.4 | 0.9 | 33.7 |
| ALF | 0.33 | 4.2 / 2.7 | 32.7 | 111.6 | 1.1 | 32.9 |
| 2SF | 0.34 | 4.8 / 3.7 | 34.1 | 131.6 | 0.9 | 35.7 |
| DM | 0.32 | 4.3 / 3.1 | 34.9 | 115.7 | 1.0 | 35.2 |
| IHC | 0.31 | 2.9 | 31.8 | 107.0 | 0.7 | 31.8 |

**Table 3-7. Minimum equivalent work for various configurations at 150 °C and using 8 m PZ.**

| Configuration | Opt. Lean Loading | Pressure | $W_{eq}$ | Heat Duty | Pump Work | $W_{eq}$ @ $P^*_{CO2}$<= 0.5 kPa |
|---|---|---|---|---|---|---|
| | *mol $CO_2$/mol alk* | *bar* | *kJ/mol $CO_2$* | | | *kJ/mol $CO_2$* |
| 1SF | 0.33 | 11.0 | 35.3 | 124.7 | 1.9 | 36.1 |
| SS | 0.31 | 9.3 | 33.1 | 111.9 | 1.4 | 33.1 |
| ALF | 0.30 | 11.3 / 6.5 | 32.3 | 102.2 | 1.7 | 32.3 |
| 2SF | 0.32 | 14.2 / 10.1 | 34.0 | 119.0 | 2.1 | 34.1 |
| DM | 0.29 | 12.2 / 8.1 | 32.2 | 209.5 | 3.5 | 32.2 |
| IHC | 0.28 | 7.6 | 30.9 | 99.9 | 1.0 | 31.2 |

The improvement in the equivalent work between 120 °C and 150 °C was marginal, only 1% to 3% for the cases with optimized lean loadings, but when considering the equivalent work for lean loadings at saturation or lower, 150 °C demonstrated a 2% to 8% improvement. The effect of complexity on the equivalent work was still noticeable, with a 5% and 6% maximum improvement over the simple stripper base case for 120 and 150 °C, respectively. Additionally, the reduced capital cost of the multistage compressor would favor operating at the elevated temperature of 150 °C. Based on the lowest pressure vessel in each configuration, the 120 °C cases all required six compression stages to maintain a compression ratio of 2 or less, and 150 °C cases mostly required five compression stages, with the exception of the 1- and 2-stage flash configurations that required four compression stages.

## 3.4. COMPARING PERFORMANCE OF MEA AND PZ

Since PZ was expected to have better performance than MEA in the stripper, a comparison of the results of the two solvents was done. The heat duty should drastically be reduced for concentrated PZ because it has twice the $CO_2$ carrying capacity of the standard 7 m MEA solvent. Potentially counteracting qualities of concentrated PZ were its lower heat of absorption and higher ceiling stripping temperature. A lower heat of absorption reduces the $CO_2$ equilibrium partial pressure at stripping conditions, but stripping at 150 °C could have a counteracting effect. Additionally, concentrated PZ has been shown to have twice the reaction rate with $CO_2$ compared to 7 m MEA. The reaction rate with $CO_2$ did not have a direct impact in the stripper since the reactions were assumed to be instantaneous; however, a faster reaction rate should result in better

absorber performance. Therefore, when considering a constant absorber height, the rich loading in 8 m PZ should be higher than the rich loading in 9 m MEA when comparing on a common basis of $P^*_{CO2}$ at 40 °C. The absorber was not directly coupled to the stripper in this analysis, so an approximation of the performance with both solvents was needed.

### 3.4.1. Absorber performance approximation

In order to appropriately compare the performance of the stripper using 9 m MEA and 8 m PZ, it was desired to determine a rich loading for each solvent which accounted for the difference in reaction rates in the absorber. The overall reaction rate constant, $k_g$', combined the kinetic and mass transfer effects and can be used to calculate $CO_2$ flux with the gas side driving force between the bulk gas and interface concentrations:

$$N_{CO_2} = k'_g\left(P_{CO_2} - P^i_{CO_2}\right) \qquad \textbf{3-4}$$

Data for $k_g$' in MEA and PZ was measured by Dugas (2009) as a function of loading, which was directly indicative of the $P^*_{CO2}$ at 40 °C of the solution. The rate constant was also measured with varying temperature and solvent concentration, both of which had little effect between 40 °C and 60 °C. This data was gathered and correlated to predict $k_g$' as a function of $P^*_{CO2}$ at 40 °C for MEA using 40 °C and 60 °C data for 7 m, 9 m, 11 m, and 13 m MEA. A similar correlation was derived for PZ using 40 °C and 60 °C data for 2 m PZ, 5 m PZ, and 8 m PZ. The final correlation for each solvent is:

$$\textbf{MEA}: \quad ln\, k'_g = -0.40 \cdot ln\, P^*_{CO_2,40°C} - 14.35 \qquad \textbf{3-5}$$

$$\textbf{PZ}: \quad ln\, k'_g = -0.41 \cdot ln\, P^*_{CO_2,40°C} - 13.44 \qquad \textbf{3-6}$$

To calculate approximate absorber performance, a saturated lean loading was specified where its equilibrium partial pressure was 10% of the rich equilibrium partial

pressure since 90% removal in the absorber was expected. Assuming a constant absorber height for all cases, the normalized $CO_2$ absorption rate was calculated as the log mean flux:

$$N_{CO_2,\mathrm{LM}} = \frac{N_{CO_2,\mathrm{rich}} - N_{CO_2,\mathrm{lean}}}{\ln\left(N_{CO_2,\mathrm{rich}} / N_{CO_2,\mathrm{lean}}\right)} \qquad \textbf{3-7}$$

Next, corresponding rich and lean loading sets for MEA and PZ were calculated that made the log mean fluxes for the two solvents equal to each other, thereby indicating equivalent absorber performance. These estimates assumed an isothermal absorber at 40 °C. Rich and lean loadings sets were calculated for both solvents for two cases:

1. 0.50 rich loading for 9 m MEA
2. 0.50 rich loading for 8 m PZ

**Table 3-8. Loadings of 9 m MEA and 8 m PZ to match absorber log mean flux. Loadings predicted by isothermal absorber approximation at 40 °C**

| Case | MEA rich | | MEA lean | | PZ rich | | PZ lean | |
|---|---|---|---|---|---|---|---|---|
| | $P^*_{CO2}$ (kPa) | ldg | $P^*_{CO2}$ (kPa) | ldg | $P^*_{CO2}$ (kPa) | ldg | $P^*_{CO2}$ (kPa) | ldg |
| 1 | 5.0 | 0.50 | 0.50 | 0.45 | 8.4 | 0.42 | 0.84 | 0.33 |
| 2 | 1.5 | 0.48 | 0.15 | 0.40 | 5.0 | 0.40 | 0.50 | 0.31 |

Prior work (Oyenekan et al., 2007) used a common rich and lean loading set for MEA corresponding to 5 kPa/0.5 kPa of $P^*_{CO2}$ at 40 °C. Table 3-8 shows that these loadings for MEA corresponded to loadings for PZ that provided 8.4 kPa/0.84 kPa $P^*_{CO2}$ at 40 °C. It was expected that a more realistic rich loading with PZ would have a $P^*_{CO2}$ at 40 °C of 5 kPa, so this case (case 2 in Table 3-8) was used for the comparison simulations.

### 3.4.2. 9 m MEA and 8 m PZ performance with similar absorber specification

Using the rich and lean loadings for MEA and PZ detailed in case 2 of Table 3-8, five configurations were evaluated at the respective maximum temperatures for each solvent. The five configurations were the 1-stage flash (Figure 3-3), 2-stage flash (Figure 3-4), simple stripper (Figure 1-2), stripper with adiabatic lean flash (Figure 3-7), and interheated column (Figure 3-8) configurations. The equivalent work at saturation as well as the optimal lean loading for each configuration are shown for 9 m MEA and 8 m PZ in Tables 3-9 and 3-10, respectively. These tables also detail the normalized reboiler duty and work contributions for each configuration. The vessel pressures are also reported, and these demonstrate one of the most significant benefits of using concentrated PZ: by running at 150 °C, the stripper ran at significantly higher pressures. Table 3-11 shows the performance of 8 m PZ at 120 °C. Considering the two solvents at the equivalent temperature of 120 °C, the vessel pressures were consistently lower when using 8 m PZ.

The use of 8 m PZ at high temperature in the place of 9 m MEA yielded a 3% to 11% improvement depending on the configuration. When changing the solvent from 9 m MEA to 8 m PZ, the simple stripper showed the greatest improvement of all the configurations with a decrease of 11%, followed by the interheated column with an improvement of 10%, and the adiabatic lean flash had the third-best improvement of 9%. The 1- and 2-stage flash configurations did not benefit much by using 8 m PZ, demonstrating only a 4% and 3% improvement, respectively.

Another significant difference between the two solvents was that the optimal lean loading when using 9 m MEA was overstripped, but the optimal lean loading when using 8 m PZ was understripped or near saturation. At a low lean loading, the dominating effect that would increase the total equivalent work was the stripping steam requirement.

Since MEA has a high heat of absorption, the stripping steam requirement was generally lower, so it ran more optimally at lower lean loading than PZ.

**Table 3-9. Performance of 9 m MEA at 120 °C with a 0.48 rich loading, $CO_2$ compression to 150 bar. Pressure, total heat duty, and work contributions at optimal lean loading.**

| Configuration | Process units | Equivalent Work | | Lean Loading | Pressure | Total Q | $W_{heat}$ | $W_{pump}$ | $W_{comp}$ |
|---|---|---|---|---|---|---|---|---|---|
| | | *kJ/mol $CO_2$* | | *mol $CO_2$/mol alk* | *bar* | *kJ/mol $CO_2$* | | | |
| Lean loading → | | 0.4 ldg | Optimal | | | | | | |
| 1-Stage flash | 2 | 37.4 | 37.2 | 0.39 | 5.1 | 153 | 24.6 | 1.2 | 11.4 |
| Simple Stripper | 3 | 37.0 | 35.9 | 0.36 | 3.9 | 137 | 21.9 | 1.4 | 12.6 |
| Stripper with adiabatic lean flash | 3 | 36.8 | 35.4 | 0.36 | 5.2 / 2.9 | 132 | 21.1 | 1.5 | 12.8 |
| 2-Stage flash | 4 | 36.2 | 35.5 | 0.38 | 7.1 / 4.4 | 145 | 23.1 | 1.5 | 10.8 |
| Interheated column | 5 | 35.3 | 34.2 | 0.35 | 3.5 | 129 | 20.6 | 0.5 | 13.0 |

**Table 3-10. Performance of 8 m PZ at 150 °C with a 0.40 rich loading, $CO_2$ compression to 150 bar.**

| Configuration | Process units | Equivalent Work | | Lean Loading | Pressure | Total Q | $W_{heat}$ | $W_{pump}$ | $W_{comp}$ |
|---|---|---|---|---|---|---|---|---|---|
| | | *kJ/mol $CO_2$* | | *mol $CO_2$/mol alk* | *bar* | *kJ/mol $CO_2$* | | | |
| Lean loading → | | 0.31 ldg | Optimal | | | | | | |
| 1-Stage flash | 2 | 36.1 | 35.3 | 0.33 | 11.0 | 125 | 25.1 | 1.9 | 8.3 |
| Simple Stripper | 3 | 33.1 | 33.1 | 0.31 | 9.3 | 112 | 22.6 | 1.5 | 9.0 |
| Stripper with adiabatic lean flash | 3 | 32.3 | 32.3 | 0.31 | 12.1 / 7.1 | 103 | 20.7 | 1.7 | 7.9 |
| 2-Stage flash | 4 | 34.1 | 34.0 | 0.32 | 14.2 / 10.1 | 119 | 24.0 | 2.0 | 7.3 |
| Interheated column | 5 | 31.2 | 30.9 | 0.28 | 7.6 | 100 | 20.1 | 1.0 | 9.8 |

**Table 3-11. Performance of 8 m PZ at 120 °C with a 0.40 rich loading, $CO_2$ compression to 150 bar.**

| Configuration | Process units | Equivalent Work | | Lean Loading | Pressure | Total Q | $W_{heat}$ | $W_{pump}$ | $W_{comp}$ |
|---|---|---|---|---|---|---|---|---|---|
| | | *kJ/mol $CO_2$* | | *mol $CO_2$/mol alk* | *bar* | *kJ/mol $CO_2$* | | | |
| Lean loading → | | 0.31 ldg | Optimal | | | | | | |
| 1-Stage flash | 2 | 39.2 | 35.6 | 0.35 | 3.9 | 139 | 22.2 | 0.8 | 12.6 |
| Simple Stripper | 3 | 33.7 | 33.5 | 0.33 | 3.3 | 120 | 19.3 | 0.9 | 13.3 |
| Stripper with adiabatic lean flash | 3 | 32.9 | 32.7 | 0.33 | 4.2 / 2.7 | 112 | 17.9 | 1.1 | 12.2 |
| 2-Stage flash | 4 | 35.7 | 34.1 | 0.34 | 4.8 / 3.7 | 132 | 21.1 | 0.8 | 11.8 |
| Interheated column | 5 | 31.8 | 31.8 | 0.31 | 2.9 | 107 | 17.1 | 0.7 | 13.9 |

### 3.4.3. Comparison of solvent/configuration combinations

Table 3-12 summarizes the results of important solvent/configuration combinations. The minimum total equivalent work, optimal lean loading, vessel pressure, total heat duty, and work contributions are all detailed.

**Table 3-12: Noteworthy Solvent/Configuration Combinations. 9 m MEA at 120 °C and 8 m PZ at 150 °C.**

| System | Equivalent Work | Lean Ldg | Pressure | Total Q | $W_{heat}$ | $W_{pump}$ | $W_{comp}$ |
|---|---|---|---|---|---|---|---|
| | *kJ/mol $CO_2$* | *mol/mol* | *bar* | *kJ/mol $CO_2$* | | | |
| MEA - SS - 0.5 rldg | 33.8 | 0.39 | 5.1 | 131 | 21.1 | 1.3 | 11.5 |
| MEA - SS - 0.48 rldg | 35.9 | 0.36 | 3.9 | 137 | 21.9 | 1.4 | 12.6 |
| MEA - 2SF - 0.48 rldg | 35.5 | 0.38 | 7.1 / 4.4 | 145 | 23.1 | 1.5 | 10.8 |
| PZ - SS - 0.40 rldg | 33.1 | 0.31 | 9.3 | 112 | 22.6 | 1.5 | 9.0 |
| PZ - 2SF - 0.40 rldg | 34.1 | 0.31 | 13.4 / 9.4 | 120 | 24.2 | 1.8 | 8.1 |
| PZ - IHC - 0.40 rldg | 30.9 | 0.28 | 7.6 | 100 | 20.1 | 1.0 | 9.8 |

Various mechanisms within the stripper dictated the improvement of each combination. Changes in compression and pump work were straightforward. Compression work decreased due to any increase in the pressure of the vessel(s), and pump work increased due to any increase in the pressure of the vessel(s). However, pump work also decreased with reduced optimal lean loading due to increased capacity and decreased solvent circulation rate. Several mechanisms directed changes in the heating work. First, increased reboiler temperature at a constant total heat duty raised the heating work since the steam used was of higher quality. Next, improved solvent capacity decreased the heat duty due to the lower sensible heat requirement. Finally, the difference in the heats of absorption of $CO_2$ of the solvents affected the amount of heat

duty needed to desorb $CO_2$. The improvements of each combination in Table 3-12 can be explained using these mechanisms. The general conclusion was that 8 m PZ consistently performed better than 9 m MEA, mostly due to the fact that it was run at 150 °C. At the higher temperature, the vessel pressures were significantly higher in the PZ cases, drastically reducing the compression work.

The first and second cases both used 9 m MEA in a simple stripper, but the rich loading varied between 0.5 and 0.48. As expected, the total equivalent work was lower with a high rich loading. The optimal lean loading with a rich loading of 0.50 resulted in a stripper pressure of 5.1 bar, compared to 3.9 bar for a rich loading of 0.48. Consequently, the compression work was reduced by 1.1 kJ/mol $CO_2$, or 8.7%. The reboiler duty (and heating work) also decreased with the higher rich loading because the $CO_2$ equilibrium partial pressure was higher at the top of the column, so the $CO_2$ selectivity was better.

A comparison which demonstrated a major difference between the two solvents was the difference between the simple stripper and 2-stage flash with each solvent. The flash configuration was capable of reducing the total work requirement with MEA, but the performance worsened when transitioning from the simple stripper to 2-stage flash with PZ. By examining the changes in work contributions for this modification with each solvent, it was clear that MEA experienced a drop in compression work of 1.8 kJ/mol $CO_2$, but PZ only experienced a drop of 0.9 kJ/mol $CO_2$. Both solvents experienced an increase in heating work since more stripping steam escaped from the equilibrium flashes, but MEA had a smaller increase due to its higher heat of absorption. Combining all of the contributions, the 2-stage flash configuration was a beneficial change from the simple stripper when using MEA, but not for PZ.

Table 3-12 clarifies the source of improvement of the interheated column over the simple stripper. First, since the rich solvent entering the top of the column was cooler, the stripping steam exiting in the vapor from the top of the column decreased. Since the stripping steam requirement decreased, the reboiler duty and heating work also decreased. Next, the column pressure was lower with the lower lean loading, so the rich pump pressure change decreased by 15%. The lower optimal lean loading caused the solvent rate to decrease by 25%, so the overall decrease in rich pump work was 33%. The compression work increased by 9% due to the lower column pressure, but the other savings resulted in a much more efficient configuration.

### 3.4.4. Update to Absorber Approximation

The difference in optimal lean loadings between MEA and PZ needed to be addressed. As previously pointed out, the process optimally utilized overstripping for MEA, but only typically optimized with a saturated lean loading for PZ. The rich loadings of 0.48 and 0.4 for MEA and PZ, respectively, were calculated to be an accurate comparison in section 3.4.1 when paired with the respective lean loadings corresponding to 90% removal. All amine solvents demonstrated trends of $k_g$' that increased with decreasing loading. Since MEA optimized with lower lean loading, the actual log mean $CO_2$ flux in the absorber was greater, so the rich and lean loadings for PZ needed to also be lower to similarly increase its log mean flux in the absorber. Table 3-13 summarizes a supplemental set of rich and lean loadings for 9 m MEA and 8 m PZ. The optimized runs for 9 m MEA in section 3.4.2 demonstrated variable optimal lean loadings, so a representative value of 0.36 was selected. The new calculated loadings for PZ were not significantly different than the originally selected values. Consequently, the simple

stripper at 150 °C had an energy requirement of 33.6 kJ/mol $CO_2$ using the new rich and lean loadings, only 0.4 kJ/mol $CO_2$ (1.4%) greater than the requirement with a rich loading of 0.4. Approximately the same change could be expected for the other configurations.

**Table 3-13. Rich and lean loadings for 9 m MEA and 8 m PZ predicted by isothermal absorber approximation based on optimal performance of 9 m MEA in stripper**

| Solvent | Rich | | Lean | |
|---|---|---|---|---|
| | $P^*_{CO2}$ *(kPa)* | *ldg* | $P^*_{CO2}$ *(kPa)* | *ldg* |
| MEA | 1.5 | 0.479 | 0.09 | 0.360 |
| PZ | 4.5 | 0.394 | 0.45 | 0.308 |

## 3.5. RECOMMENDED FLOWSHEET IMPROVEMENTS

The performance of the heat exchanger was important to evaluate in order to make adequate recommendations for future flowsheet modifications. The heat exchanger was simulated in this work using a constant cold side temperature approach, which assumed a variable exchanger area to attain the desired temperature approach. However, an imbalance of heat capacity flows as well as excessive flashing of the rich solvent could result in a hot side temperature approach that was significantly higher than the cold side. Table 3-14 shows the heat exchanger performance of the important combinations of solvent and configuration that were presented in Table 3-12. When the pressure was sufficiently high to prevent flashing of the rich solvent, the hot side approach was between 6.1 and 7.7 °C. However, at the pressures that were modeled in the simulations, flashing occurred and the hot side approaches were increased to 6.6 to 13.9 °C. Such a drastic difference in the approach temperatures indicated a source of inefficiency. Tactics to balance the temperature driving force in the heat exchanger could include

overpressurization of the rich solvent to reduce flashing, reflux in the stripper to balance the heat capacity flows, and rich solvent bypass around the heat exchanger to balance the heat capacity flows.

**Table 3-14. Heat exchanger performance of important solvent/configuration combinations, with and without rich solvent flashing. 9 m MEA at 120 °C and 8 m PZ at 150 °C.**

| System | Cold Side Approach<br>*C* | Hot Side Approach<br>*C* | Hot Side Approach (no flashing)<br>*C* |
|---|---|---|---|
| MEA - SS - 0.5 rldg | 5.0 | 9.3 | 7.0 |
| MEA - SS - 0.48 rldg | 5.0 | 8.8 | 7.0 |
| MEA - 2SF - 0.48 rldg | 5.0 | 13.9 | 7.7 |
| PZ - SS - 150C | 5.0 | 9.7 | 6.1 |
| PZ - 2SF - 150C | 5.0 | 8.7 | 6.4 |
| PZ - IHC - 150C | 5.0 | 6.6 | 6.5 |

The intercoolers in the multi-stage compressor were also a potential source of low grade heat. The amount of recoverable heat varies with the inlet pressure of $CO_2$, but a saturated feed with a pressure of 2 bar and intercooling to 40 °C had 20.6 kJ/mole $CO_2$ of total heat available for recovery. However, this value assumed that the heat could be used all the way down to 40 °C. Less heat would be available at a higher feed pressure. Nonetheless, recycling the heat removed in the intercoolers could be a way to reduce the impact of the heating requirement in the stripper.

Lastly, configurations were explored in this chapter that utilized high stripper pressure. For example, the optimum flowsheet with 8 m PZ in an interheated column with a reboiler temperature of 150 °C had a column pressure of 7.6 bar. The required feed pressure of the absorber is typically only 1 atm. The extra pressure to overcome head and pressure drop would be approximately 2.5 bar. Therefore, whenever the lean return pressure was greater than 3.5 bar, the extra pressure could theoretically be

recovered in a liquid expanding turbine. Due to pressure drop in pipes and process units, the heights of the absorber and stripper, and inefficiencies in the pumps and liquid expander, the rich pump work could not be fully recovered, but a slight benefit may be realized.

**Table 3-15. Potential improvement in stripper performance by using lean solvent expansion with turbine 100% efficiency. 9 m MEA (0.48 rich loading) and 8 m PZ (0.40 rich loading).**

| | **Lean Loading** *mol/mol* | **No Lean Recovery Equivalent Work** *kJ/mol $CO_2$* | **Lean Recovery Equivalent Work** *kJ/mol $CO_2$* |
|---|---|---|---|
| MEA-2SF-120 °C | 0.38 | 35.50 | 35.31 |
| PZ-IH-150 °C | 0.28 | 30.95 | 30.61 |

The 2-stage flash configuration with 9 m MEA had a high LP pressure and low equivalent work, so it was chosen for analysis with lean solvent expansion. The high vessel pressures in the PZ configurations made them better candidates for recovering energy with lean expansion. The interheated column with 8 m PZ had the best overall performance, so it was also of interest for further improvement. Even so, the maximum recoverable energy was about 0.3 kJ/mole $CO_2$, or 1%. This result suggested that pursuing the use of a liquid expansion turbine to recover pressure energy from the lean solvent would only be worthwhile if scraping for every possible energy benefit.

## 3.6. CONCLUSIONS

1. Using either MEA or PZ, greater complexity in the stripper usually resulted in better energy efficiency due to a closer approach to a reversible process. The type of complexity added to the simple stripper dictated the relative magnitude of the improvement.

2. The 2-piece compressor correlation assuming 72% polytropic efficiency and no pressure drop in intercoolers provided nearly the same approximation as 80% polytropic efficiency and 20% pressure drop in each intercooler.

3. Evaluating performance by equivalent work accounted for the impact of variable vessel pressure and steam quality required when considering different reboiler temperatures and solvents.

4. Increasing the number of pressure stages of a multi-stage flash from 1 to 2 with 9 m MEA decreased the equivalent work by 4.2%. There was a reduced benefit of 0.5% when the number of pressure stages in a multi-stage flash was increased from 3 to 4 with 9 m MEA.

5. The most beneficial single addition of complexity was interheating of a packed column. The actual improvement varied by solvent, temperature, and rich loading, but the interheated column consistently required 4.8% to 7.8% less equivalent work.

6. Reducing the rich loading of the MEA runs to a more conservative value of 0.48 reduced the efficiency of each configuration by 2%-9%. The configuration least affected by the loading change was the interheated column.

7. Increasing the stripping temperature of 8 m PZ from 120 °C to 150 °C reduced the work requirement by 1% to 3% at optimal lean loadings, depending on the configuration.

8. Using laboratory rate data and an isothermal absorber approximation at 40 °C, rich/lean loadings sets of 0.48/0.40 and 0.40/0.31 for 9 m MEA and 8 m PZ, respectively, were found to require an equivalent packed area in the absorber.

9. The minimum equivalent work for the stripper was found with understripped lean loadings when simulating 9 m MEA, but the optimal lean loadings for 8 m PZ were higher, hovering around the saturation $CO_2$ equilibrium partial pressure at 40 °C.

10. A simple stripper had the best improvement of 11% when changing the system from 9 m MEA at 120 °C to 8 m PZ at 150 °C.

11. Compared to a simple stripper, 9 m MEA benefited from the 2-stage flash due to a reduction in compression work. In contrast, 8 m PZ showed a decrease in efficiency because its benefit in compression work was smaller than the increase in heat work.

12. 8 m PZ consistently had a lower energy requirement than 9 m MEA when using a rich loading which accounted for the faster reaction rate of PZ in the absorber. The simple stripper and complex configurations with packed columns demonstrated substantial improvement of 9% to 11% better energy performance with PZ. The multi-stage flash configurations were 3% to 4% better with PZ.

13. Equivalent work optimization yielded higher optimal lean loadings than heat duty optimization.

14. The heat exchangers were imbalanced due to unequal rich and lean heat capacity flows and rich solvent flashing. Rich bypass around the exchanger could resolve this inefficiency.

15. Heat recovery from the intercoolers of the multi-stage compressor and energy recovery from the lean solvent through a liquid expansion turbine could both reduce the energy requirement, but the benefit would be marginal. Heat recovery from intercoolers could recycle 20.6 kJ/mol $CO_2$ assuming a stripper pressure of 2 bar, and the maximum benefit of using a liquid expansion turbine would be 1% of the total equivalent work.

# Chapter 4: Optimization Case Studies

The previous chapter focused heavily on the potential improvement in stripping efficiency by increasing configuration complexity or switching to a new solvent like PZ with more favorable qualities. Though the equivalent work requirement was reduced by 14%, further work should be done to continue reducing the energy usage and approach the thermodynamic minimum. This chapter focuses on several case studies to improve the stripper performance or address the accuracy of calculations in the current approach. Bypass of the cold rich solvent around the main cross exchanger directly to the stripping vessel(s) was used as a method of condensing stripping steam by direct contact cooling. Geothermal heat was explored with a modified 2-stage flash configuration. Lastly, a collaboration helped to more accurately calculate the penalty of $CO_2$ separation and compression, and it also allowed for a comparison to the current calculation approach.

## 4.1. Room for Expansion of Analysis

Chapter 3 demonstrated that increasing stripper complexity can improve the energy performance. Additionally, 8 m PZ further reduced the energy requirement by decreasing compression work through increased stripper pressure and by reducing the solvent circulation rate. The minimum work requirement was 30.5 kJ/mole $CO_2$, but the thermodynamic minimum work of separation and compression to 150 bar is 17.3 kJ/mole $CO_2$. Some inefficiencies in the process are unavoidable due to mechanical limitations;

this includes the inefficiencies in the pumps and compressors. Heat exchangers also have implied irreversibility since a moderate approach temperature is required to use a reasonable exchanger size.

Chapter 3 focused on applying individual types of complexity to configurations to see how each affected energy performance. A common source of wasted heat was stripping steam. The water vapor that escaped with $CO_2$ could only be reduced to equilibrium conditions at the top of the columns. All of the heat that supplied the energy to generate the water vapor went to waste when the gas was cooled and water was condensed. Water condensing was done before the multi-stage compressor as well as between stages. A majority of the water was condensed in the pre-cooler which ran at 40 °C. Therefore, recycling the heat contained in the water vapor instead of using the cold sink of cool water could improve the overall efficiency.

A downside of using steam for the stripper that was generated in the boiler of the coal plant is that this steam would feasibly only be available at one temperature. A plant would be designed to draw steam at a single point at the IP/LP crossover, which would be at a specific pressure and temperature. Although isothermal stripping is the most reversible approach from a thermodynamic standpoint, a large temperature swing exists between the absorber and stripper. Therefore, methods should be explored that utilize heat at multiple temperature levels. With this consideration, non-isothermal configurations could be designed to take advantage of heat sources that are available at multiple temperature levels.

The decomposition method was adopted for this work to simplify the analysis of the stripper. The absorber and stripper each have problems that are very different from each other, so it was helpful to evaluate the stripper without considering the impact of the absorber. Additionally, the stripper has always been simulated without considering the

direct impact of drawing steam from the power generation cycle. While it was fair to assume that these two sections have little direct impact on the optimization of the stripper, a fully rigorous and credible analysis should expand its scope as much as possible. This type of analysis could confirm or refute the assumptions that have been made for the types of simulations that were done in Chapter 3 and other previous work by different authors.

## 4.2. COLD RICH BYPASS TO IMPROVE 2-STAGE FLASH PERFORMANCE AT PILOT PLANT

In previous configurations, high mole fraction of non-$CO_2$ components in the overhead vapor resulted in reduced performance. Water vapor in the overhead stream, stripping steam, was especially present in configurations without packing as well as when 8 m PZ was used. Since the configurations were modeled with the hot overhead streams being condensed with cooling water, heat trapped in the form of stripping steam was wasted. Volatilized amine also represented non-optimal performance. The vapor amine concentration was always low compared to $CO_2$ and water, but its presence in the vapor could cause operational issues. Condensing amine on the compressor blades would cause corrosion, and high amine concentration in the return of condensate would increase its viscosity. In the case of 8 m PZ, high amine concentration in the condensate without dissolved $CO_2$ could risk precipitation and clog process units or pipes. Therefore, a method to reduce the vapor concentrations of both highly condensable impurities could improve the performance of various configurations/solvent systems.

Cold rich bypass was proposed as a simple modification to the 2-stage flash configuration. The flowsheet of bypass for a 2-stage flash is shown in Figure 4-1. This method has previously been used to take advantage of the heating capability of exiting

vapor (Leites et al., 2003; Mak, 2006). The rich solvent was bypassed around the cross exchanger and then directly to the flash vessels. A small amount of packing was used in the top section of each flash to countercurrently contact the cold rich solution with the rising hot vapor from the flash. This vapor/liquid contact served as a direct contact cooler for the vapor, condensing both water and amine vapor. In turn, $CO_2$ was also released from the rich solvent due to released latent heat of the condensing water and amine. This concept was expected to improve the energy performance and reduce the amine volatility of all configurations with both solvents. The analysis of this concept was limited to its application to a 2-stage flash, a simple stripper, and an interheated column. 8 m PZ was expected to have the greatest benefit with bypassed solvent due to its higher stripping steam requirement and high risk of precipitation with PZ. The 2-stage flash should experience the greatest improvement since it had no packing, so its vapor concentrations were at the equilibrium conditions of the high temperature reboilers.

Figure 4-1 used the pilot plant skid as the basis for the rich bypass flowsheet. The unique aspect of this process was the presence of two separate heat exchangers to perform the main heat exchange. The plant was originally designed to have a stripper temperature of 100 to 120 °C. The new high-temperature 2-stage flash skid was designed for operating PZ at 150 °C, so a second, high-pressure heat exchanger was added. This heat exchanger was designed to deliver the heat exchange necessary to attain 150 °C as well as withstand the high-pressure of PZ at elevated temperature.

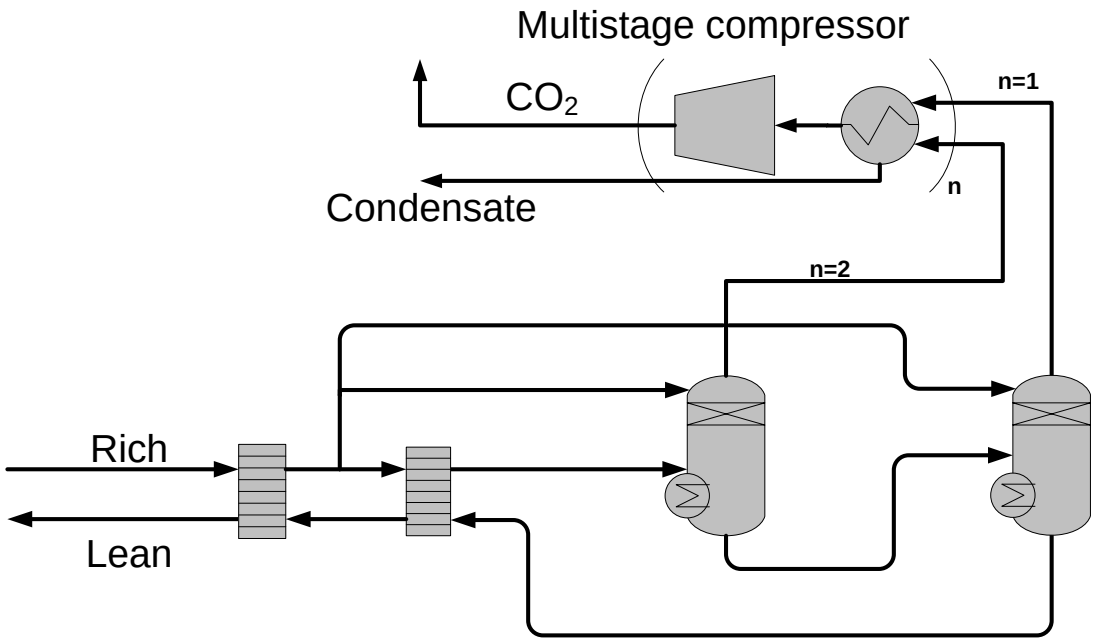


Figure 4-1. Cold rich bypass to both vessels of a 2-stage flash.

### 4.2.1. Benefit of Cold Rich Bypass for Pilot Plant Flowsheet

The first analysis of cold rich bypass considered drawing the bypass from this stream of rich solvent between the two heat exchangers, as shown in Figure 4-1. Bypass modifications were evaluated in two configurations:

1. Rich bypass to both the high-pressure and low-pressure vessels (2SF-LP/HP Byp).
2. Rich bypass to only the low-pressure vessel (2SF-LP Byp).

Bypass to both vessels was analyzed as a best case scenario for performance with bypass. However, since the low-pressure vessel was at the lowest loading, its vapor had the lowest concentration of $CO_2$ and the highest concentration of amine and water vapor. Therefore, rich bypass only this vessel was also considered to see whether bypass to both vessels was necessary.

The flowsheets were simulated with the Fawkes model for PZ to ensure correct representation of the amine volatility. Bypassing solvent around the high-pressure exchanger was going to change the balance of its approach temperatures, as well as change the amount of flashing that occurred within the exchanger. For that reason, a method more rigorous than specifying the cold side approach was needed. Assumptions were imposed on each heat exchanger to maintain constant performance. A constant LMTD of 5 °C was specified for the low-pressure heat exchanger. A constant average U was specified for the high-pressure heat exchanger. The total area of the high-pressure heat exchanger was 219.6 $ft^2$. The following fundamental equation for heat exchangers was used for this analysis:

$$\boldsymbol{Q = U\,A\,\Delta T} \qquad \textbf{4-1}$$

where $Q$ is the heat duty exchanged, $U$ is the overall heat transfer coefficient, $A$ is the heat exchanger area, and $\Delta T$ is the temperature difference between the hot and cold streams. Unless considering ideal cases, both the overall heat transfer coefficient and the temperature difference change throughout the exchanger area. Therefore, the expression must either be integrated along the exchanger area or approximated by calculating in pieces. The latter approach was used by utilizing a base case simulation of the 2-stage flash. The following calculations were for a 2-stage flash simulation with a 5 °C LMTD on the low-pressure exchanger, a rich loading of 0.4, and a lean loading of 0.26. The temperature profile in the high-pressure exchanger was calculated by splitting the heat duty into 5 segments. The profile is shown in Figure 4-2, and the conditions in the exchanger are detailed in Table 4-1.

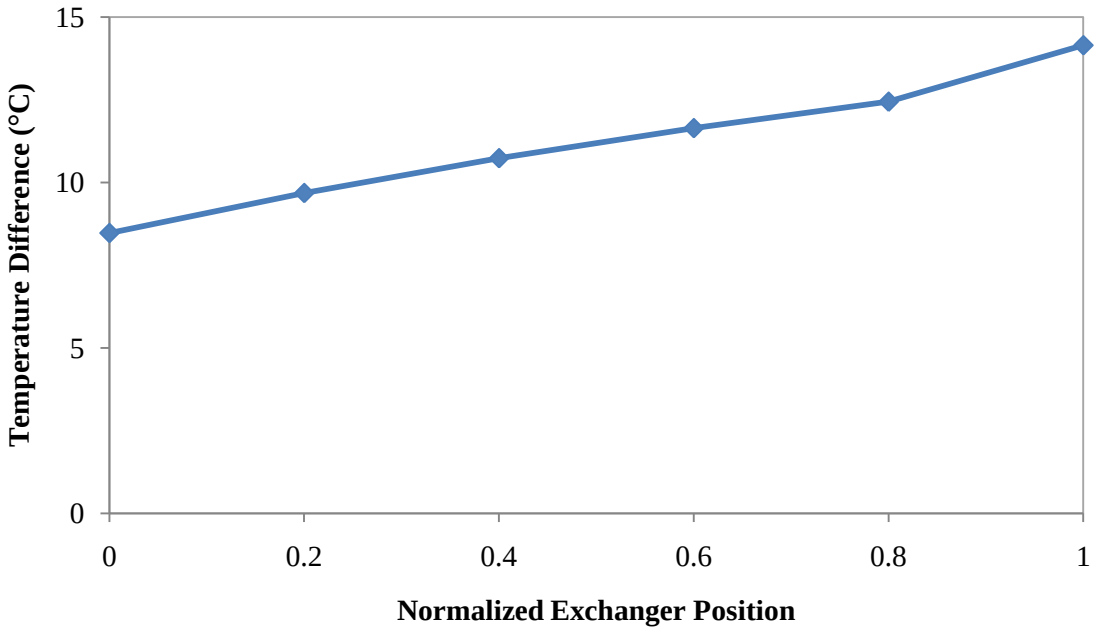


Figure 4-2. Profile of Temperature Difference between hot and cold streams in High-Pressure Heat Exchanger of 2-Stage Flash. 0 = cold side, 1 = hot side. 0.4 rich loading, 0.26 lean loading, 5 °C LMTD on low-pressure heat exchanger.

**Table 4-1. High-Pressure Exchanger Conditions for 2-Stage Flash Base Case, HP pressure = 13.5 bar.**

| Segment | Exchanger Position | Cold T | Hot T | Q | dT | UA |
|---|---|---|---|---|---|---|
| | | *°C* | *°C* | *kW* | *°C* | *kW/°C* |
| 0 | 0 | 90.0 | 98.5 | | 8.5 | |
| 1 | 0.2 | 99.2 | 108.9 | 36.0 | 9.7 | 3.96 |
| 2 | 0.4 | 108.5 | 119.3 | 36.0 | 10.7 | 3.52 |
| 3 | 0.6 | 117.9 | 129.6 | 36.0 | 11.6 | 3.22 |
| 4 | 0.8 | 127.4 | 139.8 | 36.0 | 12.4 | 2.99 |
| 5 | 1 | 135.9 | 150.0 | 36.0 | 14.2 | 2.71 |

The total heat duty in the high-pressure heat exchanger was 179.9 kW, so each of the five segments exchanged 36.0 kW. The temperature difference for each segment was assumed to be the average of its hot side and cold side values of ΔT. Therefore, the UA for each segment could be calculated as follows:

$$UA_i = \frac{Q_i}{(\Delta T_i + \Delta T_{i+1})/2} \qquad 4\text{-}2$$

where *i* is the segment. The sum of all $UA_i$ values gave an overall UA and was divided by the exchanger area (219.6 $ft^2$) to give a calculated average U. This calculation gave an average U of 0.804 kW/m-K.

For all following calculations, the same average U was specified for the high-pressure heat exchanger. Several beneficial effects were observed by splitting the rich solvent and contacting the high temperature vapor in either stream with the cold liquid, detailed in Table 4-2. The bypass to each vessel was 5% of the total rich solvent, and the packed sections were 12 in of Mellapak 500Y. The diameter of the packing was set to be the same as the packing in the stripper column, 16.8 inches. The flood at this diameter varied from 4 to 10% with a range of rich bypass from 0 to 25%. The total PZ contained in the vapor was calculated as the combined molar flow rate of PZ released from both flash vessels, and it was normalized by the stripped $CO_2$ rate.

A simple stripper under the same heat exchange specifications was reported for a baseline comparison. The data in Table 4-2 demonstrated the importance of improving performance and reducing volatility at low lean loading where water and amine concentrations in the vapor were high. In the simple stripper baseline, total released PZ increased by 18% when the lean loading decreased from 0.30 to 0.26 because the PZ concentration increased from 527 to 576 ppm and the $CO_2$ concentration decreased. There was a substantial increase in PZ volatility and equivalent work when switching from a simple stripper to 2-stage flash at both lean loadings. Bypassing solvent to only the low-pressure flash significantly improved the volatility and performance. At lean loadings of 0.26 and 0.30, the released PZ improved by 54 and 63%, and the equivalent work decreased by 8.3 and 6.7%, respectively. Including bypass to the high-pressure

vessel improved performance more, but the effect was not as significant as bypassing to the low-pressure vessel. The lower amine and water concentration in the high-pressure vapor meant that there was less room for improvement than in the low-pressure vessel. Additionally, the pressure ratio of 2 resulted in the production vapor being weighted toward the low-pressure flash. Since more vapor was produced at the low pressure, it was more important to treat the low-pressure vapor with cold rich bypass.

Alternate cases were run with a pressure ratio between flash stages of 1.5. This lower pressure ratio yielded vapor flows that were more balanced on a molar basis. Table 4-3 shows the performance and decrease in PZ volatility at these conditions.

Since this pressure ratio of 1.5 balanced the production of vapor from the two flashes, the performance for these cases was better than the cases with a pressure ratio of 2. Another important conclusion from these cases with balanced vapor production was that adding bypass to the high-pressure vessel was nearly as important as adding bypass to the low-pressure vessel, especially when considering the reduction in the equivalent work. The cases with bypass to both vessels demonstrated equivalent work values less than the simple stripper baseline values presented in Table 4-2. The downside to implementing bypass to both flash vessels would be the implication of higher process complexity, which would result in a larger capital investment and more difficult process control. However, adding a short section of packing to the top of a flash vessel would be a less significant increase in capital compared to other high complexity configurations suggested in Chapter 3. The simulations were more difficult to converge when there were two interacting packed sections with countercurrent rate based vapor/liquid calculations.

**Table 4-2. Improvement with 5% Cold Rich Bypass in 2-Stage Flash. 150 °C reboilers, rich loading = 0.40, $P_{HP}/P_{LP}$ = 2, compression to 150 bar. LP HX = 3 °C cold side approach, HP HX = constant UA (16.4 kW/K).**

| Rich loading | Lean loading | Configuration | Total heat duty | HP PZ | LP PZ | Total PZ in vapor | Equivalent work | Cold approach | Hot approach |
|---|---|---|---|---|---|---|---|---|---|
| *mol/mol* | *mol/mol* | | *kJ/mol $CO_2$* | *ppm* | | *mmol PZ/ kmol $CO_2$* | *kJ/mol $CO_2$* | *°C* | *°C* |
| 0.4 | 0.26 | SS | 106.1 | - | 576 | 0.92 | 33.2 | 8.0 | 17.5 |
| 0.4 | 0.26 | 2SF | 130.1 | 894 | 3949 | 6.64 | 38.7 | 7.7 | 12.6 |
| 0.4 | 0.26 | 2SF-LP Inj | 113.7 | 873 | 2138 | 3.08 | 35.5 | 8.3 | 10.4 |
| 0.4 | 0.26 | 2SF-LP/HP Inj | 107.4 | 15 | 2211 | 2.79 | 34.2 | 8.5 | 9.0 |
| 0.4 | 0.3 | SS | 101.0 | - | 527 | 0.78 | 32.5 | 6.8 | 13.4 |
| 0.4 | 0.3 | 2SF | 108.7 | 557 | 2106 | 3.00 | 36.4 | 6.5 | 8.1 |
| 0.4 | 0.3 | 2SF-LP Inj | 96.0 | 548 | 848 | 1.10 | 34.0 | 6.5 | 6.8 |
| 0.4 | 0.3 | 2SF-LP/HP Inj | 93.7 | 33 | 918 | 1.00 | 33.4 | 6.7 | 5.7 |

**Table 4-3. Improvement with 5% Cold Rich Bypass in 2-Stage Flash. Rich loading = 0.40, $P_{HP}/P_{LP}$ = 1.5, compression to 150 bar. LP HX = 3 °C cold side approach, HP HX = constant UA (16.4 kW/K).**

| Rich loading | Lean loading | Configuration | Total heat duty | HP PZ | LP PZ | Total PZ in vapor | Equivalent work | Cold approach | Hot approach |
|---|---|---|---|---|---|---|---|---|---|
| *mol/mol* | *mol/mol* | | *kJ/mol $CO_2$* | *ppm* | | *mol PZ/ kmol $CO_2$* | *kJ/mol $CO_2$* | *°C* | *°C* |
| 0.4 | 0.26 | 2SF | 127.1 | 1560 | 3918 | 5.59 | 37.3 | 7.8 | 14.5 |
| 0.4 | 0.26 | 2SF-LP Inj | 112.5 | 1555 | 1673 | 2.80 | 34.4 | 8.4 | 12.7 |
| 0.4 | 0.26 | 2SF-LP/HP Inj | 101.5 | 167 | 1741 | 1.49 | 32.2 | 8.5 | 11.1 |
| 0.4 | 0.3 | 2SF | 107.4 | 927 | 2090 | 1.81 | 34.5 | 5.7 | 10.1 |
| 0.4 | 0.3 | 2SF-LP Inj | 96.3 | 925 | 456 | 0.74 | 32.3 | 6.8 | 8.8 |
| 0.4 | 0.3 | 2SF-LP/HP Inj | 86.6 | 49 | 476 | 0.24 | 30.7 | 6.7 | 7.5 |

### 4.2.2. Balancing Temperature Difference Driving Force in Heat Exchanger with Bypass

Typically the lean solvent flow rate is smaller than the rich flow since $CO_2$ and water exit in the overhead. This effect reduces the temperature increase of the rich solvent, so the rich solvent does not approach the lean solvent temperature as closely. Additionally, the rich solvent can begin to flash in the heat exchanger, which reduces its temperature increase even further. Therefore, the hot side approach is typically higher than the cold side approach in optimized flowsheets. Bypassing rich solvent around the heat exchanger can undo this effect by equalizing the capacity flow rates for the countercurrent streams and overcompensating for flashing that occurs in the rich solvent. This effect is shown in Figure 4-3. The trends were shown with a lean loading of 0.30 and bypass only to the low-pressure vessel, but the trends were similar for all lean loadings and bypass configurations. The main variables that affected balancing temperature differences across the heat exchanger was the total bypass percentage around the main heat exchanger.

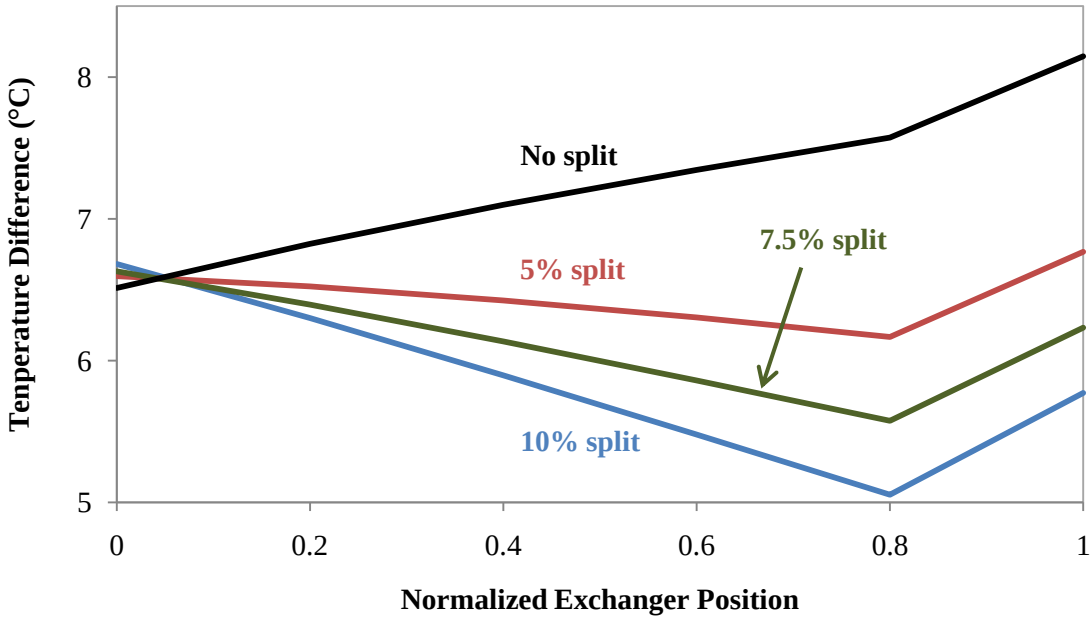


Figure 4-3. Temperature difference profile of the high-pressure heat exchanger with varying bypass percentage to low-pressure flash. 8 m PZ, 0.4 rich loading, 0.3 lean loading.

The temperatures within the heat exchanger were calculated at the hot and cold ends as well as for evenly spaced points within the exchanger. The cold side approach was fairly constant with varying split percentages because the low-pressure heat exchanger performance was constant and had consistent rich and lean flow rates between cases. The hot side approach decreased as the bypass around the high-pressure exchanger increased. The amount of flashing increased with more bypass as the less rich solvent was being heated by the same amount of lean solvent. In Figure 4-3, the sharp increases in temperature difference toward the hot end of the exchanger indicated the relative magnitude of flashing. This flashing would become especially important in the design of the heat exchanger if a smaller temperature approach were used along with a high bypass percentage. In such a scenario, although the cold and hot temperature approaches might

suggest a feasible exchanger design, there could be a temperature pinch within the exchanger.

### 4.2.3. Sensitivity Analyses

The goal of this work was to simulate conditions that might be expected at the pilot plant is bypass concept were implemented and determine the optimal operating conditions. In section 4.2.1 bypass was evaluated 5% split, 12 inches of Mellapak 500Y packing with a diameter of 16.8 inches, and lean loadings of 0.26 and 0.30. In this section, the sensitivity of the flowsheet performance to each of these variables was evaluated. The flowsheets were not being evaluated as upgrades to existing processes, so an arbitrary rich solvent flow rate of 50 kmol/s was used. Consequently, the diameter of packing was not a meaningful result, but the flood was maintained at 80% by varying the diameter.

First, the required height of packing was analyzed, shown in Figures 4-4 and 4-5. These figures demonstrated that the base case of 12 inches of packing was sufficient to maximize both performance and PZ capture. When considering a lean loading of 0.26, the minimum height of packing to reach minimum equivalent work was approximately 8 inches, but 24 inches was required to reach the minimum PZ release rate at a lean loading of 0.30. Nonetheless, 12 inches of packing approached the minimum equivalent work and minimum PZ release rate at lean loadings of 0.26 and 0.30.

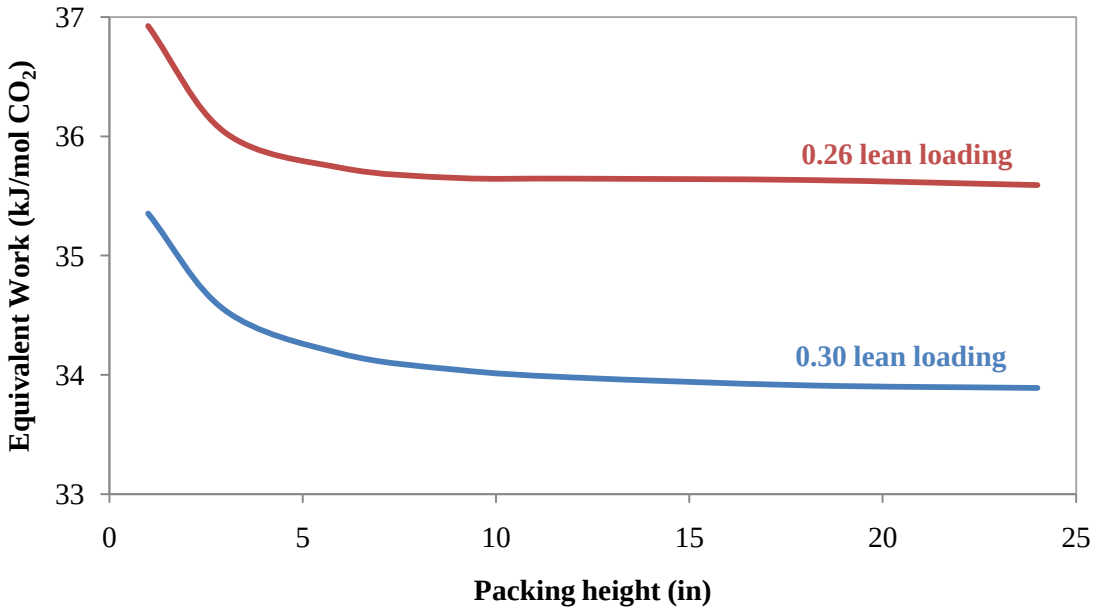


Figure 4-4. Decrease in equivalent work with greater packed height. 8 m PZ, 150 °C reboilers, 0.40 rich loading, 5% bypass of rich solvent before high-pressure cross exchanger, bypass only to low-pressure flash, pressure ratio = 2.

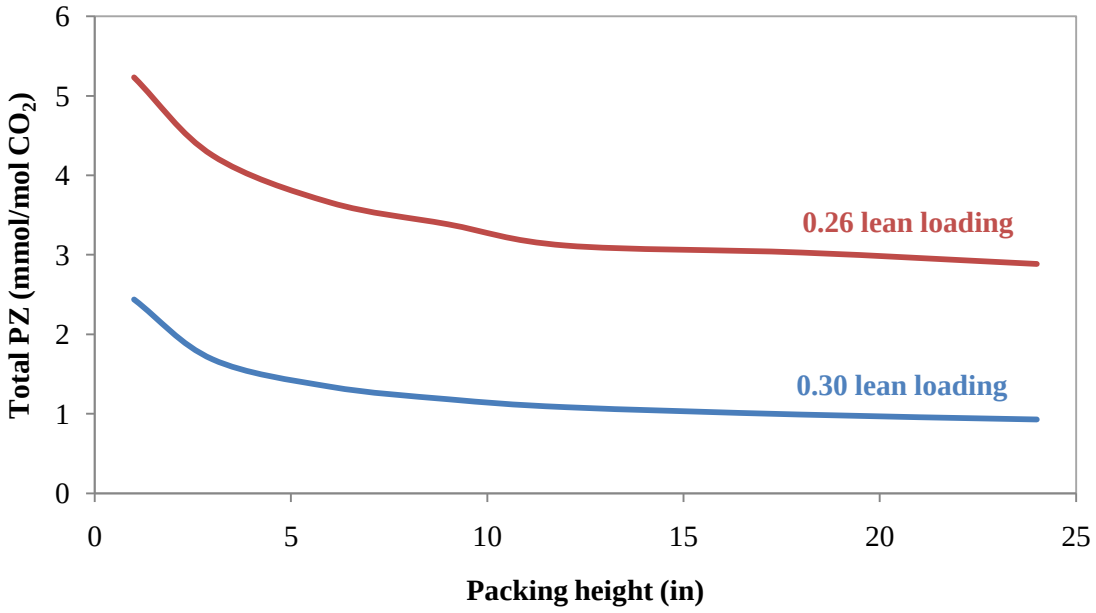


Figure 4-5. Decrease in released PZ with greater packed height. 8 m PZ, 150 °C reboilers, 0.40 rich loading, 5% bypass of rich solvent before high-pressure cross exchanger, bypass only to low-pressure flash, pressure ratio = 2.

A lean loading of 0.3 was closer to optimal with the base case 2-stage flash than 0.26, so the predicted equivalent work with 5% bypass was also lower at all packed heights. The volatility of PZ was also lower at the lean loading of 0.3 since less free anime was available in solution. Consequently, the total released PZ was lower for all packing heights at a lean loading of 0.3 than at 0.26.

The sensitivity of equivalent work and released PZ to bypass percentage was also analyzed. Again, this analysis was performed with bypass only the low-pressure flash vessel, but a similar trend would be seen with split to the high-pressure vessel. Unlike the effect of packing height, bypass percentage did not have the same effect on equivalent work as it did on PZ release rate. The effects for equivalent work and PZ release rate are shown in Figures 4-6 and 4-7, respectively.

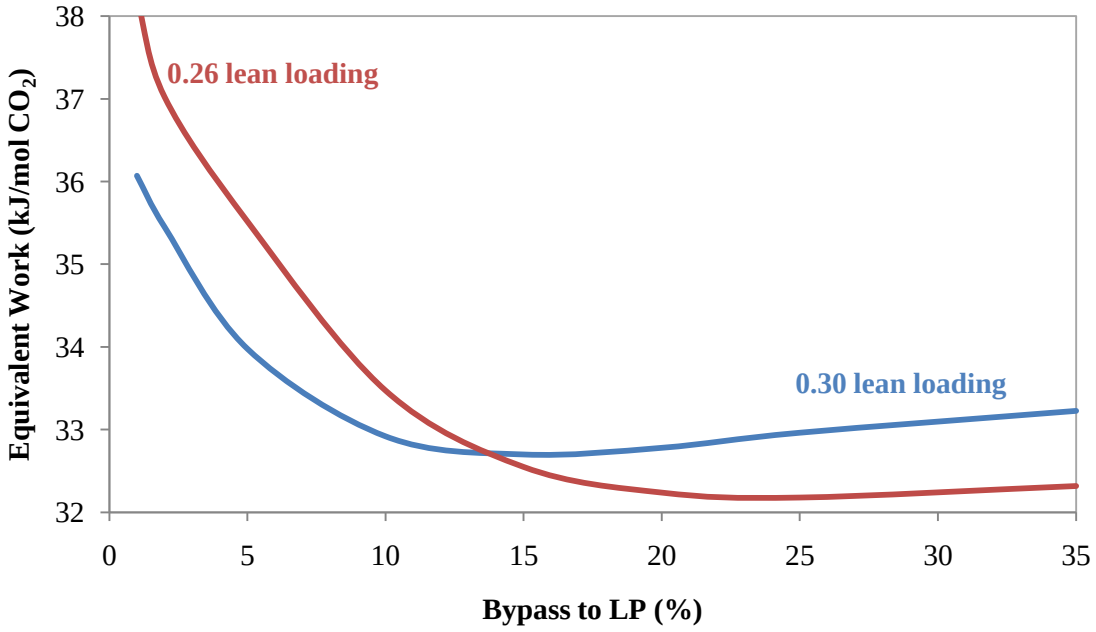


Figure 4-6. Minimization of equivalent work with bypass to low-pressure flash vessel. 8 m PZ, 150 °C reboilers, 0.40 rich loading, bypass only to low-pressure flash, bypass to 12 in of Mellapak 500Y packing, pressure ratio = 2.

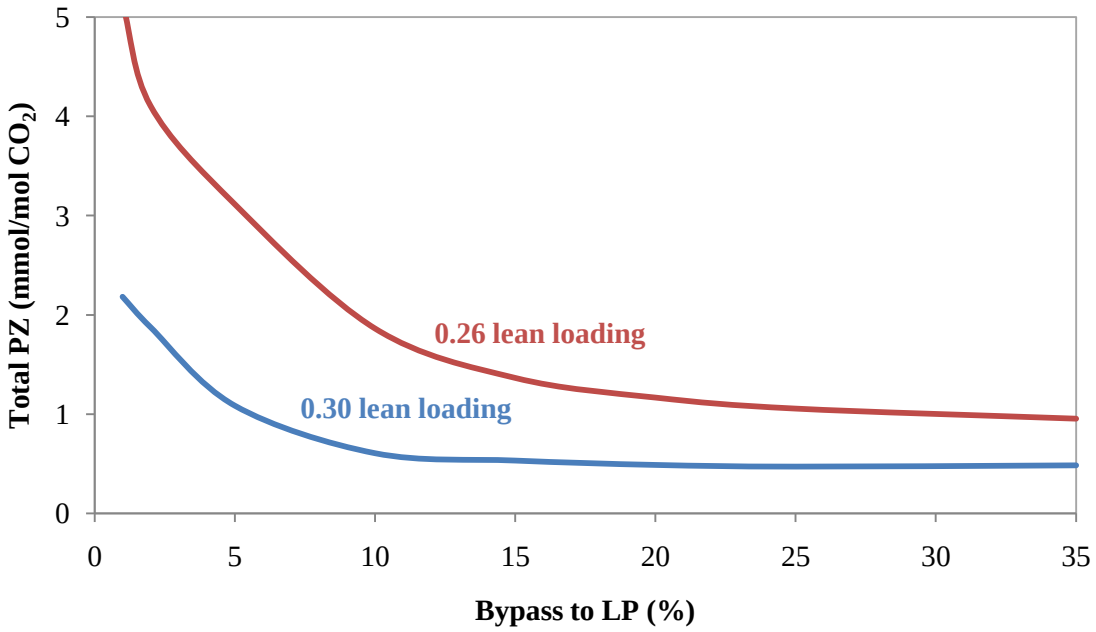


Figure 4-7. Decrease in released PZ with higher bypass to low-pressure flash vessel. 8 m PZ, 150 °C reboilers, 0.40 rich loading, bypass only to low-pressure flash, bypass to 12 in of Mellapak 500Y packing, pressure ratio = 2.

Surprisingly, the minimum equivalent work with a lean loading of 0.26 dropped below the predictions for a lean loading of 0.3 when the bypass was greater than 15%. A higher bypass percentage transitioned the flowsheet more to a simple stripper as opposed to a 2-stage flash. The main heat exchanger was not properly utilized at high bypass, and heat was used to increase the solvent temperature instead of cross exchange or countercurrent contact the vapor. As seen in Figure 4-8, the optimal lean loading decreased with increasing bypass.

If the split to the high-pressure vessel was also included in this type of analysis, the ratio of bypass split to the high-pressure and low-pressure vessels would also need to be optimized. The water and PZ vapor content of each stream would be different, so the optimal bypass to each vessel would be unique.

Figure 4-8 shows the optimization of lean loading when considering bypass to the low-pressure flash vessel. The curves of equivalent work and total released PZ are shown for 5% and 10% bypass the low-pressure vessel. This analysis showed that bypass improved the performance and reduced the amount of volatilized amine, but the process conditions must be re-optimized. When increasing the bypass from 5 to 10%, the minimum equivalent work was reduced from 33.9 to 32.6 kJ/mol $CO_2$, and the optimal lean loading was reduced from 0.293 to 0.285.

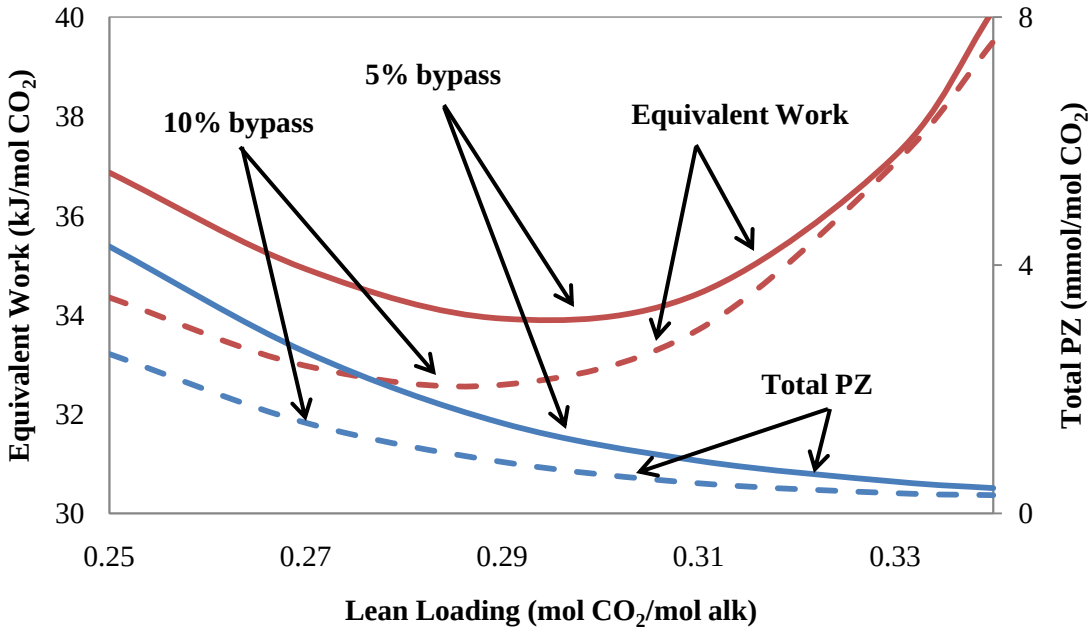


Figure 4-8. Equivalent work and total released PZ variations with lean loading. 8 m PZ, 150 °C reboilers, 0.40 rich loading, bypass only to low-pressure flash, bypass to 12 in of Mellapak 500Y packing, pressure ratio = 2.

When using bypass only to the LP flash vessel and a pressure ratio of 2, the optimal run conditions were 10% bypass and a lean loading of 0.29. The predicted liquid and vapor temperatures within the 12 inches of packing are depicted in Figure 4-9. The concentration of $CO_2$ in the vapor is also described. From this plot it was apparent that 12 inches of packing was not enough to attain equilibrium at the top of the column; the

temperatures and compositions of the liquid and vapor were still changing at the top. However, as shown in Figure 4-5, 12 inches of packing was nearing the height of minimum equivalent work. At these conditions, the 2-stage flash base case with no bypass had an LP vapor $CO_2$ concentration of 49.1%, and Figure 4-9 shows the improvement to 72.5% at the top of the column. It was clear that this bypass modification benefited performance by improving the $CO_2$ selectivity and reducing the temperature of the overhead vapor. The reduced temperature of the vapor cut down on the wasted heat in the condenser.

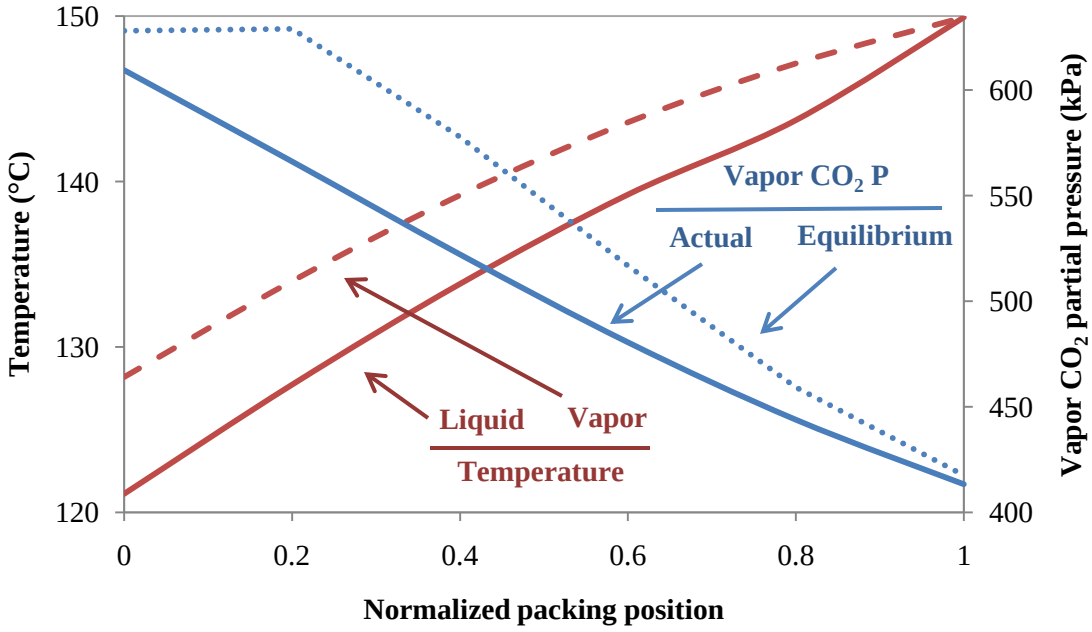


Figure 4-9. Predictions of vapor and liquid temperatures and vapor $CO_2$ concentration for optimum bypass case with 2-stage flash using 8 m PZ. 10% bypass to LP flash, 0.40 rich loading, 0.29 lean loading, 12 inches Mellapak 500Y, pressure ratio = 2.

The McCabe-Thiele plot for the same case is shown in Figure 4-10. The column nears an equilibrium pinch toward the bottom of the column, right above the reboiler. The other noticeable characteristic of the diagram was $CO_2$ absorption that occurred at the top of the column where the cold bypass entered. The cool rich solvent was 113 °C in

this case, and Figure 4-9 shows that it quickly heated up to 121 °C upon contacting the 128 °C vapor. The rich solvent condensed water and absorbed a small amount of $CO_2$, increasing the loading by 0.002. As the liquid continued down the packing, it cooled the vapor, condensed water, and released $CO_2$. This effect was similar to the "free stripping" effect that was observed in the double matrix configuration (Figure 3-5). However, in this case the flowsheet was not complicated by adding a semi-lean stream that should be introduced to an optimized absorber mid-point.

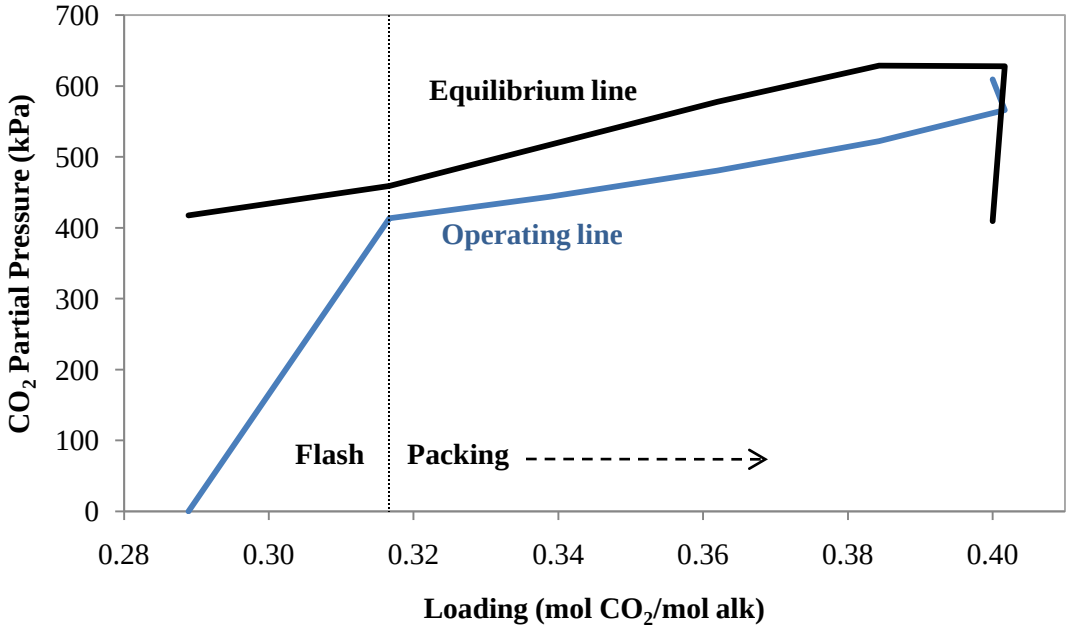


Figure 4-10. McCabe-Thiele diagram for optimum bypass case with 2-stage flash using 8 m PZ. 10% bypass to LP flash, 0.40 rich loading, 0.29 lean loading, 12 inches Mellapak 500Y, pressure ratio = 2.

The performance of the main heat exchanger is plotted in Figure 4-11. The temperature difference driving force was more balanced compared to the 2-stage flash base case. More flashing occurred toward the hot end of the exchanger, qualitatively described by the sharper change in steepness on the hot side of the exchanger. The

variability in the temperature difference was reduced by balancing the heat capacity flows of the rich and lean streams.

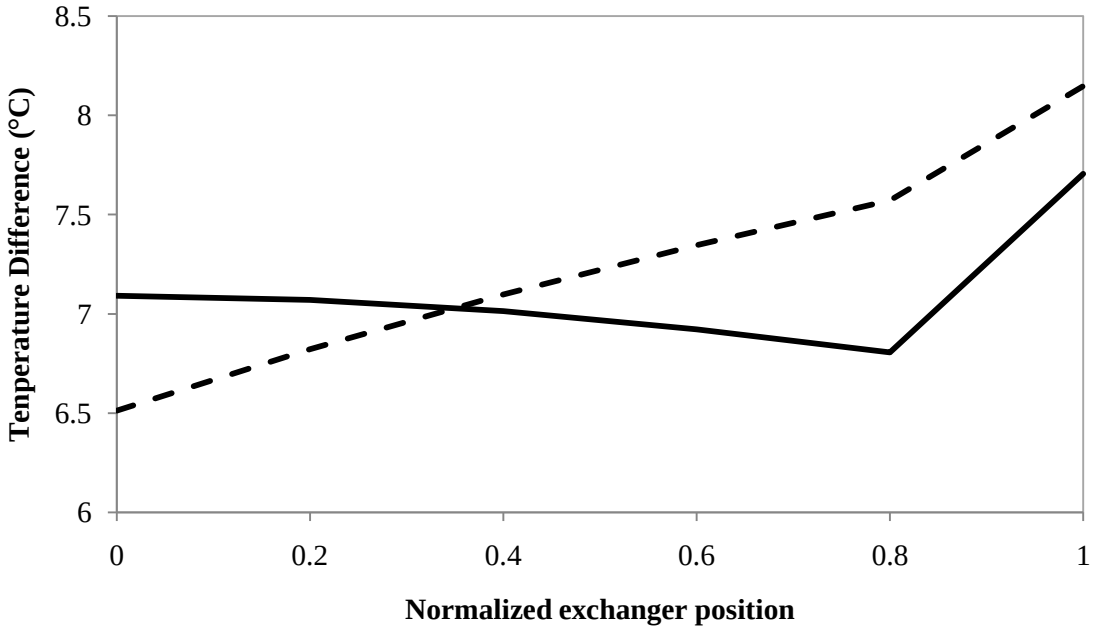


Figure 4-11. Cross exchanger performance of optimum bypass case. Lines-solid: 10% rich bypass, dashed: no bypass. Constant UA between cases calculated from pilot plant performance and exchanger area.

This analysis demonstrated that cool rich bypass would be an advisable upgrade to the 2-stage flash flowsheet of the pilot plant skid. 12 inches of packing was sufficient to approach minimum equivalent work and volatilized PZ. Performance improved with increasing bypass, but excessive bypass had a negative effect on equivalent work because very little stripping occurred at the high-pressure. When using a pressure ratio between flashes of 2, bypass to the low-pressure vessel had a greater effect than bypass the high-pressure vessel because the majority of the vapor was produced in this flash. However, bypass to the high-pressure vessel was also beneficial when considering a pressure ratio between flashes of 1.5 where the vapor production rate of the two vessels was more balanced. In fact, bypass to both flash vessels dropped the work requirement below that

of a simple stripper under similar heat exchange conditions when a pressure ratio of 1.5 was used. Using the heat exchanger performance from the pilot plant, the equivalent work requirement with a lean loading of 0.30 was 32.5 kJ/mol $CO_2$. A 2-stage flash with bypass to both vessels, a lean loading of 0.30, and a pressure ratio of 1.5 had a predicted performance of 30.7 kJ/mol $CO_2$. The total amount of released PZ was decreased by 87% from the standard 2-stage flash at these conditions.

When considering a pressure ratio of 1.5 and bypass only to low-pressure flash, the optimal lean loading decreased to 0.285 and the minimum equivalent work was 32.6 kJ/mol $CO_2$. This performance required 12 inches of packing to contact 10% bypass.

## 4.3. Cold Rich Bypass Applied to Generic Configurations

The analysis in section 4.2 was directed toward an application specific for the pilot plant skid that we used at the J. J. Pickle Research Center. A main hindrance of this analysis was the specific performance of the heat exchanger. A fully optimized process would have a heat exchanger designed specifically for the process to obtain a desirable approach temperature. For this reason, 8 m PZ was evaluated again with bypass to a 2-stage flash. This same flowsheet was also evaluated with 9 m MEA as a comparison. Next, these two solvents were evaluated with cold rich bypass to a simple stripper. Finally, bypass to an interheated column using 8 m PZ was also evaluated since this flowsheet without bypass was the most efficient option that was explored in Chapter 3. The simulations with PZ were modeled using the 5deMayo model, and the simulations with MEA were modeled using the Hilliard model. The packed section for contacting the vapor with the bypassed solvent was held constant at 12 inches of Mellapak 500Y, and the main cross exchange performance was held constant with a 5 °C LMTD. A constant

UA in the exchanger was not used as it was in the previous section because a single heat exchanger was modeled and it was not designed from pilot plant specifications. The heat exchangers in this section could be designed to meet the 5 °C LMTD specification.

### 4.3.1. Bypass with 8 m PZ and 2-Stage Flash

This system was reevaluated using the bypass approach that would be applied to each of the other combinations of solvent and configuration. As seen in Figure 4-12, the rich bypass was taken before the main cross exchanger, so the solvent being injected to the top of the vessels was colder than in the analysis in section 4.2.

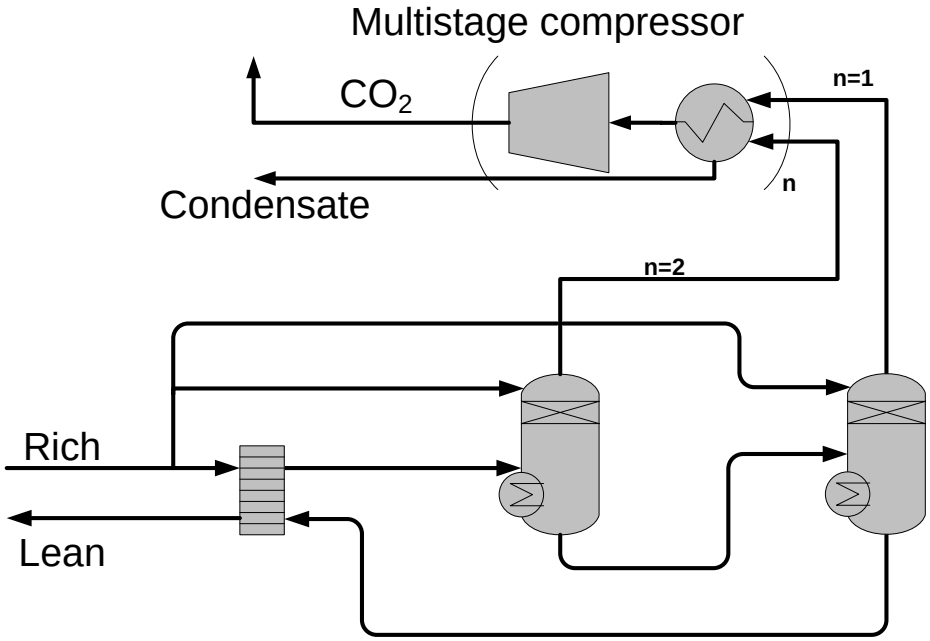


Figure 4-12. Cold rich bypass to low-pressure vessel of 2-stage flash. Bypass drawn before main cross exchanger.

The trend of equivalent work with changing bypass was similar to what was seen in section 4.2. The trends are shown in Figure 4-13. The minimum work requirement without bypass was 32.5 kJ/mol $CO_2$, and the optimal bypass flowsheet reduced the work

requirement to 29.8 kJ/mol $CO_2$, a reduction of 8.2%. This flowsheet used a bypass of 7.5%. When using low values of lean loading, the optimal bypass percentage was higher because more water was contained in the vapor. Therefore, more cold solvent was usable to cool the vapor and condense water. In contrast, running with a high lean loading and high bypass introduced a parasitic use of heat to bring the cold solvent up to the stripper temperature of 150 °C.

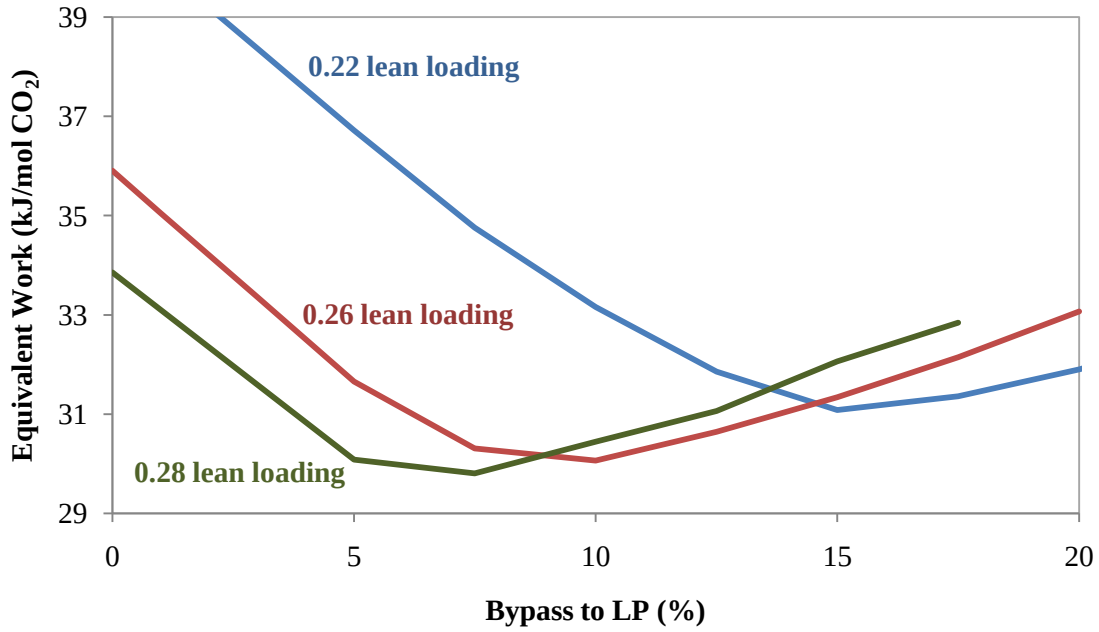


Figure 4-13. Equivalent work requirement for 8 m PZ in 2-stage flash with bypass to low-pressure flash. 150 °C reboilers, 0.40 rich loading, equal molar vapor production per stage, 5 °C LMTD in main cross exchanger, compression to 150 bar.

The temperature profile of the liquid and vapor as well as the loading profile of the optimum case are displayed in Figure 4-14. The profiles with this cold rich bypass were more complicated than the previous results in section 4.2.3 with the bypass taken midway through the heat exchange. Since the bypass entered the packing at 50 °C in this case, the liquid and vapor temperatures were both significantly colder at the top of the packing when compared with Figure 4-9. Since the liquid was so cold, its equilibrium

$CO_2$ partial pressure was lower than the $CO_2$ partial pressure in the vapor, so $CO_2$ absorption occurred in the top 20% of the column as the liquid heated up. It must be re-emphasized that this simulation assumed equilibrium reactions within the packing. Future simulations should consider the implementation of kinetic reaction calculations since the reaction rates would start to become rate limiting at the lower temperature in the top of the column.

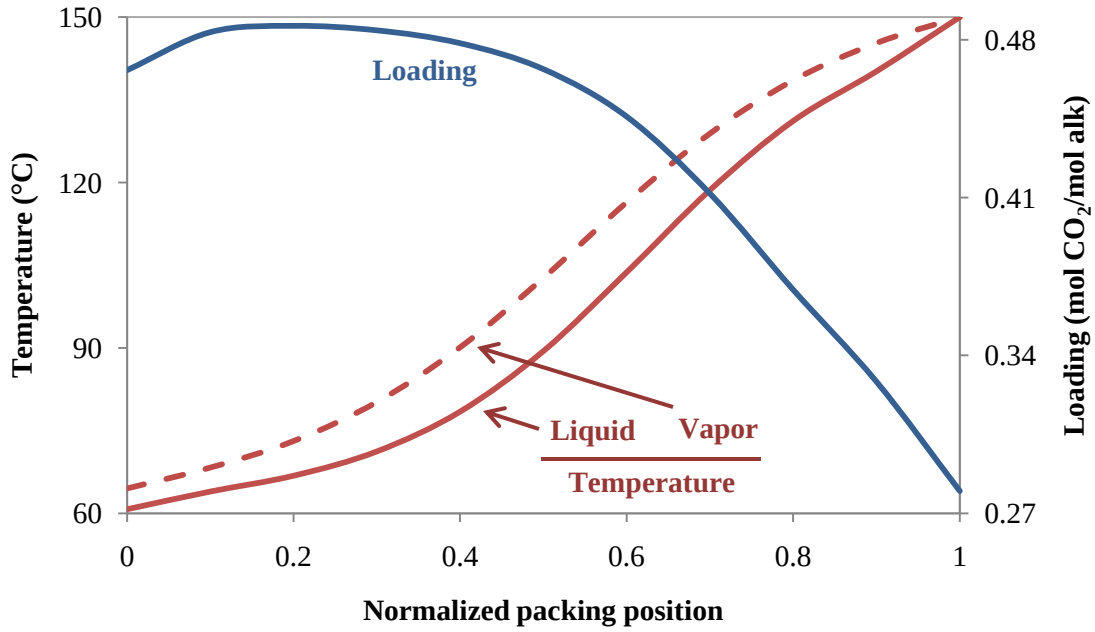


Figure 4-14. Temperature and loading profiles of optimum bypass case with 2-stage flash using 8 m PZ. 7.5% bypass to LP flash, 0.40 rich loading, 0.28 lean loading, 150 °C reboilers 12 inches Mellapak 500Y, equal molar vapor production per pressure stage.

The McCabe-Thiele plot for the same case is shown in Figure 4-15. The absorption at the top of the column was apparent in this diagram; the equilibrium partial pressure of the entering liquid was below the operating line until the loading increased to 0.486. As the liquid continued further down the packing, it cooled the vapor, condensed water, and released $CO_2$.

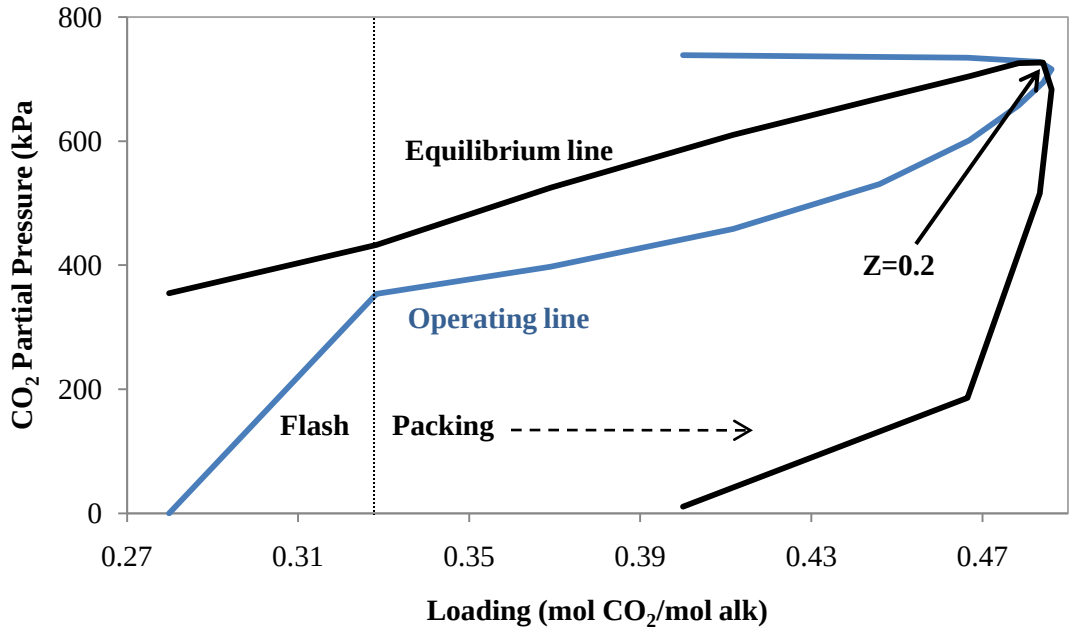


Figure 4-15. McCabe-Thiele diagram for optimum cold bypass case with 2-stage flash using 8 m PZ. 7.5% bypass to LP flash, 0.40 rich loading, 0.28 lean loading, 150 °C reboilers 12 inches Mellapak 500Y, equal molar vapor production per pressure stage.

Compared to the main analysis in section 4.2.3, the minimum work requirement with these specifications was lower. The colder temperature of the rich solvent condensed more water in the existing vapor and yielded a nearly pure stream of $CO_2$ to be fed to the multi-stage compressor. The $CO_2$ purity of the low-pressure vapor in the optimum case was 97%, improved from 46% without bypass. The high-pressure vapor only had a purity of 65%, so it could also realize some benefit from cold rich bypass. However, the required bypass rate would be lower all of the water would be condensed with a smaller amount of cold solvent.

### 4.3.2. Bypass with 9 m MEA and 2-Stage Flash

A 2-stage flash configuration was the ideal flowsheet with which to evaluate cold rich bypass. The vapor leaving the flashes was at high temperature and had high water

content, so contacting the overhead vapor with cold rich bypass could purify the stripped $CO_2$. MEA has a higher heat of absorption than PZ, so the water content of the overhead vapor was not as significant as with 8 m PZ, but it could still realize benefit. Similar to the previous section, the packed section for contacting the vapor with the bypassed solvent was held constant at 12 inches of Mellapak 500Y, and the main cross exchange performance was held constant with a 5 °C LMTD. The trends with varying lean loading and bypass are shown in Figure 4-16.

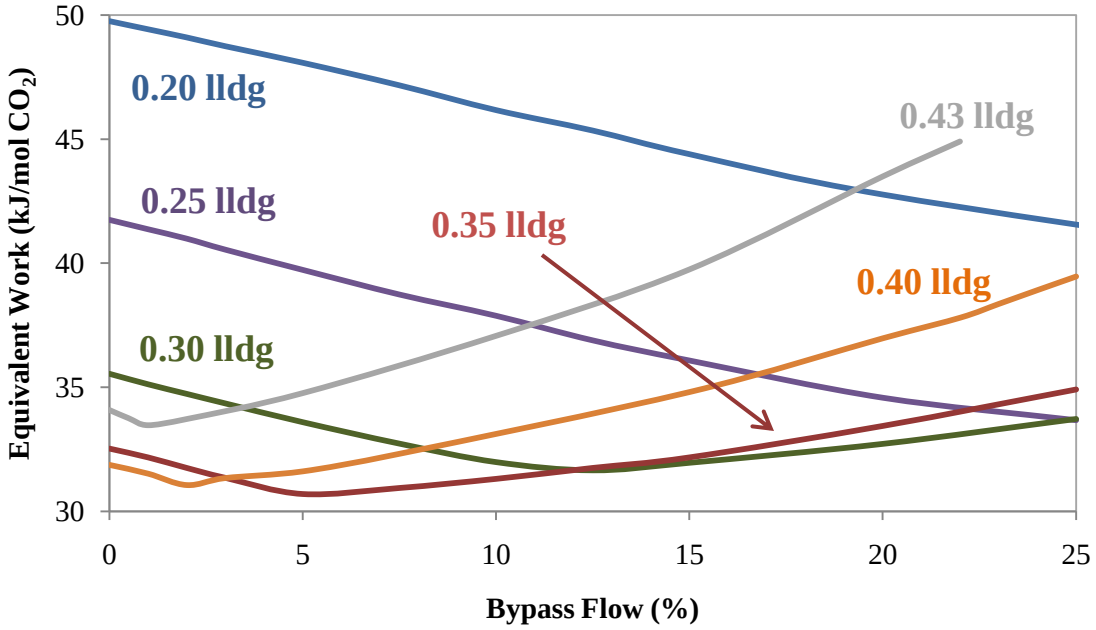


Figure 4-16. Equivalent work requirement for 9 m MEA in 2-stage flash with bypass to low-pressure flash. 120 °C reboilers, 0.50 rich loading, equal molar vapor production per stage, 5 °C LMTD in main cross exchanger, compression to 150 bar.

These simulations showed a much more distinct optimal bypass than the PZ simulations. The minimum equivalent work for each lean loading was not subtle and rounded, but there was a sharp upward inflection at the point where additional water vapor was not condensed with increasing bypass. These results also demonstrated the decreasing optimal value of bypass as lean loading increased. The optimal bypass was

1% for a lean loading of 0.43, but the optimal bypass increased to 5% at a lean loading of 0.35. The magnitude of optimal bypass was explained by the amount of water that needed to be condensed from the gas. The $CO_2$ purities of the overhead vapor with no bypass at these two loadings were 80% and 57%, respectively. The global optimum with bypass was 30.7 kJ/mol $CO_2$ with a lean loading of 0.35 and 5% bypass to the low-pressure vessel, compared to 31.7 kJ/mol $CO_2$ at a lean loading of 0.39 with no bypass. The improvement using this configuration with MEA was less than with PZ, only 3.2%. The difference was because the $CO_2$ purity of the low-pressure vapor in the optimum case using MEA without bypass was 69%, compared to 46% with PZ.

### 4.3.3. Bypass with 8 m PZ and Simple Stripper

The benefit of bypass in a simple stripper flowsheet was analyzed as a comparison to the 2-stage flash. Although the simple stripper contained packing that counter currently contacted rich solvent with vapor rising from the reboiler, cold rich bypass would cool the gas further and more effectively condense water vapor exiting from the column. The additional packed section for contacting the vapor with the bypassed solvent was held constant at 12 inches of Mellapak 500Y, and the main cross exchange performance was held constant with a 5 °C LMTD. The trends with varying lean loading and bypass are shown in Figure 4-17.

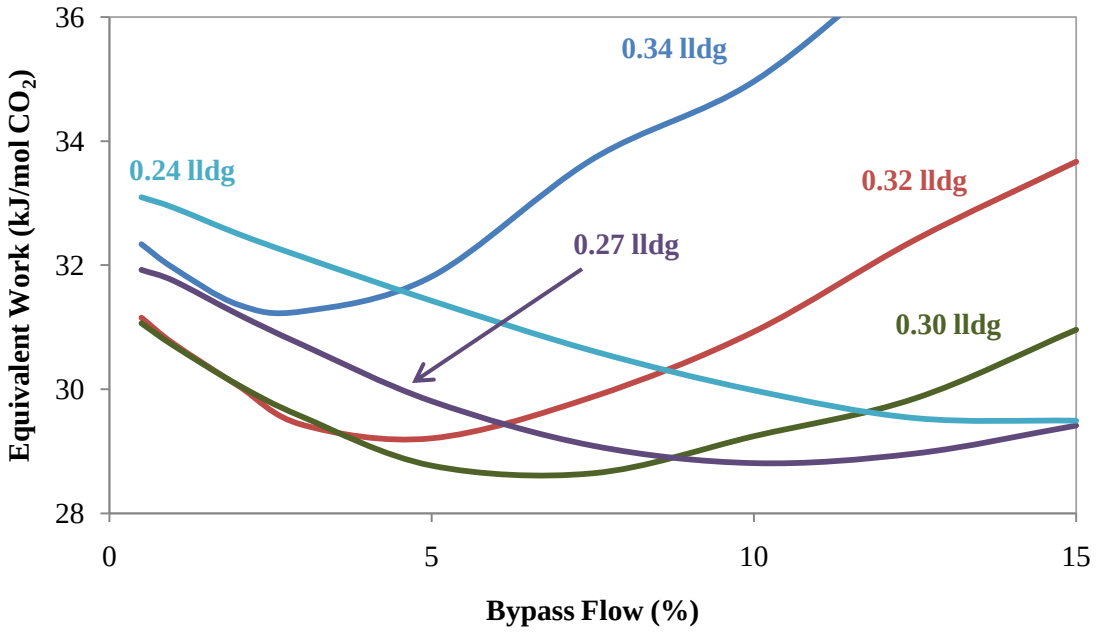


Figure 4-17. Equivalent work requirement for 8 m PZ in simple stripper. 150 °C reboiler, 0.40 rich loading, 5 °C LMTD in main cross exchanger, compression to 150 bar.

The simple stripper also showed a decrease in optimal bypass with increasing lean loading due to reduced water vapor content from the bypass case. The optimum case with no bypass had a $CO_2$ purity of 65% and an equivalent work of 31.4 kJ/mol $CO_2$. The minimum equivalent work when using bypass was 28.6 kJ/mol $CO_2$ at a lean loading of 0.30 and 7.5% bypass.

### 4.3.4. Bypass with 9 m MEA and Simple Stripper

Bypass was also analyzed in a simple stripper using 9 m MEA. This was the base configuration in the analysis of Chapter 3. The additional packed section for contacting the vapor with the bypassed solvent was held constant at 12 inches of Mellapak 500Y, and the main cross exchange performance was held constant with a 5 °C LMTD. The trends with varying lean loading and bypass are shown in Figure 4-18.

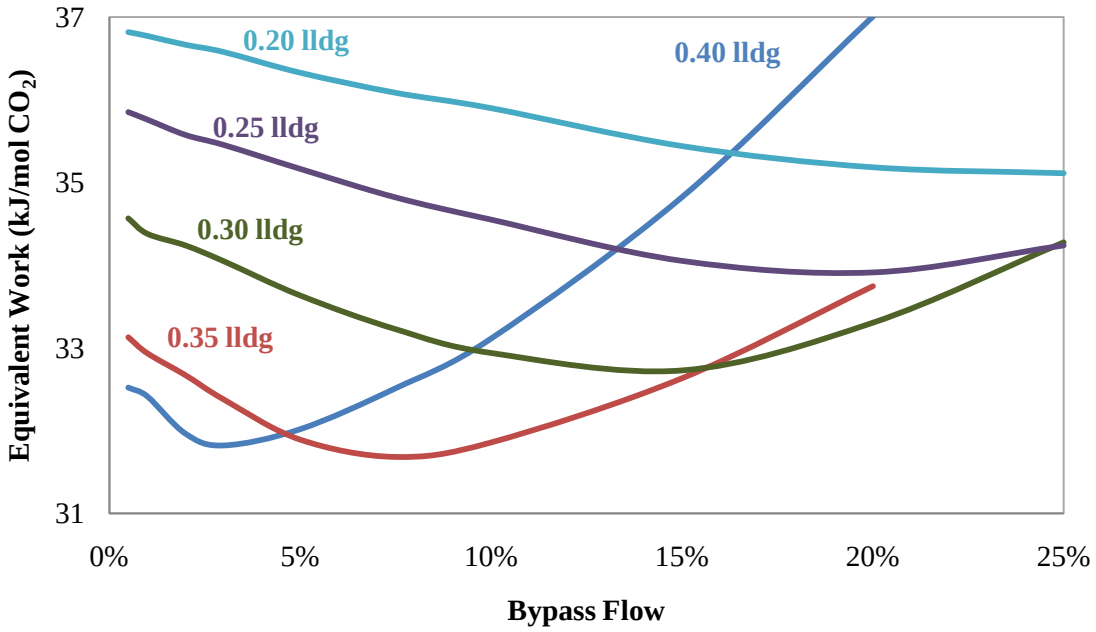


Figure 4-18. Equivalent work requirement for 9 m MEA in simple stripper. 120 °C reboiler, 0.50 rich loading, 5 °C LMTD in main cross exchanger, compression to 150 bar.

The equivalent work showed a sharp minimum with a lean loading of 0.40, like the other results with MEA in section 4.3.2. However, the optima were flatter for lower lean loadings. The equivalent work for the optimum case with no bypass was 32.8 kJ/mol $CO_2$ with a $CO_2$ purity of 75%. Since the vapor had comparatively less water content than the 2-stage flash simulations and the simple stripper simulation with PZ, the improvement with bypass was marginal, only 4.2% down to 31.4 kJ/mol $CO_2$. This analysis demonstrated that bypass would not be as important to implement if using a simple stripper with 9 m MEA. The packing combined with the high heat of absorption yielded low water content in the overhead vapor, so direct contact with bypassed cold rich solvent yielded only a small improvement.

### 4.3.5. Bypass with 8 m PZ and Interheated Column

The interheated column was the most energy-efficient configuration that was explored in Chapter 3. This configuration combined with 8 m PZ was able to attain a 14% improvement over the base case of 9 m MEA with a simple stripper. Since the interheated column was the most efficient, it was desired to quantify the potential improvement by implementing bypass into the configuration. The additional packed section for contacting the vapor with the bypassed solvent was held constant at 12 inches of Mellapak 500Y, and the main cross exchange performance was held constant with a 5 °C LMTD. The trends with varying lean loading and bypass are shown in Figure 4-19.

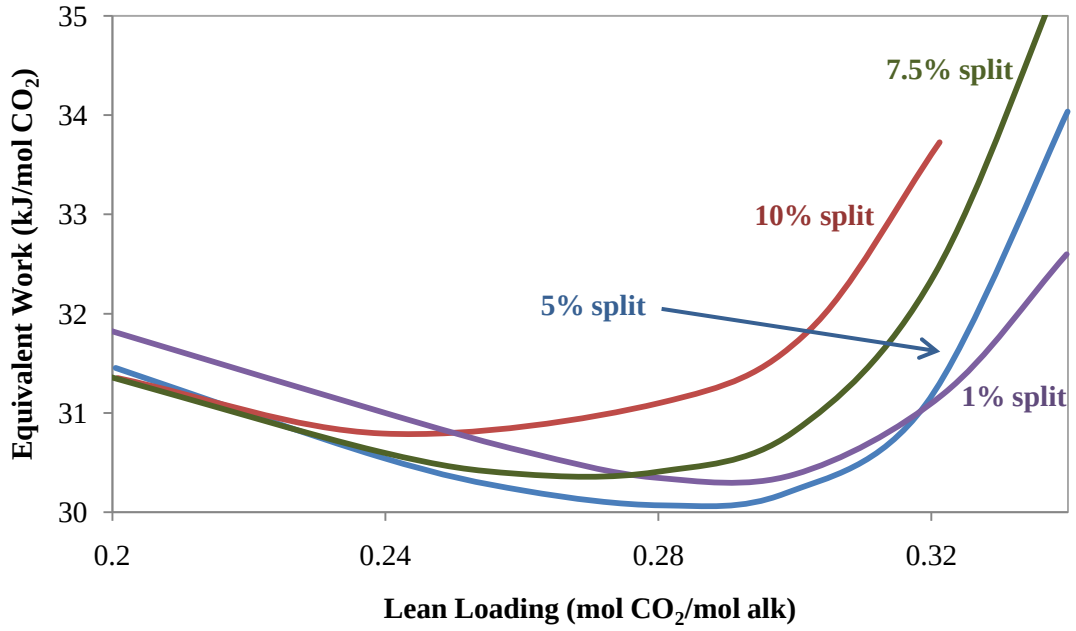


Figure 4-19. Equivalent work requirement for 8 m PZ in interheated column. 150 °C reboilers, 0.40 rich loading, 5 °C LMTD in main cross exchanger, compression to 150 bar, 80% liquid extraction for interheating.

This configuration and solvent had an equivalent work of 30.3 kJ/mol $CO_2$ and a $CO_2$ purity of 77%. Figure 4-19 demonstrated that the global minimum had a lean loading of 0.28, a split of 5%, and resulted in an equivalent work of 30.1 kJ/mol $CO_2$.

This analysis demonstrated a very minimal improvement of 1.4%. The benefit was much less than the other configurations when using PZ because the water content of the vapor was already low. The interheating had a secondary effect on the temperature of the overhead vapor. Since a portion of the heat from the lean solvent was exchanged with liquid from the middle of the column, less heat was transferred in the main heat exchanger. Therefore, the rich solvent entering the column was cooler than in a simple stripper, so the overhead vapor was also cooler. Since this effect existed, cold rich bypass had a smaller impact.

The format of Figure 4-19 also demonstrated another effect of bypass. At low values of bypass, the optimal lean loading stayed constant while the minimum equivalent work decreased. At higher levels of bypass, the minimum equivalent work increased while the optimal loading decreased substantially.

### 4.3.6. Bypass Summary

Cold rich bypass resulted in a benefit for both solvents in every configuration, though the improvement was different for each solvent and configuration. Table 4-4 compares the minimum equivalent work with and without using bypass. The absolute and percent improvements are also tabulated for each bypass option compared to its base case with no bypass. The 2-stage flash cases had the option of bypassing solvent to the low-pressure vessel, high-pressure vessel, or both. The low-pressure vessels had higher water content than the high-pressure vessels because the $CO_2$ partial pressure was lower at the lower lean loading. Therefore, bypass to only the high-pressure vessel was not explored because if only one vessel received bypass, the low-pressure vessel should be selected.

**Table 4-4. Summary of improvement with bypass for combinations of solvents and configurations. Optimized bypass split, 5 °C LMTD, compression to 150 bar. 8 m PZ: 0.40 rich loading, 150 °C. 9 m MEA: 0.50 rich loading, 120 °C.**

| Solvent | Rich ldg | Configuration | Base case | Bypass optimum | Improvement | | Ldg @ opt | P @ opt |
|---|---|---|---|---|---|---|---|---|
| | *mol/mol* | | *kJ/mol $CO_2$* | | | | *mol/mol* | *bar* |
| 8 m PZ | 0.4 | 2-stage flash, bypass to LP | 32.5 | 29.8 | 2.7 | 8.2% | 0.28 | 12.9 / 7.7 |
| 8 m PZ | 0.4 | 2-stage flash, bypass to HP/LP | 32.5 | 28.8 | 3.7 | 11.3% | 0.28 | 12.0 / 7.7 |
| 9 m MEA | 0.5 | 2-stage flash, bypass to LP | 31.7 | 30.7 | 1.0 | 3.2% | 0.35 | 7.6 / 3.6 |
| 9 m MEA | 0.5 | 2-stage flash, bypass to HP/LP | 31.7 | 29.9 | 1.8 | 5.7% | 0.35 | 7.3 / 3.6 |
| 8 m PZ | 0.4 | PZ, simple stripper | 31.4 | 28.6 | 2.8 | 8.9% | 0.3 | 8.8 |
| 9 m MEA | 0.5 | MEA, simple stripper | 32.8 | 31.4 | 1.4 | 4.2% | 0.375 | 4.3 |
| 8 m PZ | 0.4 | PZ, interheated column | 30.5 | 30.1 | 0.4 | 1.4% | 0.28 | 7.7 |

Configurations with PZ demonstrated a greater reduction in equivalent work due to the high concentration of water in the overhead vapor. The cold bypassed solvent effectively condensed the water to improve overall efficiency. Considering the simple stripper and 2-stage flash cases, the absolute improvement by adding bypass with PZ as the solvent was always at least twice as significant as the improvement seen with MEA.

The simple stripper base cases both had better $CO_2$ purity than the 2-stage flash cases since the packed column condensed water from the vapor as it contacted the slightly cooler rich solvent. Since the simple stripper cases had less water in the vapor, they had less opportunity for potential improvement. Adding cold rich bypass to only the low-pressure flash had approximately the same benefit as bypass to the simple stripper. These 2-stage flash cases specified equal vapor production in each flash vessel, so a lesser, but still substantial amount of water vapor also escaped with the high-pressure vapor. Sensitivity analyses were not performed with bypass to both flash vessels, but the performance was evaluated for the 2-stage flash with MEA and PZ using optimized bypass to both vessels. In each case, the optimal bypass split to the high-pressure vessel was less than the split to the low-pressure vessel because the water composition in the vapor was lower at high-pressure. With each amine, bypassing solvent to both flash vessels yielded a greater overall improvement than bypassing to a simple stripper. However, the additional benefit of bypassing to the high-pressure vessel was not as great as the improvement seen when bypassing to the low-pressure vessel.

The interheated column with PZ realized very little benefit with cold rich bypass. The secondary interheating effect that cooled the rich solvent in the base case as compared to a simple stripper significantly reduced the opportunity to reduce the work requirement. Bypass improved its performance only by 1.4%. Overall, bypass was most beneficial with a 2-stage flash and 8 m PZ. Using a rich loading of 0.4, a lean loading of

0.28, 4% bypass to the high-pressure vessel, and 7.5% bypass to the low-pressure vessel, the equivalent work was 28.8 kJ/mol $CO_2$, compared to 32.5 kJ/mol $CO_2$ without bypass.

## 4.4. STRIPPING WITH GEOTHERMAL HEAT

Geothermal heat is proposed as an alternative to using steam heat in the stripper. Freeing the steam cycle from the heating requirement in the stripper would be beneficial for power production at a coal-fired power plant; the steam cycle would not be subject to the disruptions that the stripper might cause. The IP/LP crossover in a new-build power plant would be designed for a preferred operating point, and inefficiencies in the steam cycle would arise from fluctuations from the design point. Therefore, an alternate source of heat could be an advantage since the stripper is coupled with the power generation facility.

### 4.4.1. Stripper Flowsheets Using Geothermal Heat

Using geothermal heat would be much different than using steam because the heat would be supplied from the brine at variable temperature. Steam supplies heat at a single temperature where it condenses. A typical steam reboiler would not make efficient use of geothermal brine because there would be a large approach temperature on the hot side of the exchanger where the brine is supplied, and there would be a pinch on the cold side. From an exergy standpoint, the high imbalance of temperature driving forces yields inefficiencies. From the viewpoint of the process itself, a large hot side driving force indicates that the heat source is not being utilized to its maximum capacity; the heat could be used at a higher temperature. Alternatively, using a cross exchanger with the hot brine and cool rich solvent could more effectively take advantage of the high temperature brine

by balancing the temperature approach throughout the exchanger. Using a cross exchanger in place of a reboiler is not a matter of simply replacing the processing unit, but the flowsheet must be redesigned to use heat in such a manner.

The earlier work demonstrated the effectiveness of a multi-stage flash configuration for stripping $CO_2$. The designs explored in Chapter 3 considered constant temperature flashes where the heat supplied was delivered in a reboiler with steam. A form of the multi-stage flash configuration is proposed in this section that incorporated cross exchangers to contact hot brine with cool rich solvent to heat the solvent with brine, and the solvent was flashed at two different pressures.

This work collaborated with a student in petroleum engineering who stimulated the practicality of drawing brine for $CO_2$ stripping (Gupta, 2011). Modeling of real geothermal reservoirs was important to predict the expected brine temperature, maximum extraction rate, and life of the geothermal reservoir. This work considered the use of the Wilcox group of brine reservoirs due to its proximity to coal-fired power plants in Texas. The brine at this location was available at 150 °C, so PZ was selected as the solvent to avoid thermal degradation. The 5deMayo thermodynamic model for PZ was used for these simulations (Rochelle et al., 2010). 8 m PZ was simulated in an advanced 2-stage, 2-pressure flash (2T2PFlash) (Figure 4-20). The configuration utilized an arrangement of five heat exchangers to remove heat from brine and the returning lean solvent more reversibly than with single exchangers for each of solvent and brine cross exchanging. The heating in this configuration was different from the flowsheets in previous simulations in that the rich solvent was fully heated before entering the two adiabatic flash vessels in series. The first flash had the highest temperature and pressure, and the second flash dropped in both temperature and pressure. The drop in temperature between

the high and low pressure flashes was lower than what would be observed in a typical 2-stage flash because heat exchanger 4 was implemented.

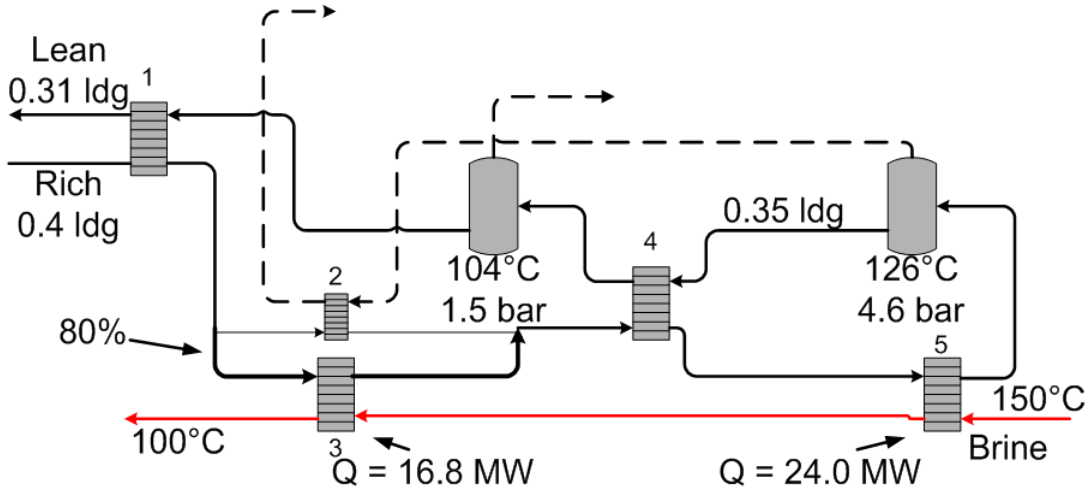


Figure 4-20. Advanced 2-Stage, 2-Pressure Flash (2T2Pflash) for amine solvent regeneration with geothermal brine heating. Conditions shown for the optimal case, designed for a 60 $MW_e$ coal-fired power plant, removing 1195 ton $CO_2$/day.

As with previous simulations of multi-stage flash configuration, all unit operations were modeled with chemical equilibrium within and between the gas and liquid phases. Several conditions were specified to be constant while others were optimized. A constant rich loading of 0.4 mol $CO_2$/mol alkalinity was specified, which represented a $CO_2$ partial pressure of 5 kPa at 40 °C. The input temperature of the rich solvent coming from the absorber was specified to be constant at 50 °C. The LMTD was 5 °C for all exchangers, and a minimum approach of 1 °C was specified for either side. The temperature difference between flash vessels was varied to ensure that equal moles of vapor were generated in each flash. This specification was made to maximize the reversibility of the process. The multi-stage compressor work was calculated using the correlation in Equation 3-1. The split of solvent between exchangers 2 and 3 was set to 80% toward exchanger 3.

The heat capacity flows of the streams in heat exchanger 1 were mostly balanced, so the hot and cold side temperature approaches were both always approximately the same. Therefore, the outlet temperature of the brine in exchanger 3 was closely connected to the equilibrium temperature in the low-pressure flash. The low-pressure flash temperature was 5 °C higher than the rich outlet in exchanger 1, and this temperature was approximately 5 °C cooler than the cold brine temperature. The geothermal well models required a constant drop in brine temperature of 50 °C between extraction to re-injection, and this stripper design allowed the low-pressure flash temperature to be the manipulated variable to achieve the desired drop in brine temperature.

The brine was simulated as pure water, but the final value of importance was the total heat rate of the brine. Simulating the flow of brine ensured that the split of heat rate in exchangers 3 and 5 represented accurate performance with the predicted temperatures. The lean loading was manipulated by varying the brine flow rate. The overall work requirement including the pumps, multi-stage compressor, and heat duty was calculated using equivalent work. For this work with variable temperature heating, the previous calculation method for heating work (Equation 2-5) was integrated between the inlet and outlet temperatures to account for the changing value of heat at different temperatures, which assumed that each unit of heat flow resulted in the same change in temperature along the entire temperature range. The inlet and outlet temperatures in each heater *i* were $T_{i,o}$ and $T_{i,f}$, respectively. This integration gave Equation 4-1 for the heat work.

$$\boldsymbol{W_{heat}} = \sum_{\boldsymbol{i=1}}^{\boldsymbol{n_{heaters}}} \boldsymbol{0.75 Q_i} \left( \frac{\boldsymbol{T_{i,f} - T_{i,o} - T_{sink} \ln\left(\frac{T_{i,f}}{T_{i,o}}\right)}}{\boldsymbol{T_{i,f} - T_{i,o}}} \right) \qquad \textbf{4-3}$$

A comparison study that would be applied at a demonstration being planned by NRG Energy (Stopek et al., 2011) was also simulated. The comparative configuration that was analyzed used 9 m MEA with a simple stripper and an adiabatic flash on the lean solvent (Figure 4-21). MEA was represented the Hilliard thermodynamic model (Hilliard, 2008). This configuration is patented by Fluor (Reddy et al., 2007) when using steam heating. The flowsheet is used in a planned demonstration that is designed for MEA, so the same solvent was selected for this modeling with geothermal heating. The brine heated a reboiler and a rich feed preheater that was added to extract additional heat from the brine. Unfortunately, the reboiler had a large hot side approach temperature since the solvent temperature was constant, but this case represented a reconfiguration that could adapt the Fluor configuration to use brine if it was already constructed to use steam from the power plant. The only additional process unit would be the cross exchanger to preheat the rich feed. The same constants were specified as for the 2-stage flash. The rich loading was specified to be 0.5 mol $CO_2$/mol alkalinity, representing a $CO_2$ partial pressure of 5 kPa at 40 °C.

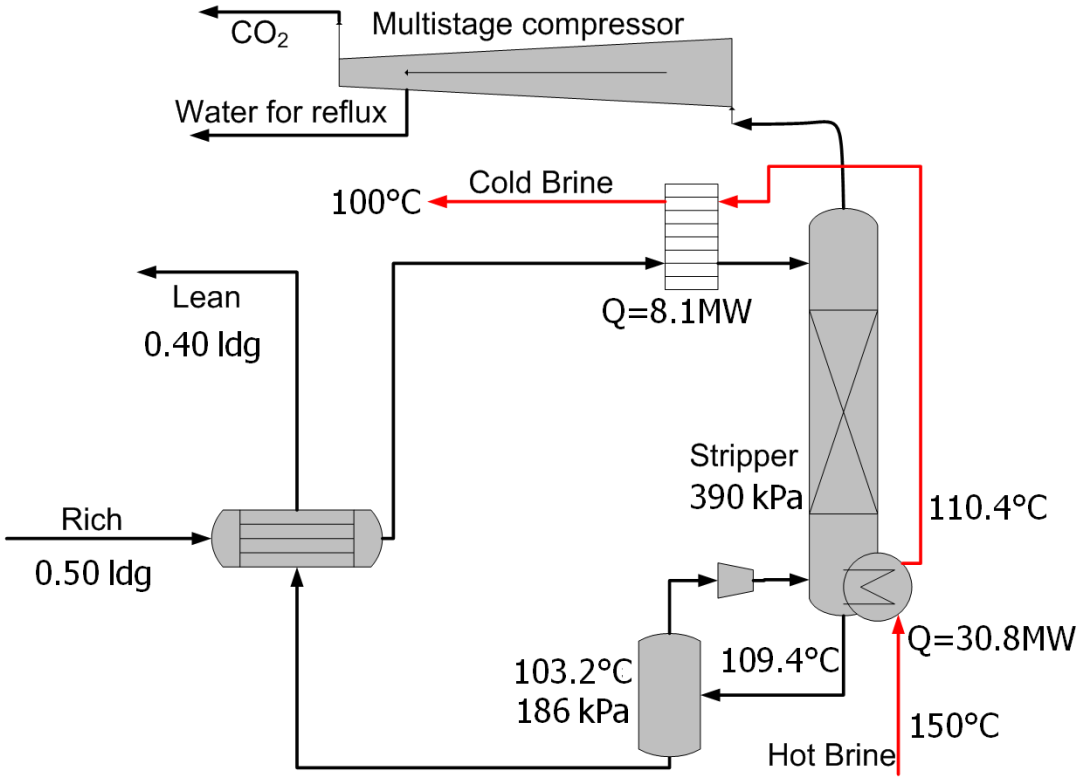


Figure 4-21. Fluor configuration modified for geothermal heating. Conditions shown for the optimal case, designed for a 60 $MW_e$ coal-fired power plant, removing 1195 ton $CO_2$/day.

### 4.4.2. Geothermal Stripping Results

The stripper was scaled to regenerate enough solvent to treat the flue gas of a 60 $MW_e$ power plant. The flue gas rate and composition from this size power plant was estimated by scaling an industrial estimate. Approximately 1195 ton $CO_2$/day would be removed for 60 $MW_e$ (Fisher et al., 2005). The lean loading was optimized to minimize the overall work requirement.

Figure 4-22 shows the behavior of both equivalent work and total heat duty as a function of lean loading in the 2T2PFlash. The optimum equivalent work was at a lean loading of approximately 0.33, but the heat duty was minimized at a slightly higher lean

loading of 0.335. These results were calculated using a rich loading of 0.4, corresponding to a $P^*_{CO2}$ of 5 kPa at 40 °C. At the lean loading of 0.33, the equivalent work was 35.1 kJ/mole $CO_2$.

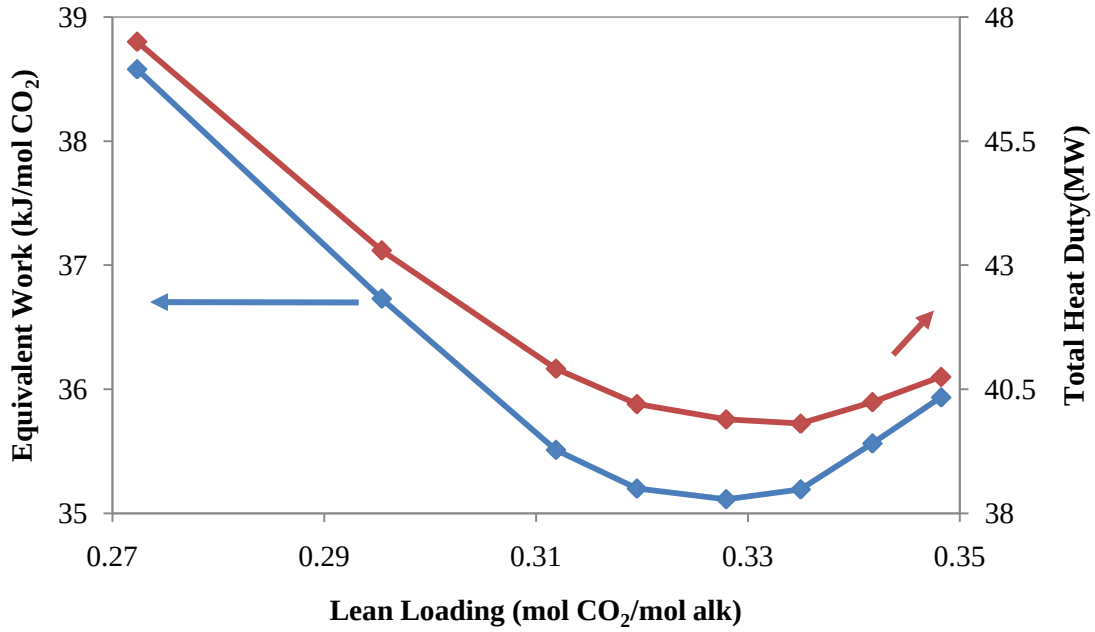


Figure 4-22. Lean loading optimization for 2T2Pflash with 8 m PZ applied to a 60 $MW_e$ power plant. 0.40 rich loading, $T_{brine,in}$ = 150 °C, $T_{brine,out}$ = 100 °C, 5 °C LMTD on heat exchangers, $CO_2$ compression to 150 bar.

The $P^*_{CO2}$ at 40 °C for the optimal lean loading of 0.335 was approximately 0.85 kPa. Solvent concentrations representing a gas side removal of less than 90% might not provide adequate absorber performance since the acceptable loadings were calculated for 90% removal. An overstripped lean solvent would perform well in the absorber because it would have a significant driving force to achieve the desired clean gas purity. Additionally, the lower lean loading would reduce the solvent circulation rate. Conversely, an understripped lean solvent would have trouble attaining the desired purity of 1.2% without using chilled water for cooling or excessive packing. For this reason, the

operation point was chosen to have a lean loading of 0.31, where the $P^*_{CO2}$ at 40 °C was 0.5 kPa. At this lower lean loading, the equivalent work was 35.5 kJ/mole $CO_2$.

Since the temperature of the extracted brine was expected to decline over the length of the project, the sensitivity of the stripper performance with brine temperature was investigated. The change in temperature of the brine across the process was held constant at 50 °C for all extraction temperatures. The base case temperature of 150 °C required 40.8 MW of heat. The expected decrease in brine temperature over a 30 year period was 2 °C (Gupta, 2011). A reduction in brine temperature from 150 °C to 148 °C would change the heat duty to 41.2 MW, only a 2.4% increase from the design case. An extreme scenario where the brine temperature dropped to 145 °C required 42.4 MW of heat, only 3.7% greater than the design case. If a brine formation that could supply heat at 160 °C was found, the heat duty would decrease to 38.8 MW, a 4.5% drop from the design case. Figure 4-23 displays the increase in heat duty and the equivalent work with decreasing brine temperature. Each simulation converged multiple heat exchange recycle loops at once, and the tolerance set on each recycle loop resulted in a small variability of each point. However, a general negative linear trend was observed.

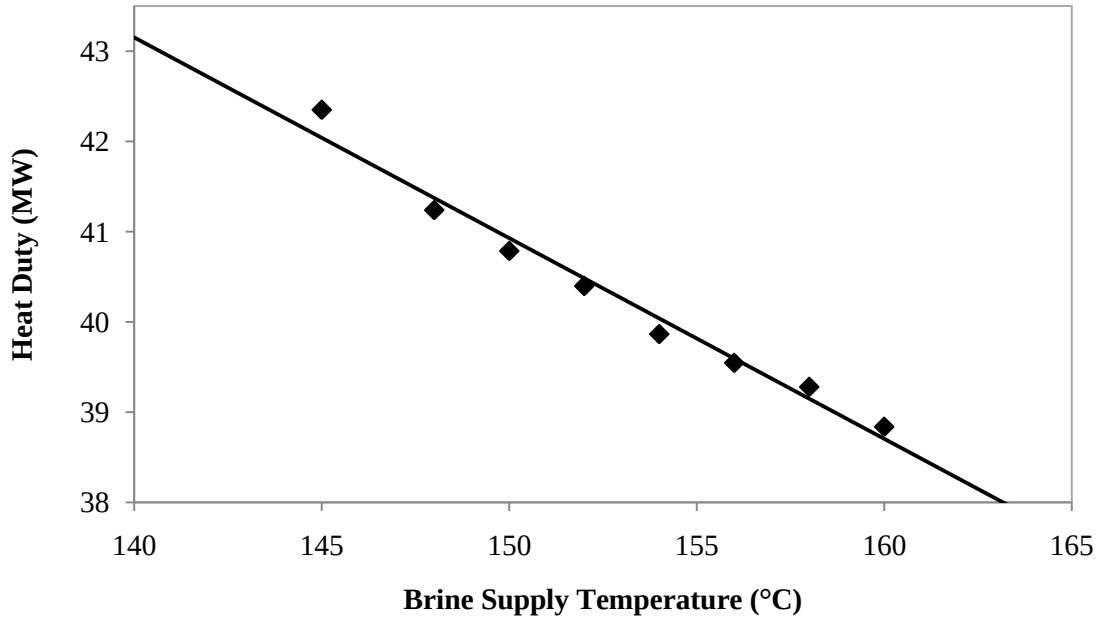


Figure 4-23. Reduction in total heat duty with increasing brine temperature for 2T2Pflash with 8 m PZ. 0.40 rich loading, $\Delta T_{brine}$ = 50 °C, 5 °C LMTD on heat exchangers, $CO_2$ compression to 150 bar. Points = simulation results, line = approximate linear representation.

The Fluor configuration with brine heating was also optimized for lean loading with 9 m MEA. As had been found in previous work with MEA (Van Wagener et al., 2010), the optimal lean loading was in the overstripping region. The minimum equivalent work was 36.3 kJ/mole $CO_2$ at a lean loading of 0.39, seen in Figure 4-24. The overall heating requirement for a 60 $MW_e$ plant was 38.6 MW, a lower heat duty than the 40.8 MW required in the PZ calculation. Previous work demonstrated a similar outcome, where a 2-stage flash with 8 m PZ had a higher heat duty than a simple stripper with 9 m MEA. Even though the heat duty was less for MEA, the PZ solvent made up in overall performance by operating at a higher pressure, so the 2-stage flash had a significantly smaller compression work. Overall, 9 m MEA had a higher equivalent work requirement than for 8 m PZ. These calculations with MEA used a rich loading of 0.5 with a $P^*_{CO2}$ at 40 °C of 5 kPa, and the optimal lean loading of 0.39 had a $P^*_{CO2}$ at 40 °C

of 0.13 kPa. Therefore, the optimal lean loading was an acceptable range to be coupled with an absorber and expect adequate performance.

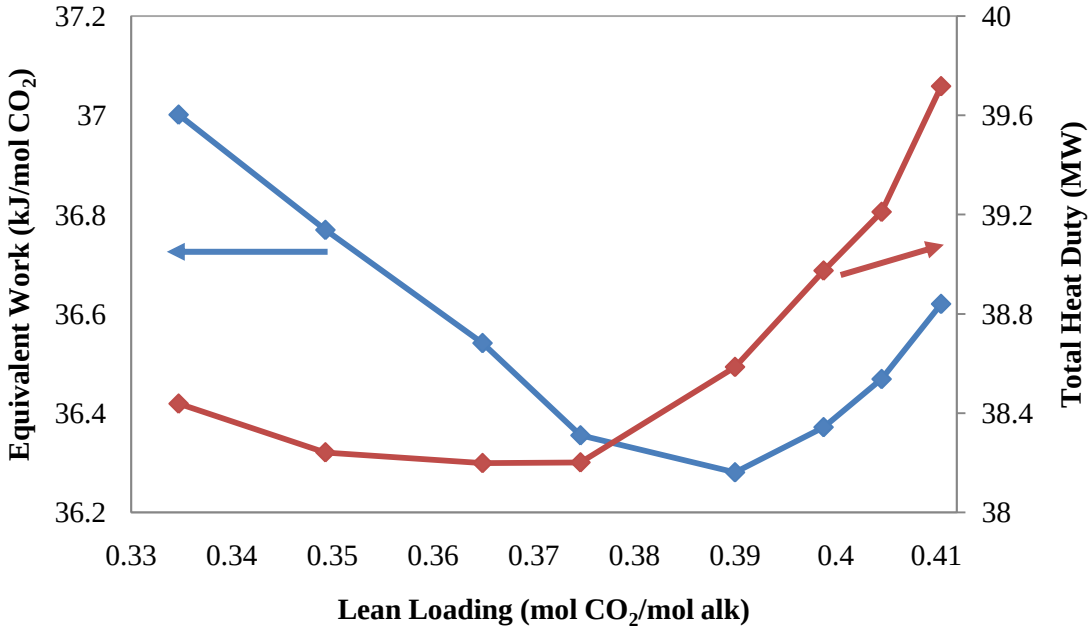


Figure 4-24. Lean loading optimization for Fluor configuration with 9 m MEA. 0.5 rich loading, $T_{brine,in}$ = 150 °C, $T_{brine,out}$ = 100 °C, $CO_2$ compression to 150 bar.

The difference in proportions of the three work contributions demonstrated that each configuration/solvent combinations could have its own application. Using the 2T2Pflash with 8 m PZ would be advantageous when aiming to minimize the overall energy usage. However, the Fluor configuration with 9 m MEA would be advantageous if electricity was cheap and the goal was to minimize the heat usage as much as possible. The Fluor configuration with 9 m MEA reduced the heat duty from the 2-stage flash design case by 5.3%

### 4.4.3. Conclusions

The 2T2PFlash configuration with 8 m PZ optimized with the lowest equivalent work, but the Fluor configuration with 9 m MEA optimized with the lowest heat duty. The individual work requirements for each of these systems are shown in Table 4-5 at their respective optimum operating conditions.

**Table 4-5. Energy requirement of 2T2PFlash with 8 m PZ and Fluor configuration with 9 m MEA. Brine supplied at 150 °C, $CO_2$ compression to 150 bar.**

| Work contribution | 9 m MEA, Fluor configuration | 8 m PZ , 2T2PFlash configuration |
|---|---|---|
| | *kJ/mol $CO_2$* | |
| $\mathbf{Q_{heat}}$ | 123.1 | 130.1 |
| $\mathbf{W_{heat}}$ | 19.7 | 20.7 |
| $\mathbf{W_{comp}}$ | 15.0 | 13.6 |
| $\mathbf{W_{pump}}$ | 1.6 | 1.2 |
| $\mathbf{W_{eq}}$ | 36.3 | 35.5 |

The design case was selected to be the advanced 2-stage flash using 8 m PZ, treating flue gas generated by the production of 60 $MW_e$. A conservative estimate of the brine extraction temperature was 148 °C, allowing for heat loss during the transportation from underground reservoir to well head along the wellbore. Assuming a rich loading of 0.40, the heating requirement was 41.2 MW, and the overall equivalent work was 11.1 $MW_e$, or 35.6 kJ/mol $CO_2$. Of the overall equivalent work, the total contribution from heating was 6.5 $MW_e$, or 20.6 kJ/mol $CO_2$. The balance of the total work, 4.6 $MW_e$, was electricity directly drawn for pump work and $CO_2$ compression to 150 bar. This electricity would be drawn directly from the generation of the turbines, as in any proposed post-combustion carbon capture with amines. However, this flowsheet would

avoid disrupting the steam cycle to draw heat for the solvent regeneration. The process integration and control of this heating option, therefore, could be very beneficial.

## 4.5. Optimized Interheated Column with Absorber Integration

In Chapter 3, the interheated column with 8 m PZ was the most energy-efficient combination of configuration and solvent. A downside of the decomposition method used in this work was that its assumption that the stripper can be modeled separate from the absorber could bring about scrutiny regarding the accuracy of predictions. Moreover, the equivalent work calculation made numerous assumptions, mainly that the value of steam used in the stripper could be adequately calculated using a Carnot calculation. In this section, the interheated column was optimized through a collaboration that provided real absorber result inputs in the stripper calculations and rigorous steam cycle calculations to determine the actual penalty on a coal-fired power plant. This section describes a collaborative effort that used results from UT absorber modeling (Plaza, 2011 (expected)) and TUHH steam cycle and compressor models (Liebenthal, 2011 (expected)).

### 4.5.1. Integrated Model

The interheated column (Figure 3-8) was simulated with the PZ solvent within Aspen Plus® using the 5deMayo thermodynamic framework that was regressed in-house (Rochelle et al., 2010). The simulation method was the same as in Chapter 3. The interheated column configuration had the best performance in the complexity analysis because it more reversibly recycled heat from the lean solvent back to the column and

reduced the temperature at the top of the column compared to a simple stripper. The optimal lean loading was also reduced when using the interheated column.

The stripper simulation was separate from the absorber to promote convergence of the individual simulations, but the rich and lean solvent specifications from the absorber simulations were used as inputs for the stripper. The stripper simulations included the stripper column and the cross exchange section with pumps and the main heat exchanger. The following flowsheet constants were specified:

1. Rich pump achieved 250 kPa above stripper pressure to account for head and frictional losses
2. Lean pump achieved 350 kPa to account for head and frictional losses
3. 5 °C cold side approach on main cross exchanger
4. 5 °C LMTD on interheater cross exchanger
5. 80% solvent extraction for interheating

The stripper simulations were used to calculate the reboiler heat duty, lean, rich, and interheating pump duties, and stripper vapor pressure. The reboiler heat duty was used by the steam cycle model to calculate the required steam rate. The power plant model also calculated the compression work of the multi-stage dresser using the stripper overhead vapor pressure. The reboiler temperature was held constant with varying L/G by changing the column pressure.

The absorber was modeled separately from the stripper. It used 15 m of Mellapak 2X packing, intercooling to 40 °C at the column midpoint, and the work requirements of the blower and intercooler pump were calculated. The column was simulated at varying values of lean loading, and 90% removal of $CO_2$ was achieved by varying the L/G. The lean loading and resulting rich loading as a function of absorber L/G are plotted in Figure 4-25. This plot also demonstrates the benefit of using intercooling in the absorber.

Without intercooling the rich loading dropped significantly when the temperature bulge coincided with the mass transfer pinch. When using intercooling, the rich loading stayed fairly constant at 0.40 because there was no longer a temperature-based mass transfer pinch and the solvent was permitted to approach equilibrium more closely (Plaza, 2011 (expected)).

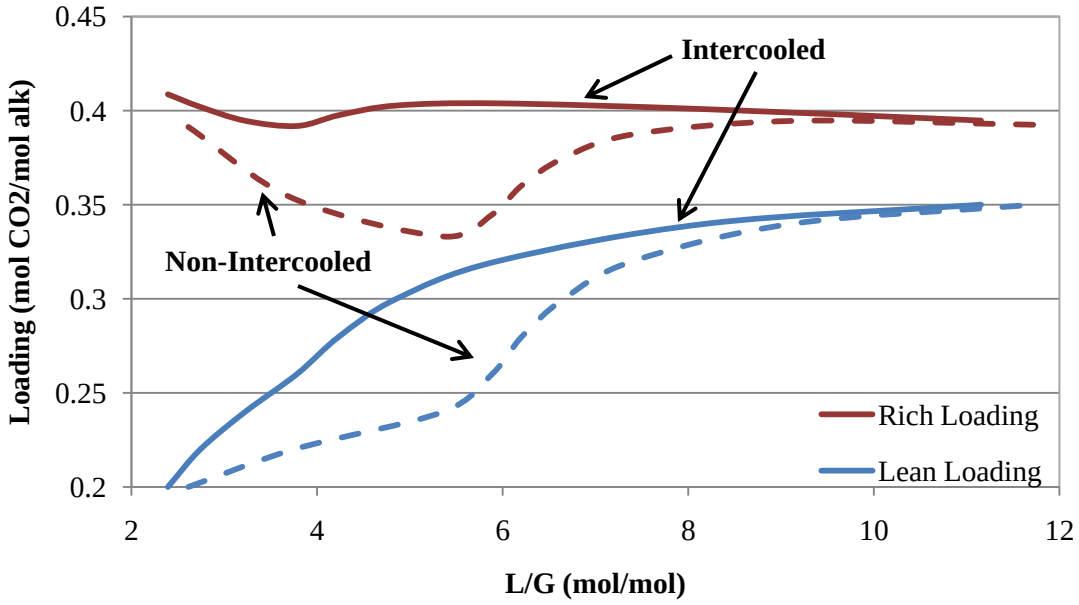


Figure 4-25. Intercooled absorber predictions of rich and lean loadings for 90% removal with 15 m of Mellapak 2X.

### 4.5.2. Stripper Model Results

The stripper was evaluated at stripper temperatures between 100 and 150 °C in 10 °C increments. The effect of L/G on the individual outputs for each reboiler temperature are shown in the figures: 4-26 shows the total heat duty, 4-27 shows the total cooling duty, 4-28 shows the total electric usage, and 4-29 shows the stripper pressure. These calculations were used by the steam cycle model of a greenfield (new-build) power

plant to determine the net penalty in efficiency and specify the optimal operating conditions. The compressor work was excluded from the total electric usage because it was calculated by a compressor model by the TUHH students.

The steam cycle calculations from TUHH showed that the efficiency loss was minimized with a reboiler temperature of 140 °C and an absorber L/G of 4.9. This solvent circulation rate corresponded to rich and lean loadings of 0.40 and 0.30, respectively. The net efficiency of the power plant was 38.4%, a reduction of 7.4% from 45.8%. The efficiency did not significantly decrease when the reboiler temperature was increased to 150 °C, but it experienced a slight reduction in net efficiency to 38.3%. This analysis demonstrated that the equivalent work and compressor work analyses that were used in previous work did not necessarily fully capture the intricate details that affected the penalty of the stripper.

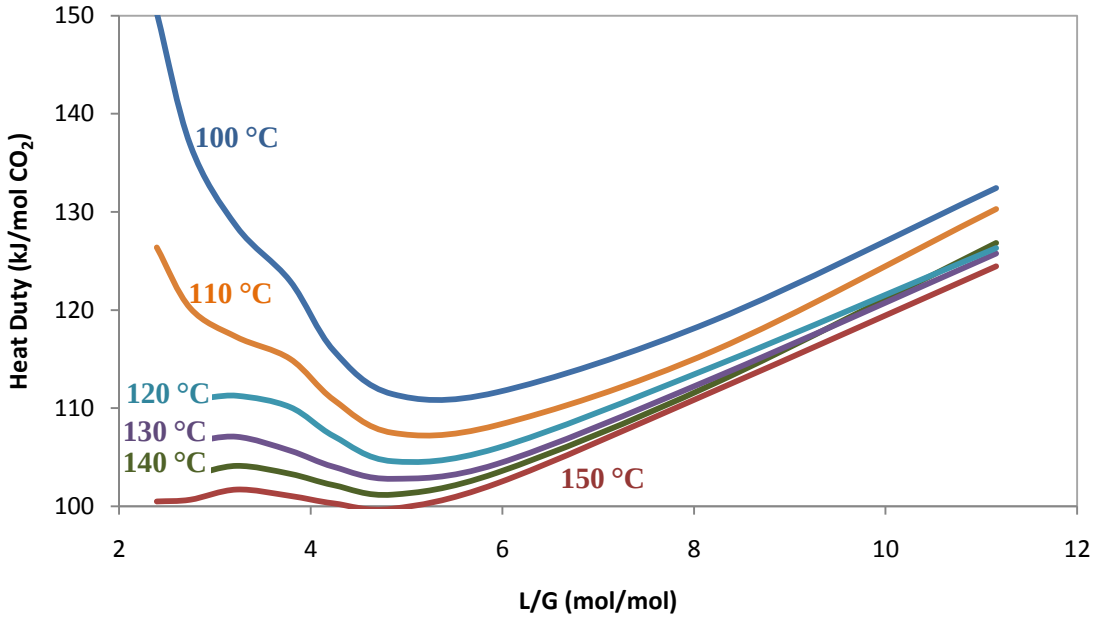


Figure 4-26. Total reboiler duty.

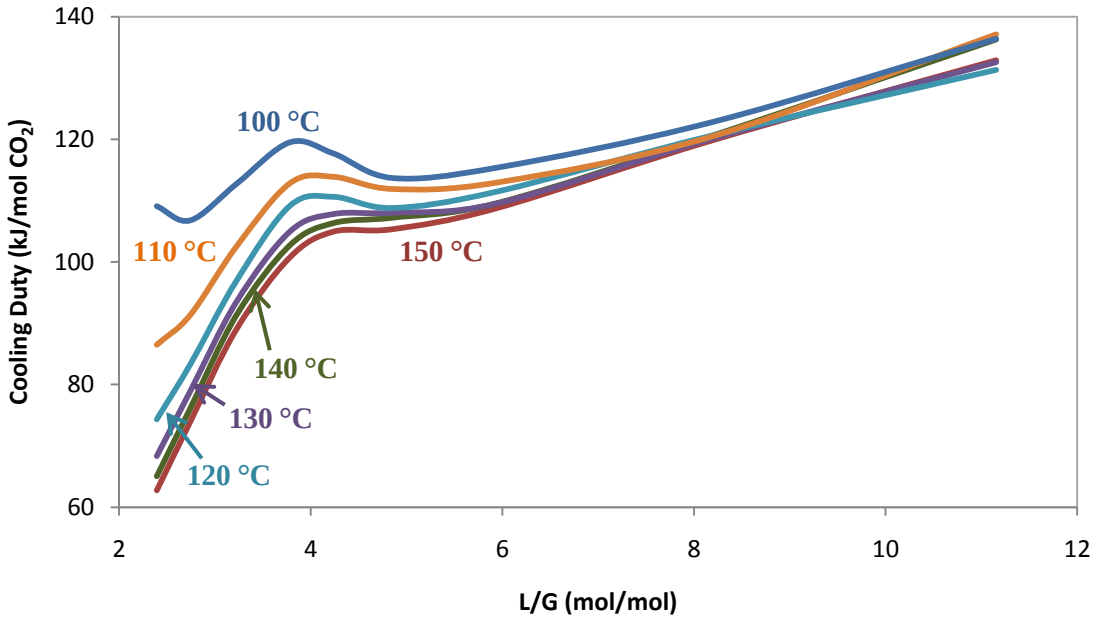


Figure 4-27. Total cooling duty. Includes absorber intercooling, lean trim cooler, and first vapor condenser.

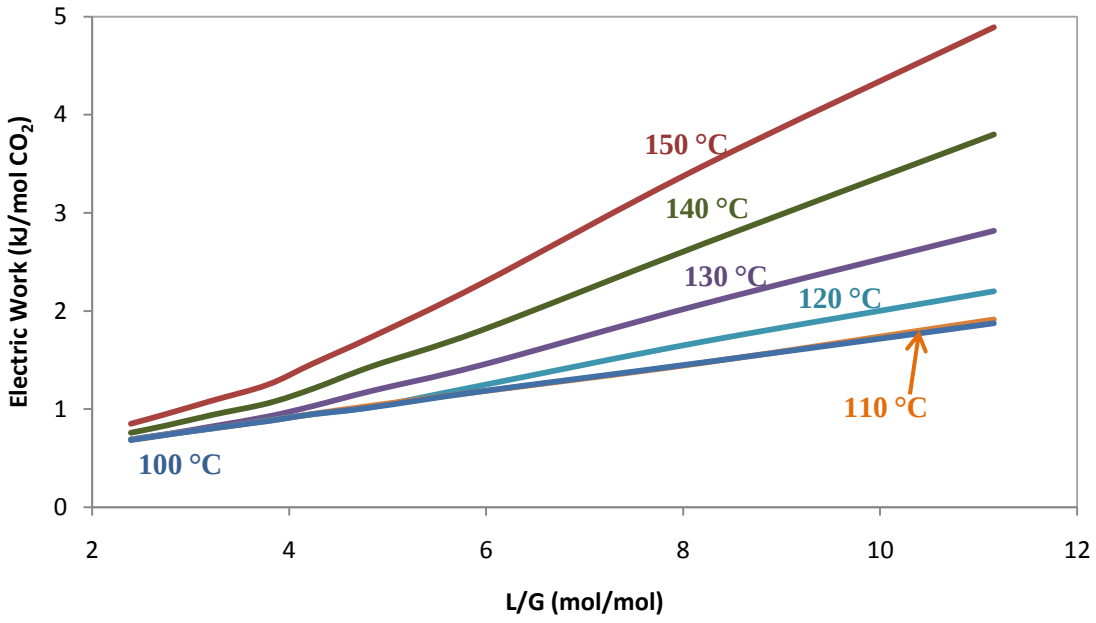


Figure 4-28. Total electric usage. Includes blower, intercooler pump, interheater pump, rich pump, and lean pump.

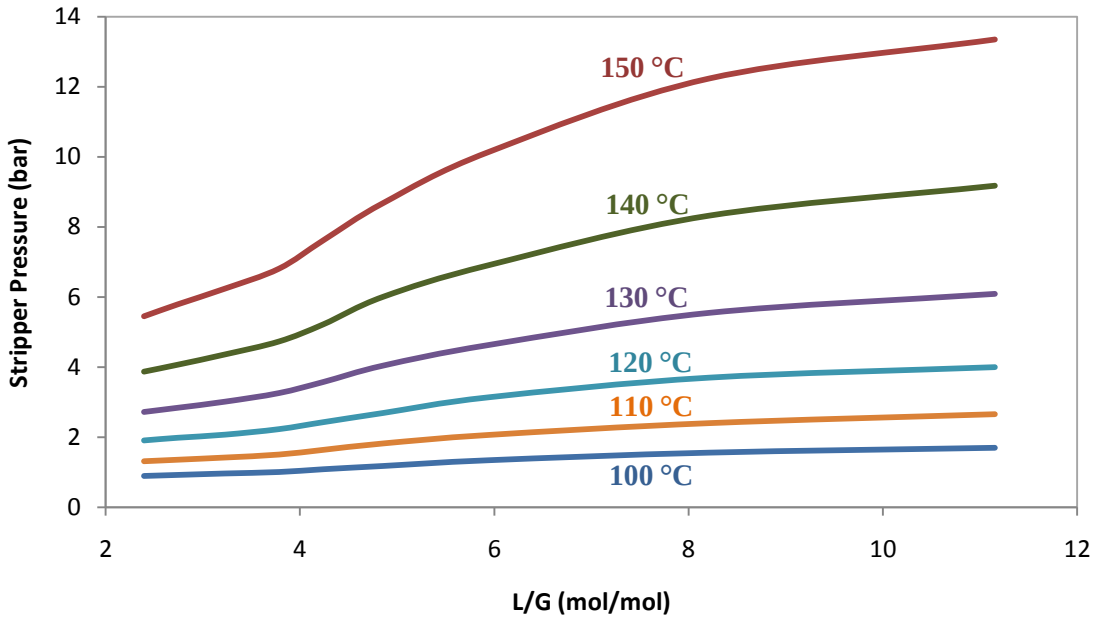


Figure 4-29. Column pressure.

The relationship between the reboiler duty and total cooling duty was confounded by several interacting factors. At a low lean loading and low L/G, the rich loading of the solvent provided by the absorber increased and was higher than 0.40. Even at constant rich loading, the interheated column already demonstrated a minimal increase in total work at low lean loading. The interheating served to provide a cooler rich feed to the column, which reduced the water content of the overhead vapor. The total cooling duty decreased at low L/G with the combination of three factors: a decrease in intercooling duty in the absorber due to lower circulation rate, a decrease in trim cooler duty due to lower circulation rate, and a minimal decrease in $CO_2$ selectivity. There was a local maximum in cooling duty at an L/G of about 4.25 where there was a peak in intercooler duty.

Unlike the analysis of the interheated column in Chapter 3, the rich loading was not constant in this study, though it was constantly close to 0.40. Figure 4-30 compares

the calculated equivalent work of these cases at 120 °C and 150 °C to the simulations with a constant rich loading of 0.40. The equivalent work predictions in these runs with a real absorber feed varied within close deviation from the constant rich loading simulation results. Although the equivalent work appeared to flatten out at low lean loading with a reboiler temperature of 150 °C, the effect was only due to the slight increase in the rich loading.

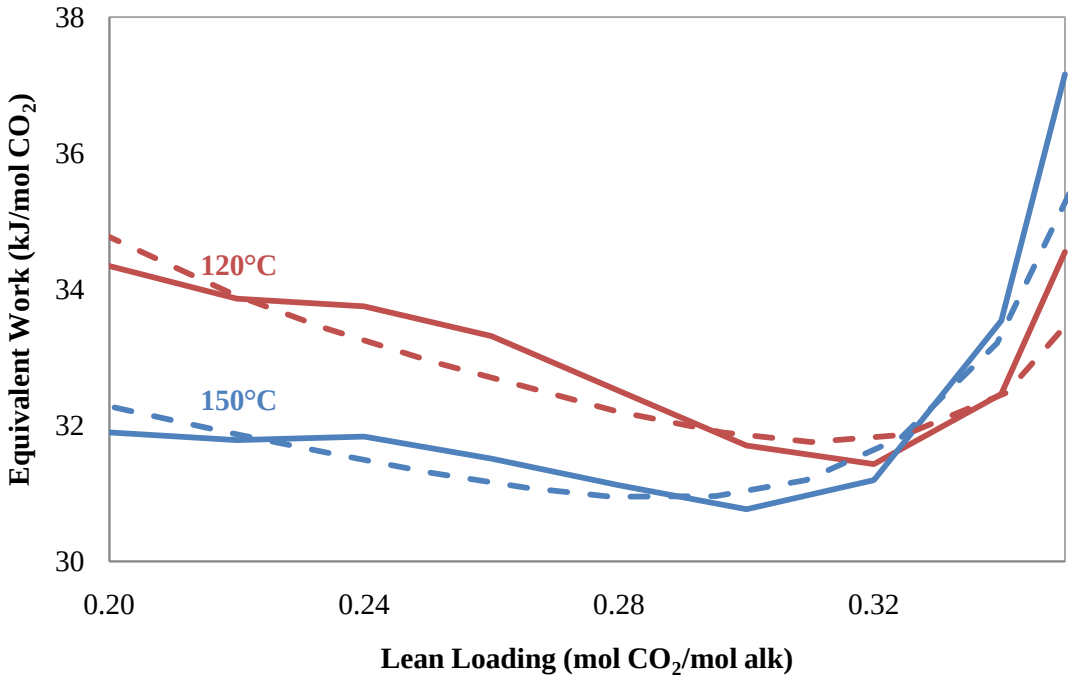


Figure 4-30. Equivalent work calculations for interheated column with 8 m PZ. Solid lines: rich feed calculated by absorber results, Dashed lines: constant rich loading of 0.40. 5 °C cold side approach on main cross exchanger, 5 °C LMTD on interheating exchanger, $CO_2$ compression to 150 bar, 80% liquid extraction for interheating.

### 4.5.3. Assessing the accuracy of heating work calculation

In the previous interheated column simulations, the performance was evaluated using equivalent work. In the equivalent work calculation, the net penalty on electricity

production of a coal plant due to steam usage was calculated. This portion of the equivalent work was the heat work, $W_{heat}$, and it was calculated using Equation 2-5. This expression calculated the electricity production potential of steam that was used in the stripper. It incorporated a Carnot efficiency term and an additional 75% efficiency term. This turbine efficiency value was based on approximations, but it had not been validated. Since this work included work from TUHH with simulations of a real steam cycle for a coal-fired power plant, the effectiveness of this heat work calculation was evaluated. The heating work was calculated for the interheated column simulations using Equation 2-5. A 10 °C approach in the reboiler was used for the steam cycle calculations, so this same approach was used to calculate the heating temperature, $T_{heat}$. The sink temperature, $T_{sink}$, was assumed to be that of cooling water, 32 °C. The calculated heat work values from each Equation 2-5 and the greenfield steam cycle calculations were compared. The two work values for all temperatures were simultaneously used to regress an updated turbine efficiency value in Equation 2-5 to minimize the sum of squared errors. The original efficiency with 75%, and a new turbine efficiency of 96% was found to give the closest match between the Greenfield calculations and heating work calculations. A graphical representation of the match between the heating work calculations and greenfield steam cycle penalty from steam usage is shown in Figure 4-31. The match between work prediction methods was very good. The maximum deviation of the heating work prediction from the steam cycle calculation was 2% with the updated turbine efficiency of 96%.

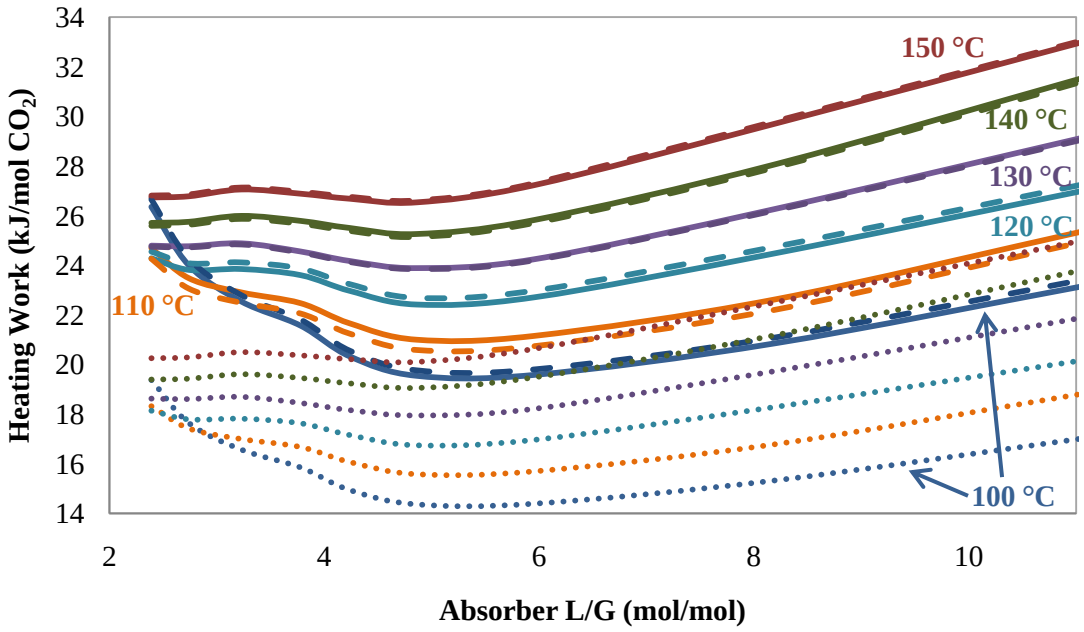


Figure 4-31. Heating work estimates by greenfield plant calculation (- -), heating work calculation with 75% turbine efficiency (···), and heating work calculation updated efficiency of 96% (—).

### 4.5.4. Assessing the accuracy of the compressor work correlation

The TUHH $CO_2$ compressor model results from this collaboration were compared against the predictions by the correlation that was used for this work. In this optimized case study for a greenfield plant, an integrally-geared compressor was considered. The calculation method accounted for the non-ideal behavior of $CO_2$ when compressing into the super critical fluid region. Similar to the simulations were done to generate the compression work correlation, the number of compression stages were varied to achieve a pressure ratio per stage between 1.4 and 2. The collaborative work only compressed $CO_2$ to 110 bar, so the original correlation was updated to this specification to adequately compare the two predictions. Equation 4-3 shows an updated correlation generated by

Aspen Plus predictions. It predicted the work required to compressed $CO_2$ to 110 bar with the minimum number of stages that yielded a compression ratio less than 2.

$$W_{comp}\left(\frac{\mathbf{kJ}}{\mathbf{mol\ CO_2}}\right) = 4.332\ ln\left({}^{110}/_{P_{in}}\right) - 2.275 \qquad \textbf{4-4}$$

The compression work predicted by this correlation was compared against the calculations of the rigorous compressor model. This comparison is graphically Figure 4-32.

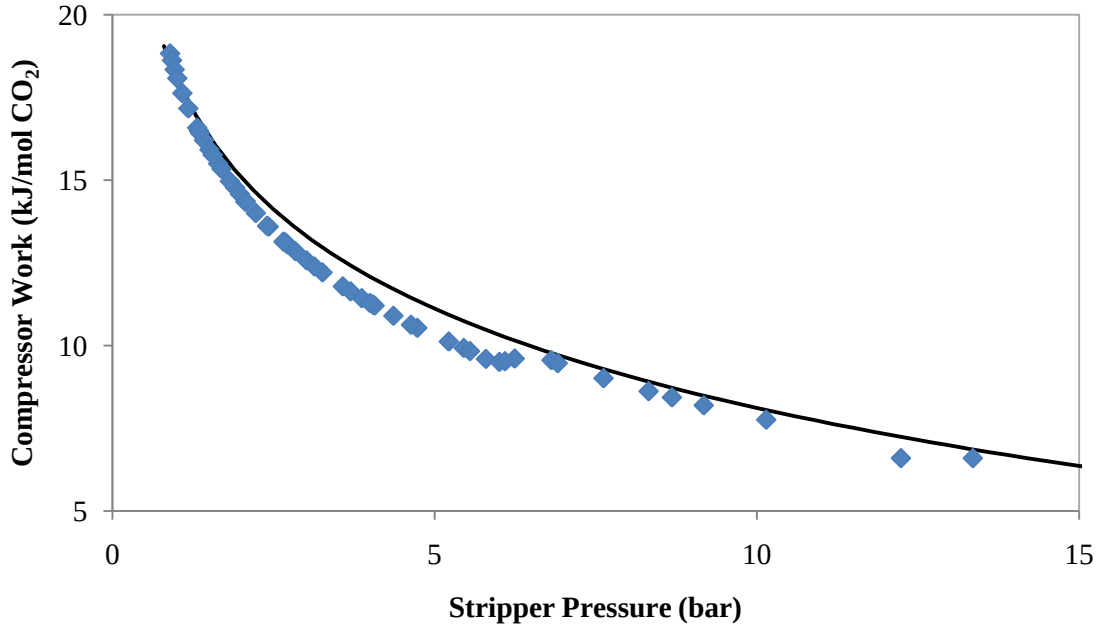


Figure 4-32. Work predictions for $CO_2$ compression to 110 bar. Points = TUHH predictions, line = correlation prediction (Eq. 4-3).

The predictions by the compression work correlation were only slightly higher than the more rigorous predictions by TUHH. The maximum deviation between the two methods was 0.88 kJ/mol $CO_2$. Correlating the TUHH predictions with the same framework as the previous correlation gave Equation 4-4.

$$W_{comp}\left(\frac{\mathbf{kJ}}{\mathbf{mol\ CO_2}}\right) = 4.494\ ln\left({}^{110}/_{P_{in}}\right) - 3.372 \qquad \textbf{4-5}$$

### 4.5.5. Optimized integrated model conclusions

When integrated with the absorber, the stripper model predicted relatively equivalent performance compared to the predictions when only the stripper was considered. The performance was similar because intercooling in the absorber provided a fairly constant rich loading of 0.40 regardless of the lean loading. Additionally, the steam cycle models from TUHH predicted an optimal loading identical to what was predicted by the equivalent expression. However, the heating work expression was found to be inaccurate when calculating the electricity penalty due to steam usage. By adjusting the turbine efficiency from 75% to 96%, the heating work calculations were much closer to the TUHH predictions with their steam cycle model. When considering the lower discharge pressure of 110 bar that was used for this analysis, the correlation from Aspen Plus® data closely predicted the work requirement for the intercooled multi-stage compressor. The correlation from Aspen Plus® always overpredicted the work requirement. The error between the two methods varied with stripper pressure, but the maximum deviation was 0.88 kJ/mol $CO_2$.

## 4.6. CONCLUSIONS

1. Cold rich bypass is an advisable upgrade to the 2-stage flash skid at the pilot plant. A majority of the vapor was produced in the low-pressure vessel, so bypass to only this flash tank had the greatest benefit.

2. Compared to the base case 2-stage flash with 8 m PZ, the predicted equivalent work requirement decreased by 6.6 % to 34.0 kJ/mol $CO_2$. The total volatilized PZ decreased by 63 %. This performance considered 10% cool rich bypass to the LP vessel,

a rich loading of 0.4, and a lean loading and 0.3. These simulations used the exchanger performance from the pilot plant.

3. Changing the pressure ratio to 1.5 balanced the vapor production rates of each flash. Bypassing cold rich solvent to both flash vessels under these conditions dropped the equivalent for further to 30.7 kJ/mol $CO_2$.

4. PZ and 2-stage flash were the solvent and configuration that benefited most from rich bypass due to elevated water content in the overhead vapor. Although the interheated column was the most efficient configuration that was previously simulated, it only experienced minor improvement with bypass.

5. The minimum work requirement for an advanced 2-stage flash configuration using 8 m PZ and 150 °C brine was 35.5 kJ/mol $CO_2$. The required heat rate for a 60 $MW_e$ coal-fired power plant was 40.8 MW.

6. The modified Fluor configuration using geothermal heating with 9 m MEA had a total energy requirement of 36.4 kJ/mol $CO_2$ and a heat rate of 38.6 MW for a 60 $MW_e$ coal-fired power plant.

7. The 2T2PFlash with PZ had a lower work requirement than the Fluor configuration because its cross exchangers were able to take better advantage of the high-temperature brine compared to the reboiler in the Fluor configuration.

8. Integrating the stripper section with the absorber had little effect on the prediction of the energy requirement. The rich loading had only slight variation with different values of lean loading when intercooling was used.

9. The predicted values of heating work were compared against steam cycle model calculations. A turbine efficiency of 96% in the heating work calculation matched the two methods well.

10. The compressor work correlation developed from Aspen Plus calculations only slightly overpredicted work values that were rigorously calculated by a TUHH model. The maximum overprediction was 0.88 kJ/mol $CO_2$.

# Chapter 5: Pilot Plant Modeling

This chapter describes reproduction of pilot plant results using solvent models that were introduced in the earlier work. The pilot plant campaigns used either 9 m MEA or 8 m PZ. Several campaigns were run with each solvent, and deviations between pilot plant measurements and simulation values are analyzed in this chapter. In addition to the traditional simple absorber and simple stripper configuration, the pilot plant experimented with a new 2-stage flash skid to demonstrate the practicality of predictions in this work. Additionally, an intercooled absorber was used in some campaigns to achieve better $CO_2$ removal and higher rich loading. The simulations generally fit the data, but the temperature profile and heat loss was difficult to replicate.

## 5.1. PILOT PLANT FOR $CO_2$ CAPTURE

An ongoing project at The University of Texas at Austin is pilot plant campaigns to demonstrate the practicality of new solvents and configurations. The pilot plant is located at the J. J. Pickle Research Center in North Austin. It is a multi-functional facility with the ability to run $CO_2$ capture campaigns as well as distillation. The $CO_2$ absorption/stripping unit runs with synthetic flue gas comparable to a 0.1 to 0.2 MW coal-fired power plant. The removed $CO_2$ runs in a closed loop, and the balance of the flue gas is air. The pilot plant has gone through many modifications, but it typically runs with a simple absorber and simple stripper configuration (Chen, 2007; Plaza et al., 2010).

In the past the pilot plant has been run with the baseline solvent, 7 m MEA, as well as a promising blend of $K^+$/PZ. Over the course of this work, campaigns were run using 9 m MEA as well as 8 m PZ. The regeneration was usually accomplished using a simple stripper. Based on preliminary results from this work, a 2-stage flash skid was constructed at the pilot plant to evaluate the effectiveness of high temperature stripping with concentrated piperazine. Consequently, a campaign in December 2010 was run with the 2-stage flash. The general simple stripper configuration and measurements taken from the pilot plant are shown in Figure 5-1. This flowsheet applied to all simple stripper campaigns except for the single 9 m MEA run in October 2007. The difference in the flowsheet for this early run is described in section 5.2.1.

Each campaign ran for multiple weeks and operating conditions were collected for 8 to 14 runs. Each run attained steady-state using a Delta V control system from Fisher Rosemount. Each run condition was measured in real time, and the steady-state value of each parameter was determined by averaging a series of values for that parameter after reaching steady-state. All of the relevant time-averaged conditions around the stripper from each run were used to assess the accuracy of the simulation results as well as the pilot plant measurements.

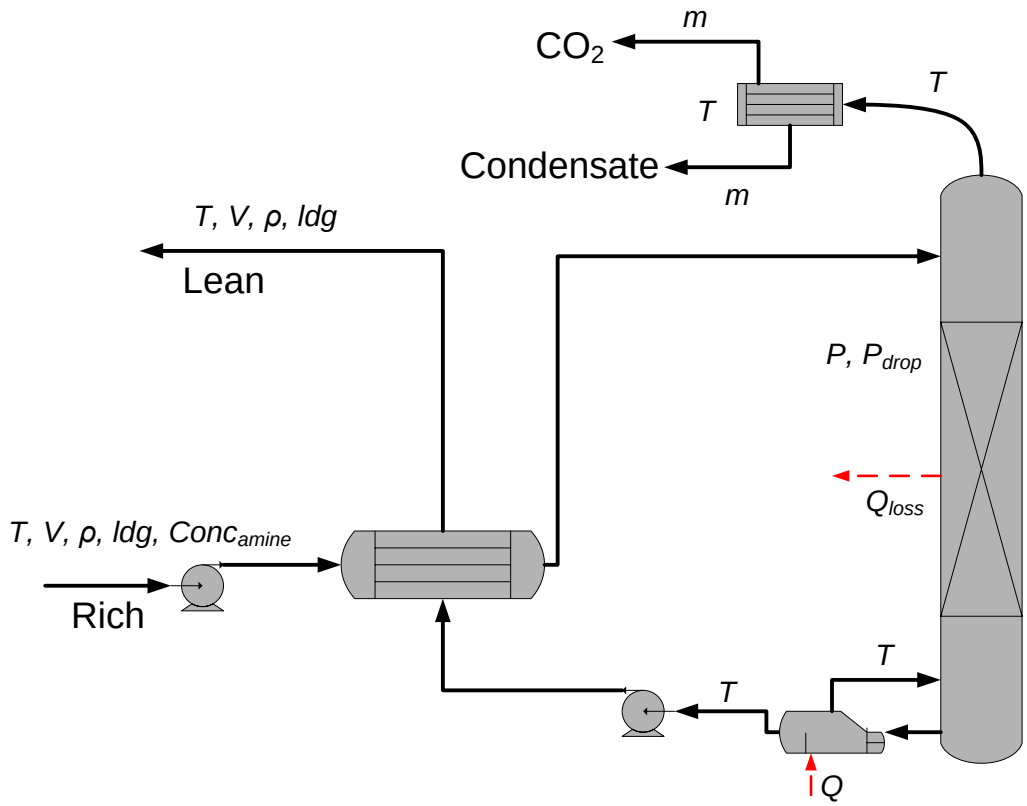


Figure 5-1. J. J. pickle pilot plant simple stripper configuration and measurements. Measured conditions listed in italics.

### 5.1.1. On-Site Heat Balance Calculations for the Stripper

Since the stripper operated at high temperature, it experienced heat loss even though there was insulation around the column. The pilot plant operators derived a correlation to calculate the expected heat loss of the stripper. This correlation was used for every campaign, regardless of the solvent and operation type (stripping or distillation). Steam was boiled in the stripping column to calibrate the temperature sensors, and the closure of the energy balance was evaluated considering the reboiler and condenser duties. The heat loss for each test trial was calculated as the difference

between the reboiler and condenser duties. Finally, a correlation for predicted heat loss was derived in the form of Equation 5-1.

$$\boldsymbol{Q_{Loss}}\left(\frac{\boldsymbol{BTU}}{\boldsymbol{hr}}\right) = \boldsymbol{C}\,(\boldsymbol{T_{T2075}} - \boldsymbol{T_{T902}}) \qquad \textbf{5-1}$$

$T_{T2075}$ was the internal stripper temperature and $T_{T902}$ was the ambient temperature. The constant, ***C***, was the regressed parameter. Its value for the different process configurations and process conditions are displayed in Table 5-1. The heat loss was correlated for both the stripping column and the 2-stage flash skid. In the case of the stripping column, different values of ***C*** were found for reboiler duties greater than and less than 0.4 MMBTU/h. The correlation for the 2-stage flash heat loss used temperature sensor $T_{T530B}$ for the internal temperature in place of $T_{T2075}$. $T_{T2075}$ was a mid-column measurement of the stripper, and $T_{T530B}$ was the temperature measurement of the liquid exiting the first flash vessel.

**Table 5-1. Heat loss correlation coefficient for Equation 5-1 with various pilot plant configurations.**

| **Configuration** | **Reboiler duty** *MMBTU/h* | **C** *BTU/h-F* |
|---|---|---|
| Column | > 0.4 | 500 |
| Column | < 0.4 | 300-400 |
| 2-stage flash | All | 350 |

The heat loss prediction at the pilot plant was to be a rough estimate of heat loss and not an exact value. The ***C*** coefficient was designed to empirically represent a pseudo UA value, combining both the overall heat transfer coefficient and the exposed surface area of hot process units and piping (Seibert, 2011).

This predicted heat loss was considered to be a variable in the Aspen Plus® simulations of the pilot plant campaigns. Many of the heat loss predictions appeared to agree with the simulations, but the heat loss was a key variable to match the material and

energy balances for the Fall 2008 PZ campaign and Summer 2010 MEA campaign. In these two campaigns, the "measured heat loss" referred to the value calculated by the pilot plant correlation (Equation 5-1), and the "simulation heat loss" referred to the final heat loss value used in the simulation that matched the material and energy balances.

The heat balance of the stripper was also calculated during every run at the pilot plant. This balance was calculated as the sum of all cooling duties and stream enthalpy flows ratioed to the reboiler duty, shown in Equation 5-2. This heat balance with the reboiler and condenser duties, correlated heat loss, simple representations of stream enthalpies, and an assumed heat of absorption was typically within 10% error. The enthalpies of the material streams were calculated using heat capacity and calculating the change from a reference temperature. They did not account for the change in enthalpy due to the desorption of $CO_2$, so the heat of absorption term, $Q_{abs}$, was included.

$$\%\,\boldsymbol{Balance} = \frac{\boldsymbol{Q_{cond} + Q_{loss} + Q_{abs} + Q_{bottom} + Q_{CO2} - Q_{feed}}}{\boldsymbol{Q_{reboiler}}} \qquad \textbf{5-2}$$

For the purposes of this work, when the energy balance of the simulations of pilot plant runs were evaluated, the net unaccounted heat flux was used instead of the percent balance value:

$$\boldsymbol{Q_{balance} = Q_{reboiler} + Q_{feed} - Q_{cond} - Q_{loss} - Q_{abs} - Q_{bottom} - Q_{CO2}} \qquad \textbf{5-3}$$

Aspen Plus® calculated the change in enthalpy of the material streams using model parameters which accounted for the changing composition between the rich and lean solvent. Therefore, this calculation of the change in enthalpy accounted for the desorption of $CO_2$, so the heat of absorption term was not required for the calculation of the simulation energy balance.

### 5.1.2. Analysis of campaign simulation accuracy

The simulation of each pilot plant run provided results to be compared with the pilot plant measurements. The mean absolute percentage error (MAPE) was used to collectively quantify the error across a single campaign. The calculation of this statistic for all of the conditions of one run is as follows:

$$\boldsymbol{MAPE = \frac{1}{n}\sum_{i=1}^{n}\left|\frac{S_i - M_i}{M_i}\right| \cdot 100\%} \qquad \textbf{5-4}$$

where $\boldsymbol{n}$ was the number of measurements, $\boldsymbol{S_i}$ was the simulation results for condition $\boldsymbol{i}$, and $\boldsymbol{M_i}$ was the pilot plant measurements for condition $\boldsymbol{i}$. The MAPE was also calculated for each condition across all the runs to find the average percentage deviation in that condition. Finally, an overall MAPE value for the campaign was calculated by averaging the MAPE values for each run.

### 5.1.3. Evaluating pilot plant performance

The heat duties of the runs in each campaign were normalized by the $CO_2$ gas rate to quantify the performance. The heat duties were also corrected for heat loss by subtracting the respective heat loss value from the duty. This calculation was performed for the simulation values as well as the measured values. In each case, the heat loss that paired with each duty was used for the calculation; the measured heat loss values were used to correct the measured heat duties, and the simulation heat loss values were used to correct the simulation heat duties.

A projected equivalent work was also calculated for the pilot plant runs. The simulation results for each run calculated a pump work, and the expected compression work was calculated using the previously derived correlation, Equation 3-1. The equivalent work was calculated both with and without heat loss correction of the heat

duty. Considering the minimum predicted equivalent work for each campaign made it possible to compare the performance of the pilot plant to the simple stripper predictions in Chapter 3.

## 5.2. MEA PILOT PLANT CAMPAIGNS

Two sets of pilot plant data were collected using 9 m MEA, a more concentrated variation of the baseline solvent. This solvent needed to be evaluated in the pilot plant to determine if it could be a practical improvement from the baseline, or whether it caused any operational difficulties. The first campaign was only a single run in October 2007. This run served to demonstrate that 9 m MEA was operationally practical for absorption/stripping. The second campaign with 9 m MEA was in September 2010, and it included a full set of 12 runs. This campaign also ran without problems. The Hilliard model for MEA was used for the simulations. The data from these two campaigns are evaluated in the next two sections. However, as seen in Figure 2-3, the Hilliard model for 9 m MEA overpredicted the $CO_2$ partial pressure at elevated temperature. The analysis of the MEA pilot plant campaigns demonstrated this issue.

### 5.2.1. 9 m MEA Baseline Run (Fall 2007)

Data was available from a single run that was executed in October 2007 using 9 m MEA. Since 7 m MEA is the typical concentration, the data from this run was used as a preliminary evaluation tool for the practicality of MEA at this concentration. Additionally, the new Hilliard model for MEA needed to be validated against real plant data. There was not a full campaign of runs, but the single run was enough to address the accuracy of the thermodynamic model when used at pilot scale.

The column contained 6.1 m of Mellapak 250Y packing with an inner diameter of 0.43 m. The stripper was coupled with a simple absorber with identical dimensions. The stripper configuration was different from what would typically be expected, and it is depicted in Figure 5-2. The reboiler was configured to heat only a fraction of the sump drawoff, but the split fraction was not recorded at the pilot plant. While this was a source of uncertainty when evaluating the stripper performance, it provided an additional variable for fitting the pilot plant data.

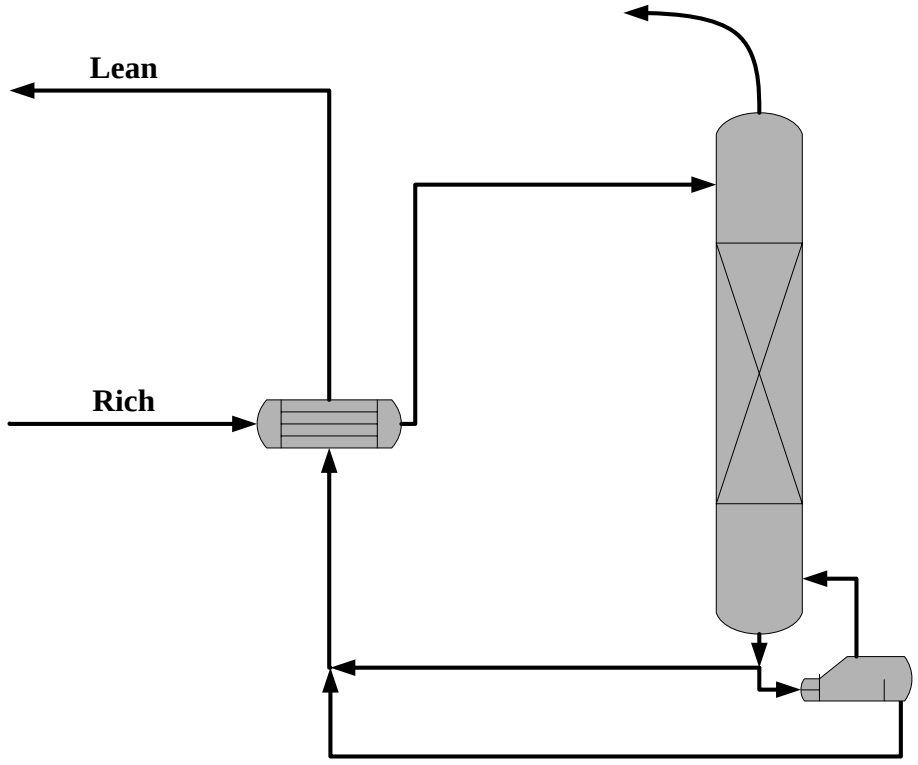


Figure 5-2. Fall 2007 pilot plant stripper flowsheet. Sump stream split between reboiler and main cross exchanger.

This Aspen Plus® simulation work assumed equilibrium reactions in the stripper. The RateSep™ tool rigorously calculated the heat and mass transfer for each stage of the simple stripper. The packing mass transfer and interfacial area model by Onda et al.

(1968) was used to estimate liquid mass transfer coefficients and interfacial area. The reboiler was modeled as equilibrium.

Temperature, composition, and flow rates were measured for the rich and lean streams. The reboiler heat duty, column pressure, and column pressure drop were also measured. The pilot plant used the existing correlation for measuring heat loss from the column, which was also reported. Finally, temperature was measured at six points throughout the column, in the reboiler, in the sump, and in the overhead vapor. The heights in packing of the six thermocouples are detailed in Table 5-2, measured from the top of the packing. The pilot plant measurements of the operating conditions around the stripper are listed in Table 5-3.

**Table 5-2. Thermocouple locations in stripper packing for pilot plant run in October 2007 run with 9 m MEA**

| Thermocouple | ID | d from top (m) |
|---|---|---|
| $T_1$ | T20710 | 0 |
| $T_2$ | T2078 | 0.99 |
| $T_3$ | T2076 | 2.92 |
| $T_4$ | T2075 | 3.05 |
| $T_5$ | T2073 | 4.01 |
| $T_6$ | T2071 | 6.08 |

The data-fit package within Aspen Plus® was used to reconcile the individual differences between pilot plant measurements and simulation predictions. The most significant deviations between pilot plant data and simulation values were the temperatures in the column. The data-fit reconciliations initially failed to produce close agreement of the temperature measurements in the column, but the best solution method was determined to be adjusting heat duties in selected stages within the column to estimate a heat loss profile. Since the heat loss predicted by the pilot plant correlation was a single value as opposed to a profile, these individual heat duties on stages were specified to match the estimated temperature profile with the six given measurements.

To reduce the number of free variables, the split ratio to the reboiler and its duty were adjusted to match the reboiler temperature and lean loading. The agreement between the values in Table 5-3 demonstrates that the $CO_2$ removal at the pilot plant was verified with the model.

**Table 5-3. October 2007 simple stripper pilot plant run measurements and simulation results (9 m MEA)**

| Variable | Pilot Plant | Aspen Plus® | Variable | Pilot Plant | Aspen Plus® |
|---|---|---|---|---|---|
| *Lean stream* | | | *Column data* | | |
| T (°C) | 44.9 | 44.9 | $T_1$ (°C) | 87.6 | 86.7 |
| Flow (kg/min) | 73.3 | 70.9 | $T_2$ (°C) | 86.3 | 86.3 |
| Ldg (mol/mol) | 0.36 | 0.36 | $T_3$ (°C) | 87.9 | 87.9 |
| *Rich stream* | | | $T_4$ (°C) | 90.4 | 90.4 |
| T (°C) | 50.2 | 50.4 | $T_5$ (°C) | 91.0 | 91.0 |
| Flow (kg/min) | 70.6 | 69.0 | $T_6$ (°C) | 95.3 | 95.3 |
| Ldg (mol/mol) | 0.48 | 0.48 | Reboiler T (°C) | 102.7 | 102.7 |
| *Heat exchanger Ts* | | | Q (kW) | 143.0 | 143.3 |
| Rich in (°C) | 44.9 | 44.9 | Q loss (kW) | 22.6 | 24.9 |
| Rich out (°C) | 91.6 | 93.1 | Sump T (°C) | 98.2 | 97.8 |
| Lean in (°C) | 98.6 | 99.7 | Column P, bot (kPa) | 105.0 | 105.0 |
| Lean out (°C) | 50.2 | 50.4 | ΔP, top (kPa) | 0.14 | 0.14 |
| *Performance* | | | ΔP, bot (kPa) | 0.15 | 0.15 |
| Eq Work (kJ/mol $CO_2$) | - | 41.2 | Outlet vapor T (°C) | 87.4 | 87.0 |
| | | | Packing ht (m) | 6.10 | 2.13 |

The stripper was run with a reboiler temperature of 103 °C, which was much cooler than the ceiling temperatures for MEA of 120 °C. The solvent model was able to match this temperature well with the column pressure and lean loading. The simulation predicted a nearly identical reboiler duty, and the heat loss was only 12% greater than the calculated heat loss at the pilot plant. The average variation between measured and calculated values was 3.8%. The most significant change was the packing height, which was reduced to about 35% of the actual height. The packing height was reduced so significantly in order to match the measured temperature profile while maintaining an overall heat loss close to the pilot plant prediction. This result suggested that the Onda

correlation for interfacial area was insufficient for this application in aqueous amine based $CO_2$ capture. Due to the speed of the reactions and the high mass transfer rates, very little packing height was required in the stripper to attain equilibrium between the vapor and liquid at the top of the column.

Other than the significant change in the packing height, the property predictions and overall energy balance were confirmed using the Hilliard MEA model, and the temperature profile was matched using on-stage heat duties. Figure 5-3 displays the measured column temperature profile as a function of relative column height, the initial Aspen calculation with no heat loss, and the final Aspen calculation with a matched temperature profile by adjusting the heat loss.

However, the liquid and vapor were at a mass transfer pinch at the top of the column for all cases. Therefore the temperature profile, packing height, and ability to match other data should be a weak function of operating conditions. This pilot plant operation is primarily a validation of the equilibrium model at these conditions. Although the partial pressure of $CO_2$ was shown to be fit poorly by the model at high temperature (Figure 2-3), the temperature of this stripper run was low enough that only very minor deviation was observed. Additionally, split ratio around the reboiler was used to match its temperature, and the increase in heat duty to match the column profile also served to match the performance of the column. These available variables were enough to force the stripper material and energy balances from the simulation to match the measurements, even though there should have been deviations.

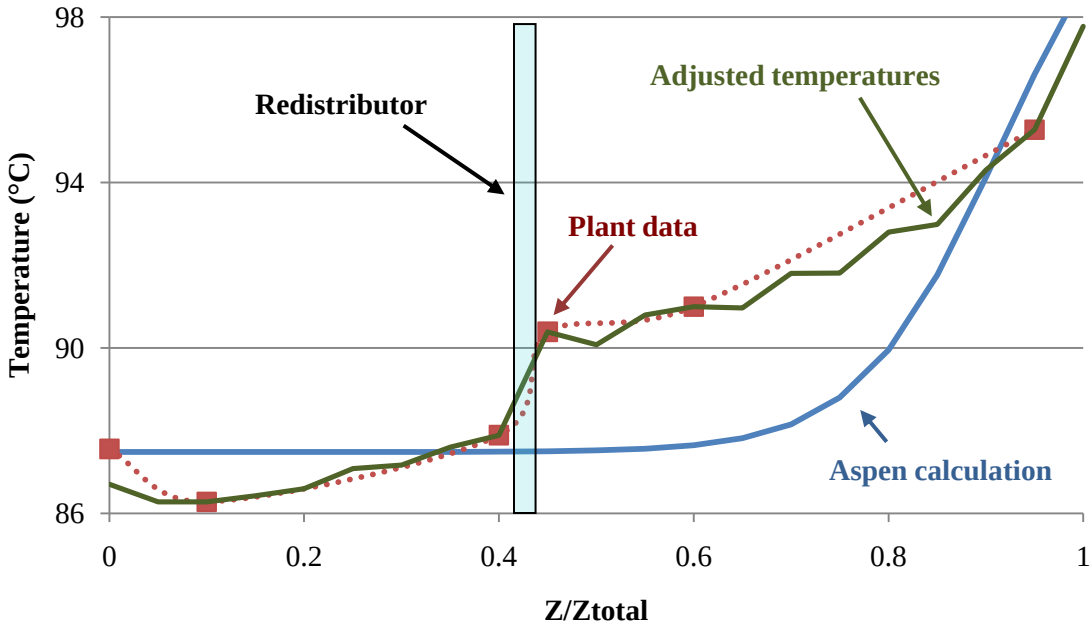


Figure 5-3. Temperature Profiles in Pilot Plant and Aspen Simulation. Rich loading = 0.48, 63% removal in absorber. "Aspen calculation": no heat loss, 75% split to reboiler, 6.1 m MP250Y packing. "Adjusted temperatures": 1.5 m MP250Y packing, heat loss adjusted to match T profile.

It was anticipated that the heat duties on individual stages would help predict the heat loss profile. However, the heat loss did not follow a believable profile; the simulation predicted heat gains in some sections. Heat duties were imposed on only 12 of the 20 packed stages, so the heat loss profile was smoothed for graphical representation by averaging $\boldsymbol{Q_{n-1}}$ through $\boldsymbol{Q_{n+1}}$ for each stage $\boldsymbol{n}$. This demonstration is shown in Figure 5-4. The majority of the heat loss was predicted to occur at the bottom of the column. This prediction was expected since the column temperature was highest at the bottom. The exact heat loss values predicted by the simulation are shown in Table 5-4.

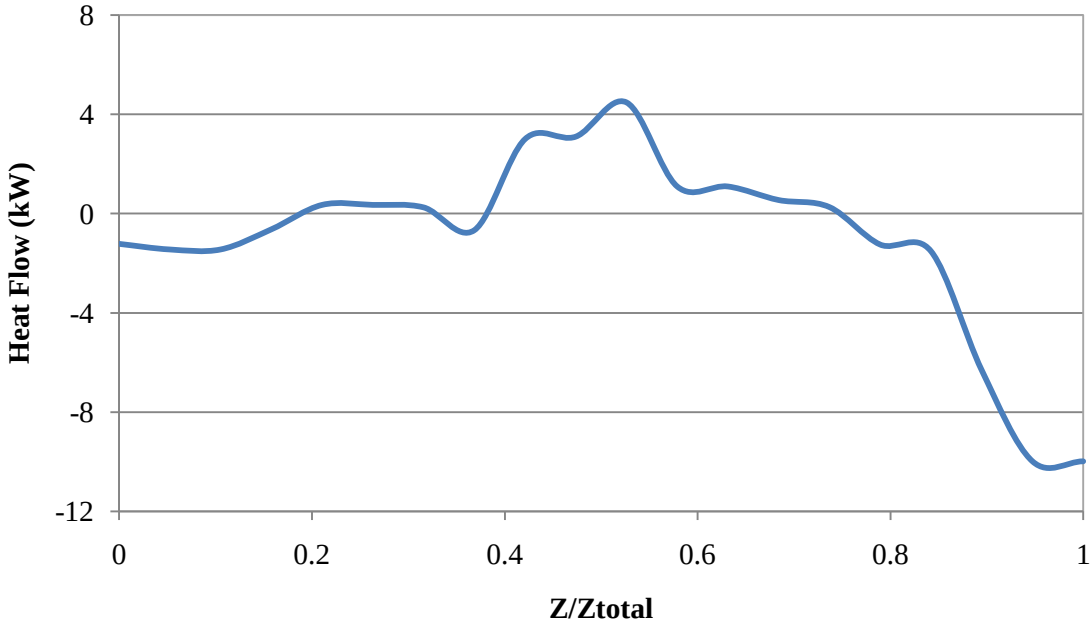


Figure 5-4. Heat flow profile to match temperature profile in pilot plant run with 9 m MEA. 0 = top of column, 1 = bottom of column.

**Table 5-4. Heat duties imposed in stripper column to match temperature profile.**

| Relative distance from top | Heat Flow *kW* |
|---|---|
| 0.05 | -2.43 |
| 0.11 | -1.90 |
| 0.26 | 1.06 |
| 0.37 | -0.30 |
| 0.42 | -1.71 |
| 0.47 | 11.02 |
| 0.58 | 2.44 |
| 0.63 | 0.85 |
| 0.74 | 0.80 |
| 0.84 | -4.54 |
| 0.95 | -14.40 |
| 1.00 | -15.56 |

Due to the large temperature increase through the redistributor from the top section to bottom section, a significant heat gain was predicted in the middle of the column. This behavior could not happen since the temperature of the stripper was about 90 °C, far above the ambient temperature of about 25 °C. The reason for this sharp

increase in temperature would require an in-depth analysis of the internal flow patterns and heat transfer of the column. However, the increase in the bottom packing section could have been due to the redistribution of hot liquid to the outside of the column where the thermocouples were measuring temperature. Another possible explanation for the increase in temperature from the transition from the top to bottom packing sections was a reduced amount of insulation around the redistributor where significant heat loss could have occurred. While this explanation could explain a drastic temperature change of the vapor when traveling from the bottom to top packing section, the simulation results suggested that heat loss alone could not induce the temperature change that was observed.

In summary, the Hilliard MEA model appropriately predicted process conditions and energy performance at the pilot plant using 9 m MEA, even though the VLE predictions of the model should have been inaccurate. The available variables permitted the simulation material and energy balances to match the measurements. The Onda model did not predict the interfacial area of the packing well, and the simulation only required 35% of the packing height that the pilot plant column used. A balanced heat loss profile in the column did not accurately predict the temperature profile. Imposed heat duties on 12 of the 20 packing stages were adjusted to match the temperature profile. This method demonstrated that there was more complexity to the temperature change within the column than the model predicted. This difference could have been due to a non-distributed heat loss profile, complex liquid or vapor flow patterns, or temperature measurements of only a single phase. A significant temperature increase from the top to bottom packing sections required a heat input in the simulation. The flow patterns of liquid in the column may have been such that it did not migrate from the middle to outside of the column, or vice versa. If this were to happen, the liquid at the outside of the column would cool substantially compared to the liquid flowing through the middle

of the column. An analysis of flow patterns through the packing could provide insight to this result.

### 5.2.2. 9 m MEA Intercooled Absorber and Simple Stripper Campaign (Summer 2010)

9 m MEA was run in the pilot plant again in August 2010. The stripper configuration was still a simple stripper, but the absorber was intercooled to attain higher rich loadings. The configuration of the stripper and the available measurements are detailed in Figure 5-1. This campaign was used mostly to evaluate the impact of intercooling, but it provided another opportunity to validate the Hilliard MEA model at stripper conditions.

The stripper used two 10-foot beds of Raschig-Jaeger RSP 250 packing. The ceiling temperature of MEA is 120 °C, but the goal temperature for these runs was 115 °C. Consequently, the stripper pressure varied from 1.5 to 2.2 bar. The data-fit package was not used for the simulations because it did not provide results that represented converged mass and energy balances. The optimal evaluation method was determined to be running the stripper simulation using pilot plant measurements for the required inputs. The deviations of the results were evaluated.

The initial run using pilot plant measurements as inputs yielded low deviations for most result variables except the $CO_2$ gas rate and lean loading. Further inspection revealed that not only were all of the simulation predictions for these two result variables higher than their pilot plant measurements, but they were also roughly linearly correlated. As Figure 5-5 shows, the deviations followed the x-y line when plotted as percent deviations. This outcome suggested that the predicted amount of $CO_2$ stripped from

solution was equally over predicted on the gas and liquid sides. A parity plot of the pilot plant measurements of $CO_2$ removal based on gas and liquid measurements confirmed that the large deviations were not due to gross inaccuracies in either the gas side or liquid side measurements, Figure 5-6. It was concluded that the energy balances of the measurements and simulations were inconsistent. The energy balance could have been incorrect either through model predictions or pilot plant measurements. Not only was the heat of absorption in 9 m MEA matched in the thermodynamic model within the error of the laboratory measurements, but manipulating the model parameters to attempt to correct this energy balance issue would have created more problems than it fixed. Therefore, the focus of correcting the energy balance was directed toward pilot plant measurements. Since the pilot plant heat loss prediction was only a rough estimate, this value was used as an adjustable parameter.

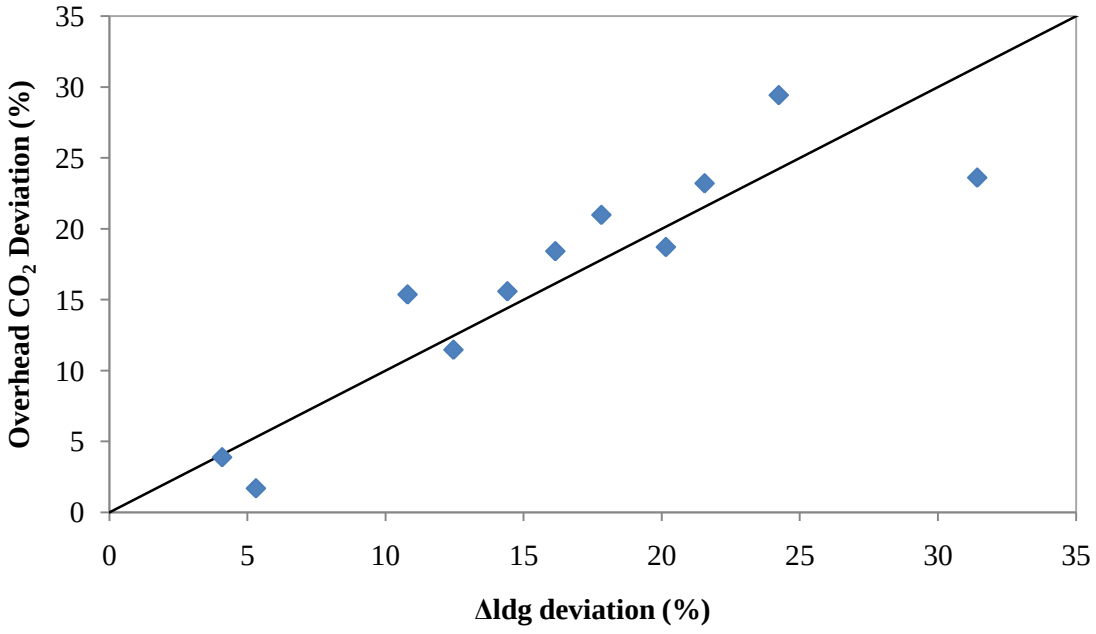


Figure 5-5. Simulation results without heat loss manipulation for 2010 simple stripper campaign with 9 m MEA. Percent deviations of overhead $CO_2$ rate and Δldg were correlated.

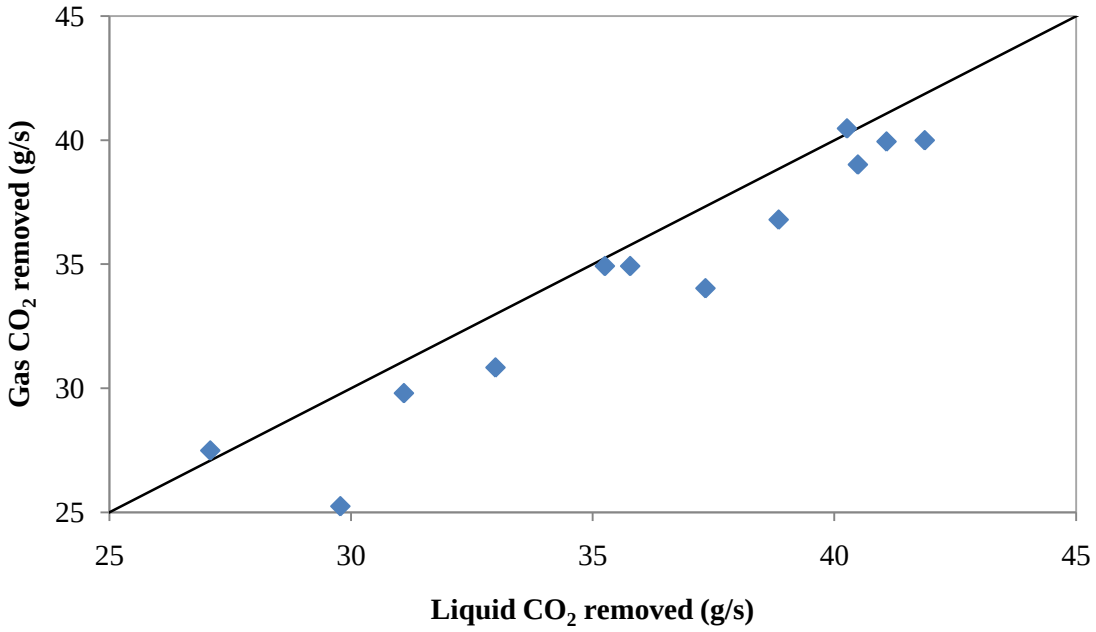


Figure 5-6: Parity plot of measured $CO_2$ removal by gas side (measured $CO_2$ flow rate) and liquid side (product of solvent rate and change in loading) measurements at pilot plant.

Adjusting the heat loss of the stripper column in the simulations effectively reduced the deviations of the lean loading and overhead $CO_2$ rate. The mean average percentage error (MAPE) was used to evaluate the deviations of the simulation results from the pilot plant measurements. Using the measured heat loss as a variable to match the material balance, the MAPE of each run was between 0.9 and 3.7%. The simulation heat loss values needed to be increased by 35 to nearly 180% compared to the measured pilot plant heat loss values. The raw pilot plant measurements for the stripper are in Table 5-5. Simulations were run using heat loss to match lean loading, and the deviations between the final simulation results and the corresponding pilot plant measurements are in Table 5-6. The heat loss was adjusted significantly, but it was not included in the

calculation of the MAPE since the heat loss values that were provided were rough predictions, not raw measurements.

**Table 5-5. Pilot plant measurements from Fall 2010 simple stripper-campaign with 9 m MEA.**

| Variable | Run → | 1 | 2 | 3 | 4 | 5 | 6 | 7 | 8 | 9 | 10 | 11 | 12 |
|---|---|---|---|---|---|---|---|---|---|---|---|---|---|
| **Rich flow** | *kg/s* | 1.16 | 1.16 | 0.77 | 0.77 | 1.20 | 1.16 | 1.04 | 1.05 | 1.19 | 1.19 | 0.63 | 0.64 |
| **Rich T** | *C* | 51.2 | 48.1 | 46.7 | 46.1 | 53.2 | 51.2 | 45.3 | 44.9 | 49.8 | 44.2 | 36.5 | 36.5 |
| **Lean flow** | *kg/s* | 1.10 | 1.10 | 0.73 | 0.73 | 1.14 | 1.10 | 0.98 | 1.00 | 1.12 | 1.17 | 0.58 | 0.59 |
| **Lean exit T** | *C* | 53.1 | 50.3 | 48.4 | 47.9 | 55.1 | 53.1 | 47.5 | 47.0 | 52.0 | 47.5 | 38.1 | 38.0 |
| **Reboiler T** | *C* | 113.7 | 113.8 | 116.8 | 116.0 | 116.5 | 113.7 | 116.6 | 116.3 | 117.8 | 118.0 | 114.7 | 114.7 |
| **Rich feed T** | *C* | 51.2 | 48.1 | 46.7 | 46.1 | 53.2 | 51.2 | 45.3 | 44.9 | 49.8 | 44.2 | 36.5 | 36.5 |
| **Rich hot T** | *C* | 108.8 | 108.7 | 111.0 | 110.2 | 111.5 | 108.8 | 110.8 | 110.5 | 110.9 | 112.6 | 107.3 | 107.4 |
| **Rich P** | *kPa* | 431 | 434 | 425 | 424 | 401 | 431 | 416 | 425 | 422 | 424 | 352 | 358 |
| **Overhead T** | *C* | 103.5 | 103.3 | 102.5 | 101.6 | 106.3 | 103.5 | 103.6 | 102.7 | 103.7 | 104.0 | 100.4 | 100.2 |
| **$CO_2$ rate** | *kg/s* | 0.035 | 0.037 | 0.030 | 0.031 | 0.034 | 0.035 | 0.039 | 0.040 | 0.025 | 0.027 | 0.040 | 0.040 |
| **Cond. rate** | *kg/s* | 0.026 | 0.037 | 0.000 | 0.013 | 0.000 | 0.026 | 0.022 | 0.056 | 0.003 | 0.017 | 0.015 | 0.014 |
| **Condenser T** | *C* | 33.3 | 33.9 | 27.9 | 31.1 | 32.9 | 33.3 | 25.4 | 26.6 | 31.1 | 32.5 | 24.7 | 24.5 |
| **Reboiler duty** | *kW* | 166.4 | 171.3 | 136.5 | 139.8 | 175.8 | 166.4 | 176.7 | 175.7 | 121.5 | 123.1 | 177.4 | 177.2 |
| **Heat loss** | *kW* | 19.5 | 19.4 | 25.7 | 31.8 | 31.4 | 19.5 | 25.9 | 25.7 | 26.0 | 26.0 | 26.8 | 26.7 |
| **Column P** | *kPa* | 165.4 | 165.4 | 182.7 | 177.1 | 177.8 | 165.4 | 177.5 | 177.5 | 219.2 | 219.2 | 158.5 | 158.5 |
| **Pressure drop** | *kPa* | 0.528 | 0.595 | 0.176 | 0.235 | 0.509 | 0.528 | 0.233 | 0.255 | 0.387 | 0.430 | 0.039 | 0.041 |
| **Reboiler liq T** | *C* | 113.7 | 113.8 | 116.8 | 116.0 | 116.5 | 113.7 | 116.6 | 116.3 | 117.8 | 118.0 | 114.7 | 114.7 |
| **Reboiler vap T** | *C* | 112.8 | 112.9 | 116.2 | 115.4 | 115.2 | 112.8 | 115.5 | 115.2 | 115.2 | 115.4 | 114.6 | 114.5 |
| **Lean ldg** | *mol/mol* | 0.314 | 0.292 | 0.285 | 0.280 | 0.284 | 0.288 | 0.280 | 0.277 | 0.364 | 0.362 | 0.197 | 0.199 |
| **Rich ldg** | *mol/mol* | 0.416 | 0.431 | 0.457 | 0.460 | 0.407 | 0.407 | 0.441 | 0.446 | 0.460 | 0.464 | 0.483 | 0.474 |
| **MEA conc** | *m* | 9.15 | 8.98 | 8.97 | 9.10 | 9.46 | 9.27 | 8.91 | 8.79 | 8.66 | 8.67 | 8.49 | 8.57 |

**Table 5-6. Deviation in result variables from pilot plant measurements of Fall 2010 pilot plant simple stripper campaign with 9 m MEA. Heat loss used to match lean loading.**

| Variable | 1 | 2 | 3 | 4 | 5 | 6 | 7 | 8 | 9 | 10 | 11 | 12 | MAPE |
|---|---|---|---|---|---|---|---|---|---|---|---|---|---|
| **Lean flow** | 1% | 1% | 0% | 0% | 1% | 1% | 0% | 0% | 4% | -1% | -2% | -1% | 1.1% |
| **Rich hot T** | -2% | -1% | -3% | -3% | -2% | -1% | -2% | -1% | -3% | -6% | -2% | -1% | 3.0% |
| **Overhead T** | -3% | -3% | -3% | -3% | -4% | -2% | -3% | -2% | -2% | -3% | 1% | 1% | 2.5% |
| **$CO_2$ rate** | -2% | 3% | 2% | 4% | 5% | -5% | -1% | 2% | 1% | -1% | -1% | -4% | 2.5% |
| **Reboiler liq T** | -3% | -3% | -3% | -3% | -4% | -3% | -3% | -2% | -6% | -6% | 0% | 0% | 4.0% |
| **Lean ldg** | -6% | 0% | 0% | 0% | 0% | 0% | 0% | 0% | 0% | 0% | 1% | 1% | 3.0% |
| **MAPE** | 2.3% | 2.2% | 2.4% | 2.7% | 3.4% | 2.5% | 1.9% | 1.5% | 3.6% | 3.7% | 0.9% | 1.3% | 2.7% |
| **Heat loss** | 179% | 148% | 71% | 35% | 91% | 192% | 106% | 81% | 66% | 40% | 62% | 74% | 101% |

Figure 5-7 shows the behavior of the normalized heat duty as a function of lean loading. The heat duty was normalized as described in section 5.1.3. The measured heat duty was corrected by the measure heat loss, and the simulation heat duty was corrected by the simulation heat loss. There was a significant difference in the normalized heat duty values from measurements and simulations. This was due to the drastic increase in heat loss for the simulations, which reduced the heat duty when corrected for heat loss. Prior modeling results suggested that a minimum heat duty should be reached at a specific lean loading, and the heat duty should decrease with increasing rich loading. Even though the runs were categorized by rich loading, the rich loading still varied slightly, and the reboiler temperature was also not constant. Nonetheless, a general decrease in heat duty with increasing rich loading was observed. The highest rich loading of 0.47 had the largest variety of lean loadings, and a minimum heat duty appeared to occur around a lean loading of 0.29. However, the optimum was flat and may have been an illusion of data scatter. The optimal lean loading in Chapter 3 was approximately 0.4 for this solvent when the rich loading was 0.5.

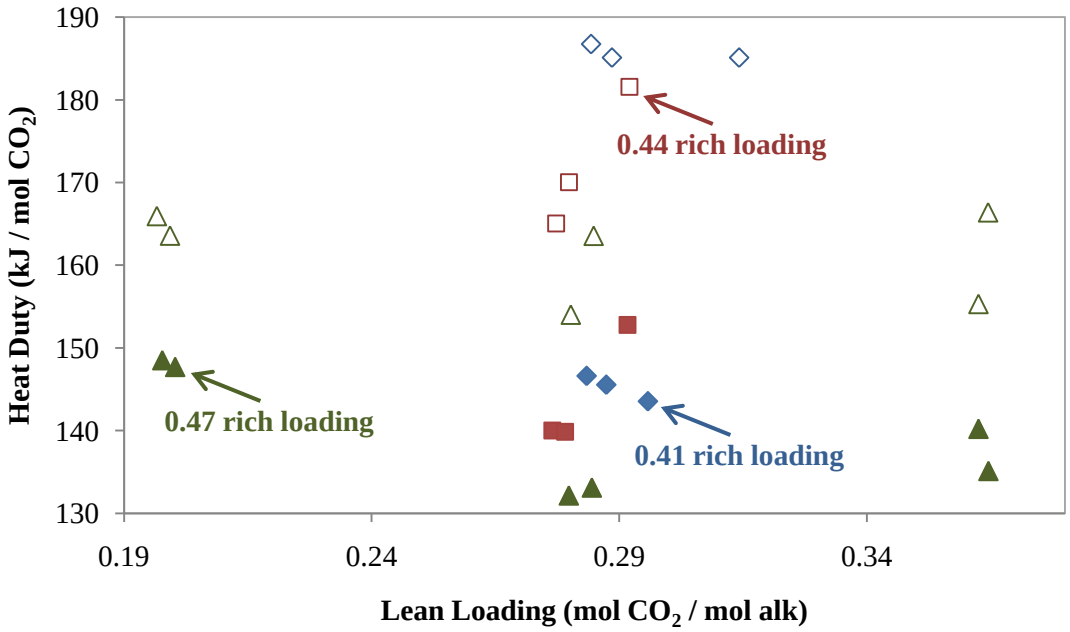


Figure 5-7. Normalized heat duty for 9 m MEA calculated from pilot plant measurements and simulation results, corrected for heat loss. Solid points = modeling results, Hollow points = pilot plant results.

The runs had reboiler temperatures between 109 and 114 °C, and the minimum heat duty in the simulations was 132 kJ/mol $CO_2$ when corrected for heat loss, and the stripper pressure was 1.8 bar. The heat work based on the heat duty for this minimum case was 28.5 kJ/mol $CO_2$, and the heat work reduced to 19.7 kJ/mol $CO_2$ when corrected for heat loss. The calculated compression work to 150 bar was 14.5 kJ/mol $CO_2$. With a calculated 1.4 kJ/mol $CO_2$ requirement for pump work at this low stripper pressure, the equivalent work for this operating condition was expected to be 44.4 kJ/mol $CO_2$, or 35.6 kJ/mol $CO_2$ when corrected for simulation heat loss. This performance was competitive with the optimal predicted conditions for 9 m MEA at 110 °C in Table 3-2, which was 35.1 kJ/mol $CO_2$.

The hefty increases in heat loss from the measured values were determined to be due to an inaccurate representation of the 9 m MEA solvent by thermodynamic model.

Figure 2-3 shows the overprediction of $CO_2$ partial pressure at the higher temperature expected in the stripper. This error, coupled with a high heat of absorption prediction, yielded the errors in performance estimates.

Table 5-7 shows the measured and simulation energy balances for Run 2 as an example of the issue. The heat of absorption requirement is listed for both energy balances, though it was only used in the calculation for the measured energy balance (see Equations 5-2 and 5-3). The overprediction of the heat of absorption by the simulation is apparent in this table, and it was also visible in Figure 2-6. The high heat of absorption in the simulation required a higher heat rate than what was measured at the pilot plant, which would reduce the simulation heat loss compared to the measured value.

**Table 5-7. Energy Balance of 2010 MEA Run 2 for Measured Values and Aspen Plus® Simulation**

| Heat Term | Simulation | Measured |
|---|---|---|
| | *kW* | *kW* |
| **Reboiler** | 171.30 | 171.30 |
| **Condenser** | -36.07 | -81.61 |
| **Heat loss** | -48.17 | -19.43 |
| **Stream enthalpy** | -87.25 | -4.63 |
| **Heat of absorption** | (-85.97) | -50.58 |
| **Balance** | -0.19 | 15.05 |

The overprediction of the heat of absorption had a secondary effect. Table 5-8 shows the simulated conditions at the top of the stripper column of Run 2. According to the Hilliard thermodynamic model, the rich solvent flashed to a loading of 0.396 and a temperature of 100.1 °C upon entry. The model also predicted a $CO_2$ partial pressure of 87.4 kPa. Experimental data suggests that the $CO_2$ partial pressure at 100 °C and a loading of 0.396 should be 28.7 kPa. Therefore, the predicted $CO_2$ mole fraction in the overhead was too high in the simulation, which reduced the simulation value of the

condenser duty, seen in Table 5-15. Therefore, the simulation heat loss was greater in order to balance this difference. Measured values of most of the conditions in this table were not available for comparison because they could not be measured with the available instrumentation. In the future, measurements of the overhead gas composition could help verify this conclusion.

**Table 5-8. Aspen Plus® Model Predictions for Conditions at the Top of the Column (2010 MEA Campaign-Run 2)**

| | | |
|---|---|---|
| **ldg at packing top** | *mol/mol* | 0.403 |
| **Predicted overhead T** | *C* | 100.2 |
| **Predicted $P_{CO2}$** | *kPa* | 87.1 |
| **Predicted $y_{co2}$** | | 0.527 |
| **Laboratory $P_{CO2}$** | *kPa* | 31.4 |

This issue needs to be addressed in the future by correcting the MEA model at this amine concentration.

In summary, the Hilliard MEA model was able to predict the performance of the simple stripper campaign by using pilot plant measurements for inputs to the simulation, but the measured heat loss had to be increased significantly for all runs. In the most extreme case, the simulated heat loss increased by 179% from the measured value. The overall MAPE for the result variables in the simulation was 2.7%. The minimum equivalent work was 35.6 kJ/mol $CO_2$ when corrected for heat loss, which was competitive with previously optimized models, but the simulation heat loss increased the equivalent work by 8.8 kJ/mol $CO_2$, or 25%.

## 5.3. PZ Pilot Plant Campaigns

Concentrated PZ (8 m) was a solvent of high interest in the time period of this work. Like 9 m MEA, this solvent needed to be evaluated in the pilot plant to determine

if it could be a practical improvement from the baseline, or whether it caused any operational difficulties. 8 m PZ was an interesting solvent to run because it had potential solubility issues. At room temperature, PZ is insoluble in unloaded solutions at concentrations greater than 2 m. 8 m PZ is soluble down to at least 40 °C within the loading range of 0.2 to 0.4, but precipitation was possible at the near-freezing temperatures in Austin during the winter, especially near the boundaries of the solubility window. The first two campaigns, in November 2008 and September 2010, used a simple stripper, shown in Figure 5-1. The last campaign in December 2010 used the new 2-stage flash skid. Each campaign had 8 to 14 usable runs. The 5deMayo model for concentrated PZ was used to run the simulations. The data from these three campaigns are evaluated in the next three sections.

### 5.3.1. 8 m PZ Simple Absorber and Stripper Campaign (Fall 2008)

This campaign started in November 2008 and ran into December. It was the first pilot trial with concentrated PZ at the Pickle pilot plant facility. There was significant hesitation due to the risk of PZ precipitation, which could clog the lines and machinery. The raw pilot plant measurements are shown in Table 5-9. As with the MEA simulations, the data-fit package was not used because it did not provide results that represented converged mass and energy balances. Instead, the required inputs for the simulation were taken directly from pilot plant measurements, and the deviations in the result variables were analyzed. The initial simulations had high deviations in both lean loading and the $CO_2$ rate exiting the condenser. The simulation predictions for lean loading and $CO_2$ gas rate were both higher than the pilot plant measurements, and they

roughly followed a linear trend when plotted against each other, Figure 5-8. This problem was similar to the issue encountered in the September 2010 9 m MEA campaign.

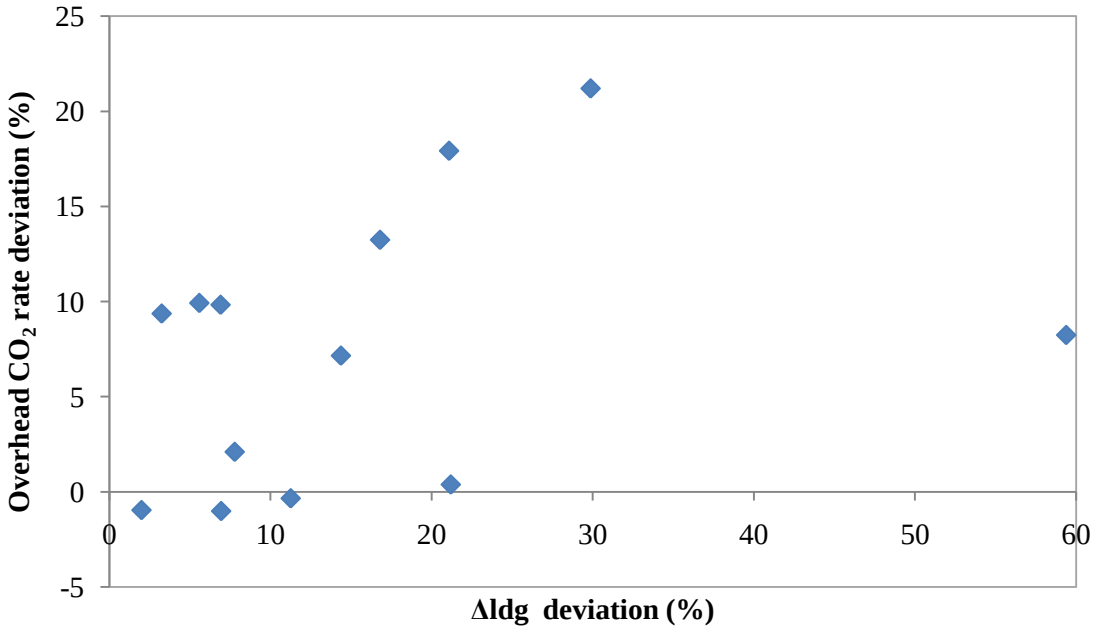


Figure 5-8: Simulation results without heat loss manipulation for 2010 simple stripper campaign with concentrated PZ. Percent deviations of overhead $CO_2$ rate and Δldg were correlated.

After checking that the measured $CO_2$ closed on the gas and liquid sides (Figure 5-9), it was concluded that the problem was not faulty measurements. Instead, an issue existed in the energy balance. Since the heat of absorption of the 5deMayo model matched well with laboratory data, parameters of the thermodynamic model were not altered. The measured heat loss was used as a variable to fit the lean loading. Since all of the simulations were overstripped compared to the pilot plant measurements, the simulation heat losses all increased from the pilot plant measurements to match the lean loadings that were measured at the pilot plant. The final deviations of the result variables are shown in Table 5-10. The deviations in heat losses are also reported because they

were used to match the lean loadings, but they were not included in the calculation of the MAPE

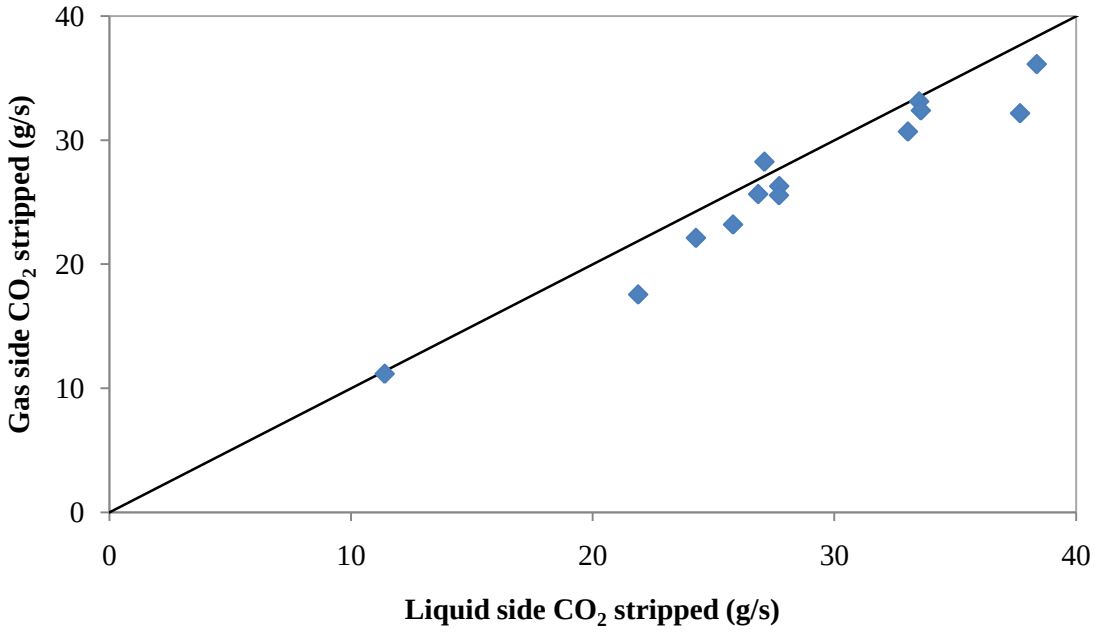


Figure 5-9: Parity plot of measured $CO_2$ removal by gas side (measured $CO_2$ flow rate) and liquid side (product of solvent rate and change in loading) measurements at pilot plant.

**Table 5-9. Pilot plant measurements from Fall 2008 simple stripper campaign with 8 m PZ.**

| Variable | Run → | 1 | 2 | 3 | 4 | 5 | 6 | 7 | 8 | 9 | 10 | 11 | 12 | 13 | 14 |
|---|---|---|---|---|---|---|---|---|---|---|---|---|---|---|---|
| **Rich flow** | *kg/s* | 1.10 | 1.11 | 1.11 | 1.12 | 0.89 | 1.33 | 1.11 | 0.89 | 1.32 | 1.11 | 1.28 | 1.28 | 1.06 | 0.85 |
| **Rich T** | *C* | 47.5 | 43.9 | 46.9 | 37.2 | 41.6 | 42.4 | 43.9 | 41.1 | 47.5 | 41.6 | 41.0 | 44.8 | 42.7 | 38.9 |
| **Lean flow** | *kg/s* | 1.04 | 1.07 | 1.05 | 1.09 | 0.84 | 1.28 | 1.07 | 0.85 | 1.26 | 1.08 | 1.24 | 1.22 | 1.01 | 0.81 |
| **Rich feed T** | *C* | 47.5 | 43.9 | 46.9 | 37.2 | 41.6 | 42.4 | 43.9 | 41.1 | 47.5 | 41.6 | 41.0 | 44.8 | 42.7 | 38.9 |
| **Lean exit T** | *C* | 49.9 | 46.5 | 49.5 | 39.7 | 44.1 | 45.4 | 48.2 | 44.9 | 51.7 | 45.3 | 44.8 | 48.6 | 46.5 | 42.6 |
| **Reboiler T** | *C* | 107.2 | 103.0 | 108.9 | 87.5 | 105.7 | 104.1 | 127.5 | 127.5 | 129.0 | 116.1 | 119.7 | 127.6 | 128.2 | 127.0 |
| **Overhead T** | *C* | 95.3 | 88.6 | 96.9 | 71.9 | 90.9 | 90.4 | 107.3 | 104.8 | 113.4 | 96.5 | 102.1 | 112.1 | 111.9 | 108.4 |
| **$CO_2$ rate** | *kg/s* | 0.033 | 0.026 | 0.036 | 0.011 | 0.028 | 0.031 | 0.026 | 0.023 | 0.032 | 0.018 | 0.022 | 0.032 | 0.031 | 0.026 |
| **Cond. rate** | *kg/s* | 0.020 | 0.008 | 0.019 | 0.002 | 0.011 | 0.012 | 0.005 | 0.004 | 0.011 | 0.013 | 0.004 | 0.011 | 0.010 | 0.009 |
| **Cond. T** | *C* | 14.9 | 15.5 | 9.0 | 22.0 | 11.3 | 4.7 | 19.6 | 16.2 | 20.1 | 25.2 | 8.0 | 11.5 | 4.8 | 4.8 |
| **Reb. duty** | *kW* | 130.6 | 101.0 | 155.5 | 45.9 | 111.1 | 125.3 | 112.7 | 105.6 | 141.3 | 79.0 | 99.8 | 134.6 | 129.0 | 114.5 |
| **Heat loss** | *kW* | 13.1 | 12.1 | 21.4 | 14.0 | 18.9 | 20.6 | 21.8 | 27.5 | 26.7 | 23.1 | 26.6 | 30.3 | 32.3 | 30.1 |
| **Column P** | *kPa* | 137.9 | 137.8 | 137.9 | 137.9 | 137.9 | 137.8 | 413.6 | 413.6 | 351.6 | 351.6 | 351.6 | 344.6 | 344.6 | 344.6 |
| **P drop** | *kPa* | 0.154 | 0.144 | 0.182 | 0.164 | 0.127 | 0.147 | 0.142 | 0.097 | 0.104 | 0.168 | 0.117 | 0.059 | 0.029 | 0.054 |
| **Reb. liq T** | *C* | 107.2 | 103.0 | 108.9 | 87.5 | 105.7 | 104.1 | 127.5 | 127.5 | 129.0 | 116.1 | 119.7 | 127.6 | 128.2 | 127.0 |
| **Reb. vap T** | *C* | 105.7 | 100.6 | 108.6 | 90.5 | 105.7 | 102.3 | 124.4 | 124.3 | 126.3 | 111.0 | 120.1 | 127.3 | 128.7 | 129.5 |
| **Rich ldg** | *mol/mol* | 0.3 | 0.372 | 0.330 | 0.404 | 0.358 | 0.361 | 0.364 | 0.369 | 0.338 | 0.381 | 0.382 | 0.362 | 0.360 | 0.382 |
| **Lean ldg** | *mol/mol* | 0.3 | 0.308 | 0.254 | 0.386 | 0.284 | 0.303 | 0.305 | 0.298 | 0.267 | 0.331 | 0.316 | 0.274 | 0.257 | 0.262 |
| **PZ conc** | *m* | 7.45 | 7.87 | 9.18 | 8.18 | 7.82 | 8.21 | 8.06 | 7.88 | 7.84 | 7.67 | 4.81 | 4.95 | 4.90 | 4.64 |

**Table 5-10. Deviation in simulation result variables from pilot plant measurements of Fall 2008 pilot plant simple stripper campaign with 8 m PZ. Heat loss used to match lean loading.**

| Variable | 1 | 2 | 3 | 4 | 5 | 6 | 7 | 8 | 9 | 10 | 11 | 12 | 13 | 14 | MAPE |
|---|---|---|---|---|---|---|---|---|---|---|---|---|---|---|---|
| **Lean flow** | 1% | 0% | 1% | 2% | 2% | 1% | 1% | 1% | 1% | 1% | 1% | 1% | 1% | 0% | 0.9% |
| **Lean ldg** | 0% | 1% | 0% | 0% | 0% | 1% | 0% | 0% | 0% | 0% | -1% | 0% | 0% | -3% | 0.4% |
| **Overhead T** | 4% | 6% | 4% | 17% | 6% | 6% | 13% | 15% | 7% | 17% | 11% | 5% | 5% | 7% | 8.8% |
| **$CO_2$ rate** | -10% | -5% | -8% | -30% | -17% | -9% | -7% | -3% | 5% | 12% | 6% | -5% | -3% | 10% | 9.2% |
| **Reboiler T** | 0% | -1% | 0% | 0% | 0% | -1% | 2% | 3% | 2% | 4% | 2% | -1% | 0% | 1% | 1.2% |
| **MAPE** | 3.0% | 2.7% | 2.6% | 9.9% | 5.1% | 3.4% | 4.6% | 4.3% | 2.9% | 6.7% | 3.8% | 2.2% | 2.0% | 4.2% | 4.1% |
| **Heat loss** | 92% | 127% | 45% | 68% | 90% | 78% | 93% | 50% | 13% | 0% | 10% | 23% | 6% | 0% | 49.6% |

Excluding the simulation heat loss, the mean absolute percentage error (MAPE) for each of the five calculated variables was between 0.4 and 9.2%. The overall MAPE was 4.1%. The simulation heat loss, however, had much higher variability from the pilot plant measurements, with a MAPE of 49.6%.

The conditions that were most accurately predicted were the lean flow rate and reboiler temperature. The average lean flow deviation was 0.9%, and the average reboiler temperature deviation was 1.2% (1.4 °C). The results with higher deviations included the overhead $CO_2$ rate and the temperature of vapor exiting the stripper. The $CO_2$ rate deviation could have been due to the method for matching lean loading with heat loss. The higher overhead temperature in simulations suggested that heat loss occurred between the top of the column and the measurement point. The simulation of the stripper column reached a rich end pinch for all of the runs, but this would not be the source of deviation in the overhead temperature. Had the pilot plant column not reached equilibrium, the partial pressure of water in the overhead vapor would have been higher than the simulation predictions, so the overhead temperature measured at the pilot plant would be higher than the simulation predictions.

The normalized heat duty demonstrated high variability (Figure 5-10), and it did not express the clear trends that appeared in the MEA campaign, in Figure 5-7. Firstly, a significant change in the lean flow rate of Run 4 resulted in a large difference between the normalized heat duties of the plant measurements and simulation predictions. A clear decrease in heat duty with increasing rich loading was not present in this campaign. The scatter in heat duties was due to variations between each run, including changes in reboiler temperature and PZ concentration. There was a decrease in the corrected heat duty from the measurement to simulation values since the simulation heat losses were

increased from the measurements. However, this effect was not as drastic as the MEA 2010 simple stripper campaign.

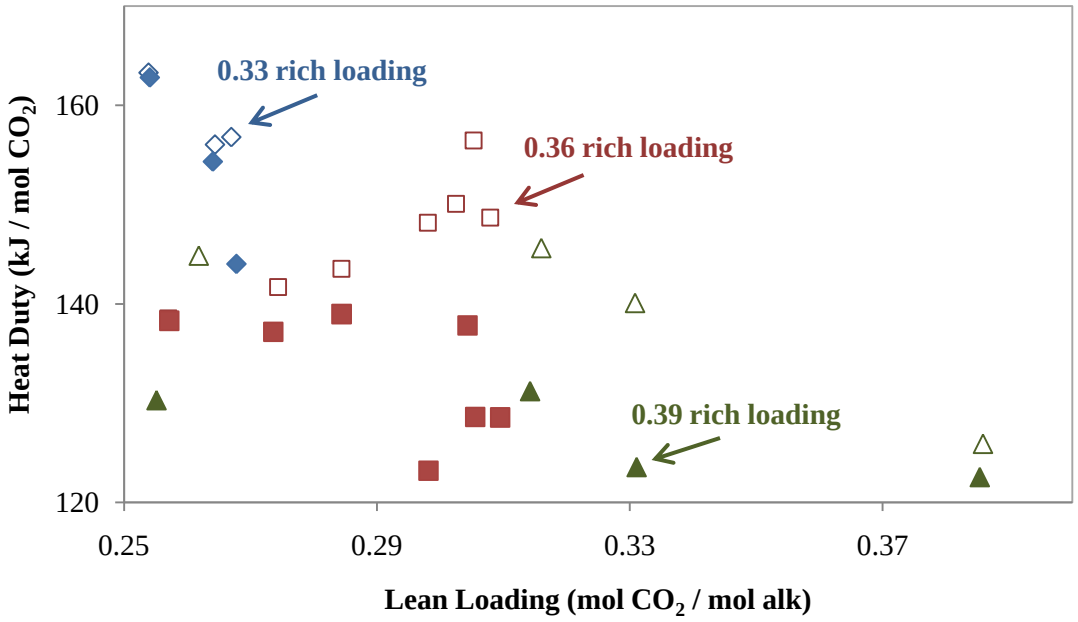


Figure 5-10. Normalized heat duty for 8 m PZ calculated from pilot plant results, Fall 2008, corrected for heat loss. Solid points = modeling results, Hollow points = pilot plant results.

The minimum heat duty was 122 kJ/mol $CO_2$, but there was a lot of scatter in the data. A decrease in heat duty with increasing rich loading was observed. The total equivalent work did not show a trend with lean loading either, and its average value was 46.2 kJ/mol $CO_2$. This average value was substantially lower than the optimum values in simulations: 33.5 and 33.1 kJ/mol $CO_2$ at 120 °C and 150 °C, respectively. This difference was attributed to non-optimal conditions at the pilot plant like lower boiler temperatures (between 88 and 131 °C), high heat loss of 19 to 35% of the reboiler duty, and most rich loading values were less than 0.40, which is achievable in the absorber and more efficient for the stripper. The minimum equivalent work without heat loss was 34.2 kJ/mol $CO_2$.

While attempting to reconcile the significant increase in the heat loss that was required in the simulation to match the material balance, it was discovered that a lean solvent recycle was split from the stream exiting the reboiler in this campaign, as in the Fall 2007 MEA run (Figure 5-2). The stripper was not modeled to account for this flow configuration, so the reboiler operated differently in the simulation than at the pilot plant. Recycling lean solvent to the sump would have reduced the loading of the collected solvent at the bottom of the column. Therefore, this solvent with lower loading would have been more difficult to strip and require a higher heat duty than if the lean solvent recycle flow pattern was not used. Since the simulation modeled a typical reboiler without lean solvent recycle, the calculations required a lower heat rate then the pilot experiment. Therefore, the simulations predicted a greater heat loss than the measured value in order to account for the lower required reboiler duty.

In summary, the simulations of this first pilot plant campaign with concentrated PZ appropriately matched the measured data. An energy balance issue existed which gave consistently lower predictions of the lean loading in the simulations. These inconsistencies were remedied by adjusting the heat losses within the column, but the average increase in the heat loss was approximately 50%. A detailed analysis of the heat loss correlation used at the pilot plant could determine whether these significant changes in the heat loss were appropriate, which was explored in section 5.4. Next, the overhead temperature was consistently over predicted by the simulation, which assumed no heat loss between the top of the column and the "measurement point". Additional installation of the vapor line at the pilot plant could ensure that these measurements are more accurate. The total equivalent work requirement including $CO_2$ compression was higher than what was predicted in Chapter 3 because the reboiler temperature was lower, there

was significant heat loss, and the rich loading in most runs was less than the previously assumed 0.40.

### 5.3.2. 8 m PZ Intercooled Absorber and Simple Stripper Campaign (Fall 2010)

This campaign ran in September 2010. It followed the August 2010 campaign with 9 m MEA that thoroughly tested intercooling. Like the MEA campaign, intercooling was used in every run for this campaign with 8 m PZ. The raw pilot plant measurements for the stripper are shown in Table 5-11. This campaign was run with the intention of keeping the reboiler temperature constant. The stripper column was not designed to withstand the high pressure of 8 m PZ at 150 °C, so it was run at approximately 120 °C. The maximum pressure was 2.7 bar. Three pressure levels were used which yielded three lean loadings since the reboiler temperature was constant. The reboiler duty was varied to maintain the desired reboiler temperature at the specified column pressure.

Once again, the data-fit package was not used because it did not provide results from fully converged runs. Instead, the required inputs for the simulation were taken directly from pilot plant measurements, and the deviations in the result variables were analyzed. Unlike the MEA campaign in summer 2010 and the PZ campaign in Fall 2008, there was no apparent issue with the energy balance. As shown in Figure 5-11, the percent deviations in overhead $CO_2$ rate and $\Delta$ldg were smaller than in the previous campaigns, and there was no correlation between the two deviations. Therefore, the heat loss predicted by the pilot plant software was not manipulated in the simulations.

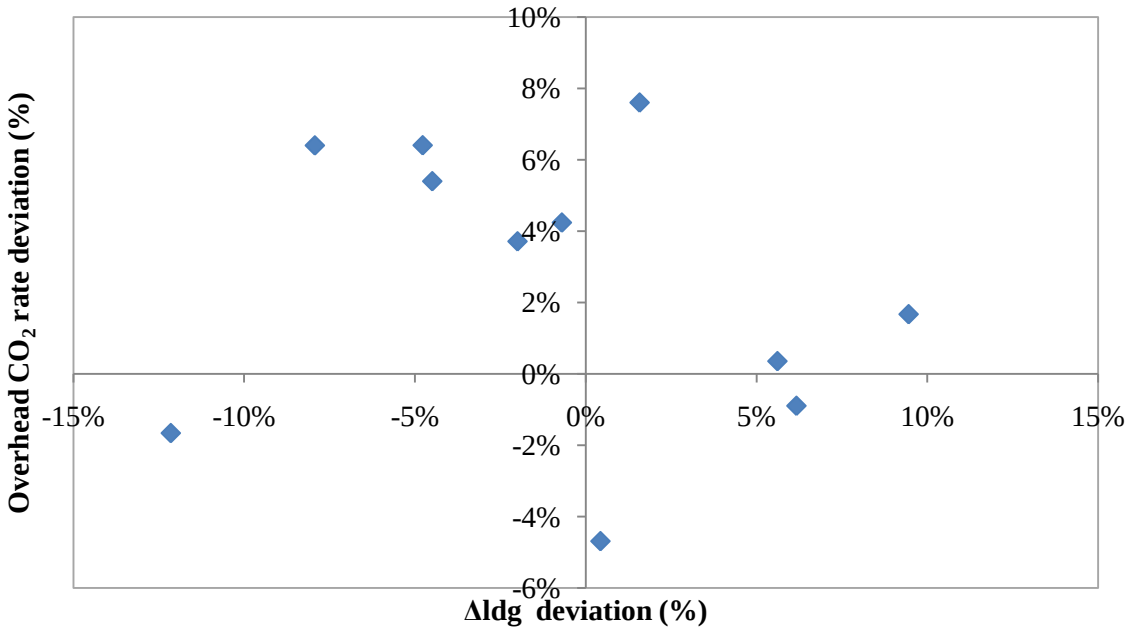


Figure 5-11: Simulation results without heat loss manipulation for 2010 simple stripper campaign with concentrated PZ. Percent deviations of overhead $CO_2$ rate and Δldg were correlated.

The deviations in the result variables of the simulations are shown in Table 5-12. Since the heat loss was not manipulated, it was not included as a result variable for this campaign. The conditions with the highest average absolute differences were the overhead temperature and the $CO_2$ gas rate. When considering the mean deviation, the average $CO_2$ gas rate discrepancy was reduced from its average absolute value difference, but the overhead gas temperature deviation was still high. The deviation signified the overestimation of the simulation temperature compared to the measured value, so the positive deviation indicated that the simulation values were consistently higher than the measured values. This result demonstrated that heat loss likely occurred in the overhead piping, which reduced the temperature of the vapor before it was measured.

The $CO_2$ gas rate was over predicted by the simulations on average, but the change in loading was not similarly over predicted. This result suggested that the

measured mass balance was slightly incorrect. The mass balance could have been thrown off by small inconsistencies in the measurements of the solvent amine concentration, rich and lean solvent $CO_2$ concentrations, and $CO_2$ gas rate.

**Table 5-11. Pilot plant measurements from Fall 2010 simple stripper campaign with 8 m PZ.**

| Variable | Run → | 1 | 2 | 3 | 5 | 6 | 7 | 8 | 9 | 11 | 12 | 13 |
|---|---|---|---|---|---|---|---|---|---|---|---|---|
| **Rich flow** | *kg/s* | 1.23 | 0.96 | 1.72 | 0.99 | 0.75 | 1.10 | 1.61 | 0.57 | 0.88 | 1.52 | 1.20 |
| **Rich T** | *C* | 48.1 | 43.5 | 45.9 | 47.9 | 42.3 | 44.7 | 45.9 | 41.7 | 40.1 | 44.0 | 41.3 |
| **Lean flow** | *kg/s* | 1.21 | 0.93 | 1.69 | 0.98 | 0.75 | 1.08 | 1.57 | 0.52 | 0.76 | 1.40 | 1.09 |
| **Rich feed T** | *C* | 48.1 | 43.5 | 45.9 | 47.9 | 42.3 | 44.7 | 45.9 | 41.7 | 40.1 | 44.0 | 41.3 |
| **Lean exit T** | *C* | 52.1 | 47.7 | 50.9 | 51.8 | 46.3 | 48.9 | 50.5 | 45.3 | 44.1 | 48.5 | 45.6 |
| **Reboiler T** | *C* | 122.3 | 122.6 | 122.4 | 123.9 | 121.8 | 122.7 | 123.1 | 120.5 | 121.7 | 122.1 | 121.4 |
| **Overhead T** | *C* | 106.8 | 105.2 | 107.6 | 108.8 | 103.5 | 106.2 | 107.4 | 103.9 | 105.0 | 107.4 | 104.6 |
| **$CO_2$ rate** | *kg/s* | 0.033 | 0.031 | 0.044 | 0.031 | 0.031 | 0.041 | 0.060 | 0.029 | 0.044 | 0.065 | 0.055 |
| **Cond. T** | *C* | 23.9 | 22.0 | 25.6 | 22.8 | 23.0 | 30.2 | 27.6 | 23.6 | 26.2 | 19.1 | 27.9 |
| **Reb. duty** | *kW* | 132.8 | 118.7 | 175.8 | 134.9 | 120.1 | 164.1 | 222.7 | 119.2 | 164.1 | 250.5 | 205.1 |
| **Heat loss** | *kW* | 27.1 | 26.8 | 33.4 | 34.2 | 32.9 | 33.3 | 33.0 | 26.2 | 33.0 | 33.1 | 32.7 |
| **Column P** | *kPa* | 272.3 | 272.3 | 272.3 | 265.4 | 248.1 | 248.1 | 248.1 | 202.0 | 208.2 | 208.2 | 208.2 |
| **P drop** | *kPa* | 0.020 | 0.020 | 0.030 | 0.015 | 0.025 | 0.035 | 0.038 | 0.022 | 0.038 | 0.043 | 0.051 |
| **Reb. liq T** | *C* | 122.3 | 122.6 | 122.4 | 123.9 | 121.8 | 122.7 | 123.1 | 120.5 | 121.7 | 122.1 | 121.4 |
| **Reb. vap T** | *C* | 119.8 | 120.6 | 119.4 | 122.2 | 120.7 | 121.0 | 120.7 | 120.7 | 120.9 | 120.1 | 119.7 |
| **Rich ldg** | *mol/mol* | 0.365 | 0.370 | 0.364 | 0.355 | 0.367 | 0.357 | 0.354 | 0.366 | 0.370 | 0.364 | 0.379 |
| **Lean ldg** | *mol/mol* | 0.287 | 0.286 | 0.290 | 0.265 | 0.261 | 0.262 | 0.261 | 0.213 | 0.215 | 0.229 | 0.230 |
| **PZ conc** | *m* | 7.98 | 8.18 | 8.33 | 7.93 | 8.09 | 8.11 | 8.36 | 7.87 | 7.85 | 7.59 | 7.69 |

**Table 5-12. Deviation in result variables of Fall 2010 simple stripper campaign with 8 m PZ.**

| Variable | 1 | 2 | 3 | 5 | 6 | 7 | 8 | 9 | 11 | 12 | 13 | MAPE | Mean |
|---|---|---|---|---|---|---|---|---|---|---|---|---|---|
| **Lean flow** | -2.1% | -1.8% | -1.6% | -3.7% | -5.5% | -3.9% | -2.7% | 0.7% | 8.3% | 1.5% | 3.0% | 3.2% | -0.7% |
| **Lean ldg** | -0.4% | -1.7% | 0.5% | 0.2% | -0.2% | -3.4% | -2.2% | 3.2% | 8.7% | 2.8% | 5.1% | 2.6% | 1.2% |
| **Overhead T** | 4.6% | 5.8% | 3.4% | 3.8% | 6.2% | 4.8% | 4.0% | 1.5% | 0.7% | -1.0% | 0.0% | 3.2% | 3.1% |
| **$CO_2$ rate** | 7.6% | 0.4% | 3.7% | 4.2% | -4.7% | 1.7% | -0.9% | 5.4% | -1.7% | 6.4% | 6.4% | 3.9% | 2.6% |
| **Reboiler T** | -0.1% | 0.3% | -0.6% | 0.2% | 1.0% | 0.9% | 0.6% | 0.1% | -1.0% | -1.6% | -1.4% | 0.7% | -0.1% |
| **MAPE** | 3.0% | 2.0% | 2.0% | 2.4% | 3.5% | 2.9% | 2.1% | 2.2% | 4.1% | 2.7% | 3.2% | 2.7% | 1.2% |

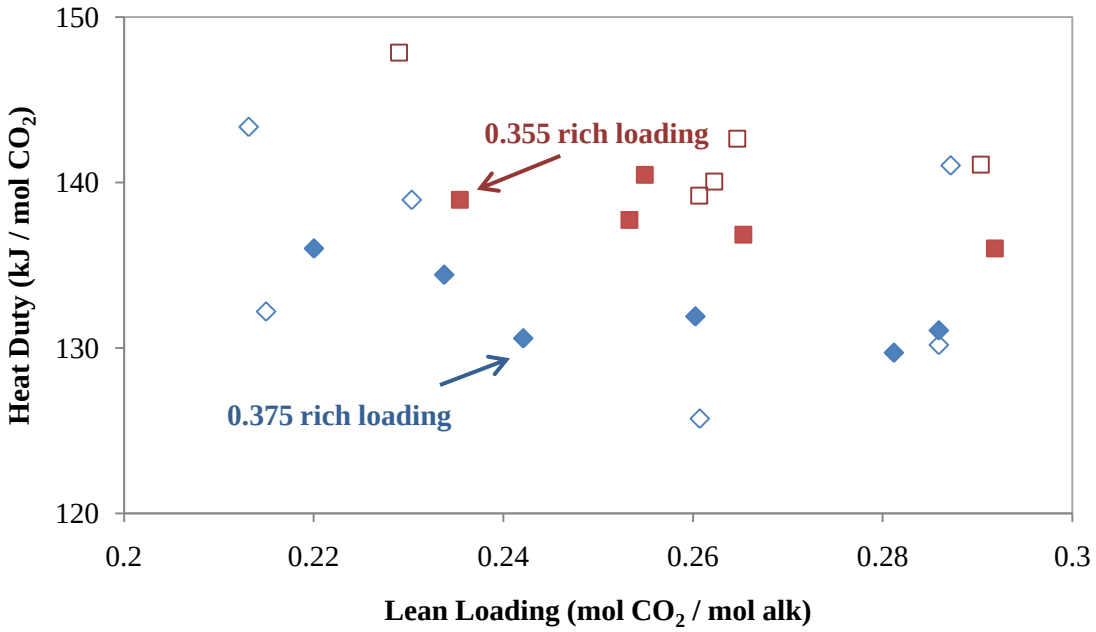


Figure 5-12. Normalized heat duty for 8 m PZ calculated from pilot plant results, corrected for heat loss. Solid points = modeling results, Hollow points = pilot plant results. 120 °C reboiler.

The measured heat duties in this campaign ranged from 154 to 181 kJ/mol $CO_2$, which showed a decrease from the 2008 campaign with the same solvent. When corrected for heat loss, the measured heat duties for this campaign ranged from 126 to 148 kJ/mol $CO_2$. Similar to the previous campaign, there was substantial scatter in the heat duty data. The pilot plant measurements had variability, but the simulations were able to distinguish trends in the data. A decrease in the corrected heat duty was observed with increasing rich loading. It was difficult to determine whether a minimum heat duty had been reached. The plot of the heat duty relationship with the lean loading suggested an optimal lean loading between 0.26 and 0.28 for a rich loading of 0.375. However, the optimum was flat and the points also suggested a continuing decrease as lean loading increased past 0.29, especially when considering the runs with lower rich loading values.

Collecting data points at slightly higher lean loading would confirm that the minimum heat duty was reached in the lean loading range from this campaign.

The expected equivalent work was also calculated. The calculation used the heat duties corrected for heat loss, a pump work calculated from the simulations, and a compressor work calculated by the work correlation. The trends of these values are shown in Figure 5-13.

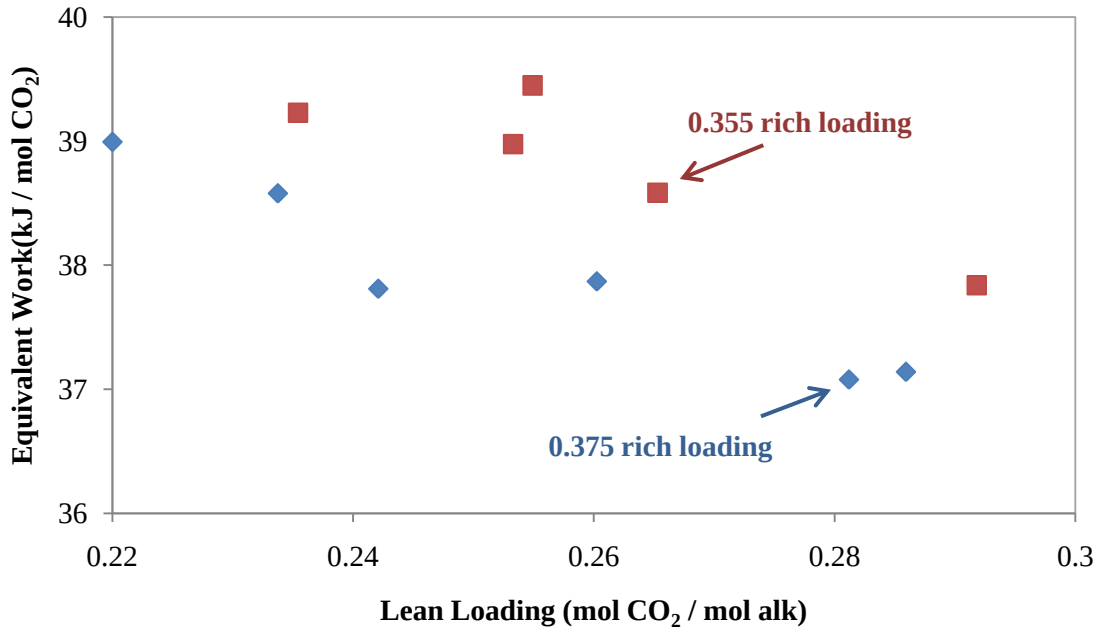


Figure 5-13. Equivalent work predictions for a simple stripper with 8 m PZ based on pilot plant results from Fall 2010. Heat duty corrected for heat loss, pump work calculated by Aspen Plus® simulation, and compressor work calculated by correlation.

It was shown in Chapter 3 that configurations using 8 m PZ typically reach a minimum equivalent work at high lean loading values. The optimized simple stripper model at 150 °C had an optimal lean loading of 0.31 when using a rich loading of 0.40. This pilot plant campaign demonstrated that the minimum equivalent work was not reached when the lean loading was increased to 0.29; rich loadings of 0.355 and 0.375 both expressed a downward trend continuing up to the highest tested lean loading of 0.29.

The relationship between equivalent work and lean loading was not as flat as corrected heat duty because equivalent work accounted for the benefit of lower compressor work at higher lean loading and higher stripper pressure.

The range in predicted total equivalent work (corrected for heat loss) was relatively small: 36.9 to 39.1 kJ/mol $CO_2$. The simulation heat loss was only 13 to 28% of the reboiler heat duty. The equivalent work predictions are shown in Table 5-13. These predictions are shown for heat duties both with and without heat loss correction

**Table 5-13. Equivalent work predictions for simple stripper with 8 m PZ based on pilot plant results from Fall 2010. Pump work calculated by Aspen Plus® simulations, and compressor work to 150 bar calculated by correlation. Lean loadings predicted by simulations.**

| Run | Loading (mol/mol) | | Q | $W_{eq}$ | Q with heat loss | $W_{eq}$ with heat loss |
|---|---|---|---|---|---|---|
| | Rich | Lean | *kJ/mol $CO_2$* | | | |
| **1** | 0.365 | 0.286 | 131.1 | 37.14 | 164.7 | 42.63 |
| **2** | 0.370 | 0.281 | 129.7 | 37.08 | 167.6 | 43.31 |
| **3** | 0.364 | 0.292 | 136.0 | 37.84 | 167.9 | 43.02 |
| **5** | 0.355 | 0.265 | 136.9 | 38.58 | 183.4 | 46.31 |
| **6** | 0.367 | 0.260 | 131.9 | 37.87 | 181.7 | 46.06 |
| **7** | 0.357 | 0.253 | 137.7 | 38.98 | 172.8 | 44.78 |
| **8** | 0.354 | 0.255 | 140.5 | 39.45 | 164.9 | 43.50 |
| **9** | 0.366 | 0.220 | 136.0 | 38.99 | 174.4 | 45.18 |
| **11** | 0.370 | 0.234 | 134.4 | 38.58 | 168.3 | 44.02 |
| **12** | 0.364 | 0.235 | 138.9 | 39.23 | 160.1 | 42.63 |
| **13** | 0.379 | 0.242 | 130.6 | 37.81 | 155.4 | 41.77 |

These predictions were not as attractive as in Chapter 3. The absorber did not achieve a rich loading of 0.4 as expected in Chapter 3. This could be a consequence of using too little wetted area in the packing of the absorber and was outside the scope of this stripper modeling. The absorber used only 20 feet of a packing with a nominal area of 250 $m^2/m^3$. Plaza showed that an intercooled absorber with 15 m of a packing with a

nominal area of 205 $m^2/m^3$ could be used to get a fairly constant rich loading of 0.4 (Figure 4-25).

In summary, the simulations of this pilot plant campaign with concentrated PZ appropriately matched the measured data. The energy balance issue that existed in previous campaigns was not present in these runs because the reboiler was run without splitting the lean solvent to recycle to the sump. This campaign was similar to the previous campaigns in that the overhead temperature was consistently overpredicted by the simulation, which assumed no heat loss between the top of the column and the measurement point. Additional insulation of the vapor line at the pilot plant could ensure that these measurements are more accurate. Scatter in the process conditions confounded the heat duty data, but a minimum heat duty for a rich loading of 0.375 may have occurred at a lean loading between 0.26 and 0.28. When corrected for heat loss, the best heat duty of the campaign was 128.5 kJ/mole $CO_2$ with a rich loading of 0.37 and a lean loading of 0.29. This run also represented the case with the smallest predicted equivalent work, 36.9 kJ/mole $CO_2$. Unlike the heat duty, the equivalent work showed a consistent downward trend with increasing lean loading. The minimum equivalent work was not reached with lean loading values as high as 0.29.

### 5.3.3. 8 m PZ Intercooled Absorber and 2-Stage Flash Campaign (January 2011)

This campaign was performed in January 2011 and it followed the success of the 8 m PZ campaign in September 2010. This was the first campaign to use the 2-stage flash skid that was designed and constructed on-site. Stripper simulations demonstrated that the 2-stage flash could result in a lower equivalent work for 9 m MEA. Unfortunately, the equivalent work of a 2-stage flash using 8 m PZ was calculated to be

slightly higher than a simple stripper with the same solvent, but the capital cost and practicality of constructing a 2-stage flash for high temperature and pressure operation with 8 m PZ would be more feasible than a full stripper column. This campaign was the first pilot scale demonstration of the multi-stage flash technology. The main goal of this campaign was to learn whether each flash vessel could achieve equilibrium, as it was modeled in the simulations. Additionally, it was desired to find out whether the configuration posed any operational issues. 14 runs were attempted, but steady-state data was extracted for only 8 runs. These steady-state runs were simulated using the 5deMayo model.

#### *5.3.3.1. Measured data from 2-stage flash campaign*

The raw pilot plant measurements for the stripper are shown in Table 5-14. The skid flowsheet and example real-time conditions from Run 1 are shown in Figure 5-14. Several measurements from the pilot plant were redundant, and only the more accurate measurement was used in each case. As an example, the temperature of the solvent in each flash was measured after the heater (TT520D/TT530C), in the flash vessel (TC522/TC524), and in the exiting liquid (TT530/TT535). The temperature of the liquid exiting from each flash was decided to be the most accurate to represent the final flash temperature that would be reported in simulations. Another example of redundant measurements was in the overhead vapor. Three sets of measurements should have provided equal estimates of the total overhead vapor flow: the sum of the individual flash overheads (FT518 & FT517), the combined overhead vapor stream (FT519), and the sum of the $CO_2$ and condensate streams exiting the overhead condenser (FT216 & FT204). However, the measurements of mixed component flows before the condenser required the

knowledge of the stream compositions to calculate the actual mass flow rate. These compositions were not measured at the pilot plant, so each of these measurements could not be used (FT517, FT518, & FT519). Lastly, the measured condensate rate was not a steady-state value because the condensate pump was only run with the accumulator (V-106) got too full. Therefore, the only reliable overhead flow measurement was the $CO_2$ rate (FT216). The cooling duty of the condenser would have been a valuable measurement, but its reliability was uncertain. The increase in temperature of the cooling water was only 1 to 3°F in each run. With such a low change in temperature, the measurements of the supply and return temperatures of the cooling water would have to be impossibly accurate to provide a useful estimate of the condenser duty.

**Table 5-14. Pilot plant measurements from January 2011 2-stage flash skid campaign with 8 m PZ campaign.**

| Variable | Tag | Units | 1 | 2 | 3 | 4 | 5 | 6 | 10 | 14 |
|---|---|---|---|---|---|---|---|---|---|---|
| **Rich flow** | *FT200* | *kg/s* | 0.844 | 0.641 | 1.115 | 0.989 | 0.986 | 1.173 | 1.293 | 0.826 |
| **Lean flow** | *FT201* | *kg/s* | 0.811 | 0.625 | 1.057 | 0.951 | 0.961 | 1.143 | 1.273 | 0.813 |
| **PZ conc** | *Lab* | *m* | 8.76 | 7.64 | 7.51 | 7.62 | 6.38 | 6.47 | 7.28 | 7.92 |
| **Rich ldg** | *Lab* | *mol/mol* | 0.351 | 0.362 | 0.372 | 0.375 | 0.365 | 0.371 | 0.377 | 0.377 |
| **Semirich ldg** | *Lab* | *mol/mol* | 0.306 | 0.309 | 0.310 | 0.310 | 0.315 | 0.328 | 0.331 | 0.343 |
| **Lean ldg** | *Lab* | *mol/mol* | 0.265 | 0.259 | 0.250 | 0.258 | 0.264 | 0.279 | 0.299 | 0.289 |
| **Rich temp** | *TT200* | *C* | 40.1 | 37.3 | 35.8 | 32.2 | 38.8 | 40.8 | 44.3 | 39.1 |
| **Rich post-LP CX T** | *TT520A* | *C* | 73.9 | 94.6 | 88.5 | 85.2 | 81.3 | 86.5 | 88.5 | 92.7 |
| **Rich pre-HP CX T** | *TT506* | *C* | 71.5 | 90.8 | 85.6 | 82.0 | 77.9 | 83.3 | 85.5 | 89.4 |
| **Rich hot T** | *TT520C* | *C* | 123.0 | 130.7 | 129.7 | 127.7 | 125.0 | 122.2 | 117.9 | 125.5 |
| **LP Flash liq. T** | *TT521A* | *C* | 145.2 | 144.9 | 145.2 | 145.3 | 144.9 | 144.8 | 137.8 | 141.9 |
| **Lean post-HP CX T** | *TT521B* | *C* | 92.5 | 104.9 | 111.0 | 100.3 | 110.6 | 115.1 | 101.4 | 103.9 |
| **Lean pre-LP CX T** | *TT215* | *C* | 88.5 | 101.7 | 107.2 | 96.4 | 108.7 | 113.5 | 100.4 | 102.3 |
| **Lean temp** | *TT212* | *C* | 56.4 | 43.4 | 57.5 | 45.2 | 60.3 | 62.4 | 43.4 | 39.1 |
| **HP Heater T** | *TT520D* | *C* | 146.0 | 144.8 | 144.2 | 146.0 | 145.8 | 145.8 | 138.5 | 142.6 |
| **HP Heater Q** | *FC525* | *kW* | 112.5 | 74.4 | 150.5 | 138.4 | 165.9 | 167.3 | 135.4 | 78.8 |
| **HP Flash P** | *PC525* | *kPa* | 877 | 876 | 835 | 877 | 896 | 1060 | 873 | 1316 |
| **HP Flash liq. T** | *TT530* | *C* | 146.4 | 145.0 | 144.6 | 146.7 | 146.5 | 145.9 | 140.7 | 145.0 |
| **LP Heater T** | *TT530C* | *C* | 146.0 | 145.9 | 146.0 | 146.0 | 145.9 | 145.9 | 138.5 | 142.6 |
| **LP Heater Q** | *FC526* | *kW* | 62.0 | 58.9 | 121.0 | 72.5 | 69.8 | 66.4 | 36.6 | 51.3 |
| **LP Flash P** | *PC528* | *kPa* | 585 | 585 | 546 | 585 | 598 | 701 | 584 | 660 |
| **LP Flash liq. T** | *TT521A* | *C* | 145.2 | 144.9 | 145.2 | 145.3 | 144.9 | 144.8 | 137.8 | 141.9 |
| **HP Overhead T** | *TT517* | *C* | 138.4 | 135.8 | 137.9 | 139.7 | 138.7 | 137.5 | 132.3 | 133.4 |
| **HP Overhead flow** | *FT517* | *kg/s* | 0.028 | 0.023 | 0.039 | 0.046 | 0.032 | 0.022 | 0.028 | 0.010 |

| Variable | Tag | Units | 1 | 2 | 3 | 4 | 5 | 6 | 10 | 14 |
|---|---|---|---|---|---|---|---|---|---|---|
| **LP Overhead T** | *TT518* | *C* | 141.6 | 141.4 | 141.6 | 141.7 | 141.4 | 141.3 | 133.9 | 138.0 |
| **LP Overhead flow** | *FT518* | *kg/s* | 0.028 | 0.024 | 0.055 | 0.032 | 0.030 | 0.026 | 0.021 | 0.024 |
| **Combined Flow** | *FT519* | *kg/s* | 0.068 | 0.058 | 0.097 | 0.085 | 0.070 | 0.063 | 0.059 | 0.051 |
| **Stripped $CO_2$** | *FT216* | *kg/s* | 0.032 | 0.027 | 0.048 | 0.044 | 0.034 | 0.032 | 0.031 | 0.026 |
| **Condenser T** | *TT225* | *C* | 10.8 | 9.7 | 13.8 | 11.0 | 10.4 | 11.4 | 9.4 | 9.6 |
| **Condenser flow** | *FT204* | *kg/s* | 0.015 | 0.011 | 0.028 | 0.022 | 0.016 | 0.011 | 0.007 | 0.000 |
| **Heat loss** | - | *kW* | 24.2 | 22.6 | 23.2 | 25.3 | 26.3 | 23.9 | 23.3 | 22.8 |

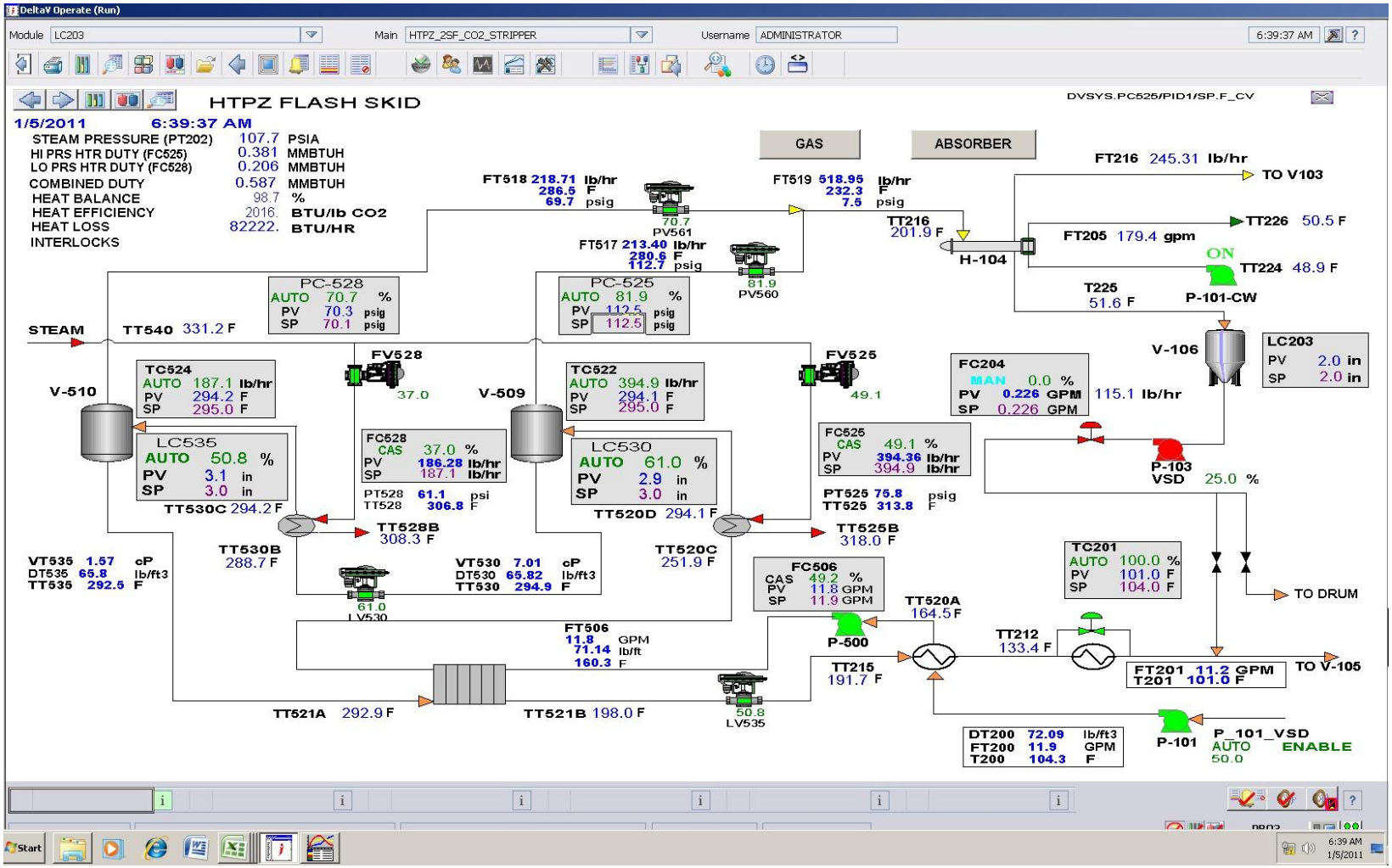


Figure 5-14. Screenshot from Run 1 of pilot plant operation with 2-stage flash skid.

The pre-existing, low-pressure exchanger was not modeled in the stripper simulations. A bypass valve existed which rerouted lean solvent around the exchanger to prevent flashing. The bypass valve was not always used, and the amount of bypass was never recorded. Although the simulations could have been used to calculate the bypass fraction, this information would not have been insightful, and it also could have confounded the results. Therefore, the scope of the simulations for the 2-stage flash included the high-pressure heat exchanger, both flash vessels, and the condenser.

Several redundant measurements were taken at the pilot plant. These measurements included the individual overhead flow rates from each flash vessel, the combined gas flow rate from these two streams, and the $CO_2$ and condensate streams exiting the condenser. Each of these three sets should have individually summed to the same value since the process was at steady-state. However, each of the gas rates was measured with an orifice meter, which required the exact gas composition to correctly report the mass flow rate. Unfortunately, the gas compositions were not measured at the pilot plant, so the only reliable gas flow rate measurement was the $CO_2$ leaving the condenser since the stream was nearly pure $CO_2$. The condensate rate was also unreliable because the liquid accumulator was not run in steady-state; instead, pump P-103 was run when the tank needed to be emptied. Due to the number of gas side measurements that were not usable, the $CO_2$ purities of the individual overhead streams could not be determined. However, the $CO_2$ balance was still analyzed.

Once again, the data-fit package was not used because it did not provide results from fully converged runs. Instead, the required inputs for the simulation were taken directly from pilot plant measurements, and the deviations in the result variables were analyzed. Even though the stripper was no longer a simple column, the pilot plant

measurements still provided an estimate of overall heat loss. In the simulations, the heat loss estimate from the pilot plant was split evenly between the two flash vessels.

#### *5.3.3.2. Approach the equilibrium of flash vessels*

One of the important analyses from this campaign was comparing the actual conditions of the flash vessels at the pilot plant against equilibrium calculations by the solvent model. This comparison checked whether the flash vessels had enough residence time to achieve a true equilibrium flash as it was previously simulated. Figure 5-15 shows the vessel pressure for various loadings of both the high-pressure and low-pressure vessels. All of the pilot plant runs kept the flash temperatures near 145 °C, but there was slight fluctuation. The pilot plant measured pressures were adjusted to the expected temperature at 145 °C by equation 5-5:

$$P_{meas}^{145°C} = P_{meas}^{T} \cdot \frac{P_{model}^{145°C}}{P_{model}^{T}} \qquad \textbf{5-5}$$

where superscripts "***T***" and "***145°C***" represented the temperature of the reported pressure, either the measured temperature of the flash in the run or 145 °C, respectively. The subscripts "***meas***" and "***model***" indicated pressures measured at the pilot plant and predicted by the model, respectively. This equation changed the vessel pressure measured at the pilot plant according to the ratio of the pressure predicted by the model at 145 °C to the pressure predicted at the actual run temperature. The adjustments were mostly small. When compared against the pressure prediction of the solvent model at the lean loadings reported at the pilot plant, it was apparent that equilibrium was achieved in the flash vessels at low loading. However, the measured pressures were generally higher at high loading. At the flash temperature of 145 °C, the measured pressure would have

been lower than the predicted pressure if the solvent did not reach equilibrium since water vapor would make up a greater proportion of the vapor than the equilibrium composition at that temperature and loading. A similar deviation between measurements and model predictions was not observed in the laboratory scale data (Figure 2-14). Therefore, these measured pressures that were higher than the model predictions were likely to be due to measurement error. The errors were probably mostly in the loading measurements because the steady-state pressure measurements were reliable.

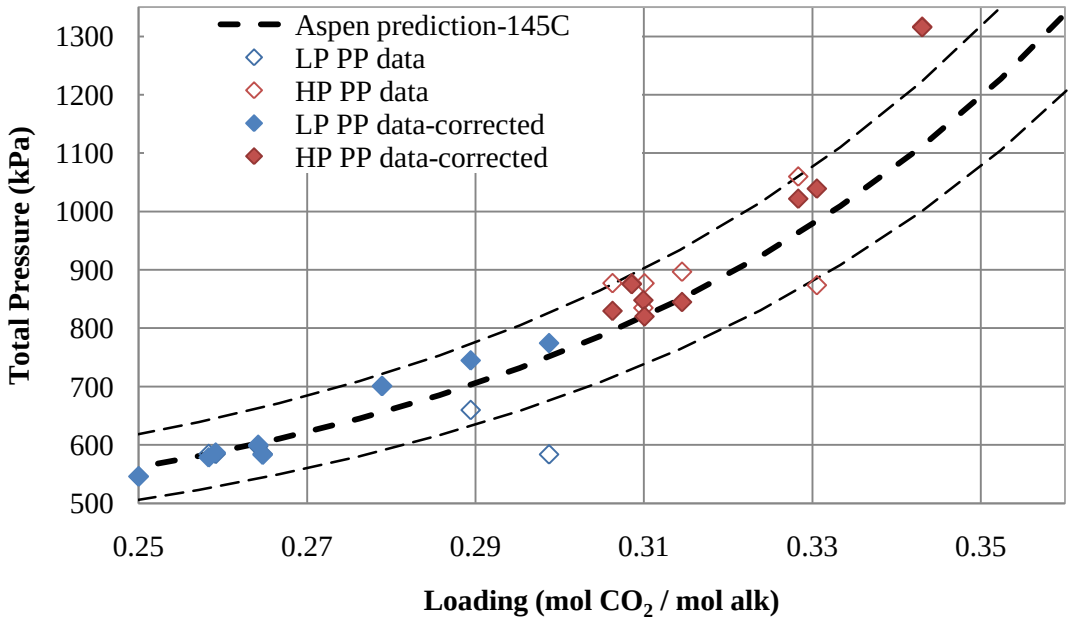


Figure 5-15. Vessel pressures from raw measurements and corrected 145 °C.

Simulations of the full stripper flowsheet were used to evaluate the performance of the pilot plant skid compared to simulation predictions. Figure 5-16 shows a parity plot of the loading calculated in the simulation compared to the loading measured at the pilot plant. The semi-rich and lean loadings were both included in this plot. As shown by the dark dotted line, the simulation predicted loadings that were mostly within an

absolute difference of 0.01 of the loadings measured at the pilot plant; the largest difference was nearly 0.02 (7.5%).

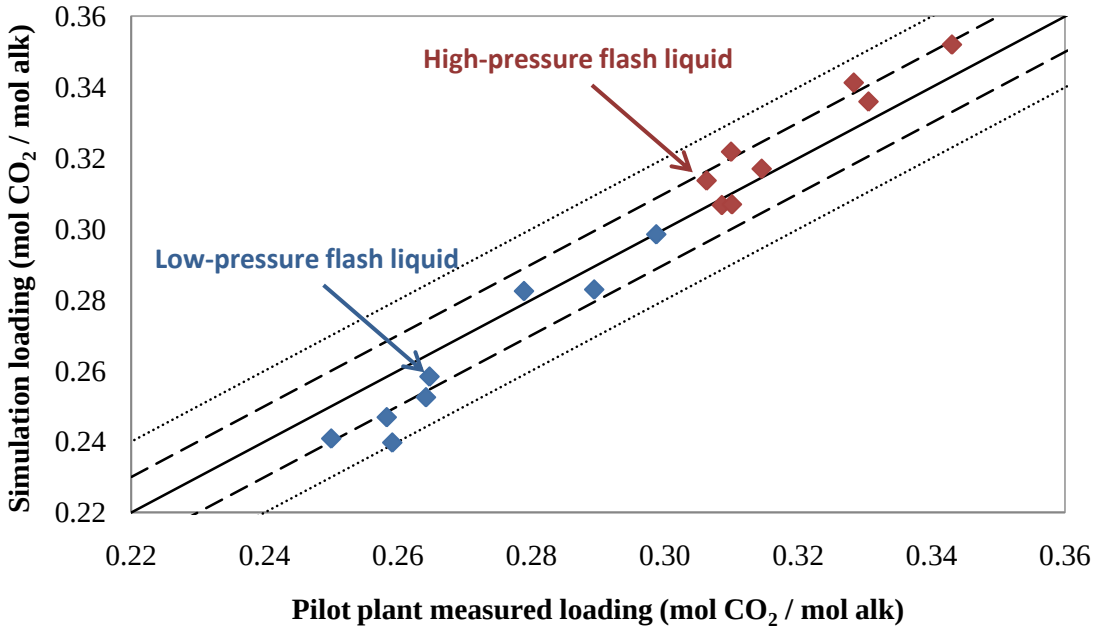


Figure 5-16. Agreement of pilot plant loading measurements with predictions by 5deMayo model under equilibrium assumptions. Solid dotted line = ± 0.01, Light dotted line = ± 0.02.

### *5.3.3.3. 2-stage flash flowsheet simulations*

This campaign was like the Fall 2010 PZ simple stripper campaign in that there was not a correlation between the deviations of overhead $CO_2$ rate and Δldg. However, the deviations in these two process conditions were two of the larger errors. Ideally, an energy balance on the whole system could be performed, but this would require an accurate measurement of the condenser duty. Using each of the heat duties and stream enthalpies estimated by the solvent model, an overall heat loss could be calculated to compare to the pilot plant estimate. As shown in Figure 5-17, the percent deviations in

overhead $CO_2$ and Δldg were smaller than in the previous campaigns, and there was no correlation between the two deviations. Therefore, the heat loss predicted by the pilot plant software was not manipulated in the simulations.

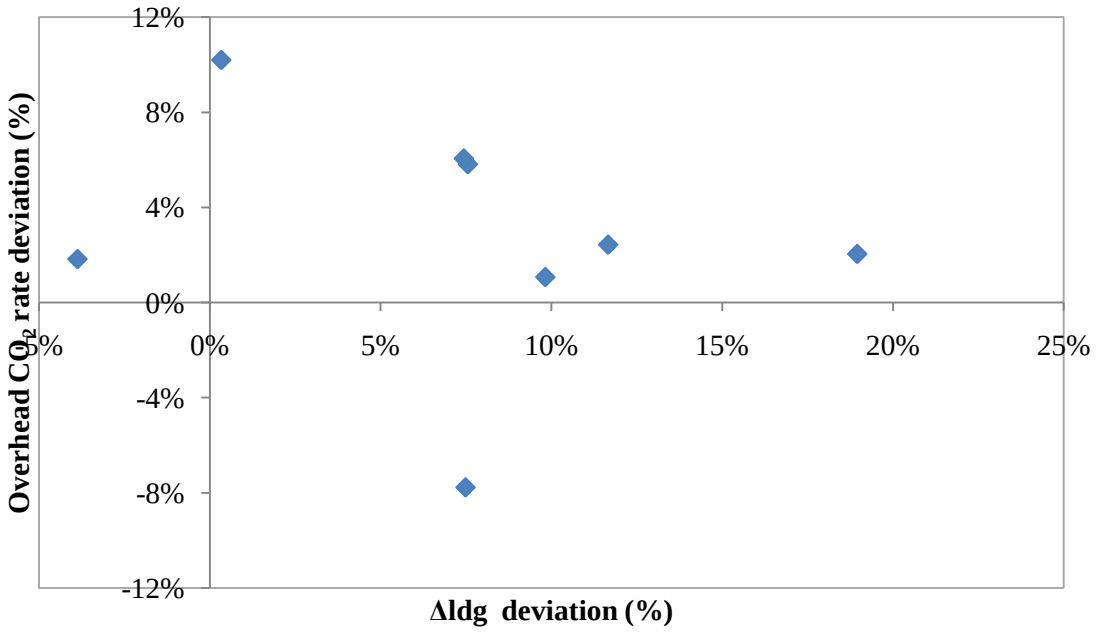


Figure 5-17. Simulation results without heat loss manipulation for 2011 2-stage flash campaign with concentrated PZ. Percent deviations of overhead $CO_2$ rate and Δldg were correlated.

The percent deviation in overhead $CO_2$ rate was less significant and more scattered than in the Fall 2008 PZ and Fall 2010 MEA campaigns, so heat loss was not used as a variable to match performance. Table 5-15 shows the percent deviation in the result variables for the simulations. The MAPE was calculated for each run as well as for each variable. The overall MAPE was only 2.9%. The deviations in the individual overhead gas flows were ignored since they did not account for the actual composition of $CO_2$ in their respective streams. The highest absolute errors were observed in the HP overhead temperature (5.7%), the LP liquid temperature (5.0%), the total overhead $CO_2$ rate (4.7%), and the lean loading (3.3%). Although the two flash vessels were generally

at the same temperature, the HP overhead gas generally had a greater temperature drop. This may have been due to its lower water content compared to the LP vessel, which allowed a greater drop in temperature while condensing an equivalent amount of water as in the LP overhead.

**Table 5-15. Deviation in result variables from pilot plant measurements of January 2011 2-stage flash skid campaign with 8 m PZ campaign.**

| Results | 1 | 2 | 3 | 4 | 5 | 6 | 10 | 14 | MAPE | Mean |
|---|---|---|---|---|---|---|---|---|---|---|
| **Lean flow** | -1.8% | -4.6% | -2.5% | -3.3% | -3.0% | -1.4% | -2.1% | -3.4% | 2.8% | -2.8% |
| **Semirich ldg** | 2.4% | -0.6% | 3.8% | -1.0% | 0.8% | 3.9% | 1.6% | 2.6% | 2.1% | 1.7% |
| **Lean ldg** | -2.4% | -7.5% | -3.7% | -4.4% | -4.4% | 1.3% | -0.1% | -2.3% | 3.3% | -2.9% |
| **Rich hot T** | -1.2% | -0.5% | -10.0% | -2.7% | -12.7% | -9.4% | 2.0% | 2.0% | 5.0% | -4.1% |
| **LP Flash liq. T** | 1.1% | 1.7% | 0.0% | 0.8% | -0.5% | -0.6% | 0.0% | 2.0% | 0.9% | 0.5% |
| **HP Heater T** | 2.1% | 3.0% | -0.3% | 1.8% | -0.3% | -1.2% | 2.1% | 4.6% | 1.9% | 1.5% |
| **HP Flash liq. T** | 0.5% | 1.3% | -1.5% | 0.2% | -2.0% | -2.3% | -0.5% | 1.2% | 1.2% | -0.4% |
| **LP Heater T** | 1.2% | 1.8% | -0.1% | 0.9% | -0.5% | -0.6% | 0.2% | 2.4% | 1.0% | 0.6% |
| **HP Overhead T** | 6.3% | 8.2% | 3.2% | 5.2% | 3.5% | 3.7% | 5.8% | 10.0% | 5.7% | 5.7% |
| **LP Overhead T** | 3.6% | 4.2% | 2.6% | 3.3% | 1.9% | 1.8% | 2.9% | 4.8% | 3.1% | 3.1% |
| **Stripped $CO_2$** | -7.8% | 2.0% | 5.8% | 1.1% | 2.4% | 1.8% | 10.2% | 6.1% | 4.7% | 2.7% |
| **MAPE** | 2.7% | 3.2% | 3.0% | 2.3% | 2.9% | 2.6% | 2.5% | 3.8% | 2.9% | 0.5% |
| **HP Overhead flow** | -43.5% | -26.6% | -34.4% | -30.9% | -38.8% | -39.5% | -17.9% | -13.5% | 30.6% | -30.6% |
| **LP Overhead flow** | 15.1% | 18.5% | 7.9% | 17.2% | 10.9% | 25.7% | 13.7% | 28.5% | 17.2% | 17.2% |

Since only eight runs were included in this analysis, there was not a clear description of the behavior of the heat duty as a function of lean loading. The three runs with low rich loadings had relatively constant lean loadings. Four of the high rich loading runs demonstrated that an optimum lean loading was between 0.26 and 0.29. These results were observed in both of the pilot plant measurements and simulation calculations (Figure 5-18).

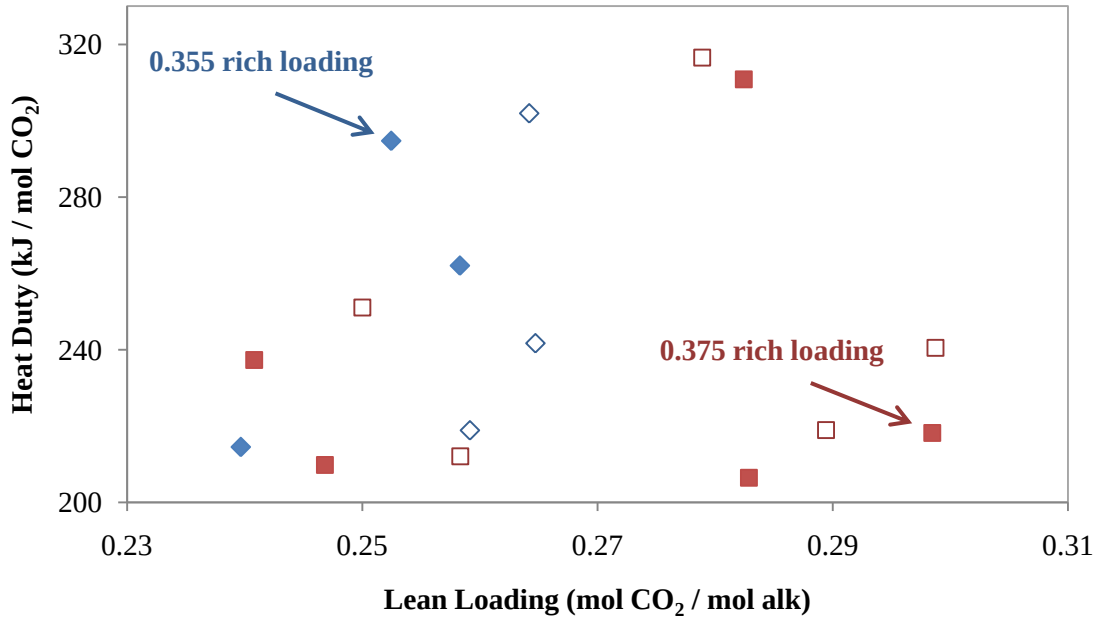


Figure 5-18. Normalized heat duty of 2-stage flash with 8 m PZ, corrected for heat loss. Solid points = simulation calculations, Hollow points = pilot plant calculations.

The heat duties in this campaign ranged from 206.4 to 310.8 kJ/mol $CO_2$. The heat duties were higher than the values for the simple stripper campaigns, which was expected from the simulation results in Chapter 3. However, even the the heat duties corrected for heat loss were significantly higher than the optimum heat duty for a 2-stage flash at 150 °C in Chapter 3. The minimum heat duty was 119 kJ/mole $CO_2$, but the lowest corrected heat duty in this campaign was 170 kJ/mole $CO_2$. Several factors led to

the inefficient operation for this campaign. The equivalent work values were also exceptionally high. The heat duties and equivalent work values both with and without heat loss correction are shown in Table 5-16. The heat duty was the dominant contribution to the equivalent work, so the trend of the equivalent work with relation to lean loading was nearly identical to the heat duty trend.

**Table 5-16. Equivalent work predictions for 2-stage flash with 8 m PZ based on pilot plant results from Winter 2011. Pump work calculated by Aspen Plus® simulations, and compressor work calculated by correlation. Lean loadings predicted by simulations.**

| Run | Loading (mol/mol) | | Q | $W_{eq}$ | Q with heat loss | $W_{eq}$ with heat loss |
|---|---|---|---|---|---|---|
| | Rich | Lean | *kJ/mol* | | | |
| 1 | 0.351 | 0.258 | 225.8 | 55.02 | 262.0 | 62.19 |
| 2 | 0.362 | 0.240 | 178.2 | 45.80 | 214.5 | 52.98 |
| 3 | 0.372 | 0.241 | 217.0 | 53.34 | 237.3 | 57.27 |
| 4 | 0.375 | 0.247 | 184.7 | 47.69 | 209.8 | 52.65 |
| 5 | 0.365 | 0.252 | 261.9 | 62.08 | 294.8 | 68.44 |
| 6 | 0.371 | 0.282 | 279.1 | 65.24 | 310.8 | 71.36 |
| 10 | 0.377 | 0.298 | 188.7 | 46.72 | 218.2 | 52.23 |
| 14 | 0.377 | 0.283 | 170.3 | 45.45 | 206.4 | 52.52 |

The calculated total equivalent work without heat loss correction varied from 52.2 to 71.4 kJ/mol $CO_2$, with an average of 58.7 kJ/mol $CO_2$. With correction for heat loss, the total equivalent work ranged from 45.5 to 65.2 kJ/mole $CO_2$, with an average of 52.7 kJ/mole $CO_2$. This represented an average increase in the equivalent work due to heat loss of 6.0 kJ/mole $CO_2$. A reason that the equivalent work was so high was that the cross exchanger network could not achieve the same hot side temperature approach that was observed in previous campaigns. The average hot side approach was 18.5 °C, compared to 6.1 °C in the previous PZ simple stripper campaign. Therefore, the sensible heat requirement in this demonstration of the 2-stage flash technology was excessive, and the total equivalent work prediction was unreasonably high. Another reason that this

campaign ran with low efficiency was that the vapor production was not evenly split between flash vessels. Table 5-17 shows the simulation estimates of overhead vapor rates for the two flash vessels. The LP vessel always produced more vapor than the HP vessel. The pressure ratio between vessels was generally 1.5, except for Run 14 where the pressure ratio was 2. This was a consequence of the low rich loading. In future campaigns, more absorber packing area will be provided to achieve a greater rich loading. This should balance the molar flow rates of the vapor streams exiting two flash vessels and make the separation more reversible and efficient.

**Table 5-17. Individual overhead vapor rates of flash vessels and ratio of molar vapor flow rates calculated by simulations**

| Run | HP vapor rate | LP vapor rate | $n_{HP}/n_{LP}$ |
|---|---|---|---|
| | *kmol/s* | *kmol/s* | |
| 1 | 0.49 | 1.16 | 0.43 |
| 2 | 0.52 | 1.04 | 0.50 |
| 3 | 0.76 | 2.20 | 0.35 |
| 4 | 0.99 | 1.37 | 0.72 |
| 5 | 0.59 | 1.19 | 0.49 |
| 6 | 0.38 | 1.06 | 0.36 |
| 10 | 0.67 | 0.79 | 0.85 |
| 14 | 0.25 | 1.05 | 0.24 |

In summary, the results of the high temperature 2-stage flash campaign with 8 m PZ demonstrated an excellent approach to equilibrium for both flash tanks in all of the runs. The simulation of the skid gave good agreement with the pilot plant measurements; the MAPE for the individual conditions ranged from 0.9 to 5.7%. The largest deviations were in the overhead temperatures, the overhead $CO_2$ rate, the lean loading, and the hot side temperature of the rich solvent. The higher prediction of overhead temperatures was simply explained through heat loss. A consistently lower lean flow rate in the simulation calculations was likely to be the main reason that the rich solvent reached a lower

temperature in the simulations than in the pilot plant. Although the overhead $CO_2$ rate and lean loading had high deviations on average, they were not linked to each other as in previous campaigns. The overall performance of these 2-stage flash runs were poor, with an average equivalent work of 58.7 kJ/mol $CO_2$. The high equivalent work in relation to previous campaigns was due to the poor cross exchanger performance which led to a high sensible heat requirement.

## 5.4. MEASURED AND SIMULATED ENERGY BALANCE DIFFERENCES

### 5.4.1. Main heat exchanger performance

The heat loss discrepancy was evaluated in more depth and all of the constituents of the energy balance were scrutinized. The energy balance, as calculated when running the pilot plant, included the stripping column and condenser, but the balance did not include the main heat exchanger; the derived heat loss correlation for estimating a measured heat loss did not include expected heat loss from the heat exchanger. However, this heat exchanger was not insulated, and loss of heat from this process unit was expected. When experimental results were compared to the simulation of the stripper, additional heat loss from the heat exchanger would be indicated by a lower hot temperature of the rich solvent. The hot lean, cold lean, and cold rich temperatures were specified in the simulation based on process measurements, so an absence of heat exchanger heat loss in the simulation would boost the temperature of the rich solvent on the hot side as well as the hot side approach. Table 5-18 summarizes the hot side temperature approaches from the measured pilot plant data and simulation values for all four campaigns. For the most part, the variability in the approach temperatures was low. The difference in heat flow to change the rich solvent temperature by this difference was

also calculated. It was generally low, except in the case of the 2-stage flash campaign. This was the only campaign where considerable heat loss in the heat exchanger was apparent. The simulation hot side temperature approach was higher than the measured hot side approach by 0.4 to 15.1 °C, with an average difference of 6 °C. While a possible explanation for this difference could have been a pressure specification in the simulation that was too low and allowed extra flashing of the solvent, this was not the case. The pressure of the rich stream in the simulation was set to match the pressure of the first flash vessel. Even without extra pressurization, no flashing of the rich solvent was observed in the simulations. The heat exchanger only brought the solvent to a temperature of 110 to 130 °C, so the high pressure of the first vessel was enough to prevent flashing in the heat exchanger. Since the higher hot side approach in the simulation was not a result of rich solvent flashing in the simulations, the energy balance of this high pressure heat exchanger was analyzed based on measured and simulated data. Table 5-19 shows the calculation of the energy balance for the high-pressure exchanger based on the measured temperatures. This method assumed no flashing of the rich solvent.

**Table 5-18. Measurement and simulation values of hot side approach of main cross exchanger for all pilot plant campaigns. Difference in heat exchanged for different approach temperature.**

| Run | | 1 | 2 | 3 | 4 | 5 | 6 | 7 | 8 | 9 | 10 | 11 | 12 | 13 | 14 | Average |
|---|---|---|---|---|---|---|---|---|---|---|---|---|---|---|---|---|
| **Fall 2010 MEA simple stripper** | | | | | | | | | | | | | | | | |
| Simulation $T_{app,h}$ | *°C* | 3.4 | 3.8 | 5.5 | 6.0 | 3.3 | 3.1 | 4.3 | 4.4 | 3.7 | 4.8 | 9.1 | 8.2 | | | 5.0 |
| Measured $T_{app,h}$ | *°C* | 4.9 | 5.1 | 5.8 | 5.8 | 5.0 | 4.9 | 5.9 | 5.8 | 6.9 | 5.5 | 7.3 | 7.3 | | | 5.9 |
| Q for $T_{app,h}$ difference | *kW* | 6.0 | 5.4 | 0.7 | 0.5 | 7.1 | 7.1 | 5.5 | 5.0 | 13.0 | 2.5 | 3.8 | 1.9 | | | 4.9 |
| **Fall 2008 PZ simple stripper** | | | | | | | | | | | | | | | | |
| Simulation $T_{app,h}$ | *°C* | 4.0 | 3.5 | 4.8 | 2.2 | 4.0 | 3.9 | 5.1 | 5.1 | 5.6 | 4.2 | 4.5 | 5.1 | 5.7 | 6.1 | 4.6 |
| Measured $T_{app,h}$ | *°C* | 4.5 | 4.4 | 5.0 | 3.8 | 4.9 | 4.7 | 6.2 | 6.5 | 6.0 | 5.3 | 5.4 | 5.6 | 6.0 | 6.2 | 5.3 |
| Q for $T_{app,h}$ difference | *kW* | 1.8 | 3.5 | 1.0 | 6.1 | 2.5 | 3.4 | 4.3 | 4.5 | 1.8 | 4.2 | 3.9 | 2.2 | 1.1 | 0.2 | 2.9 |
| **Fall 2010 PZ simple stripper** | | | | | | | | | | | | | | | | |
| Simulation $T_{app,h}$ | *°C* | 5.4 | 6.0 | 6.2 | | 5.7 | 6.6 | 6.7 | 7.0 | 7.6 | | 7.6 | 7.5 | 7.6 | | 6.7 |
| Measured $T_{app,h}$ | *°C* | 5.5 | 6.3 | 6.2 | | 5.7 | 5.9 | 6.0 | 6.3 | 6.1 | | 6.4 | 6.6 | 6.6 | | 6.1 |
| Q for $T_{app,h}$ difference | *kW* | 0.8 | 0.7 | 0.1 | | 0.2 | 1.7 | 2.5 | 3.7 | 2.9 | | 3.6 | 4.7 | 4.1 | | 2.3 |
| **Winter 2011 PZ 2-Stage Flash** | | | | | | | | | | | | | | | | |
| Simulation $T_{app,h}$ | *°C* | 25.1 | 17.4 | 28.5 | 22.2 | 35.0 | 33.2 | | | | 17.6 | | | | 16.7 | 24.5 |
| Measured $T_{app,h}$ | *°C* | 22.2 | 14.2 | 15.5 | 17.6 | 19.9 | 22.6 | | | | 20.0 | | | | 16.4 | 18.5 |
| Q for $T_{app,h}$ difference | *kW* | 8.5 | 6.9 | 49.1 | 15.4 | 50.5 | 42.1 | | | | 10.4 | | | | 1.1 | 23.0 |

In the 2-stage flash campaign, the average rich and lean heat capacities in the heat exchanger were calculated by a correlation developed in-house (Rochelle et al., 2009). The correlation was as follows:

$$C_p = \omega_{H_2O} \cdot C_{p,H_2O} + \omega_{PZ} \cdot C_{p,PZ} + \omega_{CO_2} \cdot C_{p,CO_2} \quad \text{5-6}$$

where

$$C_{p,H_2O} = \left(276370 - 2090T + 8.13\,T^2 - 0.014T^3 + 9.37e-6T^4\right)/18020 \quad \text{5-7}$$

$$C_{p,PZ} = 2.335 + 0.0056(T - 313) \quad \text{5-8}$$

$$C_{p,CO_2} = 0.763 + 0.0195(T - 313) \quad \text{5-9}$$

$\omega_{H2O}$, $\omega_{PZ}$, and $\omega_{CO2}$ were the weight fractions of water, PZ, and $CO_2$ in the solution, respectively. The average heat capacity for each stream was calculated using the amine concentration, loading, and temperatures in and out of the heat exchanger. The expected heat exchange to/from each stream $i$ could then be calculated:

$$Q_{exchanged,i} = \dot{m} C_p \Delta T \quad \text{5-10}$$

A rich new outlet temperature was calculated that made the heat absorbed by the rich solution equal to the heat delivered by the lean solution. The results of these calculations for all 8 runs are shown in Table 5-19. The new rich outlet temperature based on these calculations was always closer to the simulation value than the reported measurement. Since the measured heat exchanger performance of the previous PZ campaign with a simple stripper agreed with the simulation values, it can be assumed that the thermodynamic model for PZ and the laboratory heat capacity measurements should agree with pilot scale results. Therefore, it was most likely that the measurement of the rich outlet temperature from this high-pressure exchanger in this campaign was consistently too high.

**Table 5-19. Energy balance of high-pressure heat exchanger from 2-stage flash campaign with PZ. Rich outlet temperatures estimated by making rich Q exchanged equal to lean value based on laboratory heat capacity measurements.**

| Run | | 1 | 2 | 3 | 4 | 5 | 6 | 10 | 14 |
|---|---|---|---|---|---|---|---|---|---|
| **Cold in T** | *C* | 71.5 | 90.8 | 85.6 | 82.0 | 77.9 | 83.3 | 85.5 | 89.4 |
| **Cold out T** | *C* | 123.0 | 130.7 | 129.7 | 127.7 | 125.0 | 122.2 | 117.9 | 125.5 |
| **Hot in T** | *C* | 145.2 | 144.9 | 145.2 | 145.3 | 144.9 | 144.8 | 137.8 | 141.9 |
| **Hot out T** | *C* | 92.5 | 104.9 | 111.0 | 100.3 | 110.6 | 115.1 | 101.4 | 103.9 |
| $\mathbf{C_{p,rich,avg}}$ | *kJ/kg-K* | 3.55 | 3.46 | 3.43 | 3.44 | 3.23 | 3.25 | 3.38 | 3.51 |
| $\mathbf{C_{p,lean,avg}}$ | *kJ/kg-K* | 3.59 | 3.43 | 3.43 | 3.43 | 3.26 | 3.31 | 3.41 | 3.52 |
| **Q exchanged (rich)** | *kW* | 154.4 | 88.5 | 169.0 | 155.6 | 150.0 | 148.1 | 141.4 | 104.7 |
| **Q exchanged (lean)** | *kW* | 153.4 | 85.8 | 124.0 | 146.7 | 107.7 | 112.6 | 158.1 | 108.5 |
| **New cold out T** | *C* | 122.6 | 129.5 | 117.9 | 125.1 | 111.7 | 112.9 | 121.7 | 126.8 |
| **Cold out T (sim)** | *C* | 121.6 | 130.0 | 116.7 | 124.3 | 109.1 | 110.7 | 120.2 | 128.0 |

Three runs showed especially significant changes from the measured cold (lean) outlet temperature to the new calculated value: runs 3, 5, and 6. The measured cold outlet temperatures were not higher than in the other runs, but the measured hot outlet temperatures were hotter: the measurements for runs 3, 5, and 6 were 110-115 °C, whereas the other runs were 92-100 °C. This higher cold lean temperature resulted in less heat exchanged, so the hot rich temperature was also lower. Since these calculations resulted in new rich outlet temperatures close to the simulation predictions, it was verified that the simulation was accurately using the heat capacity according to the laboratory measurements.

### 5.4.2. Differences between Measured and Simulated Condenser Duties

The measured and simulation values of the condenser duty were correlated for the 2010 PZ simple stripper campaign and the 2011 PZ 2-stage flash campaign. The other two campaigns were ignored for this analysis since there energy balances were concluded to be inaccurate. These relationships for the two selected campaigns are

shown in Figure 5-19. Each of these data sets was correlated, and the intercept is recorded in Table 5-20. These intercepts represented the expected condenser duty by the simulation for the cases where no cooling would be required in the experimental operation. These values indicated the magnitude of the apparent heat loss in the overhead at the pilot plant. This heat flow was coupled with the condenser duty of the simulations, but it was lumped in with the measured heat loss of the pilot plant. The most overhead heat loss was observed in the 2-stage flash campaign, with an intercept of 25.8 kW. This campaign was proposed to have the highest condensation in the overhead piping for two reasons. First, the temperatures of the vapor streams were higher than in other campaigns. Second, the overhead vapor had to travel all the way from the 2-stage flash skid on the ground to the condenser at the top of the structure. In the other campaigns with the simple stripper configuration, the overhead exited the column at the top and traveled the short distance directly to the condenser. Compared to the new 2-stage flash skid, the stripper column had more exposed metal at the top and in flanges in the overhead pipe, but the data suggested that the 2-stage flash still suffered more heat loss in the overhead.

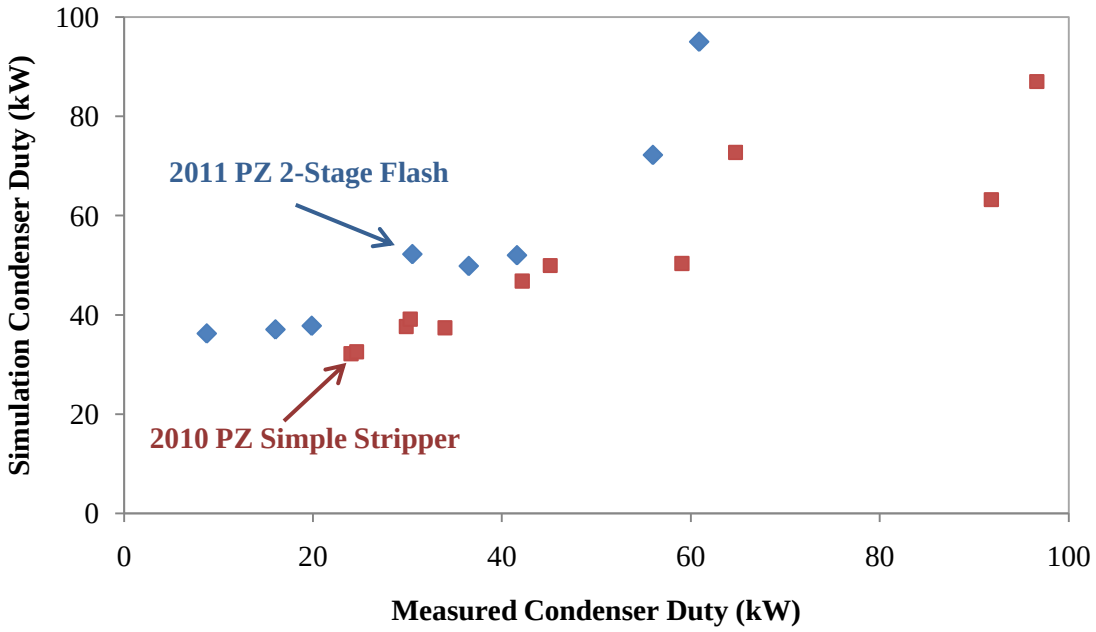


Figure 5-19. Comparison of simulation and measured values of condenser duty.

**Table 5-20. Condenser duty intercepts based on simulation and measured condenser duty parity plot**

| Campaign | Condenser duty intercept (kW) |
|---|---|
| 2010 PZ simple stripper | 18.8 |
| 2011 PZ 2-stage flash | 25.8 |

## 5.5. CONCLUSIONS

1. The 5deMayo model for concentrated PZ accurately represented the solvent in two pilot plant campaigns. The VLE was predicted well, and properties associated with the energy balance gave results with close agreement with the measured conditions.

2. The Hilliard MEA model did not predict performance of a simple stripper pilot plant campaign well. The $CO_2$ partial pressure was overpredicted, and the heat of absorption estimate was too high. Drastic increases in the measured heat loss were

required in the simulations in order to match the material balance while closing the simulation energy balance.

3. Since the Hilliard MEA model overpredicted performance at the pilot plant, estimates of the energy requirement using this solvent in earlier chapters are also likely to be overpredicted. Therefore, the performance of 8 m PZ compared to 9 m MEA was an even better improvement then what was predicted.

4. The measured data from the 2010 simple stripper campaigns with MEA and PZ both had minimum reboiler duties of 154 kJ/mole $CO_2$

5. Data-fit within Aspen Plus® would be capable of manipulating all simulation inputs to provide the best fit to pilot plant data by the least squares method, but the data-fit package did not provide results representing fully converged runs. Therefore, the pilot plant runs were simulated using plant measurements for simulation inputs, and the deviations in the result variables were analyzed.

6. The overall energy balance did not fit for the 2008 PZ and 2010 MEA campaigns. This lack of closure was apparent through a correlation between the percent deviations of stripped $CO_2$ and $\Delta$ldg.

7. The energy balance issue was addressed by manipulating the heat loss that was predicted at the pilot plant. This heat loss of most runs was increased by up to 125%, but two extreme cases required increases of 148% and 179%.

8. The overall MAPE for each campaign was between 2.7 and 4.1%. The percent deviations in the heat losses were not included in these values.

9. The conditions of the low-pressure flash in the 2-stage flash campaign demonstrated equilibrium conditions based on estimates by the solvent model. The high-pressure flash did not match equilibrium conditions as well as the low-pressure flash, which could be due to inaccurate measurements.

10. Simulations of the 2-stage flash runs fit the pilot plant data within small error by splitting the predicted heat duty evenly between the two flash vessels.

11. An area at the pilot plant that was not adequately measured was the condenser. The condenser should be run with lower cooling water flow rates to increase its $\Delta T$, and the condensation be managed in a way such that its steady-state flow can be measured. Improving these measurements would provide insight to the overall energy balance as well as the overhead vapor composition, respectively.

12. The performance of the pilot plant runs was worse than the respective optimized cases in Chapter 3 due to heat loss, higher heat exchanger approach temperatures, lower rich loading, and lower lean loadings.

13. Heat loss in the heat exchanger was located in the high temperature 2-stage flash campaign with 8 m PZ in 2011. The hot side temperature approach calculated by the simulation was consistently higher than the measured value.

14. The measured and simulated energy balances of the 2008 PZ simple stripper campaign did not match because an alternate flow pattern around the reboiler was used. The energy balances in the simulations had to be adjusted by manipulating the heat loss in the column.

15. The measured and simulated energy balances of the 2010 MEA simple stripper campaign did not match because the VLE predictions were not accurate enough for MEA. The $P_{CO2}$ and heat of absorption predictions were both too high, and these resulted in better performance in the stripper simulations than what was observed at the pilot plant. The energy balance was adjusted by manipulating the heat loss to match the $CO_2$ removal rate.

16. The measured condenser duties were consistently lower than the simulation values. This result was likely due to heat loss and condensation in the overhead pipe.

Since condensation occurred before the condenser, the required condensing duty was lower than what was predicted by the simulations. The high temperature 2-stage flash campaign had the highest average heat loss in the pipe, 25.8 kW.

# Chapter 6: Conclusions and Recommendations

This chapter summarizes the findings of this work and collates the conclusions. The conclusions are categorized by the general research areas: stripper complexity, novel stripper configurations, and pilot plant studies. Recommendations for future work are also presented.

## 6.1. CONCLUSIONS

### 6.1.1. Stripper Complexity

Interheating with the stripper column requires 4.8 to 7.8% less equivalent work than a simple stripper. An interheated stripper with 8 m PZ at 150 °C requires 30.9 kJ/mole $CO_2$.

Greater stripper complexity generally results in better energy efficiency due to a closer approach to a reversible process. A single increase in complexity does not always provide the same reduction in energy consumption. Increasing the number of pressure stages of a multi-stage flash from 1 to 2 with 9 m MEA decreases the equivalent work by 4.2%. There is a reduced benefit of 0.5% when the number of pressure stages in the multi-stage flash was increased from 3 to 4 with 9 m MEA.

Evaluating the performance with equivalent work instead of heat duty is important when considering different configurations, solvents, and reboiler temperatures because it accounts for the higher value of steam at high temperature as well as the pump and compressor work effects when the stripper pressure changes. As an example, 9 m

MEA with reboiler temperatures of 100 °C and 120 °C using a 2-stage flash and a rich loading of 0.5 is considered. The optimal lean loadings based on minimum heat duty for the two temperatures are 0.41 and 0.37, respectively. The optimal lean loadings based on the equivalent work that these two temperatures are 0.425 and 0.385, respectively.

8 m PZ requires up to 11% less equivalent work than 9 m MEA. The simple stripper is the configuration that benefits the most with PZ; the simple stripper requires 33.1 kJ/mol $CO_2$ with 8 m PZ, which is 11% less than the energy requirement with 9 m MEA. Packed configurations improve by 9 to 11% with the solvent change, whereas multi-stage flash configurations are only 3 to 4% better with PZ.

Reducing the rich loading with 9 m MEA from 0.50 to a more conservative value of 0.48 reduces the efficiency of each configuration by 5 to 7%. The configuration least affected by the loading change is the interheated column; the equivalent work decreases from 34.2 to 32.5 kJ/mole $CO_2$ when the rich loading decreases from 0.5 to 0.48.

With 8 m PZ, increasing the stripper temperature from 120 °C to 150 °C reduces the work requirement by 1 to 3% at the optimal lean loadings, depending on the configuration.

Later work with validating pilot plant campaigns revealed that the performance of 9 m MEA was overestimated with the Hilliard thermodynamic model. The conclusions of the trends with this solvent are valid, but the actual benefit of 8 m PZ over 9 m MEA will be greater than reported.

When switching from a simple stripper to 2-stage flash configuration, the equivalent work of 9 m MEA decreases by 1.1%, but the energy requirement is heightened by 3% with this switch of configurations when using 8 m PZ. This opposite behavior of the solvents demonstrates that MEA and PZ have different properties and strengths; their relative benefit with each type of complexity differs. There is a

substantial benefit in compression work for MEA that outweighs the increase in heat work. In contrast, the 2-stage flash configuration with PZ worsens the equivalent work compared to the simple stripper because the lower heat of absorption yields a higher stripping steam content in the overhead vapor compared to MEA, so its increase in heat work is greater than its benefit in compression work.

### 6.1.2. Novel Stripper Configurations

Cold rich bypass reduces equivalent work for the 2-stage flash with 8 m PZ by 6.6% to 34.0 kJ/mol $CO_2$. The total volatilized PZ decreases by 63% with the inclusion of bypass. Changing the pressure ratio from 2 to 1.5 balances the vapor production rates of the flash vessels, so bypassing cold rich solvent to both flash vessels with a pressure ratio of 1.5 dropped the equivalent work to 30.7 kJ/mol $CO_2$. PZ and the 2-stage flash are the solvent and configuration that benefit most from rich bypass due to their elevated water content in the overhead vapor. Although the interheated column is the most efficient optimized configuration, it only experiences minor improvement with bypass because the overhead vapor is already cooled.

When using an advanced 2-stage flash configuration (2T2PFlash) with 8 m PZ and geothermal brine for heating, the minimum work requirement with 150 °C brine is 35.5 kJ/mole $CO_2$. The required heat rate for a 60 $MW_e$ coal-fired power plant is 40.8 MW. The modified Fluor configuration with 9 m MEA has a total energy requirement of 36.4 kJ/mol $CO_2$ and a heat rate of 38.6 MW for a 60 $MW_e$ coal-fired power plant. The 2T2PFlash with PZ has a lower work requirement than the Fluor configuration because its cross exchangers are able to take better advantage of the high-temperature brine compared to the reboiler in the Fluor configuration.

The predictions with the isolated stripper simulations from this work match well with absorber simulation results. Integrating the stripper section with an intercooled absorber has little effect on the prediction of the energy requirement with 8 m PZ; the rich loading has only slight variation with different values of lean loading when intercooling is used. Using an intercooled absorber with 8 m PZ and 15 m of Mellapak 2X packing, the rich solvent that is provided to the stripper maintains a loading of 0.4 within a variation of 0.005.

An increase in the turbine efficiency term used in the heat work expression from 75 to 96% is required for the calculation to agree with steam cycle model predictions. With this modification, the heat work calculation closely follows the energy penalty prediction from the steam cycle model with reboiler temperatures from 100 to 150 °C.

### 6.1.3. Pilot Plant Modeling

The pilot plant campaigns in 2010 and 2011 using 8 m PZ were accurately simulated with the 5deMayo thermodynamic model. The Fall 2010 campaign used a simple stripper, and the Winter 2011 campaign used a 2-stage flash. The average absolute errors of the simulation results compared to the measurements for these campaigns were 2.7 and 2.5%, respectively.

The energy balance of the 2008 simple stripper campaign with 8 m PZ does not close in the simulations because the system used an alternative reboiler flow scheme that is not represented in the simulation. The lack of closure is apparent through a correlation between the percent deviations of stripped $CO_2$ and $\Delta$ldg. The energy balance issue is addressed in this campaign by manipulating the measured heat loss. This heat loss of

most runs is increased by up to 125%, but two extreme cases required increases of 148% and 179%.

The energy performance of the 2-stage flash campaign was significantly poorer than the predictions of the previously optimized results. The minimum normalized heat duty from the campaign was 206 kJ/mol $CO_2$, compared to a predicted minimum heat duty of 119 kJ/mol $CO_2$. The increase in heat duty was due primarily to poor cross exchanger performance.

The equilibrium flash conditions in the 2-stage flash campaign were matched within small deviation. The temperatures and compositions of the low-pressure flash in the 2-stage flash campaign demonstrated equilibrium conditions based on estimates by the solvent model. Simulations of the 2-stage flash runs fit the pilot plant data within small error by splitting the predicted heat duty evenly between the two flash vessels.

The simulation of 2010 simple stripper campaign with 9 m MEA does not match the pilot plant measurements because the Hilliard solvent model overpredicts the $CO_2$ partial pressure as well as the heat of absorption. Manipulating the measured heat loss forces the energy balance to match while simultaneously fitting the $CO_2$ removal rate. Excluding the heat loss, the MAPE is 4.1%.

The measured condenser duty at the pilot plant does not accurately reflect the actual required duty because heat loss occurs in the overhead, condensing some water vapor before it reaches the condenser. Therefore, the measured condenser duty cannot be used to calculate the condensate rate. A composition meter in the overhead or a steady-state condensate rate meter need to be installed in order to conclude on the overhead composition and, therefore, the approach to equilibrium at the top of the column.

## 6.3. RECOMMENDATIONS

### Thermodynamic Models

1. Improve the Hilliard thermodynamic model to accurately represent the 9 m MEA solvent. At an amine concentration of 9 m, the partial pressure of $CO_2$ was over predicted by Hilliard model. A following observation mandated by the Gibbs-Helmholtz relation was that the heat of absorption was also too high. This inaccuracy was apparent in the 2010 MEA simple stripper campaign. Once the new model is complete, the stripper data of the campaign should be simulated again to ensure that the measured heat loss at the pilot plant was accurate.
2. Develop new thermodynamic models for new solvents of interest like methyldiethanolamine (MDEA)/PZ. Compare the performances of new solvents in the stripper to PZ.

### Process Simulations

1. Acquire rigorous process unit models for pumps and compressors to predict their work contributions with maximum accuracy. The compressor work prediction in this work agreed within small error with rigorous compressor work models by graduate students at TUHH. However, the pump work should be verified, and the actual work requirement of a large-scale supercritical $CO_2$ compressor should be assessed.
2. Incorporate realistic heat loss profile predictions for full-scale strippers into the process models to provide better predictions of the actual energy usage that could be expected.

3. Explore new process configurations with more complex arrangements of flash vessels. Using a matrix of flash vessels at various temperatures could more efficiently strip $CO_2$ through a typical temperature range.
4. Reduce the total heat duty by integrating heat recovery recovery from the intercoolers of the multi-stage compressor and energy recovery from the lean solvent through a liquid expansion turbine. Heat recovery from intercoolers could recycle 20.6 kJ/mol $CO_2$ assuming a stripper pressure of 2 bar, and the maximum benefit of using a liquid expansion turbine would be 1% of the total equivalent work.
5. Simulate the cold rich bypass configurations using the kinetic reactions method. Since the rich solvent entering the top of the packing was approximately 50 °C, the kinetic limitations of the reactions would be important to consider. The required packing to get the same benefits as in this work would be taller.
6. Use net present value (NPV) or a similar analysis to compare steam heating to the geothermal heating alternative in the stripper.

**Pilot Plant**

1. Incorporate direct quantitative measurement of condensate or overhead vapor composition. The water content of the vapor is a direct indicator of the performance of the column and its approach to equilibrium. With either a vapor composition measurement or a condensate measurement to accompany the $CO_2$ gas rate, more conclusions can be made with regards to the stripper performance. The measured condenser duty was not reliable enough to extract this data due to a) a high cooling water flow rate, resulting in a low cooling water $\Delta T$, and b) heat loss in the overhead vapor line which liquefied water before the condenser.

2. Continue to run the reboiler flow without splitting the lean to recycle to the column sump. This unknown recycle rate yields runs that are difficult to simulate, so the results are not as useful.
3. Develop a stripper model that is capable of explaining the complex temperature behavior that was observed at the pilot plant.
4. Quantify the amount of heat loss that occurs in specific locations like the heat exchanger, reboiler, redistributor, and other exposed areas like flanges and the top of the column.
5. Update the correlation for measured heat loss at the pilot plant to include the effect of wind speed.
6. Carry out additional high temperature 2-stage flash campaigns to approach the optimal performance that was predicted in simulations. Run the flash vessels at higher pressures and reduce the heat loss.

**Industrial Recommendations**

1. Use an interheated column to maximize stripper efficiency with minimal capital cost investment.
2. Replacing a large simple stripper with a 2-stage flash can provide similar, if not lower, performance with a lower capital cost investment.
3. Implement cold rich bypass into any configuration to reduce the energy requirement and minimize amine volatility. This upgrade works especially well when using solvents with a low heat of absorption.
4. Use 8 m PZ over the industry-standard MEA. The total energy requirement decreases due to lower compressor and pump work.

# Appendix A: MEA Aspen Plus® Input File

A previously developed thermodynamic model for MEA in Aspen Plus® v7.1 was used for simulations with the solvent in this work (Hilliard, 2008). The reaction sets were cleaned up slightly to simplify the calculations. The entire input file of a simulation with a blank flowsheet is included below. It details the thermodynamic constants in the e-NRTL model that predicted the properties of loaded MEA solutions.

```
;
DYNAMICS
   DYNAMICS RESULTS=ON


IN-UNITS SI MASS-FLOW='kg/hr' PRESSURE=kPa TEMPERATURE=C  &
      MASS-HEAT-CA='kJ/kg-K' PDROP='N/sqm'

DEF-STREAMS CONVEN ALL

SIM-OPTIONS
   IN-UNITS MET VOLUME-FLOW='cum/hr' ENTHALPY-FLO='Gcal/hr'  &
      HEAT-TRANS-C='kcal/hr-sqm-K' PRESSURE=bar TEMPERATURE=C  &
      VOLUME=cum DELTA-T=C HEAD=meter MOLE-DENSITY='kmol/cum'  &
      MASS-DENSITY='kg/cum' MOLE-ENTHALP='kcal/mol'  &
      MASS-ENTHALP='kcal/kg' HEAT=Gcal MOLE-CONC='mol/l'  &
      PDROP=bar
   SIM-OPTIONS RESTART=NO GAMUS-BASIS=AQUEOUS OLD-DATABANK=NO

RUN-CONTROL MAX-TIME=10800.

DESCRIPTION "
   Electrolytes Simulation with Metric Units :
   C, bar, kg/hr, kmol/hr, Gcal/hr, cum/hr.

   Property Method: ELECNRTL

   Flow basis for input: Mass
```

```
   Stream report composition: Mass flow
   "

DATABANKS 'APV71 ASPENPCD' / 'APV71 AQUEOUS' / 'APV71 SOLIDS' &
      / 'APV71 INORGANIC' / 'APV71 PURE20'

PROP-SOURCES 'APV71 ASPENPCD' / 'APV71 AQUEOUS' / 'APV71 SOLIDS' &
      / 'APV71 INORGANIC' / 'APV71 PURE20'

COMPONENTS
   H2O H2O /
   CO2 CO2 /
   MEA C2H7NO /
   MEA+ C2H8NO+ /
   MEACOO- C3H6NO3- /
   HCO3- HCO3- /
   CO3-- CO3-2 /
   H+ H+ /
   OH- OH-

HENRY-COMPS HC-1 CO2

CHEMISTRY GLOBAL
   IN-UNITS SI MASS-FLOW='kg/hr' MOLE-FLOW='mol/hr' PRESSURE=kPa  &
      TEMPERATURE=C MASS-HEAT-CA='kJ/kg-K' PDROP='N/sqm'
   STOIC 1 H2O -1. / H+ 1. / OH- 1.
   STOIC 2 CO2 -1. / H2O -1. / H+ 1. / HCO3- 1.
   STOIC 3 HCO3- -1. / H+ 1. / CO3-- 1.
   STOIC 4 MEA+ -1. / MEA 1. / H+ 1.
   STOIC 5 MEACOO- -1. / H2O -1. / MEA 1. / HCO3- 1.

FLOWSHEET

PROPERTIES ELECNRTL HENRY-COMPS=HC-1 CHEMISTRY=GLOBAL
   PROPERTIES SRK / STEAMNBS

PROP-DATA MDH
   IN-UNITS SI MASS-FLOW='kg/hr' MOLE-FLOW='mol/hr' PRESSURE=kPa  &
      TEMPERATURE=C MASS-HEAT-CA='kJ/kg-K' PDROP='N/sqm'
   PROP-LIST DGAQFM / DHAQFM
   PVAL MEA+ -171023632 / -336961728.8
   PVAL MEACOO- -492922520 / -707209080

PROP-DATA REVIEW-1
   IN-UNITS MET VOLUME-FLOW='cum/hr' ENTHALPY-FLO='Gcal/hr'  &
      HEAT-TRANS-C='kcal/hr-sqm-K' PRESSURE=bar TEMPERATURE=C  &
```

```
      VOLUME=cum DELTA-T=C HEAD=meter MOLE-DENSITY='kmol/cum'  &
      MASS-DENSITY='kg/cum' MOLE-ENTHALP='kcal/mol'  &
      MASS-ENTHALP='kcal/kg' HEAT=Gcal MOLE-CONC='mol/l'  &
      PDROP=bar
   PROP-LIST API / DGFORM / DGSFRM / DHFORM / DHSFRM /  &
      DHVLB / FREEZEPT / HCOM / MUP / MW / OMEGA / PC /  &
      RKTZRA / SG / TB / TC / VB / VC / VLSTD / ZC
   PVAL H2O 10.0 / -54.6343 / -56.5492 / -57.7949 /  &
      -69.9627 / 9.744507 / 0.0 / 0.0 / 1.84972 /  &
      18.01528 / 0.344861 / 220.64 / 0.243172 / 1.0 /  &
      100.0 / 373.946 / 18.8311 / 55.9472 / 18.0691 /  &
      0.229
   PROP-LIST API / DGFORM / DHFORM / DHVLB / FREEZEPT /  &
      HCOM / MUP / MW / OMEGA / PC / RKTZRA / SG / TB / &
      TC / VB / VC / VLSTD / ZC
   PVAL MEA 7.5 / -24.6893 / -49.4025 / 11.88812 / 10.5 /  &
      -325.765 / 0.77646 / 61.08308 / 0.446737 / 71.24 /  &
      0.24764 / 1.0179 / 170 / 405.05 / 68.6673 / 225 /  &
      60.3415 / 0.284
   PROP-LIST DHFORM / FREEZEPT / MW / PC / VC / VLSTD /  &
      ZC / RGYR
   PVAL CO2 -94.05110000 / -56.57 / 44.0095 / 73.83 / 94 /  &
      61.6782 / 0.274 / 1.04000E-10

PROP-DATA REVIEW-1
   IN-UNITS MET VOLUME-FLOW='cum/hr' ENTHALPY-FLO='Gcal/hr'  &
      HEAT-TRANS-C='kcal/hr-sqm-K' PRESSURE=bar TEMPERATURE=C  &
      VOLUME=cum DELTA-T=C HEAD=meter MOLE-DENSITY='kmol/cum'  &
      MASS-DENSITY='kg/cum' MOLE-ENTHALP='J/kmol'  &
      MASS-ENTHALP='kcal/kg' MOLE-ENTROPY='J/kmol-K' HEAT=Gcal  &
      MOLE-CONC='mol/l' PDROP=bar
   PROP-LIST DGAQFM / DHAQFM
   PVAL HCO3- -587370182.1 / -690767961
   PVAL CO3-- -538355662.9 / -677140000

PROP-DATA CPAQ0-1
   IN-UNITS SI MASS-FLOW='kg/hr' MOLE-FLOW='mol/hr' PRESSURE=kPa  &
      MASS-HEAT-CA='kJ/kg-K' PDROP='N/sqm'
   PROP-LIST CPAQ0
   PVAL CO3-- 1334017.129 -5564.838795 5.192267274  &
      -118575111.1 0.0 0.0 0.0 2000.000000
   PVAL HCO3- 211386.984 -881.7986241 0.874689511 -18789290.32  &
      0.0 0.0 0.0 2000.000000
   PVAL MEA+ -1700442.83 7093.368695 -8.487374579 151145133.9  &
      0.0 0.0 0 2000.000
   PVAL MEACOO- -2408071.1 17268.3153 -26.0389963 0.0 0.0  &
      0.0 0.0 2000.000
```

```
PROP-DATA CPDIEC-1
  IN-UNITS MET VOLUME-FLOW='cum/hr' ENTHALPY-FLO='Gcal/hr'  &
    HEAT-TRANS-C='kcal/hr-sqm-K' PRESSURE=bar TEMPERATURE=C  &
    VOLUME=cum DELTA-T=C HEAD=meter MOLE-DENSITY='kmol/cum'  &
    MASS-DENSITY='kg/cum' MOLE-ENTHALP='kcal/mol'  &
    MASS-ENTHALP='kcal/kg' HEAT=Gcal MOLE-CONC='mol/l'  &
    PDROP=bar
  PROP-LIST CPDIEC
  PVAL H2O 78.24662286 32730.85746 298.15
  PVAL MEA 31.06961991 15128.19841 298.15

PROP-DATA DHVLWT-1
  IN-UNITS MET VOLUME-FLOW='cum/hr' ENTHALPY-FLO='Gcal/hr'  &
    HEAT-TRANS-C='kcal/hr-sqm-K' PRESSURE=bar TEMPERATURE=C  &
    VOLUME=cum DELTA-T=C HEAD=meter MOLE-DENSITY='kmol/cum'  &
    MASS-DENSITY='kg/cum' MOLE-ENTHALP='J/kmol'  &
    MASS-ENTHALP='kcal/kg' HEAT=Gcal MOLE-CONC='mol/l'  &
    PDROP=bar
  PROP-LIST DHVLWT
  PVAL H2O 40655000 100.00 0.26623503 0.09110321 0.01
  PVAL MEA 54835800 126.67 0.4041153 0.11011257 -27.37

PROP-DATA HENRY-1
  IN-UNITS MET VOLUME-FLOW='cum/hr' ENTHALPY-FLO='Gcal/hr'  &
    HEAT-TRANS-C='kcal/hr-sqm-K' PRESSURE=Pa TEMPERATURE=K  &
    VOLUME=cum DELTA-T=C HEAD=meter MOLE-DENSITY='kmol/cum'  &
    MASS-DENSITY='kg/cum' MOLE-ENTHALP='kcal/mol'  &
    MASS-ENTHALP='kcal/kg' HEAT=Gcal MOLE-CONC='mol/l'  &
    PDROP=bar
  PROP-LIST HENRY
  BPVAL CO2 H2O 170.7126000 -8477.711000 -21.95743000  &
    5.78074800E-3 273.0000000 500.0000000 0.0
  BPVAL CO2 MEA 89.452 -2934.6 -11.592 0.01644 273.0000000  &
    500.0000000 0.0

PROP-DATA NRTL-1
  IN-UNITS MET VOLUME-FLOW='cum/hr' ENTHALPY-FLO='Gcal/hr'  &
    HEAT-TRANS-C='kcal/hr-sqm-K' PRESSURE=bar TEMPERATURE=C  &
    VOLUME=cum DELTA-T=C HEAD=meter MOLE-DENSITY='kmol/cum'  &
    MASS-DENSITY='kg/cum' MOLE-ENTHALP='kcal/mol'  &
    MASS-ENTHALP='kcal/kg' HEAT=Gcal MOLE-CONC='mol/l'  &
    PDROP=bar
  PROP-LIST NRTL
  BPVAL H2O MEA -123.323712 2575.16998 0.2 0.0 22.061396  &
    -0.029745916 0.0 1000
  BPVAL MEA H2O -1.71338728 -214.123176 0.2 0.0 0.0 0.0  &
```

```
      0.0 1000
   BPVAL H2O CO2 10.06400000 -3268.135000 .2000000000 0.0 0.0  &
      0.0 0.0 200.0000000
   BPVAL CO2 H2O 10.06400000 -3268.135000 .2000000000 0.0 0.0  &
      0.0 0.0 200.0000000

PROP-DATA VLCLK-1
   IN-UNITS MET VOLUME-FLOW='cum/hr' ENTHALPY-FLO='Gcal/hr'  &
      HEAT-TRANS-C='kcal/hr-sqm-K' PRESSURE=bar TEMPERATURE=C  &
      VOLUME=cum DELTA-T=C HEAD=meter MOLE-DENSITY='kmol/cum'  &
      MASS-DENSITY='kg/cum' MOLE-ENTHALP='kcal/mol'  &
      MASS-ENTHALP='kcal/kg' HEAT=Gcal MOLE-CONC='mol/l'  &
      PDROP=bar
   PROP-LIST VLCLK
   BPVAL MEA+ OH- -390.9954000 1000.000000

PROP-DATA GMELCC-1
   IN-UNITS MET VOLUME-FLOW='cum/hr' ENTHALPY-FLO='Gcal/hr'  &
      HEAT-TRANS-C='kcal/hr-sqm-K' PRESSURE=bar TEMPERATURE=C  &
      VOLUME=cum DELTA-T=C HEAD=meter MOLE-DENSITY='kmol/cum'  &
      MASS-DENSITY='kg/cum' MOLE-ENTHALP='kcal/mol'  &
      MASS-ENTHALP='kcal/kg' HEAT=Gcal MOLE-CONC='mol/l'  &
      PDROP=bar
   PROP-LIST GMELCC
   PPVAL H2O ( H+ HCO3- ) 8.04500000
   PPVAL ( H+ HCO3- ) H2O -4.07200000
   PPVAL H2O ( H+ CO3-- ) 8.04500000
   PPVAL ( H+ CO3-- ) H2O -4.07200000
   PPVAL H2O ( H+ OH- ) 8.04500000
   PPVAL ( H+ OH- ) H2O -4.07200000
   PPVAL H2O ( MEA+ HCO3- ) 12.77005390
   PPVAL ( MEA+ HCO3- ) H2O -3.80956870
   PPVAL CO2 ( MEA+ HCO3- ) 49.15747970
   PPVAL ( MEA+ HCO3- ) CO2 -5.89256106
   PPVAL CO2 ( MEA+ CO3-- ) 15.00000000
   PPVAL ( MEA+ CO3-- ) CO2 -8.00000000
   PPVAL CO2 ( MEA+ OH- ) 15.00000000
   PPVAL ( MEA+ OH- ) CO2 -8.00000000
   PPVAL MEA ( MEA+ HCO3- ) 1.78726059
   PPVAL ( MEA+ HCO3- ) MEA -30.84763770
   PPVAL MEA ( MEA+ CO3-- ) 15.00000000
   PPVAL ( MEA+ CO3-- ) MEA -8.00000000
   PPVAL MEA ( MEA+ OH- ) 15.00000000
   PPVAL ( MEA+ OH- ) MEA -8.00000000
   PPVAL H2O ( MEA+ MEACOO- ) 19.03188830
   PPVAL ( MEA+ MEACOO- ) H2O -7.38531897
   PPVAL CO2 ( MEA+ MEACOO- ) 15.00000000
```

```
   PPVAL ( MEA+ MEACOO- ) CO2 -8.00000000
   PPVAL MEA ( MEA+ MEACOO- ) 16.87100390
   PPVAL ( MEA+ MEACOO- ) MEA -13.62627530

PROP-DATA GMELCD-1
   IN-UNITS MET VOLUME-FLOW='cum/hr' ENTHALPY-FLO='Gcal/hr'  &
      HEAT-TRANS-C='kcal/hr-sqm-K' PRESSURE=bar TEMPERATURE=C  &
      VOLUME=cum DELTA-T=C HEAD=meter MOLE-DENSITY='kmol/cum'  &
      MASS-DENSITY='kg/cum' MOLE-ENTHALP='kcal/mol'  &
      MASS-ENTHALP='kcal/kg' HEAT=Gcal MOLE-CONC='mol/l'  &
      PDROP=bar
   PROP-LIST GMELCD
   PPVAL H2O ( MEA+ HCO3- ) 156.09046700
   PPVAL ( MEA+ HCO3- ) H2O -214.82514800
   PPVAL CO2 ( MEA+ HCO3- ) 430.10816000
   PPVAL ( MEA+ HCO3- ) CO2 14444.83540000
   PPVAL CO2 ( MEA+ CO3-- ) 0.0
   PPVAL ( MEA+ CO3-- ) CO2 0.0
   PPVAL CO2 ( MEA+ OH- ) 0.0
   PPVAL ( MEA+ OH- ) CO2 0.0
   PPVAL MEA ( MEA+ HCO3- ) 3128.53045000
   PPVAL ( MEA+ HCO3- ) MEA 6981.73393000
   PPVAL MEA ( MEA+ CO3-- ) 0.0
   PPVAL ( MEA+ CO3-- ) MEA 0.0
   PPVAL MEA ( MEA+ OH- ) 0.0
   PPVAL ( MEA+ OH- ) MEA 0.0
   PPVAL H2O ( MEA+ MEACOO- ) -789.61025500
   PPVAL ( MEA+ MEACOO- ) H2O 432.17895100
   PPVAL CO2 ( MEA+ MEACOO- ) 0.0
   PPVAL ( MEA+ MEACOO- ) CO2 0.0
   PPVAL MEA ( MEA+ MEACOO- ) -2809.73880000
   PPVAL ( MEA+ MEACOO- ) MEA 1864.65113000

PROP-DATA GMELCE-1
   IN-UNITS MET VOLUME-FLOW='cum/hr' ENTHALPY-FLO='Gcal/hr'  &
      HEAT-TRANS-C='kcal/hr-sqm-K' PRESSURE=bar TEMPERATURE=C  &
      VOLUME=cum DELTA-T=C HEAD=meter MOLE-DENSITY='kmol/cum'  &
      MASS-DENSITY='kg/cum' MOLE-ENTHALP='kcal/mol'  &
      MASS-ENTHALP='kcal/kg' HEAT=Gcal MOLE-CONC='mol/l'  &
      PDROP=bar
   PROP-LIST GMELCE
   PPVAL H2O ( MEA+ HCO3- ) 24.60156680
   PPVAL ( MEA+ HCO3- ) H2O -5.89393435
   PPVAL CO2 ( MEA+ HCO3- ) 2262.77769000
   PPVAL ( MEA+ HCO3- ) CO2 659.23135400
   PPVAL CO2 ( MEA+ CO3-- ) 0.0
   PPVAL ( MEA+ CO3-- ) CO2 0.0
```

```
   PPVAL CO2 ( MEA+ OH- ) 0.0
   PPVAL ( MEA+ OH- ) CO2 0.0
   PPVAL MEA ( MEA+ HCO3- ) 66.01464320
   PPVAL ( MEA+ HCO3- ) MEA 440.40354300
   PPVAL MEA ( MEA+ CO3-- ) 0.0
   PPVAL ( MEA+ CO3-- ) MEA 0.0
   PPVAL MEA ( MEA+ OH- ) 0.0
   PPVAL ( MEA+ OH- ) MEA 0.0
   PPVAL H2O ( MEA+ MEACOO- ) -19.69365630
   PPVAL ( MEA+ MEACOO- ) H2O 1.75887248
   PPVAL CO2 ( MEA+ MEACOO- ) 0.0
   PPVAL ( MEA+ MEACOO- ) CO2 0.0
   PPVAL MEA ( MEA+ MEACOO- ) 22.41433100
   PPVAL ( MEA+ MEACOO- ) MEA 16.45050280

PROP-DATA GMELCN-1
   IN-UNITS MET VOLUME-FLOW='cum/hr' ENTHALPY-FLO='Gcal/hr'  &
      HEAT-TRANS-C='kcal/hr-sqm-K' PRESSURE=bar TEMPERATURE=C  &
      VOLUME=cum DELTA-T=C HEAD=meter MOLE-DENSITY='kmol/cum'  &
      MASS-DENSITY='kg/cum' MOLE-ENTHALP='kcal/mol'  &
      MASS-ENTHALP='kcal/kg' HEAT=Gcal MOLE-CONC='mol/l'  &
      PDROP=bar
   PROP-LIST GMELCN
   PPVAL CO2 ( MEA+ HCO3- ) .1000000000
   PPVAL CO2 ( MEA+ CO3-- ) .1000000000
   PPVAL CO2 ( MEA+ OH- ) .1000000000
   PPVAL MEA ( MEA+ HCO3- ) .1000000000
   PPVAL MEA ( MEA+ CO3-- ) .1000000000
   PPVAL MEA ( MEA+ OH- ) .1000000000
   PPVAL CO2 ( MEA+ MEACOO- ) .1000000000
   PPVAL MEA ( MEA+ MEACOO- ) .1000000000

EO-CONV-OPTI

STREAM-REPOR MOLEFLOW MOLEFRAC

PROPERTY-REP PARAMS NOPCES PROP-DATA DFMS NOPARAM-PLUS
;
;
;
;
;
```

# Appendix B: Tabulated Simulation Results

Simulation results were presented in Chapters 3 and 4 that demonstrated the performance of various stripper configurations with 8 m PZ and 9 m MEA. This appendix tabulates the data that was used to generate the figures.

**Table B-1. Predicted compressor work based on Aspen Plus® simulations and thermodynamic minimum. Data used for Figures 3-9 and 3-10.**

| Inlet Pressure | 72% eff, 0% ΔP | 80% eff, 0% ΔP | 80% eff, 10% ΔP | 80% eff, 20% ΔP | Thermodynamic Minimum@40°C |
|---|---|---|---|---|---|
| *bar* | *Compression Work (kJ/mol $CO_2$)* | | | | |
| 0.80 | 19.99 | 17.89 | 18.89 | 20.00 | 11.47 |
| 0.90 | 19.30 | 17.28 | 18.18 | 19.25 | 11.17 |
| 1.00 | 18.66 | 16.71 | 17.60 | 18.57 | 10.90 |
| 1.15 | 17.84 | 15.98 | 16.78 | 17.72 | 10.54 |
| 1.25 | 17.84 | 15.97 | 16.37 | 17.18 | 10.32 |
| 1.50 | 16.81 | 15.06 | 15.75 | 16.48 | 9.85 |
| 2.00 | 15.28 | 13.70 | 14.31 | 14.95 | 9.10 |
| 2.50 | 14.61 | 13.08 | 13.24 | 13.82 | 8.53 |
| 3.00 | 13.68 | 12.26 | 12.74 | 13.24 | 8.06 |
| 3.50 | 12.91 | 11.57 | 12.03 | 12.50 | 7.66 |
| 4.00 | 12.25 | 10.99 | 11.40 | 11.87 | 7.32 |
| 4.50 | 11.67 | 10.48 | 10.89 | 11.32 | 7.02 |
| 5.00 | 11.66 | 10.44 | 10.76 | 10.83 | 6.75 |
| 5.50 | 11.19 | 10.03 | 10.34 | 10.67 | 6.51 |

| **Inlet Pressure** | **72% eff, 0% ΔP** | **80% eff, 0% ΔP** | **80% eff, 10% ΔP** | **80% eff, 20% ΔP** | **Thermodynamic Minimum@40°C** |
|---|---|---|---|---|---|
| *bar* | *Compression Work (kJ/mol $CO_2$)* | | | | |
| 6.00 | 10.77 | 9.65 | 9.95 | 10.27 | 6.28 |
| 6.50 | 10.38 | 9.31 | 9.60 | 9.90 | 6.08 |
| 7.00 | 10.02 | 8.99 | 9.27 | 9.58 | 5.89 |
| 7.50 | 9.69 | 8.70 | 8.98 | 9.27 | 5.72 |
| 8.00 | 9.38 | 8.42 | 8.69 | 8.98 | 5.56 |
| 8.50 | 9.09 | 8.16 | 8.43 | 8.71 | 5.41 |
| 9.00 | 8.82 | 7.92 | 8.18 | 8.46 | 5.26 |
| 9.50 | 9.10 | 8.16 | 8.35 | 8.21 | 5.13 |
| 10.00 | 8.86 | 7.94 | 8.13 | 8.33 | 5.00 |
| 10.50 | 8.62 | 7.73 | 7.92 | 8.12 | 4.88 |
| 11.00 | 8.40 | 7.53 | 7.72 | 7.91 | 4.76 |
| 11.50 | 8.18 | 7.34 | 7.53 | 7.71 | 4.65 |
| 12.00 | 7.98 | 7.16 | 7.34 | 7.53 | 4.55 |
| 12.50 | 7.79 | 6.99 | 7.17 | 7.35 | 4.45 |
| 13.00 | 7.60 | 6.82 | 7.00 | 7.18 | 4.35 |
| 13.50 | 7.42 | 6.66 | 6.84 | 7.02 | 4.26 |
| 14.00 | 7.25 | 6.51 | 6.68 | 6.86 | 4.17 |
| 14.50 | 7.08 | 6.36 | 6.53 | 6.71 | 4.08 |
| 15.00 | 6.92 | 6.21 | 6.39 | 6.56 | 4.00 |
| 15.50 | 6.76 | 6.08 | 6.24 | 6.42 | 3.92 |
| 16.00 | 6.61 | 5.94 | 6.11 | 6.28 | 3.85 |
| 16.50 | 6.47 | 5.81 | | 6.14 | 3.77 |
| 17.00 | 6.33 | 5.69 | | 6.98 | 3.70 |
| 17.50 | 6.20 | 5.57 | | | 3.63 |
| 18.00 | 6.07 | 5.46 | | | 3.56 |
| 18.50 | 5.95 | 5.35 | | 6.60 | 3.50 |
| 19.00 | | | | 6.47 | 3.43 |
| 19.50 | 5.75 | 5.17 | | 6.35 | 3.37 |
| 20.00 | | | | | 3.31 |

**Table B-2a. Performance of all configurations with 9 m MEA with a reboiler temperature of 120 °C. Data used for Figures 3-11 to 3-14.**

| Lean Loading | Simple Stripper | 1-Stage Flash | 2-Stage Flash | 3-Stage Flash | 4-Stage Flash |
|---|---|---|---|---|---|
| *mol/mol* | *Equivalent Work (kJ/mol $CO_2$)* | | | | |
| 0.20 | 37.38 | 59.40 | 49.82 | 46.38 | 44.61 |
| 0.21 | 37.27 | 57.07 | 48.01 | 44.85 | 43.11 |
| 0.22 | 37.16 | 54.88 | 46.37 | 43.42 | 41.83 |
| 0.23 | 37.03 | 52.83 | 44.86 | 42.06 | 40.64 |
| 0.24 | 36.89 | 50.94 | 43.49 | 40.86 | 39.59 |
| 0.25 | 36.73 | 49.18 | 42.22 | 39.75 | 38.63 |
| 0.26 | 36.56 | 47.55 | 41.05 | 38.85 | 37.78 |
| 0.27 | 36.38 | 46.03 | 39.98 | 37.96 | 36.99 |
| 0.28 | 36.18 | 44.62 | 39.00 | 37.14 | 36.28 |
| 0.29 | 35.96 | 43.31 | 38.09 | 36.41 | 35.63 |
| 0.30 | 35.74 | 42.10 | 37.25 | 35.75 | 35.05 |
| 0.31 | 35.51 | 40.99 | 36.53 | 35.17 | 34.54 |
| 0.32 | 35.28 | 39.97 | 35.88 | 34.66 | |
| 0.33 | 35.05 | 39.04 | 35.31 | 34.21 | 33.77 |
| 0.34 | 34.82 | 38.17 | 34.77 | | 33.46 |
| 0.35 | | 37.39 | 34.34 | 33.57 | 33.22 |
| 0.36 | | 36.69 | 34.00 | 33.33 | 33.05 |
| 0.37 | 34.21 | 36.08 | 33.72 | 33.19 | 32.96 |
| 0.38 | 34.08 | 35.57 | 33.55 | 33.13 | 33.01 |
| 0.39 | 34.04 | 35.21 | 33.49 | 33.25 | 33.13 |
| 0.40 | 34.11 | 34.99 | | 33.43 | 33.37 |
| 0.41 | 34.32 | 34.94 | 33.89 | 33.81 | |
| 0.42 | 34.74 | 35.13 | 34.41 | 34.44 | 34.56 |
| 0.43 | 35.52 | 35.68 | 35.28 | 35.51 | 35.63 |
| 0.44 | 36.81 | 36.76 | | 37.05 | 37.05 |
| 0.45 | 38.80 | 38.72 | 39.10 | 39.66 | 39.66 |

**Table B-2b. Performance of all configurations with 9 m MEA with a reboiler temperature of 120 °C. Data used for Figures 3-11 to 3-14.**

| Lean Loading | Double matrix, 20% split | Double matrix, opt split | Double matrix, opt split, LP packing | 2-Stage Multipressure |
|---|---|---|---|---|
| *mol/mol* | *Equivalent Work (kJ/mol $CO_2$)* | | | |
| 0.20 | 45.13 | 39.62 | | |
| 0.21 | 43.63 | | | |
| 0.22 | 42.29 | | | |
| 0.23 | 41.06 | 38.25 | 36.96 | |
| 0.24 | 39.95 | | | |
| 0.25 | 38.93 | 36.96 | | 40.74 |
| 0.26 | 38.01 | | | 39.71 |
| 0.27 | 37.17 | | 35.30 | 38.82 |
| 0.28 | 36.43 | 35.81 | | 38.04 |
| 0.29 | 35.69 | | | |
| 0.30 | 35.11 | 34.79 | 34.23 | |
| 0.31 | 34.62 | | | 36.12 |
| 0.32 | 34.22 | | | 35.62 |
| 0.33 | 33.88 | 34.00 | | 35.17 |
| 0.34 | 33.62 | | 33.24 | 34.77 |
| 0.35 | 33.45 | 33.43 | | 34.43 |
| 0.36 | 33.37 | | | 34.15 |
| 0.37 | 33.41 | 33.19 | 32.89 | 33.95 |
| 0.38 | 33.61 | | | 33.85 |
| 0.39 | 34.00 | 33.23 | | 33.86 |
| 0.40 | 34.66 | | 33.22 | |
| 0.41 | 35.72 | 33.80 | | 34.46 |
| 0.42 | 37.38 | | 34.23 | 35.15 |
| 0.43 | 39.97 | 34.84 | | 36.44 |
| 0.44 | 44.16 | 36.70 | 36.72 | 38.41 |
| 0.45 | 51.35 | 39.01 | 42.99 | 41.55 |

**Table B-2c. Performance of all configurations with 9 m MEA with a reboiler temperature of 120 °C. Data used for Figures 3-11 to 3-14.**

| Lean Loading | 2-Stage Multipressure, packing | Stripper with lean flash | Interheated above reboiler | Interheated at mid-column |
|---|---|---|---|---|
| *mol/mol* | *Equivalent Work (kJ/mol $CO_2$)* | | | |
| 0.20 | 37.05 | 37.50 | 37.32 | |
| 0.21 | 36.87 | | | 34.89 |
| 0.22 | 36.68 | | 36.97 | |
| 0.23 | 36.48 | 37.09 | | |
| 0.24 | 36.23 | | 36.55 | |
| 0.25 | 35.98 | | | 34.38 |
| 0.26 | 35.71 | | 36.06 | |
| 0.27 | 35.42 | 36.41 | | |
| 0.28 | 35.14 | | 35.51 | 33.82 |
| 0.29 | 34.82 | 35.83 | | |
| 0.30 | 34.51 | | 34.90 | |
| 0.31 | 34.22 | 35.10 | | |
| 0.32 | 33.94 | | 34.29 | 33.16 |
| 0.33 | 33.68 | 34.58 | | |
| 0.34 | 33.48 | | 33.71 | |
| 0.35 | 33.33 | | | 32.78 |
| 0.36 | 33.21 | 33.86 | 33.20 | |
| 0.37 | 33.16 | 33.60 | | 32.48 |
| 0.38 | 33.18 | | 32.97 | |
| 0.39 | 33.31 | 33.59 | 32.96 | 32.54 |
| 0.40 | 33.56 | 33.81 | | 32.67 |
| 0.41 | 34.01 | 34.30 | 32.88 | 33.14 |
| 0.42 | 34.70 | 34.79 | 33.35 | 33.49 |
| 0.43 | 35.80 | 36.05 | | |
| 0.44 | 37.42 | | | |
| 0.45 | 39.99 | | | |

**Table B-3. Performance of 1-stage flash with 9 m MEA at various flash temperatures. Data used for Figure 3-15.**

| Lean Loading | 100 °C | 110 °C | 120 °C | 130 °C |
|---|---|---|---|---|
| *mol/mol* | *Equivalent Work (kJ/mol $CO_2$)* | | | |
| 0.20 | 67.16 | 63.91 | 59.40 | 54.29 |
| 0.21 | 65.22 | 61.75 | 57.07 | 52.13 |
| 0.22 | 63.27 | 59.58 | 54.88 | 50.10 |
| 0.23 | 61.40 | 57.44 | 52.83 | 48.25 |
| 0.24 | 59.60 | 55.58 | 50.94 | 46.56 |
| 0.25 | 57.87 | 53.67 | 49.18 | 45.05 |
| 0.26 | 56.19 | 52.00 | 47.55 | 43.59 |
| 0.27 | 54.58 | 50.30 | 46.03 | 42.30 |
| 0.28 | 53.02 | 48.76 | 44.62 | 41.12 |
| 0.29 | 51.52 | 47.30 | 43.31 | 40.04 |
| 0.30 | 50.07 | 45.92 | 42.10 | 39.07 |
| 0.31 | 48.68 | 44.63 | 40.99 | 38.20 |
| 0.32 | 47.34 | 43.41 | 39.97 | 37.42 |
| 0.33 | 46.06 | 42.27 | 39.04 | 36.73 |
| 0.34 | 44.83 | 41.21 | 38.17 | 36.12 |
| 0.35 | 43.66 | 40.21 | 37.39 | 35.60 |
| 0.36 | 42.56 | 39.30 | 36.69 | 35.17 |
| 0.37 | 41.52 | 38.44 | 36.08 | 34.85 |
| 0.38 | 40.55 | 37.66 | 35.57 | 34.64 |
| 0.39 | 39.65 | 36.95 | 35.21 | 34.58 |
| 0.40 | 38.85 | 36.39 | 34.99 | 34.70 |
| 0.41 | 38.15 | 35.97 | 34.94 | 35.07 |
| 0.42 | 37.57 | 35.72 | 35.13 | 35.76 |
| 0.43 | 37.17 | 35.72 | 35.68 | 36.95 |
| 0.44 | 37.01 | 36.10 | 36.76 | 38.88 |
| 0.45 | 37.24 | 37.19 | 38.72 | 42.03 |

**Table B-4. Equivalent work contributions for 1-stage flash with 9 m MEA at varying flash temperatures. Data used for Figure 3-16.**

| Flash T | Lean Loading | Equivalent Work | Heat Work | Compression work | Pump Work |
|---|---|---|---|---|---|
| *°C* | *mol/mol* | *kJ/mol $CO_2$* | | | |
| 100 | 0.44 | 37.01 | 21.11 | 14.98 | 0.92 |
| 110 | 0.42 | 35.72 | 21.86 | 12.96 | 0.90 |
| 120 | 0.405 | 34.94 | 22.76 | 10.82 | 1.36 |
| 130 | 0.39 | 34.58 | 23.71 | 8.88 | 1.98 |

**Table B-5. Performance of important configurations with 8 m PZ with a reboiler temperature of 150 °C. Data used for Figure 3-21.**

| Lean Loading | 1-Stage Flash | 2-Stage Flash | Simple Stripper | Adiabatic Lean Flash | Double Matrix | Interheated Column |
|---|---|---|---|---|---|---|
| *mol/mol* | *Equivalent Work (kJ/mol $CO_2$)* | | | | | |
| 0.20 | 55.84 | 46.40 | 35.43 | 34.61 | 35.11 | 32.26 |
| 0.21 | 53.41 | 44.57 | 35.24 | 34.37 | 34.67 | |
| 0.22 | 50.86 | 42.67 | 35.02 | 34.18 | 34.26 | 31.89 |
| 0.23 | 48.64 | 41.50 | 34.78 | 33.91 | 33.82 | 31.60 |
| 0.24 | 46.38 | 39.94 | 34.53 | 33.60 | 33.38 | |
| 0.25 | 44.28 | 38.69 | 34.28 | 33.35 | 32.97 | 31.30 |
| 0.26 | 42.52 | 37.61 | 33.97 | 33.02 | 32.72 | |
| 0.27 | 40.78 | 36.55 | 33.74 | 32.79 | 32.47 | 31.08 |
| 0.28 | 39.24 | 35.78 | 33.47 | 32.52 | 32.24 | 30.95 |
| 0.29 | 38.03 | 35.07 | 33.29 | 32.41 | 32.22 | |
| 0.30 | 36.91 | 34.41 | 33.13 | 32.30 | 32.24 | 30.96 |
| 0.31 | 36.06 | 34.10 | 33.11 | 32.35 | 32.59 | 31.19 |
| 0.32 | 35.53 | 34.00 | 33.25 | 32.63 | 33.04 | 31.82 |
| 0.33 | 35.31 | 34.27 | 33.64 | 33.17 | 34.13 | |
| 0.34 | 35.58 | 34.86 | 34.31 | 34.01 | 35.75 | 33.21 |
| 0.35 | 36.47 | 36.13 | 35.68 | 35.64 | 38.40 | 36.18 |
| 0.36 | 38.57 | 38.40 | 38.85 | 38.39 | 44.12 | |
| 0.37 | 42.78 | 43.46 | | 43.72 | | 42.58 |
| 0.38 | 52.66 | 53.06 | | 53.97 | | 54.89 |
| 0.39 | 81.32 | 88.89 | | 78.59 | | |

**Table B-6. Cool rich bypass based on pilot plant results with 2-stage flash in 8 m PZ. Bypass taken between LP and HP cross exchangers. 0.40 rich loading, 3 °C cold side approach on LP exchanger, constant UA on HP exchanger, pressure ratio = 2, $CO_2$ compression to 150 bar. Data used for Figure 4-8.**

| Bypass | 5% | 10% | 5% | 10% |
|---|---|---|---|---|
| Lean Loading | Equivalent Work | | PZ in vapor | |
| *mol/mol* | *kJ/mol $CO_2$* | | *mmol/kmol $CO_2$* | |
| 0.25 | 36.87 | 34.35 | 4.304 | 2.570 |
| 0.27 | 34.92 | 32.97 | 2.599 | 1.458 |
| 0.29 | 33.93 | 32.59 | 1.453 | 0.827 |
| 0.31 | 34.43 | 33.71 | 0.844 | 0.482 |
| 0.33 | 37.21 | 37.06 | 0.508 | 0.322 |
| 0.34 | 40.14 | 39.50 | 0.404 | 0.290 |

**Table B-7. Cold rich bypass with 2-stage flash and 8 m PZ. Bypass taken before cross exchanger. 0.40 rich loading, 5 °C LMTD on cross exchanger, equal molar vapor production per pressure stage, $CO_2$ compression to 150 bar. Data used for Figure 4-13.**

| Lean Loading | 0.22 | 0.26 | 0.28 |
|---|---|---|---|
| Bypass | Equivalent Work | | |
| *%* | *kJ/mol $CO_2$* | | |
| 0 | 40.84 | 35.91 | 33.85 |
| 1 | | 35.05 | |
| 3 | 38.37 | 33.36 | 33.10 |
| 5 | 36.72 | 31.65 | 30.08 |
| 7.5 | 34.76 | 30.31 | 29.80 |
| 10 | 33.16 | 30.06 | 30.44 |
| 12.5 | 31.86 | 30.64 | 31.06 |
| 15 | 31.08 | 31.34 | 32.06 |
| 17.5 | 31.36 | 32.15 | 32.84 |
| 20 | 31.90 | 33.07 | 32.88 |

**Table B-8. Cold rich bypass with 2-stage flash and 9 m MEA. Bypass taken before cross exchanger. 0.50 rich loading, 5 °C LMTD on cross exchanger, equal molar vapor production per pressure stage, $CO_2$ compression to 150 bar. Data used for Figure 4-16.**

| Lean Loading | 0.2 | 0.25 | 0.3 | 0.35 | 0.4 | 0.43 |
|---|---|---|---|---|---|---|
| **Bypass** | **Equivalent Work** | | | | | |
| *%* | *kJ/mol $CO_2$* | | | | | |
| 0 | 49.76 | 41.75 | 35.54 | 32.53 | 31.87 | 34.08 |
| 1 | 49.43 | 41.37 | 35.12 | 32.17 | 31.51 | 33.46 |
| 2 | 49.10 | 40.99 | 34.73 | 31.75 | 31.05 | 33.71 |
| 3 | 48.74 | 40.55 | 34.35 | 31.35 | 31.33 | |
| 5 | 48.08 | 39.73 | 33.59 | 30.70 | 31.60 | 34.76 |
| 7.5 | 47.17 | 38.74 | 32.73 | 30.94 | 32.31 | |
| 10 | 46.17 | 37.88 | 31.98 | 31.31 | | 37.07 |
| 12.5 | 45.35 | 36.89 | 31.65 | 31.75 | | |
| 15 | 44.40 | 36.08 | 31.95 | 32.17 | 34.80 | 39.74 |
| 20 | 42.77 | 34.58 | 32.72 | 33.44 | 36.97 | 43.49 |

**Table B-9. Cold rich bypass with simple stripper and 8 m PZ. Bypass taken before cross exchanger. 0.40 rich loading, 5 °C LMTD on cross exchanger, equal molar vapor production per pressure stage, $CO_2$ compression to 150 bar. Data used for Figure 4-17.**

| Lean Loading | 0.24 | 0.27 | 0.3 | 0.32 | 0.34 |
|---|---|---|---|---|---|
| **Bypass** | **Equivalent Work** | | | | |
| *%* | *kJ/mol $CO_2$* | | | | |
| 0 | | | 31.42 | 31.58 | |
| 0.5 | 33.10 | 31.93 | 31.06 | 31.16 | 32.34 |
| 1 | 32.93 | 31.75 | 30.70 | 30.74 | 31.95 |
| 2 | 32.50 | 31.21 | 30.07 | 30.06 | 31.37 |
| 3 | 32.13 | 30.72 | 29.55 | 29.43 | 31.26 |
| 5 | 31.43 | 29.81 | 28.77 | 29.21 | 31.82 |
| 7.5 | 30.62 | 29.09 | 28.64 | 29.88 | 33.71 |
| 10 | 29.98 | 28.81 | 29.24 | 30.93 | 34.96 |
| 12.5 | 29.53 | 28.96 | 29.85 | 32.41 | 37.02 |
| 15 | 29.49 | 29.41 | 30.96 | 33.67 | 38.73 |

**Table B-10. Cold rich bypass with simple stripper and 9 m MEA. Bypass taken before cross exchanger. 0.50 rich loading, 5 °C LMTD on cross exchanger, equal molar vapor production per pressure stage, $CO_2$ compression to 150 bar. Data used for Figure 4-18.**

| Lean Loading | 0.2 | 0.25 | 0.3 | 0.35 | 0.4 |
|---|---|---|---|---|---|
| **Bypass** | **Equivalent Work** | | | | |
| *%* | *kJ/mol $CO_2$* | | | | |
| 0.5 | 32.54 | 36.82 | 34.57 | 33.13 | 32.52 |
| 1 | 32.43 | 36.77 | 34.38 | 32.93 | 32.41 |
| 2 | 31.99 | 36.67 | 34.24 | 32.67 | 31.96 |
| 3 | 31.71 | 36.58 | 34.05 | 32.38 | 31.82 |
| 5 | 31.42 | 36.33 | 33.63 | 31.89 | 32.02 |
| 7.5 | 31.59 | 36.09 | 33.23 | 31.68 | 32.51 |
| 10 | 32.00 | 35.90 | 32.94 | 31.86 | 33.11 |
| 15 | | 35.44 | 32.73 | 32.63 | 34.82 |
| 20 | | 35.18 | 33.30 | 33.75 | 37.01 |

**Table B-11.: Rich bypass with the interheated column in 8 m PZ. Bypass taken before cross exchanger. 0.40 rich loading, 5 °C LMTD on cross exchanger, equal molar vapor production per pressure stage, $CO_2$ compression to 150 bar. Data used for Figure 4-19.**

| Split (%) | 1 | 5 | 7.5 | 10 |
|---|---|---|---|---|
| **Lean Loading** | **Equivalent Work** | | | |
| *mol/mol* | *kJ/mol $CO_2$* | | | |
| 0.20 | 31.83 | 31.45 | 31.36 | 31.35 |
| 0.24 | 30.96 | 30.56 | 30.61 | 30.79 |
| 0.26 | 30.61 | 30.21 | 30.38 | |
| 0.28 | 30.35 | 30.07 | 30.40 | 31.10 |
| 0.30 | 30.38 | 30.19 | 30.80 | 31.81 |
| 0.32 | 31.19 | 31.08 | 32.39 | 33.73 |
| 0.34 | 32.60 | 34.04 | 35.81 | |

# References


Al-Baghli NA, et al. "A rate-based model for the design of gas absorbers for the removal of CO2 and H2S using aqueous solutions of MEA and DEA." *Fluid Phase Equilibria.* 31-43. 2001.

Alie C, et al. "Simulation of CO2 capture using MEA scrubbing: a flowsheet decomposition method." *Energy Conversion and Management.* 475-487. 2005.

Aroonwilas A and P Tontiwachwuthikul. "Mass transfer studies of high-performance structured packing for CO2 separation processes." *Energy Conversion and Management.* S75-S80. 1997.

Astarita G and DW Savage. "Theory of chemical desorption." *Chem Eng Sci.* 35(3): 649-56. 1980a.

Astarita G and DW Savage. "Gas absorption and desorption with reversible instantaneous chemical reaction." *Chem Eng Sci.* 35(8): 1755-64. 1980b.

Austgen DM, et al. "Model of vapor-liquid equilibria for aqueous acid gas-alkanolamine systems 2. Representation of H2S and CO2 solubility in aqueous MDEA and CO2 solubility in aqueous mixtures of MDEA with MEA or DEA." *Industrial Engineering and Chemistry Research.* 543-555. 1991.

Bates BC and ZW Kundzewicz. "Climate Change and Water. Technical Paper of the Intergovernmental Panel on Climate Change." 2008.

Benson HE and DH McCrea. Removal of Acid Gases from Hot Gas Mixtures. Patent 4160810, July 10, 1979.

Bosch H, et al. "Kinetics of the reaction of carbon dioxide with the sterically hindered amine 2-amino-2-methylpropanol at 298 K." *Chem Eng Sci.* 45(5): 1167-73. 1990.

Cadours R, et al. "Kinetics of CO2 Desorption from Highly Concentrated and CO2-Loaded Methyldiethanolamine Aqueous Solutions in the Range 312-383 K." *Ind Eng Chem Res.* 36(12): 5384-5391. 1997.

Chen C-C and Y Song. "Generalized electrolyte-NRTL model for mixed-solvent electrolyte systems." *AIChE J.* 50(8): 1928-1941. 2004.

Chen CC, et al. "Local composition model for excess Gibbs energy of electrolyte systems. Part I: Single solvent, single completely dissociated electrolyte systems." *AIChE J.* 28(4): 588-96. 1982.

Chen E. "Carbon dioxide absorption into piperazine promoted potassium carbonate using structured Packing." 2007.

Closmann F, et al. "MDEA/piperazine as a solvent for CO2 capture." *Energy Procedia.* 1(1): 1351-1357. 2009.

Cullinane JT. "Carbon dioxide absorption in aqueous mixtures of potassium carbonate and piperazine." 2002.

Cullinane JT. *Thermodynamics and kinetics of aqueous piperazine with potassium carbonate for carbon dioxide absorption*. The University of Texas at Austin. Ph.D. Dissertation. 2005.

Cullinane JT and GT Rochelle. "Carbon dioxide absorption with aqueous potassium carbonate promoted by piperazine." *Chemical Engineering Science.* 3619-3630. 2004.
Dang H. "CO2 absorption rate and solubility in monoethanolamine/piperazine/water." 2001.
Desideri U and A Paolucci. "Performance modeling of a carbon dioxide removal system for power plants." *Energy Conversion and Management.* 1899-1915. 1999.
Dugas RE. "Carbon Dioxide Absorption, Desorption, and Diffusion in Aqueous Piperazine and Monoethanolamine." 2009.
EIA. (2006). "Electric Power Annual: Summary Statistics for the United States." http://www.eia.doe.gov/cneaf/electricity/epa/epa_sum.html
Ermatchkov V, et al. "Solubility of Carbon Dioxide in Aqueous Solutions of Piperazine in the Low Gas Loading Region." *J Chem Eng Data.* 51(5): 1788-1796. 2006.
Escobillana GP, et al. "Behavior of absorption/stripping columns for the carbon dioxide-MEA system; modeling and experiments." *Can J Chem Eng.* 69(4): 969-77. 1991.
Fisher KS, et al. "Integrating MEA Regeneration with CO2 Compression and Peaking to Reduce CO2 Capture Costs." 2005.
Frailie P, et al. "Modeling piperazine thermodynamics." *Energy Procedia.* 4: 35-42. 2011.
Freeman SA. *Thermal degradation and oxidation of aqueous piperazine for carbon dioxide capture*. University of Texas at Austin. 2011.
Freeman SA, et al. "Carbon dioxide capture with concentrated, aqueous piperazine." *International Journal of Greenhouse Gas Control*. 119-124. 2010.
Freguia S. "Modeling of CO2 removal from flue gases using MEA." 2002.
Freguia S and GT Rochelle. "Modeling of CO2 capture by aqueous monoethanolamine." *AIChE Journal.* 1676-1686. 2003.
Gupta AK. *Understanding the Plume Dynamics and Risk Associated with CO2 Injection in Deep Saline Aquifers*. The University of Texas at Austin. Masters thesis. 2011.
Hilliard MD. *A Predictive Thermodynamic Model for an Aqueous Blend of Potassium Carbonate, Piperazine, and Monoethanolamine for Carbon Dioxide Capture from Flue Gas*. The University of Texas at Austin. Ph.D. Dissertation. 2008.
Jassim MS and GT Rochelle. "Innovative absorber/stripper configurations for CO2 capture by aqueous monoethanolamine." *Industrial and Engineering Chemistry Research.* 2465-2472. 2006.
Jou FY, et al. "The solubility of CO2 in a 30 mass percent monoethanolamine solution." *Canadian Journal of Chemical Engineering.* 140-147. 1995.
Keeling CD and TP Whorf. "Atmospheric CO2 Records from Sites in the SIO Air Sampling Network." 2004.
Kim I, et al. "Enthalpy of absorption of CO2 with alkanolamine solutions predicted from reaction equilibrium constants." *Chemical Engineering Science.* 64(7): 2027-2038. 2009.

Kim I and HF Svendsen. "Heat of absorption of carbon dioxide (CO2) in Monoethanolamine (MEA) and 2 (Aminoethyl)ethanolamine (AEEA) Solutions." *Industrial & Engineering Chemistry Research.* 46: 5803-5809. 2007.
Kvamsdal HM, et al. "Modelling and simulation of the Esbjerg pilot plant using the Cesar 1 solvent." *Energy Procedia.* 4: 1644-1651. 2011.
Le Tourneux D, et al. "Solubility of carbon dioxide in aqueous solutions of 2-amino-2-hydroxymethyl-1,3-propanediol." *Fluid Phase Equilib.* 268(1-2): 121-129. 2008.
Leites IL and VM Berchenko. "Application of the Second Law of Thermodynamics for Optimization of Absorption Processes to Decrease the Energy Consumption". *Energy Systems and Ecology Conference 93*, Cracow, Poland. 1993
Leites IL, et al. "The theory and practice of energy saving in the chemical industry: some methods for reducing the thermodynamic irreversibility in chemical technology processes." *Energy.* 55-97. 2003.
Liebenthal U. *Overall Process Optimisation of Coal-Fired Power Plants using Correlations.* TUHH. Doctoral Thesis. 2011 (expected).
Mak J. Configurations and Methods for Acid-Gas Absorption and Solvent Regeneration. International Patent WO 2006/118795, November 9, 2006.
Nainar M and A Veawab. "Corrosion in CO2 Capture Process using Blended Monoethanolamine and Piperazine." *Industrial & Engineering Chemistry Research.* 48(20): 9299-9306. 2009.
Nguyen T, et al. "Volatility of aqueous amines in CO2 capture." *Energy Procedia.* 4: 1624-1630. 2011.
NIST. "NIST Chemistry WebBook, CO2 Fluid Properties." Retrieved 6/21/2011. http://webbook.nist.gov/chemistry/
Oexmann J and A Kather. "Minimising the regeneration heat duty of post-combustion CO2 capture by wet chemical absorption: the misguided focus on low heat of absorption solvents." *Int J Greenhouse Gas Control.* 4(1): 36-43. 2009.
Onda K, et al. "Mass transfer coefficients between gas ad liquid phases in packed columns." *J Chem Eng Jap.* 1(1): 56-62. 1968.
Oyenekan BA. *Modeling of strippers for CO2 capture by aqueous amines*. The University of Texas at Austin. Ph.D. Dissertation. 2007.
Oyenekan BA and GT Rochelle. "Alternative stripper configurations for CO2 capture by aqueous amines." *AIChE Journal.* 3144-3154. 2007.
Petit JR and et al. "Climate and Atmospheric History of the Past 420,000 Years from the Vostok Ice Core, Antarctica." *Nature.* 429-436. 1999.
Plaza JM. *Modeling of Carbon Dioxide Absorption Using Aqueous Monoethanolamine, Piperazine and Promoted Potassium Carbonate*. Ph.D. dissertation. 2011 (expected).
Plaza JM, et al. "Pilot plant studies of CO2 capture using concentrated piperazine". *Pacifichem 2010, International Chemical Congress of Pacific Basin Societies*, Honolulu, HI, United States. 2010
Reddy S, et al. Integrated Compressor/Stripper Configurations and Methods. International Patent WO 2007075466,

Reddy S, et al. Improved Split Flow Process and Apparatus. International Patent WO 2004005818,
Rochelle GT (2007). CO2 Capture by Aqueous Absorption/Stripping.
Rochelle GT, et al. "CO2 Capture by Aqueous Absorption, First Quarterly Progress Report 2009." Luminant Carbon Management Program. The University of Texas at Austin. 2009.
Rochelle GT, et al. "CO2 Capture by Aqueous Absorption, Second Quarterly Progress Report 2010." Luminant Carbon Management Program. The University of Texas at Austin. 2010.
Seibert AF. Personal communication. Austin, Texas, USA, 6/23/2011.
Stopek D, et al. "Carbon Capture Demonstration Project at WA Parish Station". *Electric Power 2011*, Rosemont, Illinois. 2011
Tans DP. (2010). "Trends in Carbon Dioxide-NOAA/ESRL." www.esrl.noaa.gov/gmd/ccgg/trends/
Tobiesen FA, et al. "Experimental validation of a rigorous desorber model for CO2 post-combustion capture." *Chemical Engineering Science.* 2641-2656. 2008.
Vaida PD and EY Kenig. "CO2 Capture by Novel Amine Blends." *Advances in Gas Processing.* 239-246. 2009.
van Nierop EA, et al. "Effect of absorption enthalpy on temperature-swing CO2 separation process performance." *Energy Procedia.* 4: 1783-1790. 2011.
Van Wagener DH and GT Rochelle. "Stripper Configurations for CO2 Capture by Aqueous Monoethanolamine." *Chemical Engineering Research and Design.* doi:10.1016/j.cherd.2010.11.011. 2010.
Weiland RH, et al. "Stripping of carbon dioxide from monoethanolamine solutions in a packed column." *AIChE J.* 28(6): 963-73. 1982.
Xu Q. *Thermodynamics of CO2 Loaded Aqueous Amines for CO2 Capture*. University of Texas at Austin. 2011 (expected).
Xu Q and GT Rochelle. "Total Pressure and CO2 Solubility at High Temperature in Aqueous Amines." *Energy Procedia.* 4: 117-124. 2011.
Zheng Y, et al. "Simulation and pilot plant measurement for CO2 absorption with mixed amines." *Energy Procedia.* 4: 299-306. 2009.

# Vita

David Hamilton Van Wagener was born in Cincinnati, OH in 1983. He graduated from Cherry Creek High School in Greenwood Village, CO in 2002, and then he enrolled at Bucknell University to study chemical engineering. He suffered a traumatic cervical spinal cord injury during winter break after his first semester. Even so, he returned to Bucknell in August 2003 to continue his studies, and he graduated with his incoming class in May 2006 with a Bachelor of Science degree in chemical engineering with magna cum laude honors. In the summer of 2005, he worked with Procter & Gamble in Cincinnati, OH. He started his graduate program at The University of Texas at Austin in August 2006 as a Ph.D. student working under Dr. Gary T. Rochelle. David has accepted full-time employment with ConocoPhillips in Bartlesville, OK.

Permanent e-mail address: david.vanwagener@gmail.com

This dissertation was typed by the author.